Effect of Control Techniques on the Performance of Semiactive Dampers

John W. Masi

Thesis submitted to the faculty of

Virginia Polytechnic Institute and State University

in partial fulfillment of the requirements for the degree of

Masters of Science

In

Mechanical Engineering

Mehdi Ahmadian, Chair

Daniel J. Inman

Donald Leo

December 19, 2001

Blacksburg, Virginia

Keywords: Vehicle Suspension, Semiactive, Control, Magneto Rheological, Magneto Rheological Damper, Skyhook, Groundhook, Hybrid

Effect of Control Techniques on the Performance of Semiactive Dampers

John W. Masi

Abstract

A computer simulation is used to examine the effects that various control methods have on the performance of semiactive dampers in controlling the dynamics of a single suspension (quarter car) model. The level of dynamic control of this model has a direct bearing on the ride comfort and vehicle handling, when the single suspension is interpreted as a partial model of a vehicle. The dynamic results obtained when using two alternative semiactive control methods are compared to the results obtained when using the more conventional control methods of passive damping, Skyhook control, and Hybrid control. The conventional control methods results confirm that the semiactive damper possesses a number of benefits when compared to passive damping. In addition, the alternative control methods, which are Displacement Skyhook and Displacement Hybrid, do not show benefits that are superior to passive damping or the conventional semiactive control methods.

In support of the conclusions of this report, sufficient detail of the mathematical and numerical model is provided in the event that one should wish to recreate the results presented here. Next, the simulation results of each of the five control methods are presented individually. Several of the responses used in the results chapters are the transmissibility plots for the sprung and unsprung body displacement, the frequency spectrum of acceleration, and the frequency spectrum of the rattle space. In addition, the system response to a step input is calculated and, lastly, time traces are calculated, one at a time, for system excitations at the sprung and unsprung mass natural frequencies. The key dynamic measures studied are settling times, displacements, accelerations, and jerks. The responses just listed are then used in a comparison study between each of the presented control methods.

Acknowledgments:

Dr. Ahmadian deserves most of the credit for this thesis, as its creation is the result of his inspiration, creativity, and experience. Dr. Ahmadian's advice and suggestions were critical for completing this thesis. Also, I would like to thank the Department of Mechanical Engineering at Virginia Tech for supporting me through a Graduate Teaching Assistantship.

In addition, I want to thank Dr. Leo and Dr. Inman for serving on my committee. I would also like to thank Jim Poyner and Fernando Goncalves for their experimental results, which were used in this thesis.

I thank my parents, William and Ruth Masi, for supporting me throughout the years. Without them, the path to where I am now would have been much more difficult.

Contents

List of Tables

List of Figures

Chapter 1
Introduction

This study utilizes the semiactive damper to control a simulated suspension model in an attempt to improve semiactive damper technology. Semiactive dampers are a relatively new technology that has been focused on in a number of studies. It is our goal to not only provide simulation results using existing technology, but to try and improve upon it by experimenting with two alternative controllers. First, however, we run simulations using three of the more "traditional" control methods for later comparison to the alternative semiactive laws. This chapter includes a brief introduction to semiactive damping, a list of objectives for this study, a description of the approach used here, and an outline of the rest of this report.

1.1 Introduction

Semiactive dampers change their damping force in real time according to a controller policy, which is usually based on the system dynamics. Simply adjusting the damper's resistance to motion, or damping coefficient, changes the damper force. The ability to vary the semiactive damping coefficient independently of damper velocity, within limits, has prompted a number of individuals and companies to explore the possibility of improving suspension performance by using semiactive damper technology. As noted by Pare in [3], most research concludes that, at least in certain aspects, semiactive dampers can outperform the passive damper.

To implement the semiactive control law, the semiactive damper must be adjustable in real time. Currently, semiactive dampers can be adjusted hydraulically or rheologocally. The first category uses mechanical valves driven by a solenoid or stepper motor to control damper force in a hydraulic damper. In the latter category, the rheological effect of controllable fluids, such as magneto rheological or electro rheological fluid, is used to provide adjustable damping forces. Although mechanical and rheological control

dampers have been researched and developed extensively, the rheological controllable dampers have received much more attention in the past few years, mainly due to great advances in magneto rheological fluids.

Semiactive dampers are potentially a very attractive method of controlling a suspension in order to improve its performance. As we have already begun to see, the effective use of these special dampers depends, in part, on the designer's ability to develop a suitable controller for the damper. Although several promising control laws have already been introduced, further improvements could be realized by examining alternative control laws.

1.2 Objective

The primary objectives of this study are to

1. analytically evaluate and compare various semiactive control techniques that have been proposed in the past, such as Skyhook and Hybrid control;
2. propose new control techniques that can be used for vehicle applications; and
3. evaluate the benefits of each control technique for vehicle suspensions with bounded damping force.

1.3 Approach

To achieve the objectives of this study, a single suspension computer model will be used to evaluate the effectiveness of a variety of control techniques, such as passive, Skyhook and Hybrid, in terms of selected performance measures. We will concentrate the output analysis on key performance measures, such as settling time, displacement, acceleration, and jerk. These performance measures will determine the extent to which the tested control techniques improve the ride comfort and road handling in a vehicle application.

1.4 Outline

Chapter 2 presents background information on semiactive systems, MR dampers, and semiactive controllers. In addition, a literature review is included which summarizes

selected past studies on semiactive control. Chapter 3 presents the mathematical model used for the simulations. Here, the models for the single suspension, the MR damper, the passive damper, and the semiactive controllers are presented. The SIMULINK block models are shown and the model parameters are also defined in Chapter 3. Chapter 4 contains the linear passive results. The passive results are reviewed for comparison to the semiactive cases later and to verify that the model, excluding the semiactive controllers and MR damper, is correct. Chapter 5 explains the semiactive results for Skyhook and Hybrid and also the Displacement Skyhook and Hybrid controllers. At the end of Chapter 5, bar charts are used to compare all of the different control policies. Chapter 6 is the conclusion chapter and ties everything together by presenting the important points to take from this study.

Chapter 2
Background

Much has been learned about semiactive damper technology in the last thirty years. Some of this knowledge is reviewed now in order to guide us in our study. To review the area of semiactive technology, we start with a brief description of a semiactive system, which is a feedback system. In addition, we will also review the operation the MR damper since a model of a MR damper was used in this study. Finally, in this chapter, we will also familiarize ourselves with some of the studies and results that have been carried out in the past. The information in this chapter forms the basis for the model used in this study.

2.1 Semiactive Systems

A semiactive damper suspension system varies the damping force in real time depending on the dynamics of the controlled masses. The semiactive system utilizes a feedback loop to control the damping force at any time. The feedback is usually taken as the velocities of the bodies that the suspension controls. A processor can then use the feedback data to calculate the desired damper control force, which must be converted into a control signal that will adjust the damper. The form of this signal is discussed in the next section. The signal that is sent to the damper changes the damper's resistance to velocity and therefore changes the damper force. Finally, the feedback loop is completed as the changing damper force alters the acceleration of the controlled bodies and the feedback variables in ways that would not have occurred had a passive system been used. If the system works as desired, then the semiactive system dynamics will be more favorable than the passive system dynamics.

In studying dynamic systems, whether semiactive or not, the terminology sprung and unsprung bodies (masses) are often used in dynamics literature to refer to the two bodies of a two degree of freedom dynamic model, Figure 2.1. Here, the sprung body is represented by m_1 and the unsprung body by m_2. The bodies are connected together by a

spring and the unsprung body is connected to a movable base. A movement of this base is called a base excitation of the dynamic system. In Chapter 3, this model will be used as a lumped-parameter model of a vehicle suspension.

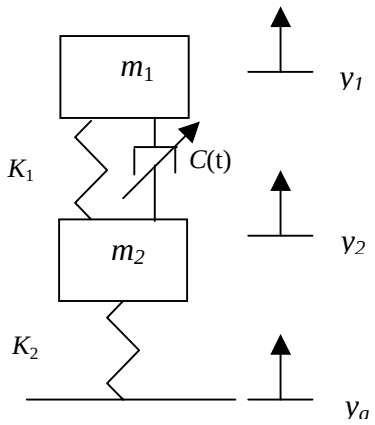

Figure 2.1 Two Degree of Freedom Single Suspension Model.

2.2 Semiactive Dampers

Semiactive dampers are an alternative to the active dampers. The semiactive dampers only *dissipate* energy in a controlled fashion. Imagine holding a rod vertically in your hand and letting the rod slip through. By tightening your grip you can control the dissipation of the potential energy stored in the rod as well as the speed of the rod as it falls. This is the basic idea behind a semiactive damper control. The active dampers are capable of *supplying* energy to the system, such as by a hydraulic piston. Now, to represent the semiactive damper in our rod analogy we can consider holding the rod loosely in one hand and firmly in the other. By pushing the rod up and down with the firmly gripped hand we can represent the concept of active control.

The advantage of semiactive dampers over active dampers is their lower complexity, cost, risk, and weight. The semiactive damper does away with the need for the compressor, reservoir, and valving. The elimination of these parts makes the system lighter in weight as noted in several studies referenced by [9]. In addition, although MR fluid is not inexpensive, neither is the mechanical setup required for the active damper, especially considering the hydraulic valves. Also, in terms of risk, a malfunction of an

active system would be more serious than that of a semiactive damper. Taken together, all of these factors suggest that the MR dampers are a favorable alternative to the hydraulic dampers.

2.2.1 Magneto Rheological Operation

The MR damper is a current controlled variable damper that takes advantage of a physical property of MR fluids. When MR fluid is placed within a magnetic field, the fluid's shear strain rate increases. A stronger magnetic field provides more resistance to the fluid being sheared or passed through a valve. The magnetic field can be created by passing a current through a coil of wire that is in the specially designed damper. The damping force, for a particular velocity, increases when the current through the damper coils increases, as shown in Figure 2.2, which depicts the damping characteristic for a typical MR damper. Additionally, the power required for operating MR dampers is relatively minimal; for instance, a maximum of 5 amps at 12 volts for the damper tested in Figure 2.2. The combination of variable damping and low power allows for relatively easy application of semiactive control laws.

MR dampers also exhibit a roll-off, which typically occurs at relatively low velocities. The steep part of the curve is associated with the pre-yield behavior of the MR fluid through the valve. The flatter part of the curve is caused by the post-yield behavior of the fluid. The details of the pre- and post-yield behavior of the fluid can be found in [7].

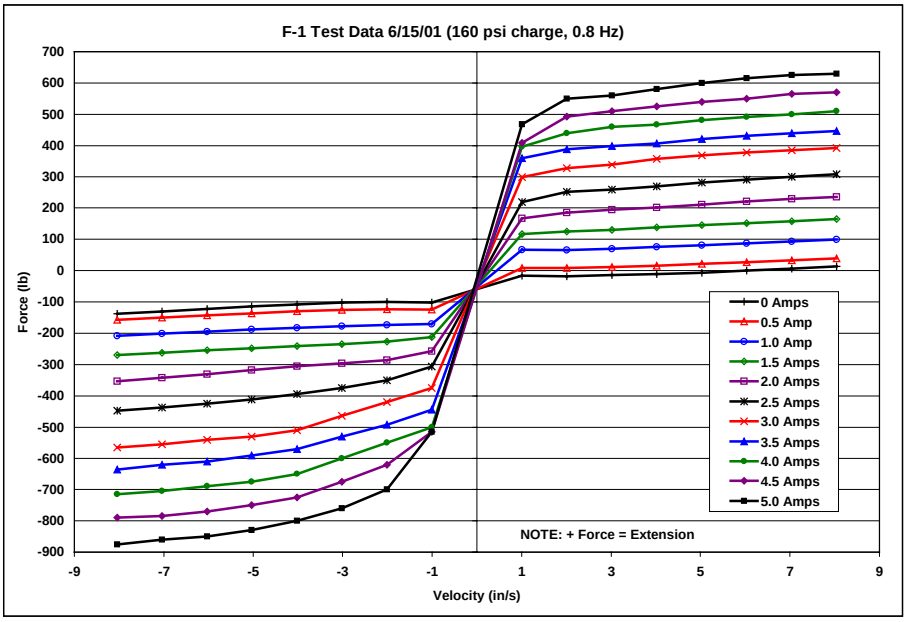

Figure 2.2 Experimental MR Damper Force/Velocity Characteristic. Adopted from [27].

2.3 Literature Review

A number of theoretical studies compare the performance of semiactive dampers to that of passive dampers. In one paper, Crosby and Karnopp [9], present the benefits of Skyhook control as a reduction in the frequency response magnitude of a single degree of freedom semiactive isolator, shown in Figure 2.3. Their simulation results show that using Skyhook to control the semiactive damper reduces the transmissibility, or the ratio of the output to the input, y/y_g, to less than the passive damper transmissibility. They also note that, "The apparent lowering of the system natural frequency with high values of b [Skyhook gain] is attained at the cost of a very discontinuous force." [9].

The effect of semiactive control on suspension performance has also been studied on a two degree of freedom system (two mass) system, such as the one depicted in Figure 2.1. One such study is an experimental investigation by Ivers and Miller [14]. In their study they use a, "quarter car test rig" (single suspension device), to generate their results. This

quarter car rig was base excited by a random velocity input to represent a, “real road input”. Their results show that Skyhook can be used to reduce the sprung body RMS acceleration to below that of the passive acceleration and therefor should improve ride quality. In addition, their results show that Skyhook can also increase the RMS tire contact force and that should improve the vehicle handling. They also found that using Skyhook control for the case of a step input reduces the percent overshoot to below the overshoot of the passive case, with in limits.

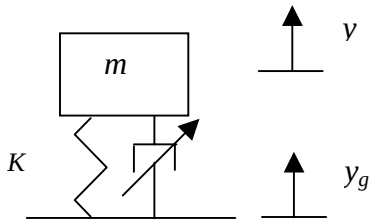

Figure 2.3 Single Degree of Freedom Isolator System.

More recently, Pare [3] has taken frequency response measures of a quarter car rig whose suspension was controlled by various methods. Pare experimentally shows that the Skyhook controller can be used to reduce the body transmissibility. Pare also has shown Hybrid control, to be discussed in more detail later, can be used to reduce both the sprung and unsprung body natural frequency transmissibilities as well as be altered to trade off sprung body performance for unsprung body performance. Goncalves [3] has extended on Pare’s work to include a more comprehensive study of Skyhook and Hybrid as well as a study of several alternative semiactive control laws, such as Displacement Skyhook and Displacement Hybrid.

Some studies are even more realistic because they use actual vehicles. For example, Ahmadian [2] has taken experimental data from a test truck fitted with sensors. The truck was driven along a road while acceleration measurements were taken from the truck. He found that for certain frequency ranges and speeds, the semiactive suspension was capable of producing lower peak acceleration intensities than the passive suspension.

Another study that uses an actual vehicle is the M551 Tank paper by Miller and Nobles [24] that presents evidence that a semiactive damper can significantly reduce acceleration power compared to the passive case. The range of power acceleration ranged from 13% to 43% of the passive results.

There are many other papers that discuss the benefits and response characteristics of Skyhook control and several that discuss Hybrid control. However, the study of semiactive control does not have to be limited to Skyhook or even Hybrid. For example, Angie Carter [5] has tested fuzzy logic controllers on a 4 degree of freedom (a model with four bodies) roll-plane model of a truck. Carter has found that the fuzzy logic controller provides a reduced dynamic response as compared to the passive control results. In addition, she has found that the fuzzy logic controller is an improvement over the on-off Skyhook by most performance measures.

The search for an alternative controller with advantages over current controllers, at least in some aspect, will probably never end. It is in this spirit that we have continued this pursuit by simulating and studying several variations to the more traditional. The results of this experimentation are presented later in this study.

Chapter 3
Dynamic Model

This chapter presents all of the details necessary to construct the semiactive single suspension model, simulate the model, and interpret the results. The mathematical model section describes the derivation of the equations for a lumped-parameter model, the damper model, and controller equations. Next, the numerical model section shows how the mathematical equations are represented in SIMULINK. The meaning and value of the model parameters are given next. Then, a justification for the test inputs is given along with a method for interpreting their results. In the next section, the solver parameters are presented. Finally, a verification section is included that explains how the model was checked. This chapter provides the means for generating and interpreting the results presented in later chapters.

3.1 Mathematical Model

The mathematical model formulation consists of the following three parts.

1) Lumped-parameter model equations
2) Passive and magneto rheological damper equations
3) Controller equations

Each one of these parts will be discussed separately.

3.1.1 Lumped-Parameter Model

The model that is used for presenting the results of this study, shown in Figure 2.1, is commonly referred to as a single suspension (quarter car) model. It represents a corner of a vehicle by including the dynamics of the sprung mass, unsprung mass, and suspension along the vertical axis of the vehicle. The sprung mass refers to the vehicle body, or the mass that is placed on the suspension. The unsprung mass refers to the bodies or components that are below the suspension, such as the vehicle axle, tire, and a portion of the suspension. The suspension includes the spring and damping elements that connect

the sprung and unsprung bodies together. The terms used to describe each part of the model are listed in Table 3.1.

The dynamics of the single suspension model in Figure 2.1 can be represented by,

$$m_1 \frac{d^2 y_1}{dt^2} + K_1 y_1 - K_1 y_2 + F_d = 0 \tag{3.1}$$

$$m_2 \frac{d^2 y_2}{dt^2} + (K_1 + K_2) y_2 - K_1 y_1 - F_d = K_2 y_g \tag{3.2}$$

The determination of the damper force, F_d, will depend upon the damper model used.

Table 3.1 Single Suspension Model Parameters.

Symbol	Description	Units
F_d	Damper force	N
F_1	Spring force	N
F_2	Tire compression/extension force	N
m_1	Sprung mass	kg
m_2	Unsprung mass	kg
$C(t)$	Damping coefficient	N/m/s
K_1	Suspension spring stiffness	N/m
K_2	Tire stiffness	N/m
y_1	Sprung body displacement	m
y_2	Unsprung body displacement	m
y_g	Ground position	m

3.1.2 Damper Model

The MR damper model presented in Figure 3.1 is based on an actual damper force/velocity characteristic. This damper model is an approximation that does not include the roll-off. The actual damper characteristic that forms the basis of this damper model is shown in Figure 2.2. There are two parts to the MR damper model. They are the,

1. force/velocity characteristic and
2. filter used for converging the jerk calculation.

Each part will be explained next.

3.1.2.1 Force/Velocity Characteristic

Regions A and B in Figure 3.1 are the available regions for the MR damper operation. The maximum damper force is bounded by the force line with slope C_{on} and the minimum damping force is bounded by the damper force line with slope C_{off}. For example, at a damper velocity of 5cm/sec, if the MR controller request a damper force greater than the C_{on} line then the damper model will limit the force at the C_{on} line. If the controller requests a damper force between the C_{on} and C_{off} line then the damper model will apply the requested force magnitude to the sprung and unsprung masses. Finally, if the requested force is below the C_{off} line then the damper will limit the damper force at the C_{off} line. The direction of the damper force will depend on whether the damper is extending (rebounding) or compressing (jouncing). The C_{on} and C_{off} lines place limits on how small and how large the damper force can be for a given velocity.

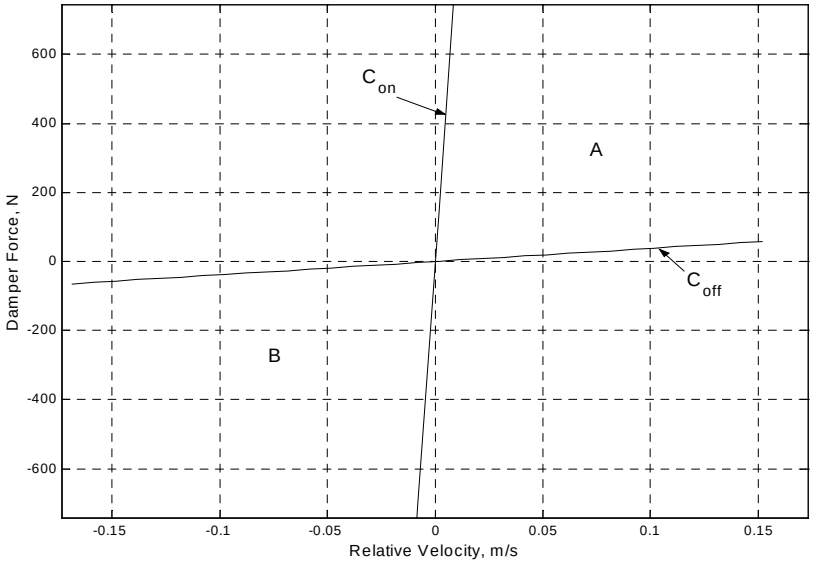

Figure 3.1 Damper Force/Velocity Characteristic for a MR Damper Model. $C_{on} = 85000$ N/m/s $C_{off} = 381.9$ N/m/s.

3.1.2.2 Filter

A first order filter, equation (3.3), such as the one used by Song [29], is used on the output of the model in Figure 3.1 for two reasons.

$$\mathrm{TF}_{\mathrm{filter}} = \frac{1}{\tau s + 1} \tag{3.3}$$

The first reason is to converge the jerk calculation and the second reason is to simulate the time delay of the damper. Concerning the first reason, jerk is the rate of change of the acceleration with respect to time. If the filter were not used, then the jerk solution would depend upon the sample time. For example, if the damper controller turns the damper force from off to full on instantaneously then the jerk on the sprung mass would be infinite since the sprung mass acceleration component, due to the damper force, would change instantaneously. Increasing the sample time would decrease the jerk by spreading out the increase in acceleration over a longer period of time.

The continuous definition of jerk is,

$$\mathrm{jerk} = \frac{da}{dt} \tag{3.4}$$

where,

$\frac{da}{dt}$ = derivative of acceleration with respect to time

The discrete definition used here is,

$$\mathrm{jerk}_{k+1} = \frac{a_{k+1} - a_k}{T_s}$$

(3.5)

where,

$a_k = k^{th}$ acceleration of the sprung body, m/s^2, for k = 1,2,3… ∞

T_s = sample period, seconds

We can see from equation (3.5) that if the sample time, T_s, were increased for the same change in acceleration, $a_2 - a_1$, then the jerk would be reduced. The filter must be used so that the jerk does not depend on the sample rate. The second reason for using the filter is to simulate the time delay of the damper. When a current is applied to a MR damper there is a finite amount of time before equilibrium is reached, as for instance stated in [19]. The time constant of this delay is taken as $\tau = 10$ msec for these simulations.

The constants were chosen as one so that the 0 Hz (constant input) response magnitude would be one. In other words, if the input to this filter were a constant, say 3, then the steady state output of the filter would be 3 as well. To understand the effect that this filter has on the results, we should examine the Bode plot of it in Figure 3.2. The filter frequency response shows that the 0 Hz response magnitude is 1. As the frequency increases, however, the filter scales down the filter input. For example, at 10.5 Hz, the filter attenuates its input by 0.835. If a 10.5 Hz sinusoid of magnitude 1 were used to drive this filter, then the filter output would be a 10.5 Hz sinusoid of magnitude 0.835. In addition, at 10.5 Hz, the filter introduces a lag of 33.4 degrees. The delay effect that the filter has can also be seen later in Chapter 3, Section 3.6.3 Semiactive Control Law Verification.

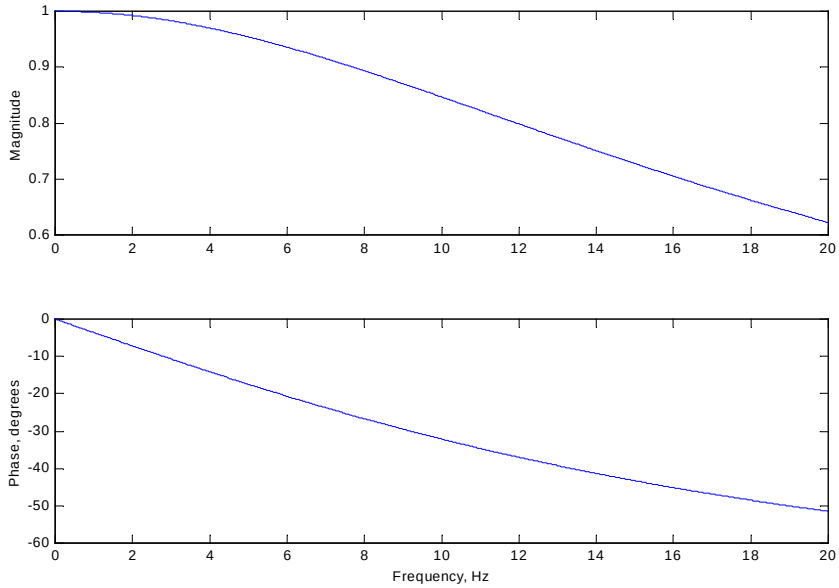

Figure 3.2 Frequency Response of the Damper Model 1st Order Filter.

Since the filter introduces a phase lag into the solution, we find that using the filter introduces a hysteresis into the solution. A damper force hysteresis has been indicated in several past studies such as [29].

3.1.3 Controller Models

There are five control methods tested in these simulations. They are linear viscous passive damping, Skyhook, Hybrid, Displacement Skyhook, and Displacement Hybrid control. The equations and a description for each of these control laws will be presented now.

3.1.3.1 Passive

The model for the passive damper is a standard linear viscous damper described by the equation,

$$F_d = Cv_{12} \tag{3.6}$$

C = passive damping coefficient, N/m/s

This damper is the standard textbook case damper whose force is a multiple of the damping coefficient and the relative velocity across it (damper velocity). The passive results will serve as a comparison basis for the other control method results.

3.1.3.2 Skyhook

The Skyhook law was patented in 1974 by Karnopp [18]. Ideally, the diagram in Figure 3.3 represents the Skyhook controlled quarter car model. Note the damper connected to the sky (a fixed y-axis coordinate). The following simple example should give an intuitive sense of how Skyhook control works. For example, if the suspension damper of Figure 3.2 is expanding and the sprung body is moving upwards, then Skyhook control turns the damper on and the damper pulls down on the sprung body. The difference between Skyhook and passive is that the Skyhook controller varies the damper force such that the damper force is equal to,

$$F_d = Gv_1 \tag{3.7}$$

The effect on the sprung body is the same as if a damper, as shown in Figure 3.3, were connected between the sprung body and the sky and was pushing down on the sprung body. The Skyhook control law is mathematically described by,

$$F_{dd} = \begin{cases} Gv_1 & v_1 v_{12} > 0 \\ 0 & v_1 v_{12} \le 0 \end{cases} \tag{3.8}$$

where,

F_{dd} = desired damper force, N

v_1 = sprung body velocity, m/s

v_2 = unsprung body velocity, m/s

v_{12} = damper velocity, m/s

G = Skyhook gain, N/m/s

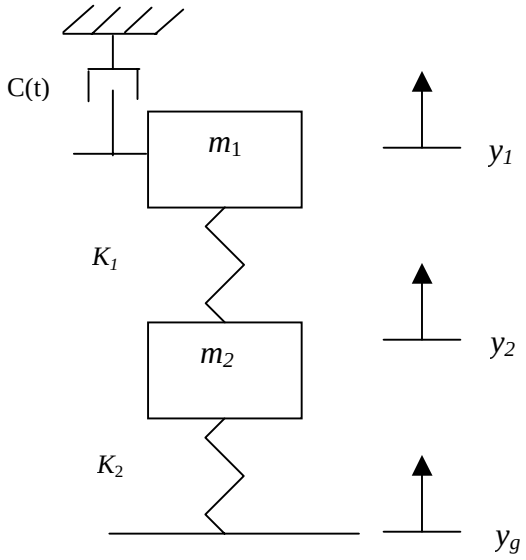

Figure 3.3 Schematic of a Single Suspension under Ideal Skyhook Control.

The switching law turns the damper off when the direction of the damper velocity is not consistent with the direction of the desired damper force. In other words, if it is desired to have the MR suspension damper pull down on the sprung body but that damper, of Figure 3.2, is being compressed, then only an upwards force is available from that damper. The control law will turn the damper off in an effort to minimize the upwards push from the suspension damper. This limitation of semiactive control is recognized in Karnopp's patent [18] and a paper by Karnopp [17]. One draw back examined here to using the switch is that it introduces a large jerk, or a rapid change in acceleration, to the bodies. Jerk can adversely affect ride comfort. The discontinuous semiactive forces are also noted in [9].

3.1.3.3 Hybrid

The Hybrid law is a combination of two control laws; a Skyhook control law that controls the sprung body and a Groundhook control law that is intended to control the unsprung mass. The goal of Hybrid control is to provide direct control of both the sprung and unsprung bodies. The ideal realization of the Hybrid law is shown in Figure 3.4. Note, that now we desire a damper connection between the *unsprung* mass and a fixed y-axis coordinate as well as a damper connection between the *sprung* mass and a fixed y-axis

coordinate. Practically, the Hybrid controller applies a Skyhook control law to both the sprung and unsprung bodies.

The equations for Hybrid control law are,

$$F_d = G\left(\alpha\sigma_{sky} - (1-\alpha)\sigma_{ground}\right)$$

$$\sigma_{sky} = \begin{cases} v_1 & v_1 v_{12} > 0 \\ 0 & v_1 v_{12} < 0 \end{cases} \qquad \sigma_{ground} = \begin{cases} v_2 & v_2 v_{12} < 0 \\ 0 & v_2 v_{12} > 0 \end{cases} \tag{3.9}$$

where,

α_{sky} = Skyhook weighting factor, unitless

α_{ground} = Groundhook weighting factor, unitless

σ_{sky} = Skyhook switch variable, m/s

σ_{ground} = Groundhook switch variable, m/s

To understand the Hybrid control, let's look at an example. Consider the case where the suspension damper is compressing and both bodies are moving up, as might happen when running over a bump in the road. The switches of equation (3.9) cause the Skyhook component to turn off and the Groundhook component to turn on. The Skyhook switch turns the *Skyhook* component of the Hybrid damper force *off* since there is no way that the compressing damper can pull down on the sprung body. The Groundhook switch turns the *Groundhook* component of the damper force *on* since we are able, under these conditions, to emulate the damper to ground connection, which pulls down on the unsprung body.

The summation of the Skyhook and Groundhook forces forms the desired Hybrid control force. Both control laws are negative feedback laws, meaning that the positive velocity of each body results (ideally) in an actuator force which resists the bodies' motion.

Equation (3.9) shows a positive sign on the Skyhook component (1st term) and a negative sign on the Groundhook component (2nd term). The signs are opposite since the derivation of the equations of motion, equations (3.1) and (3.2), for the single suspension assumes that a positive damper force acts in the negative direction on the sprung body and in the positive direction on the unsprung body. This is why equation (3.9) has a positive sign on the Skyhook component and a negative sign on the Groundhook component.

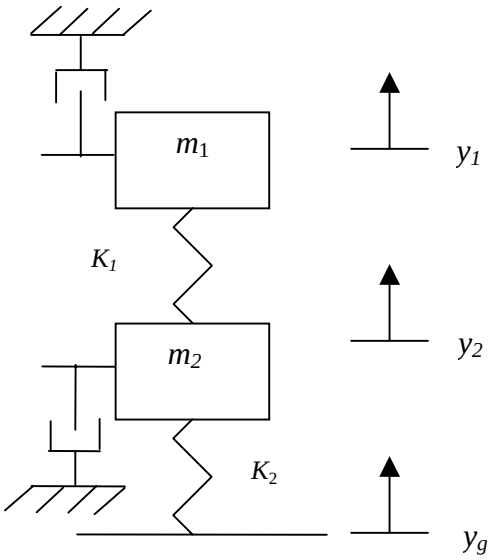

Figure 3.4 Idealized Schematic of Hybrid Control on a Single Suspension Model.

3.1.3.4 Displacement Skyhook

The Displacement Skyhook control law uses a switching policy based on sprung body displacement rather than sprung body velocity. The idea is to turn the damper off when the sprung body is positively displaced and the suspension is compressing, such as when a bump is hit. The difference between Skyhook and the Displacement Skyhook is that the suspension now turns off when the body is *displaced* upward as opposed to *moving* upward while the suspension is compressing which would also occur when hitting a

bump. Turning the suspension off should minimize the force transmitted to the body when a bump is hit. The Displacement Skyhook control law is,

$$F_d = \begin{cases} Gv_1 & x_1 v_{12} > 0 \\ 0 & x_1 v_{12} \le 0 \end{cases} \tag{3.10}$$

x_1 = sprung body displacement, m

x_2 = unsprung body displacement, m

other parameters are as defined earlier

Since the switch no longer prevents the controller from requesting a damper force that is inconsistent with the damper velocity, other arrangements were made to take care of this requirement. These arrangements are discussed later.

3.1.3.5 Displacement Hybrid

Extending the concept of Displacement Skyhook control to Hybrid control yields Displacement Hybrid. The equations for Displacement Hybrid are,

$$F_d = G\left(\alpha\sigma_{sky} - (1-\alpha)\sigma_{ground}\right) \tag{3.11}$$

$$\sigma_{sky} = \begin{cases} v_1 & x_1 v_{12} > 0 \\ 0 & x_1 v_{12} < 0 \end{cases} \qquad \sigma_{ground} = \begin{cases} v_2 & x_2 v_{12} < 0 \\ 0 & x_2 v_{12} > 0 \end{cases}$$

Displacement Hybrid operates in a similar manner to the Hybrid except that now the switches operate based on x_1 and x_2 instead of v_1 and v_2.

3.2 Numerical Model

The entire simulation was carried out using the SIMULINK block diagram models presented in this section and the variable initialization and plotting m-file routine located within the model folder attachment. The block diagrams of the single suspension model are presented next. First, the model diagrams for the bodies and the springs of the single suspension model are explained. Next, the damper model is presented followed by the

controller models. Most of the variables have been previously introduced in the mathematical section. Any new variables are defined in the Table 3.2.

Table 3.2 SIMULINK Parameters for Single Suspension Model.

Symbol	Description	Units
F_{sprung}	Force applied to the sprung body by the suspension	N
$F_{unsprung}$	Force applied to the unsprung body by the suspension and a component of the force applied by the tire compression/extension	N
jerk1	Derivative of the sprung mass acceleration	m/s^3
F_{min}	Minimum available damper force for a given damper velocity	N
F_{max}	Maximum available damper force for a given damper velocity	N
tau	Damper filter time constant	msec
Fd_2	Damper force before filter	N
Fd	Damper force after filter	N
alpha2, α	Hybrid weighting factor	unitless

Figure 3.5 is the main diagram for this model. We can see that the Controller block feeds its force request to the Suspension block. The Suspension block calculates the actual damper and spring forces to be applied to the sprung and unsprung bodies. The Sprung Mass and the Unsprung Mass blocks integrate the accelerations of each body to arrive at the body velocities and displacements. The Unsprung Mass block also calculates and applies the input force from the ground displacement to the unsprung body. The bodies' velocities and displacements are then fed back through the Controller block and the Suspension block to complete the feedback loop.

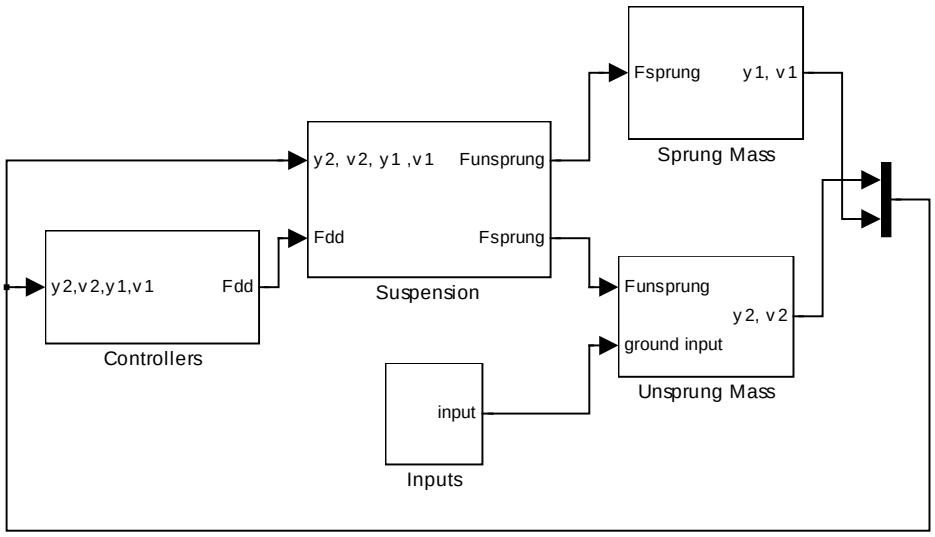

Figure 3.5 Single Suspension SIMULINK Block Diagram Model.

3.2.1 Lumped-Parameter Model

Each block, except for the Input block, of Figure 3.5 is described in this section; the input block is described later. First, the Sprung Mass block, Figure 3.6, receives the suspension force which is applied to the sprung mass. This force is divided by the value of the sprung mass, 453.6 kg, to determine the sprung body acceleration. The acceleration is then integrated once to find the velocity and then again to find the displacement. In addition, the derivative of the acceleration is taken to find the jerk. The Sprung Body block determines the sprung body dynamics based on the suspension forces applied to the sprung body.

The same basic procedure used in the Sprung Mass block is also used in the Unsprung Mass block, Figure 3.7. In addition, in this block, we calculate a component of the input force on the unsprung mass created by the tire compression due to the base displacement. This input force, caused by the base movement, is added to the suspension force. For simplicity, this portion of the input force is calculated in the Suspension block and fed to the Unsprung Mass block as part of the suspension force.

Figure 5.8, is the Suspension block. Here, the suspension forces of the spring and the damper are calculated. The suspension spring force is calculated by multiplying the appropriate displacements by the suspension spring stiffness. This block is a direct result of applying equations (3.1 and 3.2). In addition, the Damper block takes in the bodies' velocities and the controller force requests and outputs the correct damper force. The Damper block is explained later. Note that, as mentioned before, a portion of the input force is calculated in Figure 3.8 and fed straight through to the unsprung mass. This last portion of the model uses K_2. The spring and damper forces then exit the Suspension block are sent to the Sprung and Unsprung Mass blocks.

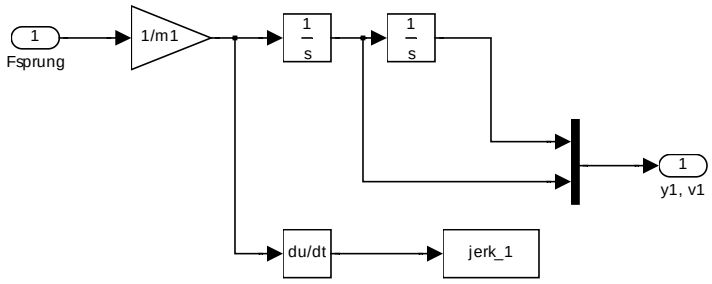

Figure 3.6 Sprung Mass Dynamics Block Diagram.

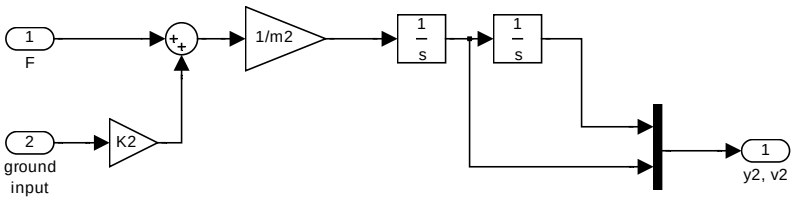

Figure 3.7 Unsprung Mass Dynamics Block Diagram.

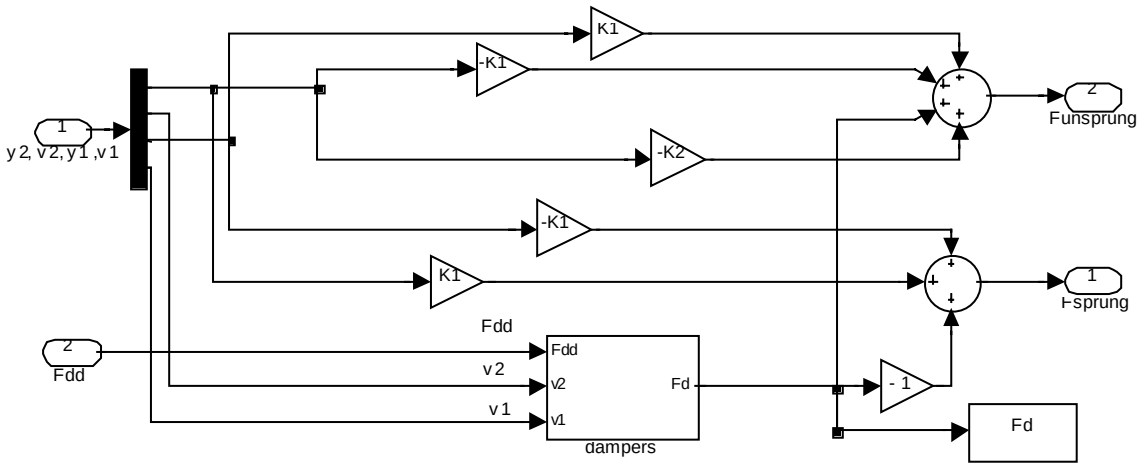

Figure 3.8 Suspension Block Diagram.

3.2.2 Damper

To avoid confusion, it should be noted that the damper modeling method used for these simulations is not the only method for obtaining these results, nor is it the simplest. We had used a version of this model previously to represent the damper roll-off, or the bilinearity, shown in Figure 2.2, and it turns out that the method used here results in shorter solution times than the more direct method described next. In fact, a more direct method for implementing the damper model is by calculating the desired damping coefficient, $C(t)$, bounding this coefficient between C_{on} and C_{off}, and then calculating the damper force by multiplying $C(t)$ with the damper velocity, v_{12}. Alternatively, the method that was used for the simulations was to bound the *damper force*, not the *damping coefficient*, since the force bounding method is faster.

In addition, this method lends itself well to being modified to represent the roll-off inherent in MR dampers. Should one desire to simulate a more detailed MR damper with the roll-off represented, the method here can be easily adapted by replacing the straight C_{on} and C_{off} lines with bilinear lines such as those in Figure 2.2. This type of line can be easily represented using block diagram models, among other methods.

At this point, we can begin examining the operation of the damper model, which bounds the forces to within physically realizable damper limits. Figure 3.9 contains the Semiactive Damper block. The $F_{\min}$ and $F_{\max}$ block provide the minimum and maximum damping force for the current velocity. The $F_{\min} / F_{\max}$ switch block bounds the damper force between $F_{\min}$ and $F_{\max}$. The filter is used to provide the time delay and to converge the jerk solution. Each of these blocks will be described next.

The Fmin block in Figure 3.10 calculates the absolute value of the minimum damping force, $F_{\min}$, for the current velocity. This force is calculated by multiplying the minimum damping coefficient available with the current absolute value of the velocity. The damper model, thus far, will not provide a force less than this minimum force.

The other force bounding block, the Fmax block, is shown in Figure 3.11 and works in a similar way to the Fmin block, except that now we are calculating the absolute value of the maximum available force for the current velocity. The maximum force, $F_{\max}$, is calculated by multiplying the maximum available damping coefficient by the current absolute value of the damper velocity. F_{min} and F_{max} are now sent to the Fmin/Fmax Switch block.

The Fmin/Fmax Switch block, in Figure 3.12, is the block that bounds the damper force in between the C_{on} and C_{off} lines. This block determines what the damper force will be depending on the values of F_{min}, F_{max}, and F_{dd}, the desired damper force. This block operates by taking in the desired damper force, F_{dd}, and comparing its magnitude to $|F_{min}|$. If $|F_{dd}|$ is greater than $|F_{min}|$ then the combination of the relational operator (>=) and the switch passes the damper force $|F_{dd}|$. However, if the magnitude of $|F_{dd}|$ is less than $|F_{min}|$, then $|F_{min}|$ is passed on.

The next combination of relational operator (<=) and switch encountered in the Fmin/Fmax Block compares its input value, which is either $|F_{dd}|$ or $|F_{min}|$ to $|F_{max}|$. If the force value is less than $|F_{max}|$ then the force value is passed through. However, if the

force value is greater than $|F_{max}|$, then $|F_{max}|$ is passed through. Finally, the sign of the damper velocity is placed on the damper force.

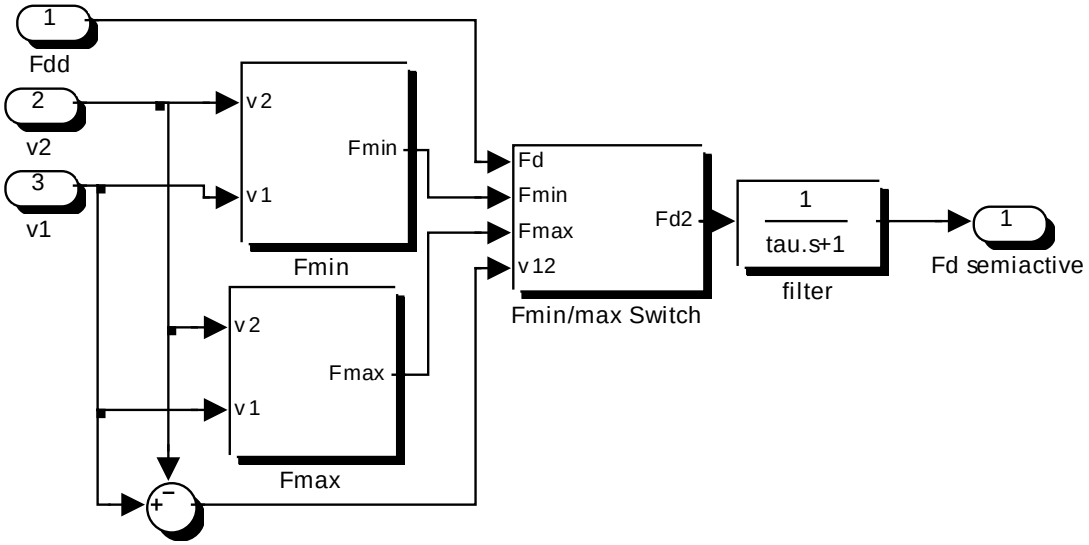

Figure 3.9 Semiactive Damper Block Diagram Model.

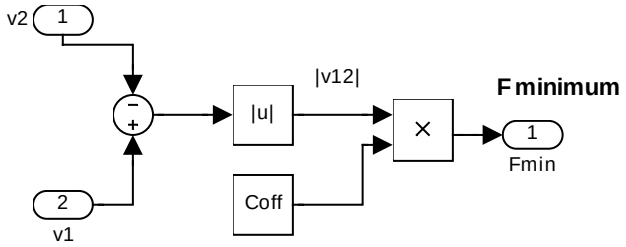

Figure 3.10 Minimum Force Calculation Block Diagram Model.

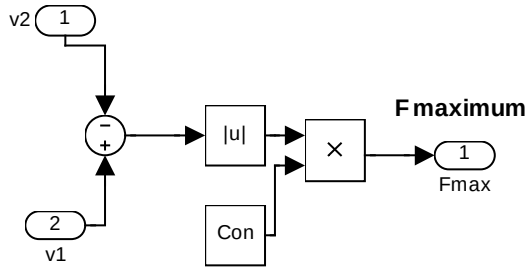

Figure 3.11 Maximum Force Calculation Diagram Model.

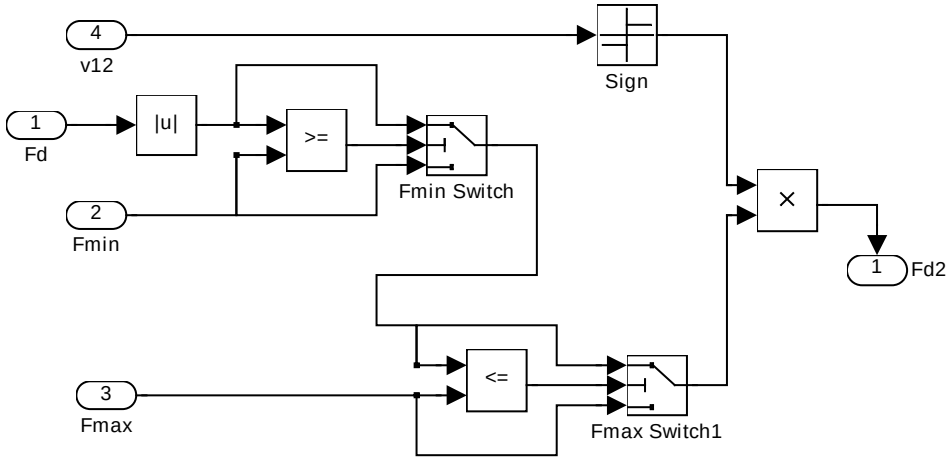

Figure 3.12 Force Bounding Block Model. (Note that any inconsistent force requests have already been zeroed in the controller diagram; this is discussed in Section 3.2.3.)

3.2.3 Controllers

It also should be noted that the correct operation of the semiactive controller law implementation requires the use of the force-limiting block, which is included in the Controller block, shown in Figure 3.13. This block will zero any force requests by the controller whose direction is not consistent with the damper's velocity. This must be done at the controller since the damper will supply a force in the wrong direction if

asked. For example, suppose you request a large *positive* damper force but the damper has a *negative* velocity. If care is not taken to zero this request, the result will be a large negative velocity, i.e. in the wrong direction.

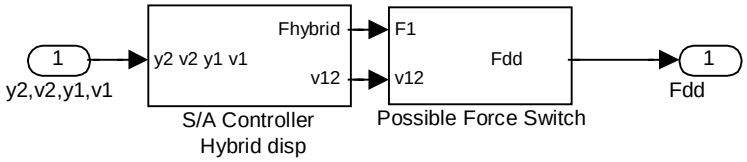

Figure 3.13 Force Limiting Block in Controller Block.
(Note: Hybrid block shown as an example controller, when another controller is used it replaces the Hybrid controller)

The first semiactive controller tested is Skyhook and its SIMULINK model is shown in Figure 3.14. The Skyhook block calculates the Skyhook force as well as switches the force on and off. The switch in equation (3.8) will turn the force off if the sign of the product of the sprung body velocity and the relative velocity is greater than zero. This switching logic is carried out using a product block and a switch.

The second semiactive controller tested is Hybrid and is shown in Figure 3.15. This block combines both the Skyhook controller and a Groundhook controller. In fact, comparing the upper section of the Hybrid block, in Figure 3.15, and the Skyhook block, Figure 3.14, reveals that they are the same. The weighted average of the Skyhook and the Groundhook forces are then taken. The weighted average is carried out by multiplying the Skyhook force by alpha (α) and the Groundhook force by 1 – alpha $(1-\alpha)$. The Hybrid force is then sent to the Possible Force Switch in Figure 3.13.

The third semiactive controller tested is Displacement Skyhook and the SIMULINK block diagram for this controller is shown in Figure 3.16. This controller differs from Skyhook in that the sprung body position, y_1, is used to determine the switching rule, as

opposed to the sprung body velocity, v_1. Comparing the Displacement Skyhook block to the Skyhook block shows that by just changing one wire we transform one controller into the other.

The last semiactive controller that is mentioned here is Displacement Hybrid. The SIMULINK diagram for this law is shown in Figure 3.17. Similar to the Hybrid case, combining Displacement Skyhook with Displacement Groundhook creates Displacement Hybrid. The upper section of the Displacement Hybrid controller, in Figure 3.17, is the Displacement Skyhook section and the lower portion is the Displacement Groundhook section. The Displacement Skyhook force and the Groundhook force are combined by multiplying the Displacement Skyhook force by α and adding this to the multiple of the Displacement Groundhook force and $(1-\alpha)$. The end result is the Displacement Hybrid force, which is then sent to the Possible Force Switch block in Figure 3.13.

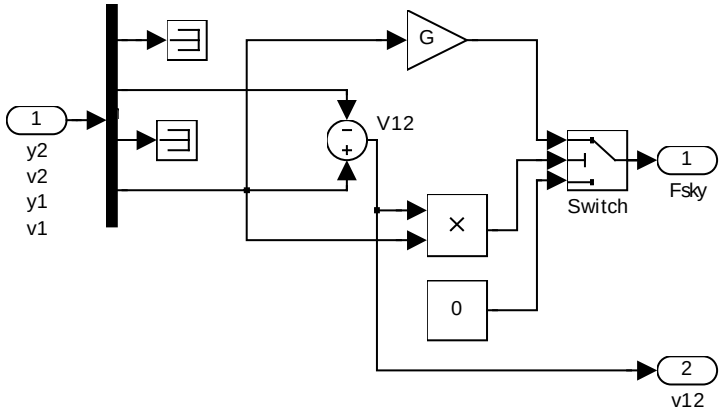

Figure 3.14 Skyhook SIMULINK Block Diagram.

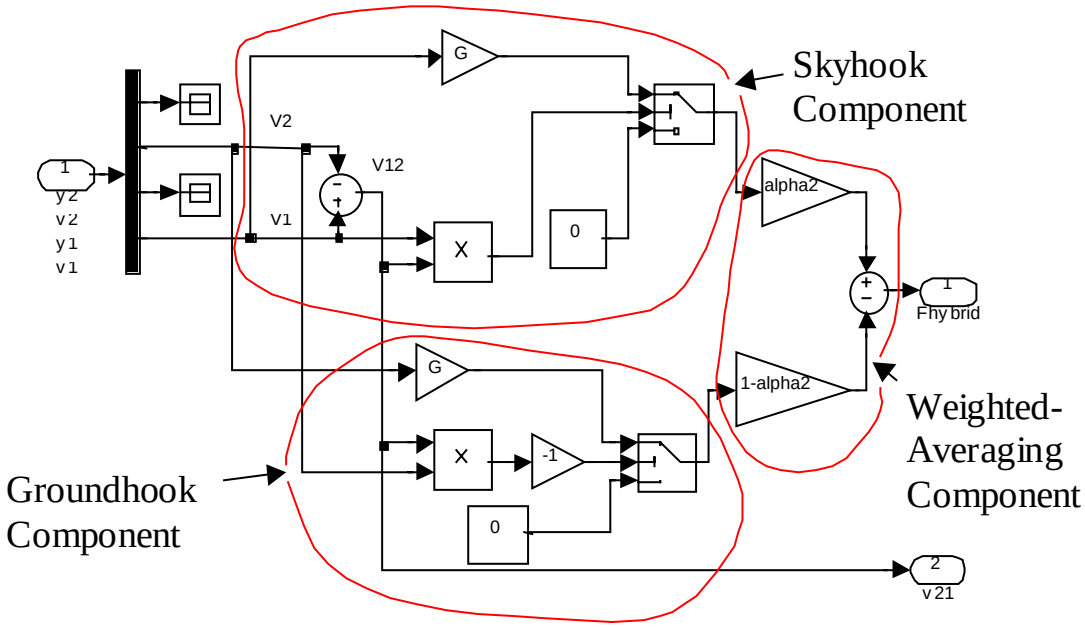

Figure 3.15 Hybrid SIMULINK Block Diagram.

(alpha2; same as α, Hybrid weighting factor)

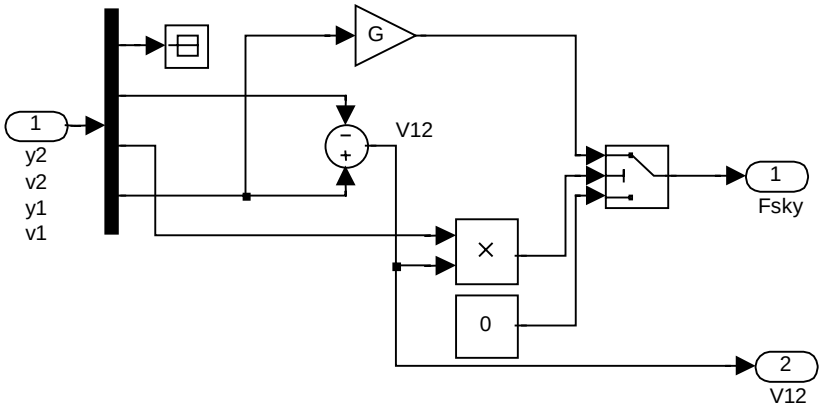

Figure 3.16 Displacement Skyhook SIMULINK Block Diagram.

(F_{sky}; Desired Skyhook damper force)

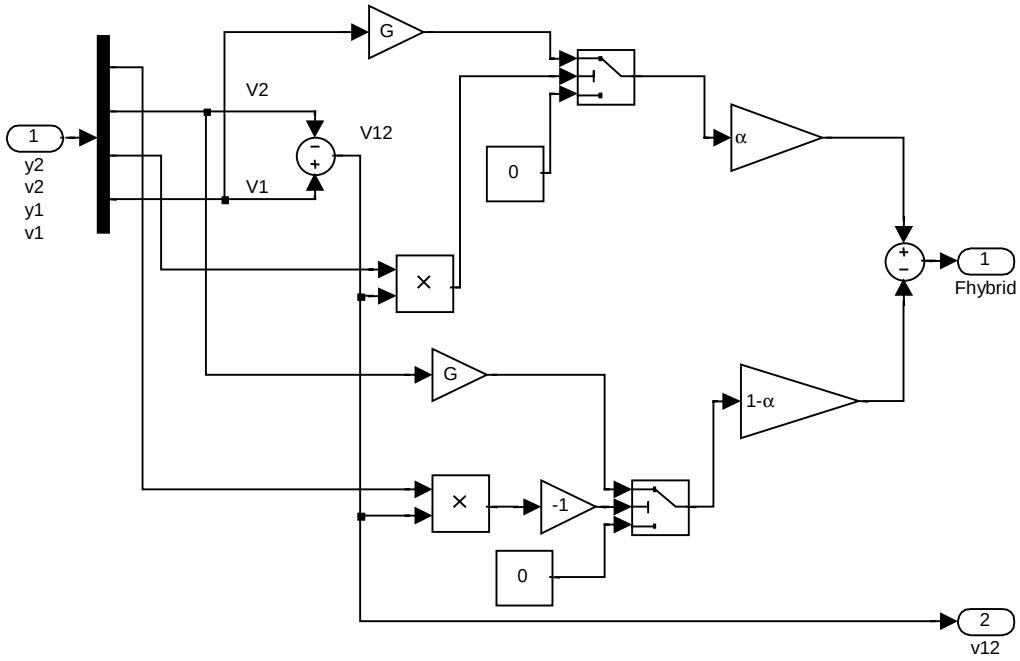

Figure 3.17 Displacement Hybrid SIMULINK Block Diagram.
(F_{hybrid}; Desired Hybrid damper force)

3.3 **Model Parameters**

The values of the model parameters used are listed in Table 3.3 and 3.4. There are several model parameters that do not change, regardless of the controller, case, or the input used. These constant parameters fall into two categories. The first category is the lumped parameter model constants, which are represented by m_1, m_2, K_1, and K_2. The second category is the MR damper constants, which are represented by C_{on}, C_{off}, and τ_{MR}. These constants are not variables that were experimented with in these studies. The rest of the variables in Table 3.2 and 3.3 are the damping coefficients for each passive damping ratio tested and the gains for the semiactive controllers.

Table 3.3 Single Suspension Model Parameter Values.

Symbol	Description	Value	Units
m_1	Sprung Mass	453.6	kg
m_2	Unsprung Mass	45.4	kg
K_1	Suspension spring stiffness	$1.5712x10^5$	N/m
K_2	Tire stiffness	$4.0288x10^4$	N/m
C_{on}	Maximum MR damping coefficient	85000	N/m/s
C_{off}	Minimum MR damping coefficient	381.9	N/m/s
τ_{MR}	MR damper filter time constant	10	msec
C	Damping Coefficient, $\zeta = 0.05$	381.9	N/m/s
	$\zeta = 0.1$	763.7	N/m/s
	$\zeta = 0.2$	1527.5	N/m/s
	$\zeta = 0.4$	3054.9	N/m/s
	$\zeta = 0.8$	6109.9	N/m/s
G	Semiactive controller gain	NA	N/m/s
α	Hybrid controller gain	NA	unitless

Table 3.4 Simulations Summary.

Control Law	**Gains**
Passive	ζ = 5%, 10%, 20%, 40%, 80%
Skyhook	G = 500, 1000, 2000, 4000, 8000
Hybrid	G = 1000, 2000, 4000, 8000 α = 0.25, 0.5, 0.75, 1
Skyhook (displacement based)	G = 625, 1250, 2500, 5000, 9000
Hybrid (displacement based)	G = 625, 1250, 2500, 5000, 9000 α = 0.25, 0.5, 0.75, 1

3.4 Model Outputs and Inputs

In order to recognize the value of the tests in this study, an interpretation of the outputs and inputs is presented in this section. The first section below provides a general means for interpreting the results of this study. The later sections give an interpretation of each of the inputs used in this study and explain the formulation of the inputs. The four test inputs used to determine the performance characteristics of the semiactive control laws are,

1) Chirp input,
2) Step input,
3) 1.34Hz Sinusoid
4) 10.5Hz Sinusoid

Each of these inputs can be interpreted as a realistic input that might be encountered during normal driving conditions. The resulting outputs are then used to determine whether the suspension performance is improved by making suspension design changes.

3.4.1 Interpreting the Outputs

Two important characteristics of a vehicle are its ride comfort and handling ability. The ride comfort is simply how comfortable one would be if they were riding in the vehicle. The ride comfort can be inferred by analyzing the sprung body dynamics. Several factors can adversely affect the ride comfort. The first factor is a large vertical sprung body acceleration [14] (14 refers to the RMS acceleration), which is generally considered unwanted, especially as its frequency increases [13]. The second factor is a large vertical sprung body displacement, is also undesirable; although the human body reacts to the acceleration and displacement differently. The third, and last factor studied here, is the sprung body jerk, which is the time derivative of acceleration. We will also consider a large jerk to be uncomfortable. Professor Ahmadian has informed this author that the acceleration, the displacement, and the jerk can cause rider fatigue and a “jelly” sensation in the affected body parts. In fact, as a contribution of unsupported evidence, this author has experienced the latter after a 3 hour car trip (as the driver) when wearing dress shoes with hard rubber soles.

The second vehicle response characteristic is the vehicle handling, which is inferred by analyzing the unsprung body dynamics. (Remember, the unsprung body contains the tire.) We will assume that larger unsprung body (tire) displacements create an inconsistent contact with the road. The poorer the contact with the road, the less the vehicle motion is constrained by the tire/road interface and the less control the driver has over the vehicles direction of travel. Since we will assume that we want the vehicle to move in the direction that the tires are rolling, we will also assume that an inconsistent tire/road contact, created by large unsprung body displacements, will result in poor vehicle handling. Ivers and Miller [14] discuss improved vehicle handling as a result of increased tire contact forces.

3.4.2 Chirp Input

An explanation of the inputs will begin with the chirp input, Figure 3.18a. The chirp input is used in a method for generating a frequency spectrum of the single suspension model. By analyzing the frequency spectrum, we can get an indirect measure of the single suspension's ability to control the sprung and unsprung body dynamics during road travel. It turns out that the random deviations in a road surface will excite the natural frequencies of a vehicle [14]. These same natural frequencies are easily visible in the frequency spectrum.

To generate the frequency spectrum, the following method is used. (this method was derived from a program by Song)

1) Excite the single suspension model at the base by the chirp input, Figure 3.18a, where,
    a. Chirp timespan: 64 seconds
    b. Starting frequency: 0.5 Hz
    c. Ending frequency: 20 Hz
    d. Solution Rate: 1000 Hz
2) Record output displacement of the body
    Figure 3.18b, (notice the resonance area)

3) Calculate the FFT magnitude of the saved output of Step 2, as shown in Figure 3.19a

4) Calculate the FFT magnitude of the saved chirp input of Step 1, as shown in Figure 3.19b

5) Calculate the transmissibility as the ratio between the transmissibilities calculated in Steps 3 and 4, as shown in Figure 3.19c.

(Note that the frequency in Hertz is determined by taking the time vector and multiplying it by 1000 Hz/64 sec, in this case.)

Basically, this method works by generating an output signal that has the model's frequency response content, which the Fast Fourier Transform can extract.

There are a couple of other factors that are related to the frequency spectrum results presented here. First, the chirp signal is necked down to represent the lower amplitudes that the higher road surface frequencies might have. Second, the semiactive frequency spectrum shows a high frequency oscillation along the data line, especially for the greater gains of the semiactive cases. An explanation is not given for this apparent noise. Lastly, the program used to generate these plots lightly filters the frequency response data. For these presentations, the order of the filter was reduced to 2 to minimize the effect that the filter has on the data. The equation for the FIR (moving average) filter is,

$$x = 0.5x_k + 0.5x_{k-1} \tag{3.12}$$

where,

$x_1 = k^{th}$ data point for $k = 1,2$

$x =$ average result

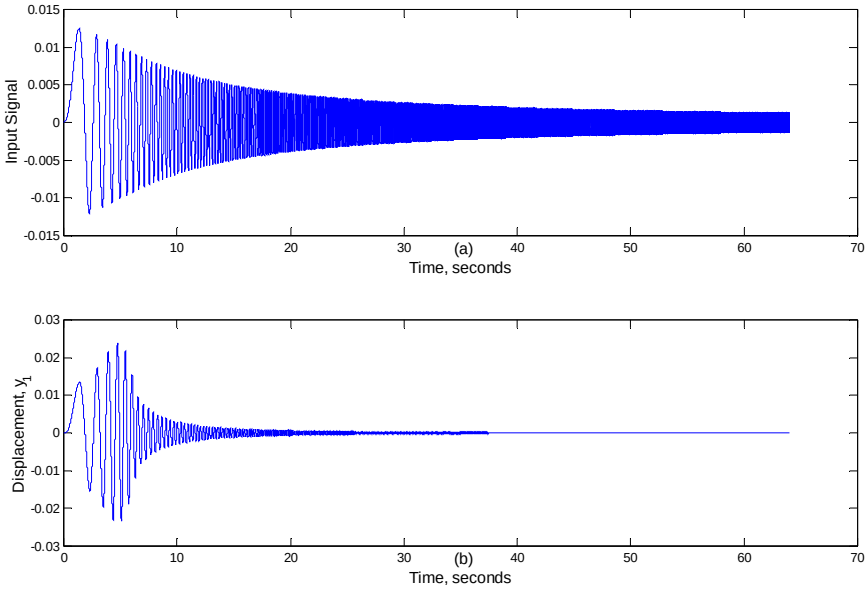

Figure 3.18 Effect of Chirp Input on Sprung Body Displacement; (a) Chirp Input Time Trace; (b) Sprung Body Time Trace.

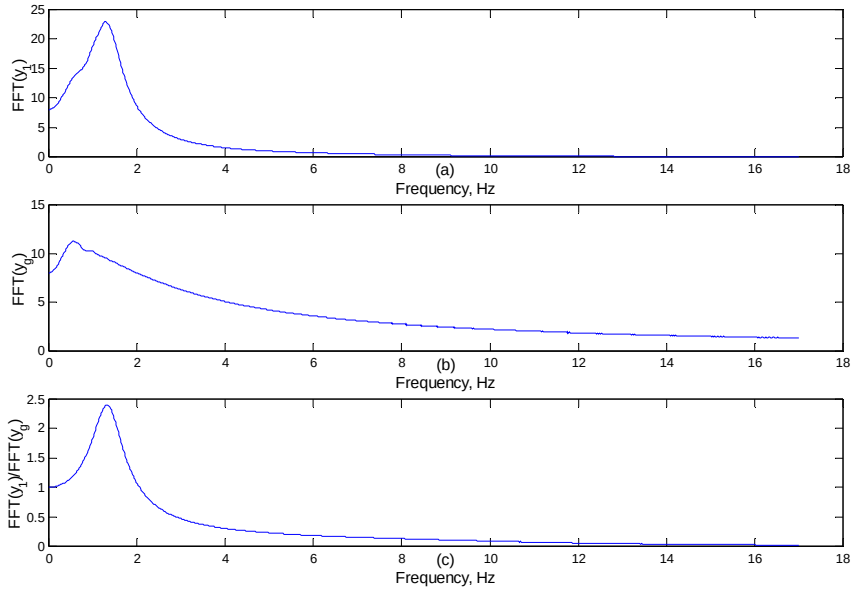

Figure 3.19 Determining the Transmissibility from the Frequency Spectrum the Input Signal and the Output Signal; (a) Output Frequency Spectrum Magnitude, (b) Input Frequency Spectrum Magnitude, (c) Transmissibility = Output FFT/Input FFT.

3.4.3 Step Input

In general, the step input excites the transient dynamics of the single suspension model, in a manner similar to a vehicle hitting a bump in the road could also excite such a transient. The step input amplitude used here has an initial value of zero and a final value of 1.27 cm. The transient response is generally considered an important performance characteristic.

3.4.4 1.34Hz Sinusoid Input

In order to focus on the steady state dynamics of the single suspension model, a 1.34 Hz, 1.27 cm amplitude sinusoid is used to excite the sprung mass natural frequency of 1.34 Hz. The sprung body resonant peak is considered because it is one of the two largest peaks on the frequency spectrum. This analysis is done to determine the effects of different control laws and gains on the steady state amplitude of the sprung body natural frequency response.

3.4.5 10.5Hz Sinusoid Input

The unsprung body natural frequency of 10.5 Hz is the second of the two largest peaks on the frequency spectrum plot. Exciting this resonant frequency allows us to focus on the effect that the different control techniques that are considered in this study have on the steady state 10.5 Hz response amplitude. It should be noted, that the unsprung body resonance can create a resonance peak in the sprung body as well, and vice versa.

3.5 Solution Method

The choice of the solution method and sample rate, shown in Table 3.5, were determined by the need for convergence of the solution and to fix the number of solution points for the root mean square (RMS) and power spectral density (PSD) calculations. To achieve convergence, the solution rate was increased by 50%, for the Skyhook case of G = 8000, until the peak-to-peak jerk changed by less than 1%. In fact, changing the solution from 2000 Hz to 3000 Hz changed the unsprung peak-to-peak jerk from 1437.853 m/s^3 to 1443.834 m/s^3. The difference between these two jerk measures is 0.416%. The fixed step method was chosen over the variable step method in order that the number of sample

points for each simulation remain the same. Maintaining the number of sample points is important for comparing various cases because the RMS, equation (3.3), and the PSD, equation (3.14), are functions of the number of sample points.

Table 3.5 Solver Parameters.

SOLUTION METHOD	fixed-step Dormand-Prince
SAMPLE RATE	
a. Frequency Response	1000 *Hz*
b. Step Response	1600 *Hz*
c. Sine Response	3000 *Hz*
TIMESPAN	
a. Frequency Response	64 sec
b. Step Response	15 sec
c. Sine Response	15 sec

The RMS function is defined by,

$$RMS = \sqrt{\frac{\left(x_1^2 + x_2^2 + ... + x_n^2\right)}{n}} \tag{3.13}$$

where,

$x_i = i^{th}$ value in the series

$n =$ number of samples in solution

The power spectral density of acceleration was calculated as,

$$a_{PSD} = \left(\frac{2\left|FFT(a(t)_{chirp})\right|}{n} \right)^2 \tag{3.14}$$

3.6.0 Model Verification

To gain some confidence in the accuracy of the SIMULINK model, a number of steps were taken to verify the model used in this study. The verification was done in several steps. First, the passive SIMULINK lumped-parameter model was verified by comparing its results with the lumped parameter state-space equations. Second, the semiactive damper model was verified by running a test signal through it and analyzing the output. Third, the semiactive controller models were verified by inspection and observing their output in the simulations. Lastly, several numerical simulations are compared to experimental results obtained from an actual test rig. Each of these verification steps are explained next.

3.6.1 Lumped-Parameter Model Verification

To check the SIMULINK model, the state-space equations for a passively damped single suspension model were derived and simulated to produce a frequency spectrum. The state-space results were then compared to the results given by the SIMULINK model, Figure 3.20. These two methods of deriving the frequency response produce the same results and indicate that the SIMULINK model is correct.

The state-space equations are,

$$\begin{bmatrix} \frac{dy_1}{dt} \\ \frac{dy_2}{dt} \\ \frac{d^2y_1}{dt^2} \\ \frac{d^2y_2}{dt^2} \end{bmatrix} = \begin{bmatrix} 0 & 0 & 1 & 0 \\ 0 & 0 & 0 & 1 \\ -K_1/m_1 & K_1/m_1 & -C/m_1 & C/m_1 \\ K_1/m_2 & -(K_1+K_2)/m_2 & C/m_2 & -C/m_2 \end{bmatrix} \begin{bmatrix} y_1 \\ y_2 \\ \frac{dy_1}{dt} \\ \frac{dy_2}{dt} \end{bmatrix} + \begin{bmatrix} 0 \\ 0 \\ 0 \\ K_2/m_2 \end{bmatrix} y_g \qquad (3.15)$$

The parameters in equation (3.15) are defined in Table 3.1.

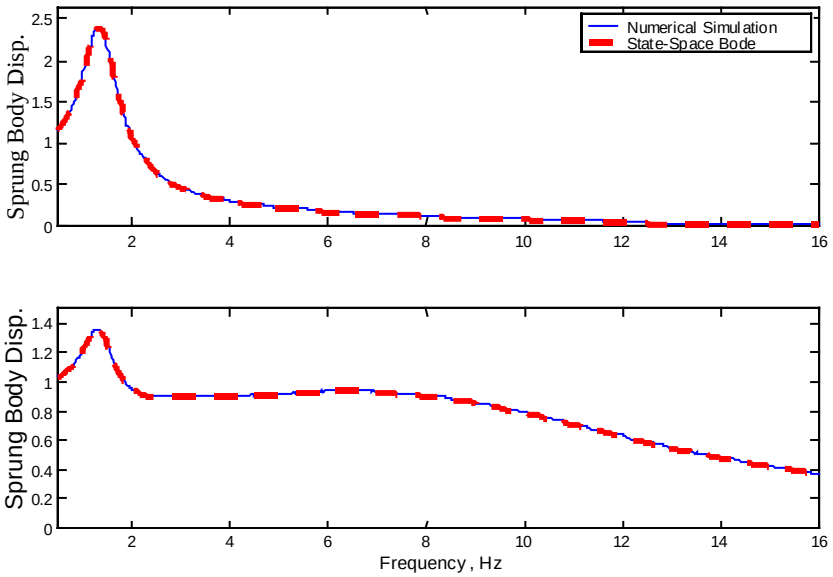

Figure 3.20 Comparison of Numerical Simulation to State-Space Bode Plot. $\zeta = 0.40$.

The frequency spectrum and state-space equations can be further verified by checking the sprung and unsprung natural frequencies with approximations. The sprung body natural frequency can be approximated by assuming that the unsprung body has zero mass (it is light compared to the sprung mass), which also means that the two springs of Figure 2.1 Are now connected in series. The equivalent stiffness for these springs is determined by,

$$\frac{1}{K_{eq1}} = \frac{1}{K_1} + \frac{1}{K_2} \tag{3.16}$$

Using the values in Table 3.1 results in an equivalent stiffness of,

$$K_{eq1} = 3.2060 \times 10^4 \, N/m$$

The expression for the sprung body natural frequency is,

$$w_n = \frac{1}{2\pi}\sqrt{\frac{K_{eq1}}{m_1}} \tag{3.17}$$

Using the values that are listed in Table 3.1 for the parameters of equation (3.7) gives,

$$w_n = \frac{1}{2\pi}\sqrt{\frac{3.060\times10^4\, N/m}{453.6kg}}$$

$$w_n = 1.338\,\text{Hz}$$

The actual pole of the state-space equations with the unsprung mass included is 1.335 Hz, for a damping coefficient of 0.

The error in the approximation due to uncoupling the masses is,

$$e_1 = \frac{1.338Hz - 1.335Hz}{1.335Hz}$$

$$e_1 = 0.22\%$$

This low error indicates that we have formulated the state-space equation correctly.

We can use a similar procedure as above to find the unsprung natural frequency, except this time we will assume that the sprung body is fixed since it is much heavier than the unsprung mass. This fixed displacement approximation means that the springs connected to the unsprung mass are connected in parallel. The equation for the equivalent stiffness is,

$$K_{eq2} = K_1 + K_2 \tag{3.19}$$

$$K_{eq2} = 4.0288\times10^4\, N/m + 1.57\times10^5\, N/m$$

$$K_{eq2} = 1.97288 \times 10^5 \, N/m$$

The expression for the unsprung natural frequency is,

$$w_{n2} = \frac{1}{2\pi}\sqrt{\frac{K_{eq2}}{m_2}} \tag{3.20}$$

$$w_{n2} = \frac{1}{2\pi}\sqrt{\frac{1.97288 \times 10^5 \, N/m}{45.4kg}}$$

$$w_{n2} = 10.49Hz$$

The unsprung body pole, calculated using Matlab, of the undamped state-space equation is 10.52 Hz. The error created by assuming that the sprung body is fixed is,

$$e_2 = \frac{10.49Hz - 10.52Hz}{10.52Hz}$$

The error is,

$$e_2 = -.29\%$$

This low error also indicates that the state-space equations were formulated correctly.

3.6.2 Semiactive Damper Model Verification

The semiactive damper model was verified at both a constant –0.5 m/s and 0.5 m/s by running a desired force sinusoid test input of amplitude 50,000 N at 1 Hz through the semiactive damper model. The output was then compared to the expected output, based on examining Figure 2.2. We expect, for a damper velocity of –0.5 m/s, that the maximum damper force would be limited at 42,500 N. This force is expected since the expected maximum force is,

$$F_{\max} = C_{on} v_{12}$$

$$F_{\max} = (85{,}000 \text{ N/m/s})(\text{-}0.5 \text{ m/s})$$

$$F_{\max} = 42{,}500 \text{ N}$$

Examining Figure 3.1 shows that this is indeed the maximum actual damper force. The minimum force and the positive damper velocity case are verified in a similar way.

It is worth noting that when a positive damper force is desired and the damper velocity is negative, the actual damper force is calculated to be negative. The reason the force is negative is that the damper is semiactive and not active; we can only vary the damping coefficient. The sign of the relative velocity across the damper determines the damper force direction.

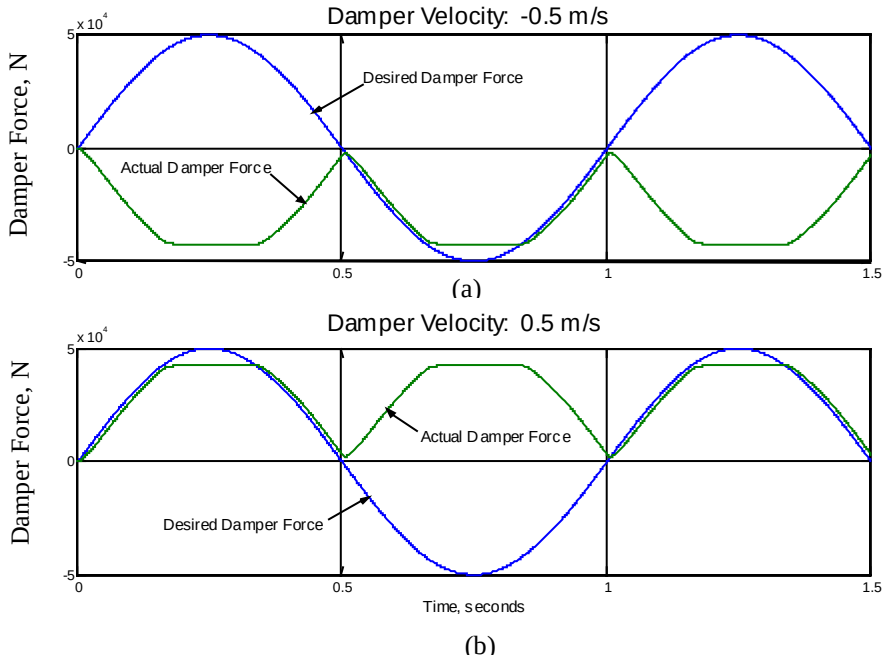

Figure 3.21 Semiactive Damper Model Test Results for a 1 Hz Sinusoid Input; (a) Damper Force for a Negative Damper Velocity; (b) Damper Force for a Positive Damper Velocity.

When the desired force test input frequency is increased to 10.5 Hz, the filter delays the damper force output by approximately 10 msec, as shown in Figure 3.22. Additionally,

the minimum damper force increases. Given this test frequency input condition, the damper force delay causes the damper to not keep up with the desired input as much as it did for the 1Hz case.

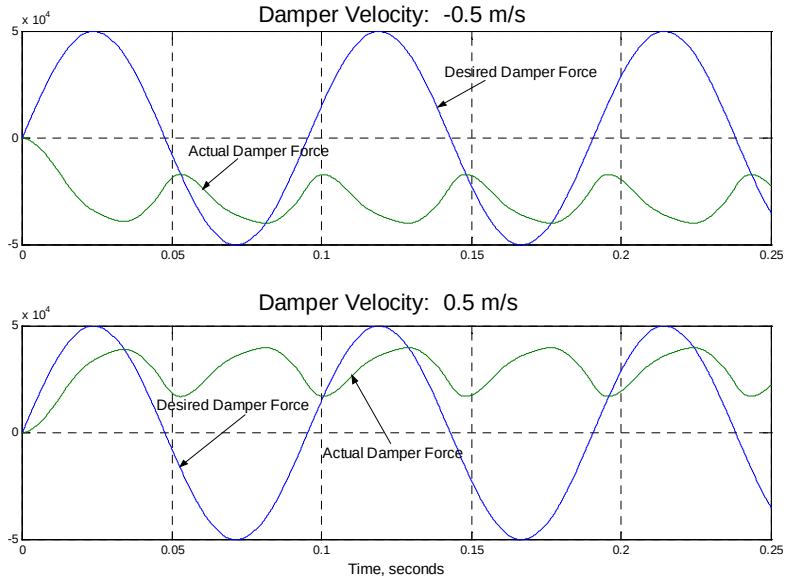

Figure 3.22 Semiactive Damper Model Test Results for a 10.5 Hz Sinusoid Input; (a) Damper Force for a Negative Damper Velocity; (b) Damper Force for a Positive Damper Velocity.

3.6.3 Semiactive Control Law Verification

We can now proceed to discuss the verification of the semiactive control laws. This verification was done mainly by careful review of the SIMULINK semiactive control diagrams as well as by inspection of the results. First, the SIMULINK models are direct implementations of the semiactive control law formulas. The SIMULINK models can be compared to their mathematical equations almost as if they were mathematical expressions themselves. Second, we can examine a time response to a 1.34 Hz sinusoidal input. Based on our understanding of how these semiactive laws should work, we can make a judgment as to whether they have been implemented correctly.

As an example, we can look at the Skyhook response to a 1.34 Hz sinusoid base excitation, as shown in Figure 3.23. We can see that when the sprung body velocity turns

positive, while the relative velocity is negative, that the desired damper force turns off. In addition, the desired damper force is a multiple (by 4000) of the sprung body velocity. This is the expected behavior of Skyhook based on equation (3.8).

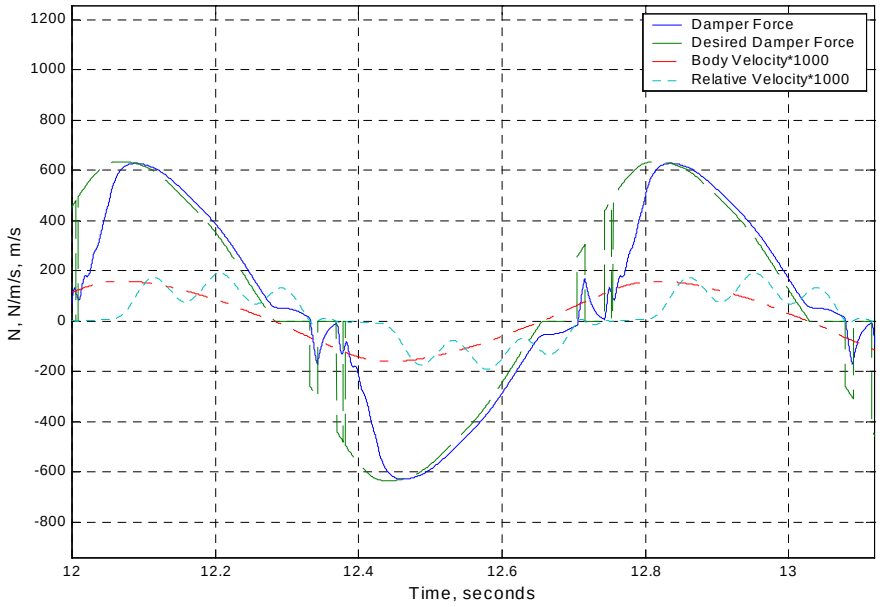

Figure 3.23 Time Response of the Skyhook Damper Force for G = 4000.

3.6.4 Comparison of Numerical Simulations to Experimental Results

As a last verification, comparing the numerical SIMULINK results with a set of experimental results checked the appropriateness of the semiactive single-suspension model. Figure 3.24 shows a damper force/velocity trajectory from a single suspension (quarter car) rig at the Advanced Vehicle Dynamics Laboratory (AVDL) of Virginia Tech, while Figure 3.25 shows a similar plot from the numerical simulation. The overall character of Figures 3.24 and 3.25 are similar. For example, in both figures, as the gain is increased, the trajectories tend to use greater maximum damping forces and lower maximum velocities. In addition, both of the figures have the same general shapes. In other words, as the gain is increased the trajectory shapes change from a low, wide rectangle to a tall, narrow rectangle. Also, an S-like curve appears on the outside of the trajectories in both figures. It appears that there are enough similarities between the numerical and experimental results to warrant using this model, at least at 1.34Hz.

There are a number of differences between Figure 3.4 And Figure 3.5. The main difference is that much larger gains are required in the numerical simulations for similar damper force/velocity trajectories. Since the numerical model was verified in several ways already, a large amount of attention was not given to determining the cause for this difference. However, it should be noted that this numerical model is relatively simple and does not take into account any non-ideal behavior that probably exists with the experimental rig.

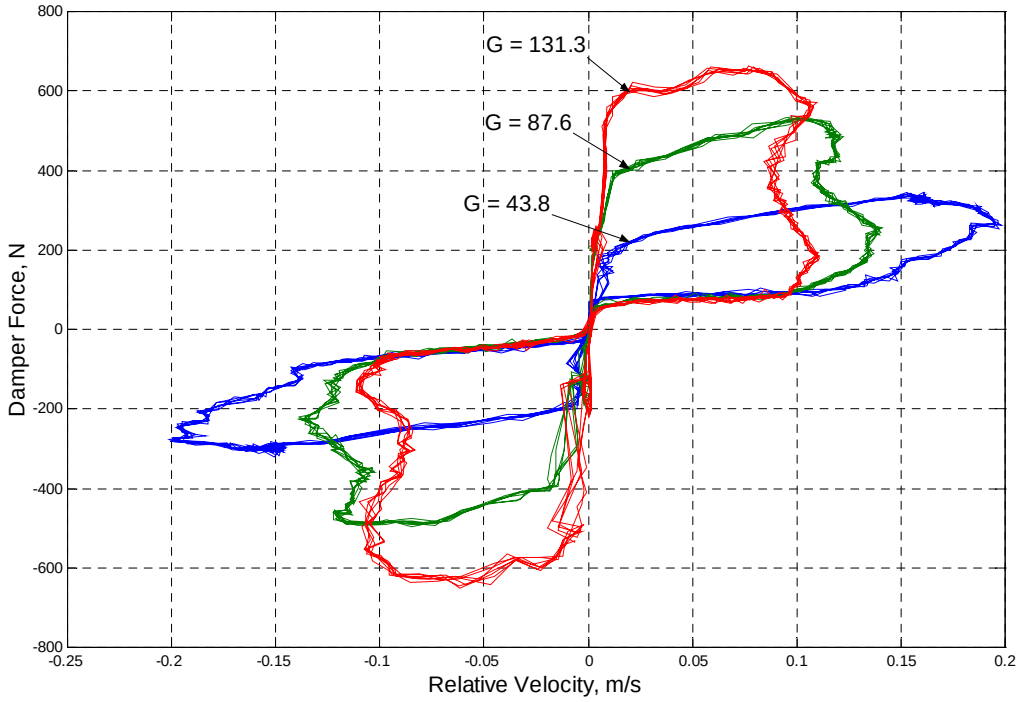

Figure 3.24 Experimental Damper Force/Velocity for Skyhook Control and a Pure Tone Base Excitation at 1.5Hz. (G is the Skyhook gain in N/m/s) (adopted from [12], where units are English)

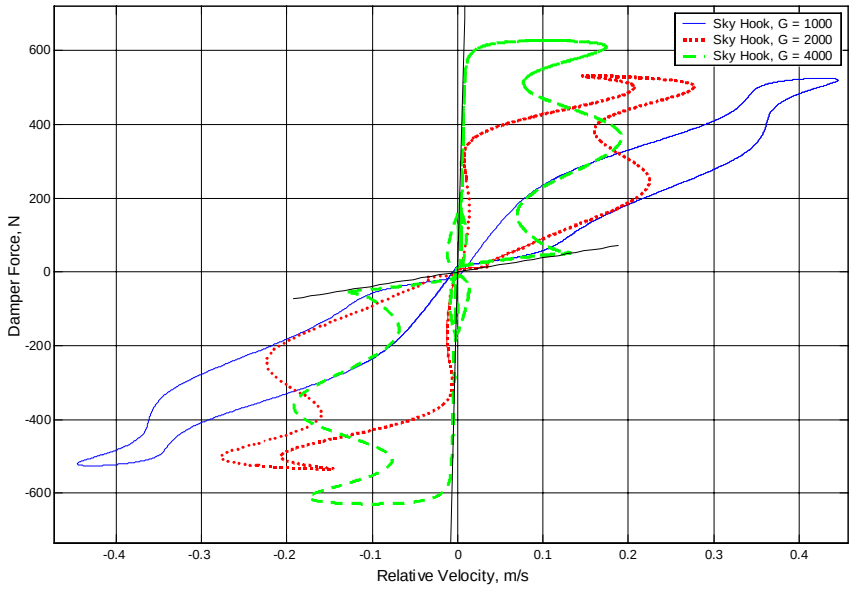

Figure 3.25 Numerical Simulation Damper Force/Velocity Plot for Skyhook and a 1.34 Hz Pure Tone Base Excitation. (G is the Skyhook gain in N/m/s)

3.7 Model Summary

This chapter presented the mathematical and numerical models that were used for this study. The suspension model is a lumped parameter model, the passive damper is the standard linear viscous model, the semiactive MR damper is a bounded linear model, and the controllers are direct implementations of their defining equations. In addition, this model was verified by using several checks. The numerical model was verified by comparing its output to the output of a state-space model for the passive case. In addition, the damper model was verified separately by running test inputs through it and checking that the output was correct. The controllers were checked by inspecting the SIMULINK block functions and checking the time response of the damper force, which are all shown in the results section. The model was also shown to be reasonable by comparing the Skyhook response damper force/velocity trajectory, at the sprung body natural frequency, of the numerical model with the equivalent experimental trajectory.

The model presented in this chapter will be used to generate the results shown in the following chapters. Chapter 4 starts the results analysis by analyzing the passive results. Chapter 5 not only analyzes previously stated control methods, but also evaluates two alternative control laws as well. The last section in Chapter 5 compares the performances of all the control laws.

Chapter 4
Passive Results

This chapter presents the base excitation responses of a passively controlled single suspension model (quarter car) to the various test inputs used in this study. The responses studied here are the frequency spectrum, the system response to a step input, the 1.34 Hz time traces, and the 10.5 Hz time traces. These responses are used in vehicle dynamics studies to assess the relative performance, interpreted in terms of ride comfort and vehicle handling, of different suspension control methods. In Chapter 5, these passive results will be compared to the semiactive damper results.

4.1 Transmissibility Analysis

The transmissibility responses are used to gain insight into the quarter car response under conditions of a road input. We will assume that a road input is a spectrum of various frequencies and therefor the transmissibility response can serve as a partial test for determining the road worthiness of a suspension. We will concentrate this analysis in the frequency range of 0 Hz to 16 Hz since this range includes the two system resonant peaks. The transmissibility response, Figure 4.1, shows that as the damping increases, the sprung and unsprung resonant peaks decrease. This means that for the sprung and unsprung resonant frequencies, the ride comfort should improve by increasing the damping since the sprung mass will oscillate at a lower amplitude. In addition, we might increase the handling ability since the unsprung mass oscillates less creating a more consistent contact with the road. However, the sprung mass transmissibility slightly increases between the sprung and unsprung resonant frequencies. We would expect that this increase would detract from the ride comfort as the sprung mass would oscillate at a greater amplitude at these frequencies. Ahmadian discusses this loss of isolation in detail in [1]. In addition, the familiar invariant points exist which occur, for this case, at approximately 1.5 Hz for the sprung mass and at 4 Hz for the tire. At the invariant points, all of the damping ratios generate the same transmissibility. Overall, we find that

increasing the damping creates a tradeoff situation between reducing the sprung and unsprung mass resonance peaks and increasing the transmissibility at frequencies in between these resonant peaks.

The suspension rattle, in Figure 4.2, shows a similar trend as does the transmissibility plot, Figure 4.1, at the sprung and unsprung resonant frequencies. As damping increases, the sprung and unsprung mass suspension rattle decreases, although isolation it not reduced in between the sprung and unsprung mass resonant frequencies. An invariant point exists as well and means that at approximately 2 Hz, for the sprung mass, changing damping does not affect the suspension rattle response. Overall, except at the invariant point, increasing damping decreases the suspension rattle. As noted in [14], the suspension rattle space is an indicator of how likely it is for the suspension to bottom out.

Increasing damping creates a trade off with the acceleration performance, see Figure 4.3. The trade off exists between reducing the acceleration at the sprung and unsprung resonant frequencies and slightly increasing the acceleration in between the sprung and unsprung resonant frequencies as the damping increases. We would expect that increasing damping would benefit ride comfort at the sprung and unsprung mass frequencies and detract from it in between these frequencies.

It appears that, just by increasing the damping, we could increase ride comfort and handling, as judged by reducing the transmissibility and acceleration, assuming that the sprung and unsprung frequencies are the key frequencies to control. This is only true for a pure tone input, which induces steady-state system response. For a step input, which is a non-stationary (transient) input, different results are observed, as will be discussed next.

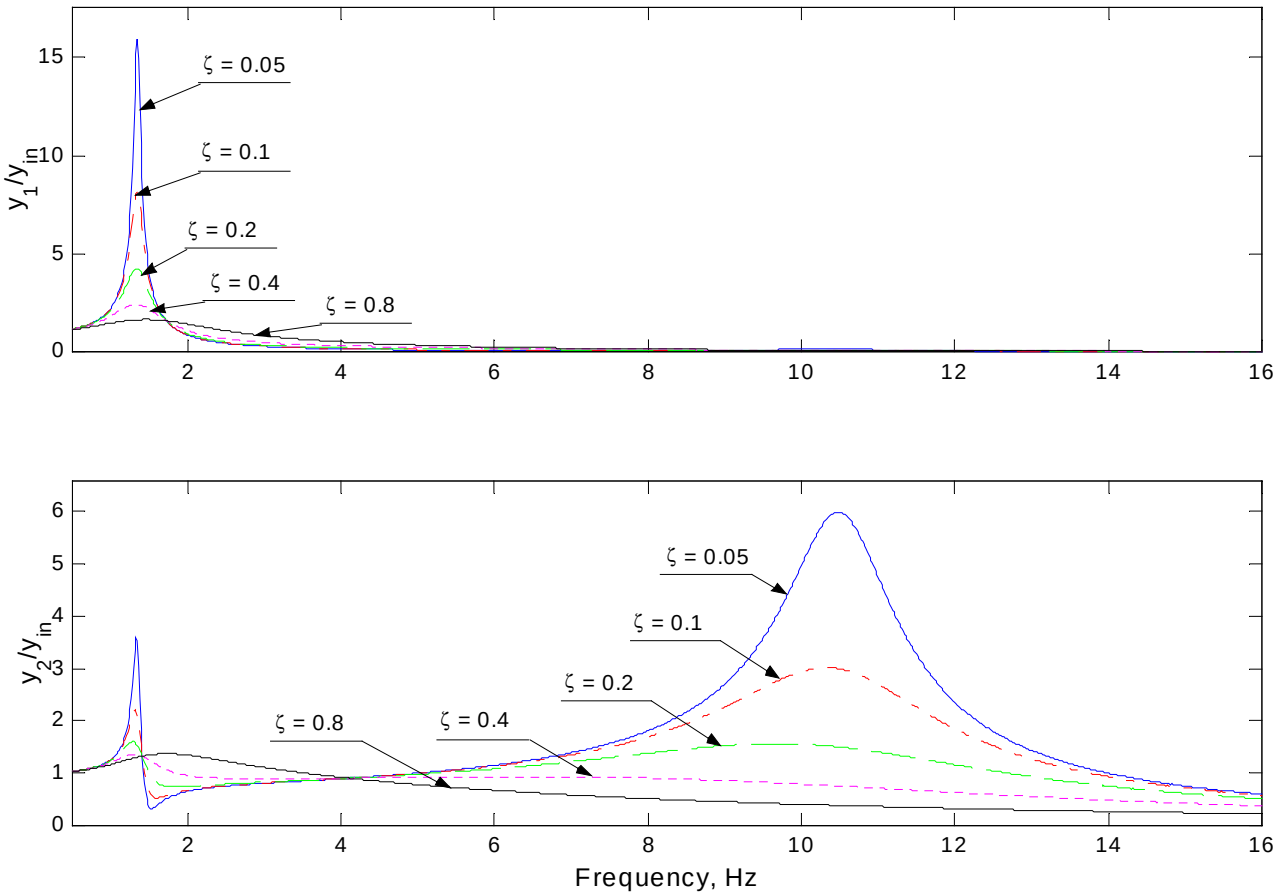

Figure 4.1 Transmissibility Plots of a Single Suspension under Passive Control. (y_1 : sprung mass displacement, y_2 : unsprung mass displacement, y_{in} : base displacement)

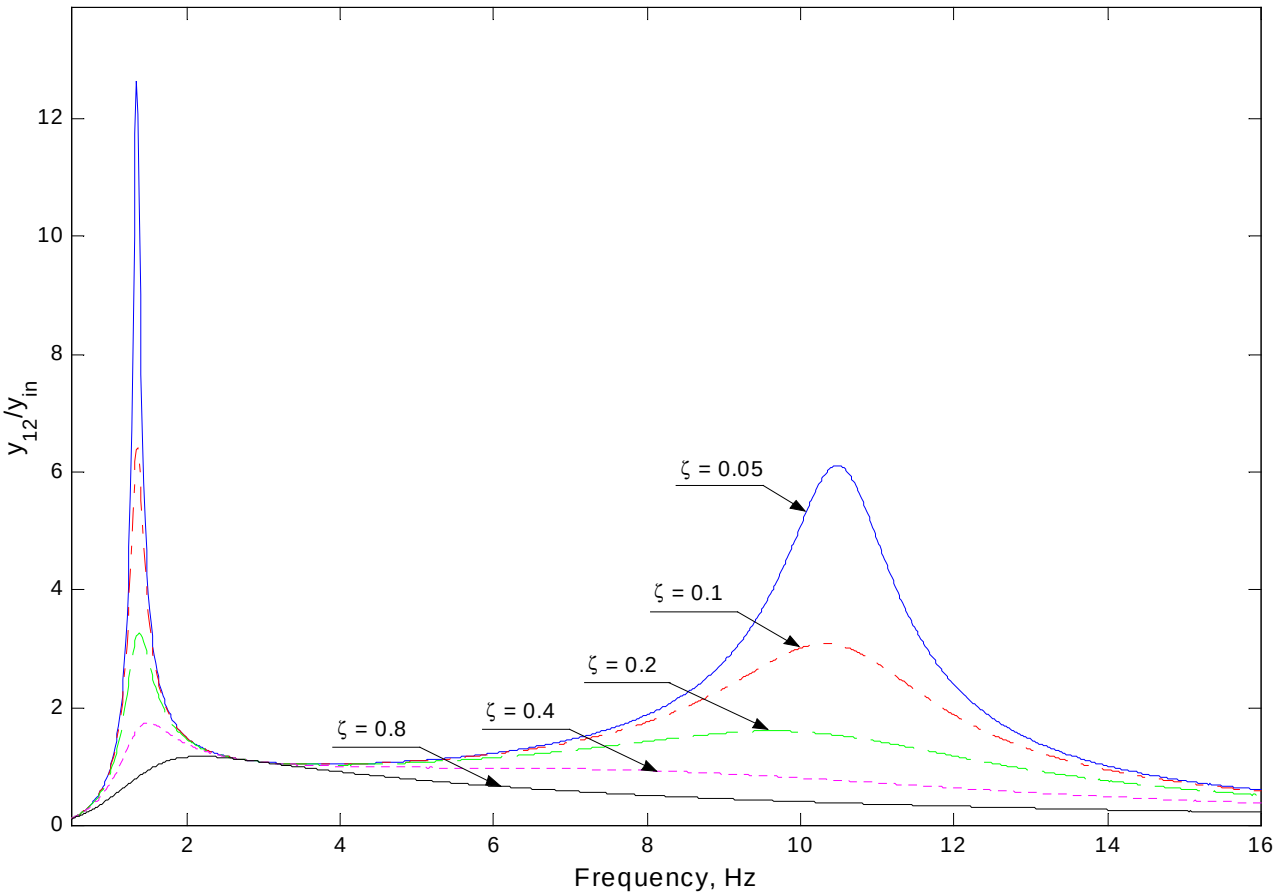

Figure 4.2 Relative Transmissibility of a Single Suspension under Passive Control.

(y_{12} : relative displacement, y_{in} : base displacement)

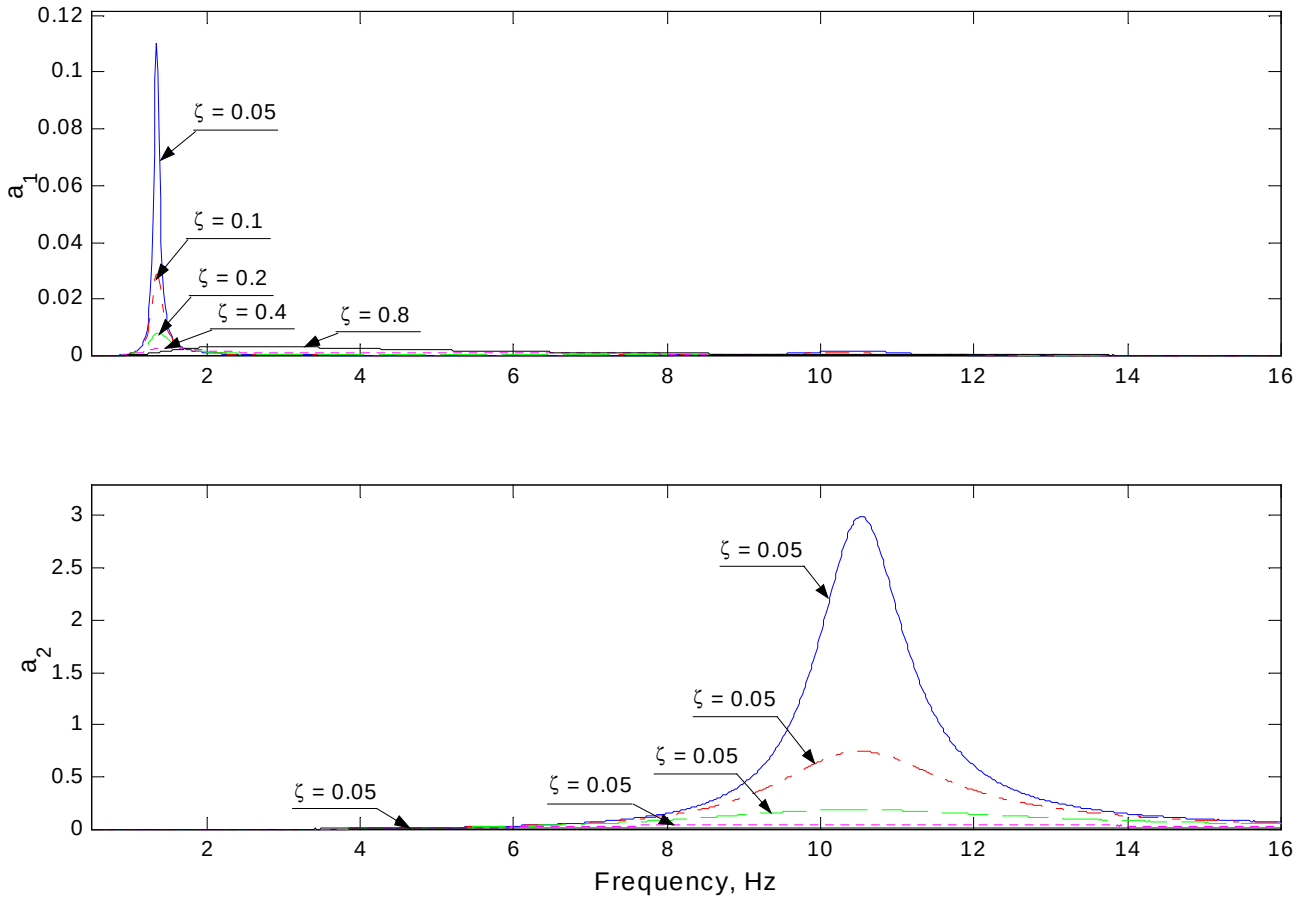

Figure 4.3 Acceleration Power Density Spectrum of a Single Suspension under Passive Control. (a_1: sprung mass acceleration power density, a_2: unsprung mass acceleration power density)

4.2 Transient Response

The step response is important for gaining insight into the behavior of a vehicle since the step input excites the transients of the system. We would like to minimize the sprung mass settling time, displacement, acceleration, and jerk in order to improve ride comfort. A reduction in the unsprung mass settling time and displacement would also improve handling. As will be discussed next, passive suspensions commonly offer a compromise among these measures [14].

A convenient method of presenting the performance measures as a function of the damping ratio is shown in Figure 4.4. The derivation of a sample point from Figure 4-4 is shown in Figure 4.5. The peak-to-peak measure is simply the distance between the maximum value, 2.7 m/s^2, and the minimum value, -0.6 m/s^2, and is 3.3 m/s^2. The rest of the points in Figure 4.5 were calculated in the same way using the appropriate time series results.

For transient dynamics, larger damping ratios result in excessive transmission of the base inputs to the sprung body, causing a harsh and uncomfortable ride. Figure 4.4, shows a fairly complete picture of the trade offs involved in maximizing the ride comfort and handling. As damping increases from 5% to 80 %, the sprung mass peak-to-peak acceleration and jerk increase from 2.7 m/s^2 up to 4.2 m/s^2 and from 120 m/s^3 up to 639.8 m/s^3 respectively. These increases detract from the ride quality. As damping is increased from 5% to 80%, however, settling time decreases from 14.6 seconds down to 0.75 seconds. In addition, the sprung mass peak-to-peak displacement decreases from 0.0224 m to 0.006 m and the unsprung mass displacement decreases from 0.014 m to 0.003 m. The decrease in the settling time and sprung mass displacement should benefit ride quality while the decrease in unsprung mass displacement should improve handling. The trade off evident in this plot, as damping increases, occurs between the sprung mass acceleration and jerk verses the sprung mass settling time and displacement as well as the unsprung mass displacement. Damping cannot simply be increased without bound in an

attempt to improve ride comfort and handling. Excessive amount of damping locks out the suspension and negates its benefits.

In order to better understand the operation of a passive damper and gain an insight into the performance measures discussed above we evaluate figure 4.6. Figure 4.6 shows the superposition of the step response damper force, damper velocity (relative velocity), and the sprung mass velocity. The results are exactly what one would expect from a linear viscous damper. The damper force is just a multiple of the relative velocity. This multiplication relationship follows directly from the linear nature of the ideal passive damper; that is, the damper force is equal to the damping coefficient multiplied by the relative velocity. The end effect of having the damper force tied directly to the damper velocity is that we get a large damper force when the relative velocity is large. A sudden large damper force, such as from a step input, will cause a large sprung mass acceleration and jerk, Figure 4.7, at the beginning of the step response. This relationship will change for systems with semiactive dampers.

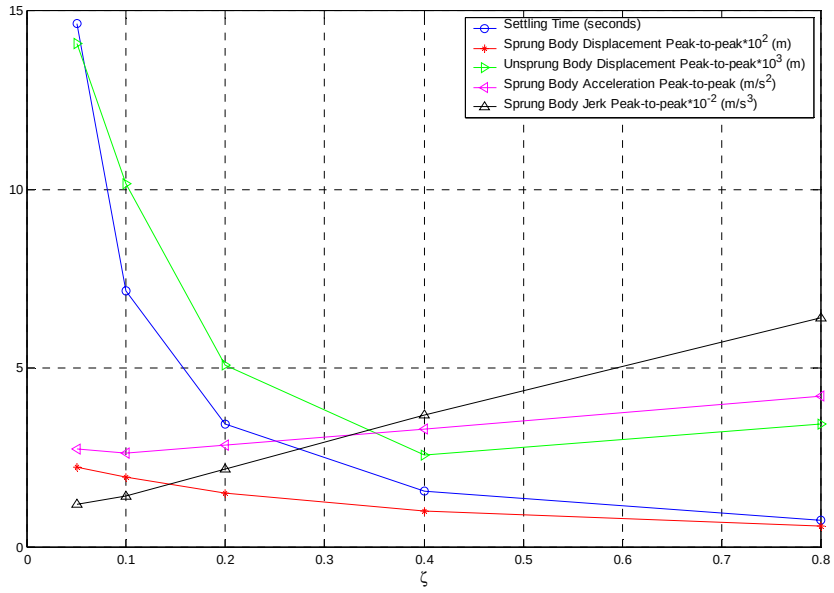

Figure 4.4 Effect of Varying ζ on the Peak-to-peak Step Response Performance Measures for a Single Suspension under Passive Control.

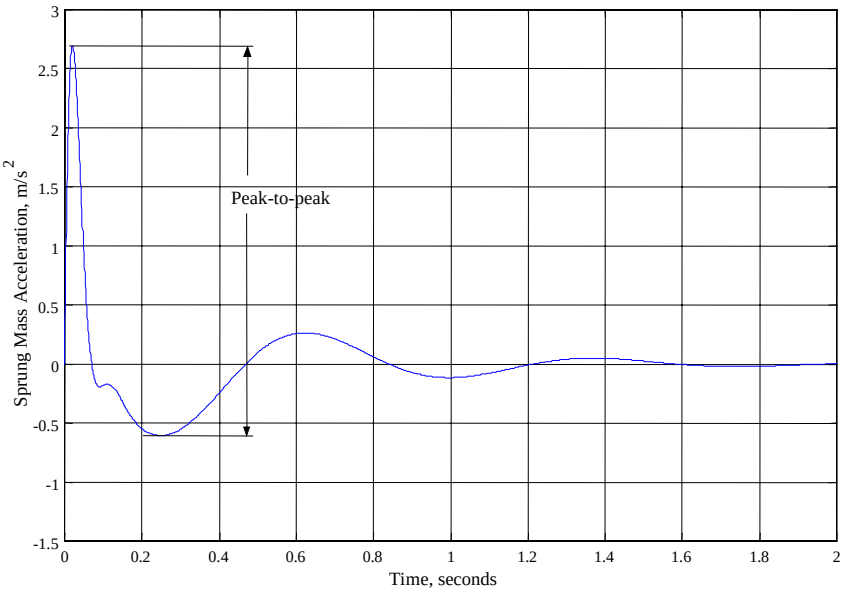

Figure 4.5 Example of the Determination of the Step Response Peak-to-peak Measure for $\zeta = 0.4$ for a Single Suspension under Passive Control.

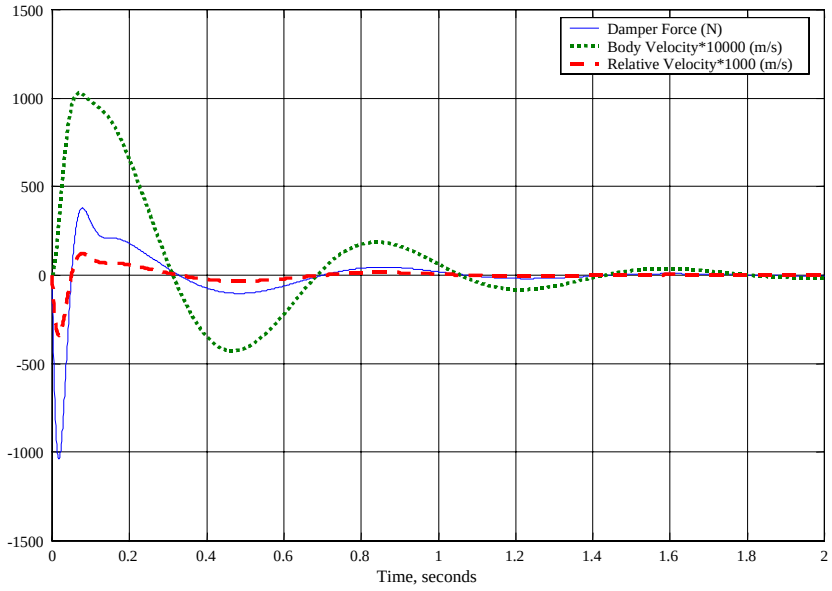

Figure 4.6 Step Response of a Single Suspension under Passive Control for $\zeta = 0.4$.

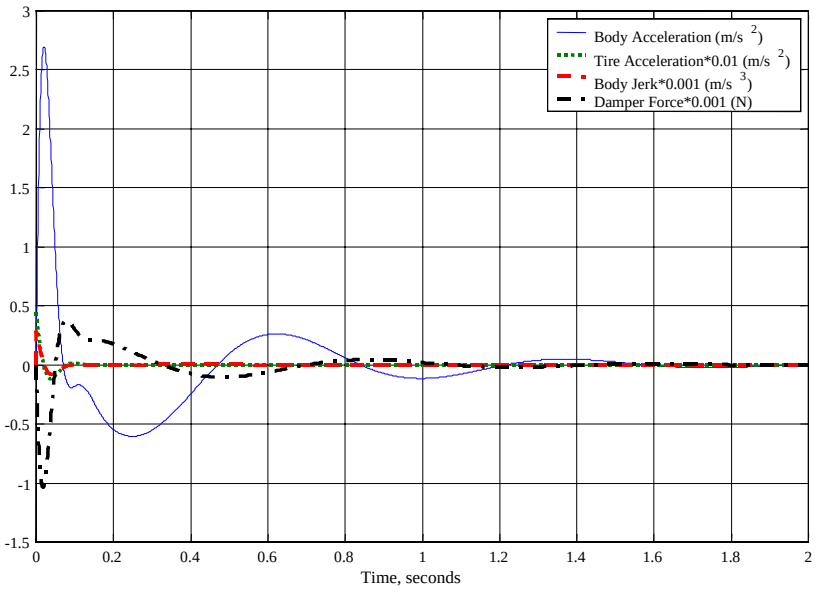

Figure 4.7 Step Response of a Single Suspension under Passive Control for $\zeta = 0.4$.

4.3 Steady State Response Analysis

Pure tone (i.e., single frequency inputs) inputs can be used to study a single aspect of a dynamic system, such as the system response at the sprung and unsprung body natural frequencies. In this section, we will excite the single suspension system with two pure tone frequencies that represent the sprung body (1.34 Hz) and unsprung body (10.5 Hz) resonant frequencies. We will analyze the time domain response in a manner similar to those presented earlier for the step input. This section analyses the sprung mass and unsprung mass peak-to-peak and RMS frequency responses at 1.34 Hz and 10.5 Hz. These two resonant frequencies are focused on in this section since they result in the largest undamped oscillations and their control is critical in determining whether or not the ride will be acceptable. The information for the frequencies in between the two resonant frequencies were discussed earlier in the transmissibility plots, Figures 4.1, 2, and 3.

4.3.1 1.34 Hz Sinusoidal Response

The critical performance measures are shown together as a function of the damping in Figure 4.8. Figure 4.9 is an example of how the peak-to-peak measure is calculated. The peak-to-peak measure, in this case, is the distance between the maximum of the response, 0.2 m, and the minimum of the response, -0.2 m,; in other words, twice the amplitude, 0.4 m. Overall, each measure is improved by increasing the damping and will benefit both the ride quality as well as the handling.

The peak-to-peak performance improvements show a diminishing return as damping increases from 5% to 80%, indicated Figure 4.8. The sprung and unsprung mass displacements are reduced from 0.4 m to 0.042 m and 0.086 m to 0.033 m, respectively. The sprung mass acceleration and jerk are reduced, respectively, from 28.0 m/s^2 to 3.00 m/s^2 and from 235 m/s^3 to 24.8 m/s^3. The sprung mass frequency response is only one performance measure and must be balanced with the step response and transmissibility responses, as well in order to find a suitable damping ratio.

As indicated in figure 4.10, the RMS performance measures show a similar response to increasing damping from 5% to 80% as does the peak-to-peak measures, see Figure 4.10. The sprung and unsprung mass RMS displacements are reduced from 0.145 m to 0.015 m and from 0.031 m to 0.011 m, respectively. The sprung mass acceleration and jerk are reduced, respectively, from 10.3 m/s^2 to 1.03 m/s^2 and from 82.1 m/s^3 to 8.87 m/s^3. Again, this response must be balanced with the step response and the transmissibility response when determining a suitable damping ratio.

We can start to understand the operation of the damper and its effect on the bodies by looking at a co-plot of the damper force, sprung mass velocity, and the unsprung mass velocity, Figure 4.11. Again, we see that the damper force is a multiple of the relative velocity and is not directly related to the sprung mass velocity. This relationship is brought out here as a first step in comparing the passive responses with the semiactive responses in Chapter 5. The acceleration of the sprung mass is caused only by the force that is applied to it by both the suspension spring and the damper. Figure 4.12 contains a

co-plot of the damper force and sprung mass acceleration and jerk. It is important to note here that the passive damper control results in a smooth response since both the passive model is linear and the input is smooth. Later, we will find out that the response with the semiactive damper is not so smooth due to the time-invariant, bounded behavior such dampers.

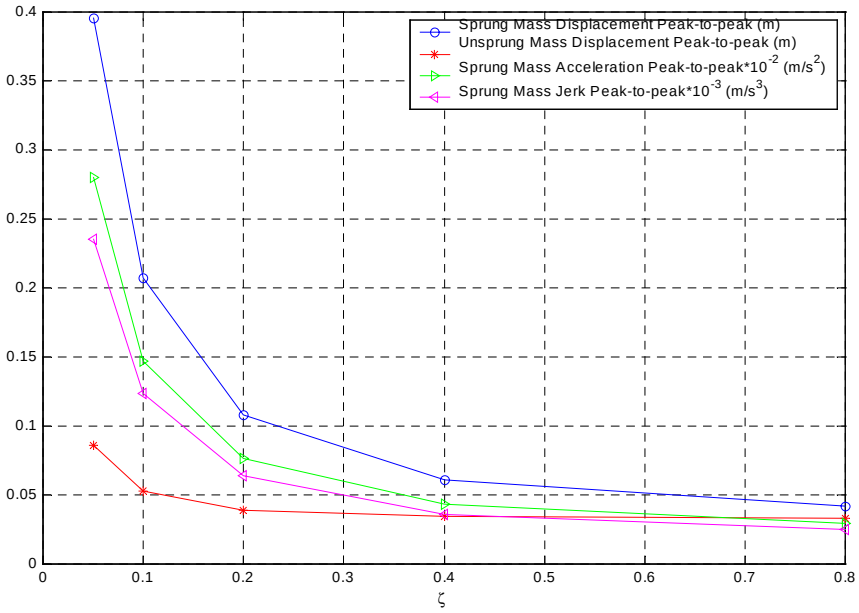

Figure 4.8 Effect of Varying ζ on the Peak-to-peak Steady State Response Performance Measures for a Single Suspension under Passive Control. (1.34 Hz Sinusoidal Input)

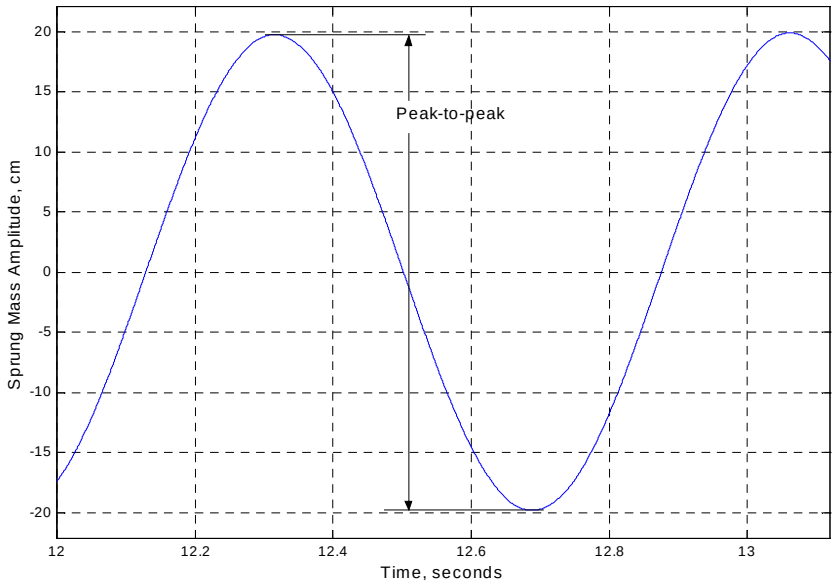

Figure 4.9 Example of the Determination of the Peak-to-peak measures for a 1.34 Hz Sinusoidal Response of a Single Suspension under Passive Control.

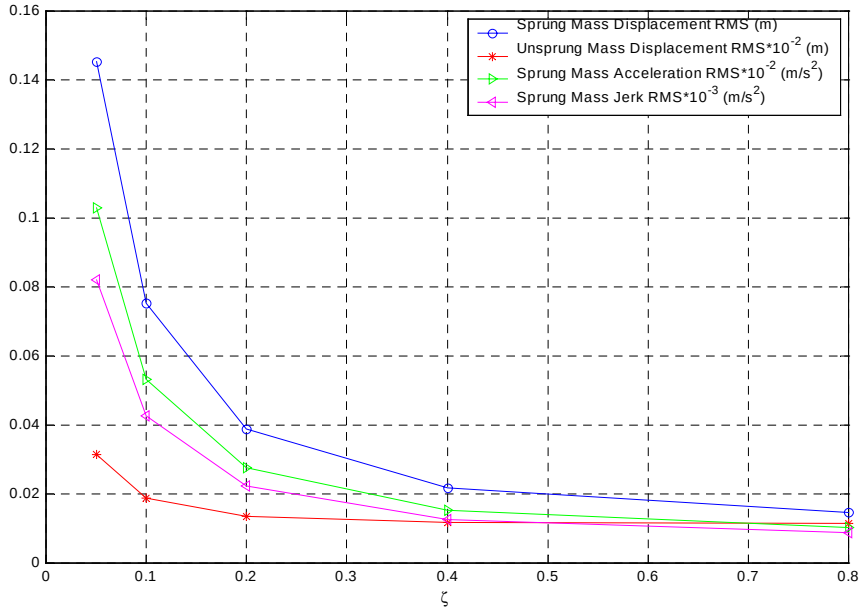

Figure 4.10 Effect of Varying ζ on the RMS Steady State Response Performance Measures for a Single Suspension under Passive Control. (1.34 Hz Sinusoidal Input)

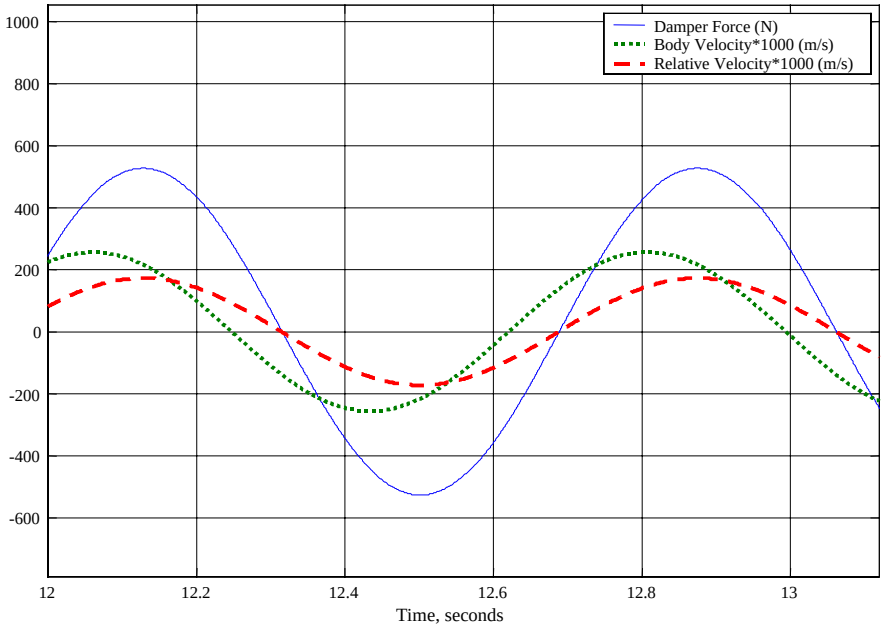

Figure 4.11 1.34 Hz Steady State Response of a Single Suspension under Passive Control for $\zeta = 0.4$.

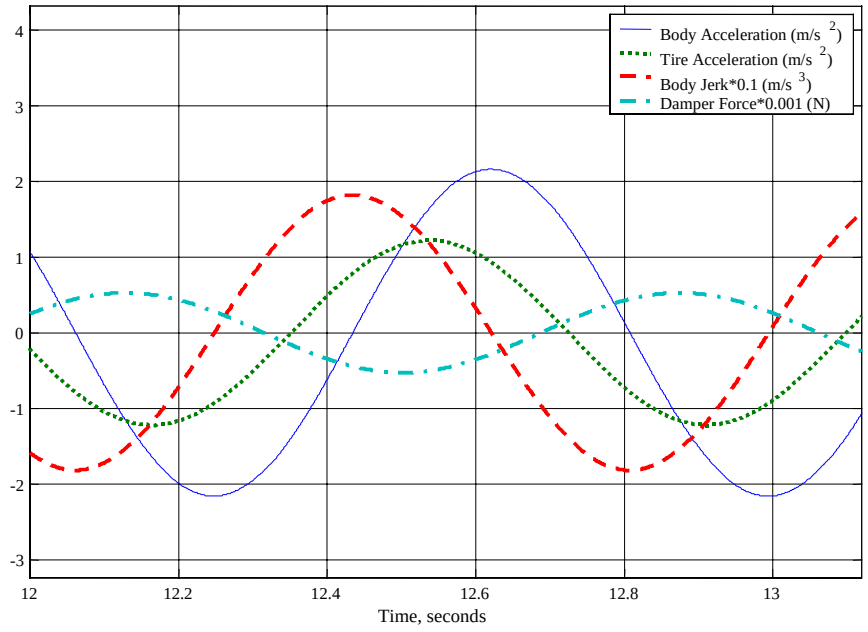

Figure 4.12 1.34 Hz Steady State Response of a Single Suspension under Passive Control for $\zeta = 0.4$.

4.3.2 10.5Hz Sine Response

If we excite the base of the single suspension model at the unsprung resonant frequency of 10.5 Hz, the unsprung mass will resonate as expected and the body response is relatively muted. This characteristic response is different than when we excite the base at the sprung mass resonant frequency, in which case the unsprung mass is affected by suspension forces caused by the resonance of the sprung mass, as was shown earlier in Figure 4.1.

Figure 4.13 conveniently summarizes the sprung and unsprung mass peak-to-peak performance measures. As with the 1.34 Hz steady state response, increasing the damping improves the performance, for increasing damping from 5% to 80%. As the damping is increased, the sprung and unsprung mass displacement decreases from 0.0038 m to 0.002 m. The sprung mass acceleration and jerk decreases from 16.3 m/s^2 down to 8.67 m/s^2 and from 1072 m/s^3 down to 572 m/s^3, respectively. The reduction of the displacement, acceleration, and jerk indicates that the ride quality and handling improve as the damping is increased.

The RMS measures are similarly improved by an increase in the damping, see Figure 4.14. Increasing damping over the same range as before reduces the sprung and unsprung mass RMS displacements from 0.0013 m to 0.0009 m, respectively. The sprung mass RMS acceleration and jerk decrease from 5.75 m/s^2 down to 3.06 m/s^2 and from 379 m/s^3 down to 202 m/s^3, respectively. Vehicle comfort and handling should improve at 10.5 Hz by increasing damping.

We can analyze a single time trace, such as shown in Figure 4.15, to give us a comparison basis for analyzing the semiactive results in Chapter 5. As expected, the damper force is a multiple of the relative velocity just as it was for the 1.34 Hz case. For the 10.5 Hz base excitation, however, the damper force is nearly in phase with the sprung mass acceleration, as indicated by Figure 4.16. Finally, as with the 1.34 Hz response, the last important thing to notice here is the smooth linear response.

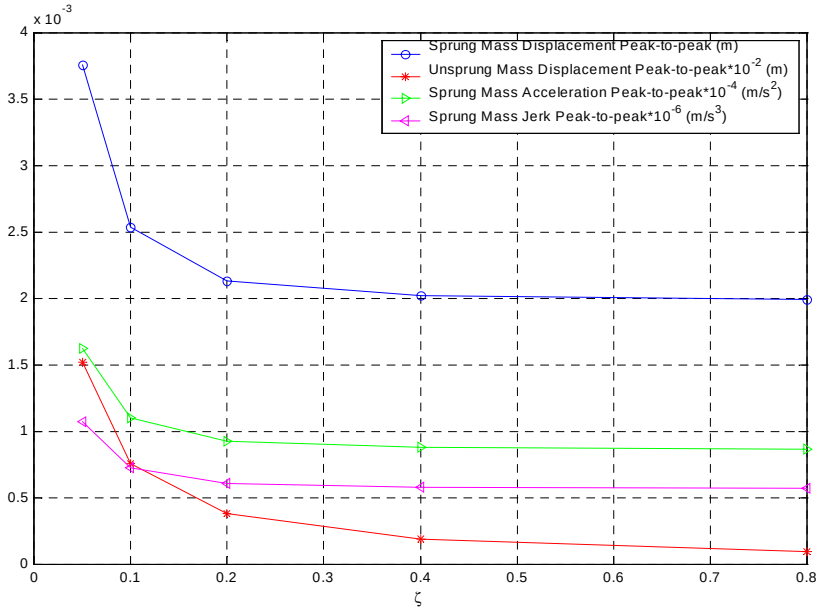

Figure 4.13 Effect of Varying ζ on the Peak-to-peak Steady State Response Performance Measures for a Quarter Car under Passive Control.
(10.5 Hz Sinusoidal Input)

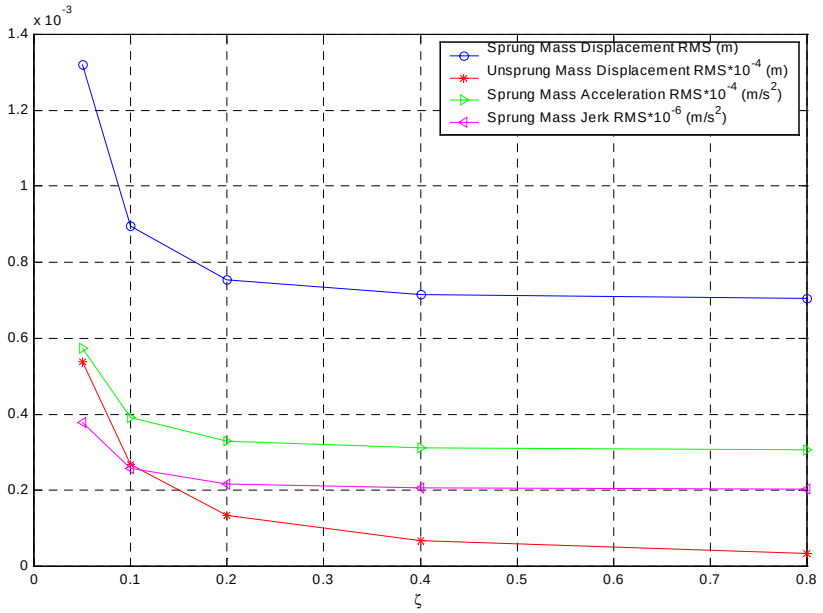

Figure 4.14 Effect of Varying ζ on the RMS Steady State Response Performance Measures for a Quarter Car under Passive Control.
(10.5 Hz Sinusoidal Input)

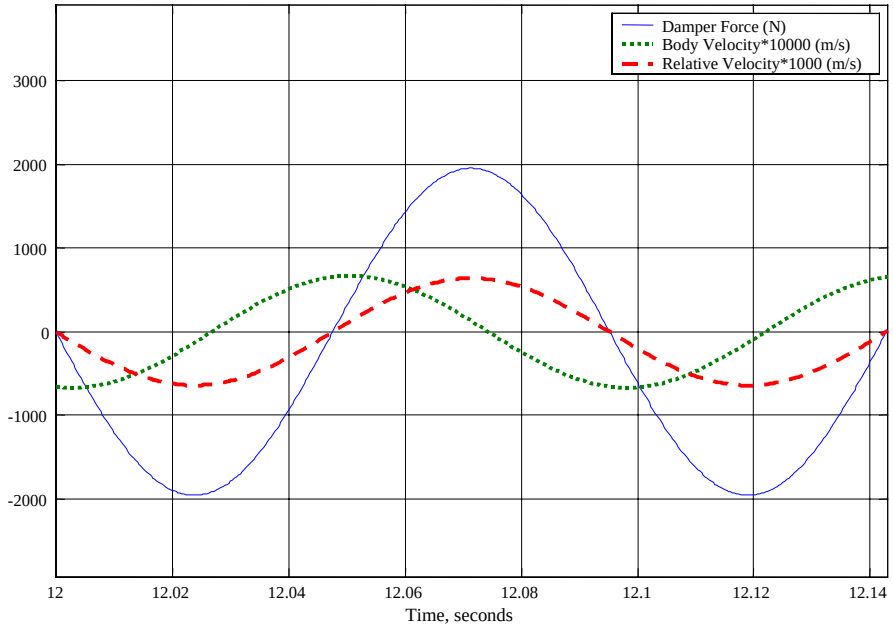

Figure 4.15 10.5 Hz Steady State Response of Quarter Car under Passive Control for $\zeta = 0.4$.

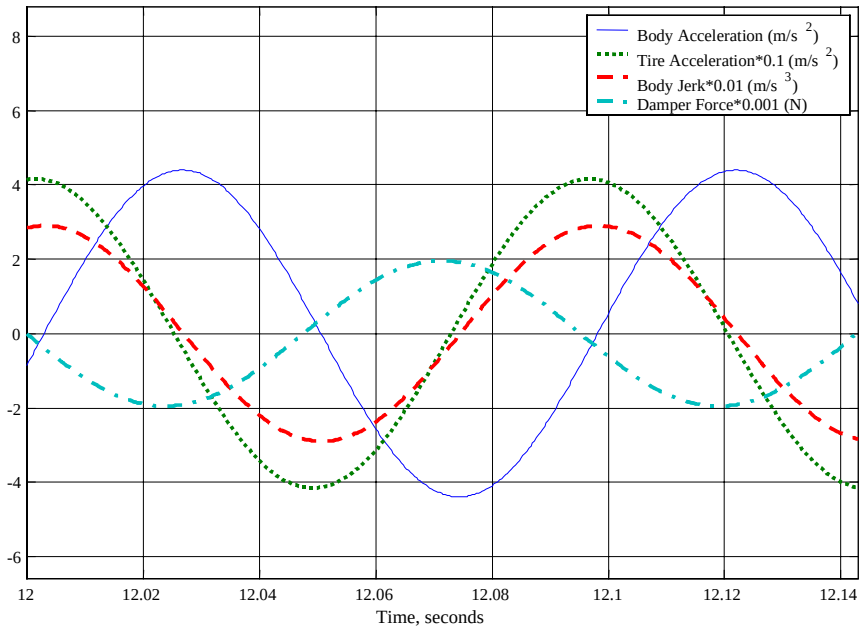

Figure 4.16 10.5Hz Steady State Response of Quarter Car under Passive Control for $\zeta = 0.4$.

4.4 Passive Results Summary

Overall, considering all of the test responses presented for the passive case, increasing damping creates two trade offs. First, increasing damping reduces the sprung and unsprung body resonance peaks but slightly increases the transmissibility at frequencies in between the resonant peaks, as shown in Figure 4.1. Similar results were shown for a single-degree of freedom system model in [1]. Second, as damping increases, the step response acceleration and jerk increase, while the settling time and sprung and unsprung mass peak-to-peak displacements decrease, which will be discussed next, are more involved.

Chapter 5
Semiactive Results

This chapter presents the simulated base excitation responses of a single suspension model under various forms of semiactive control when subjected to various test inputs. Just as was done in Chapter 4 for passive damping, the responses studied here are the frequency spectrum, the system response to a step input, the 1.34 Hz time traces, and the 10.5Hz time traces.

5.1 Skyhook Control Results

The results of the Skyhook study presented next merely confirm the understanding of Skyhook that already exists. These results are used to confirm that the model is implemented correctly, and to compare with alternative semiactive control laws that are proposed here. First, the results show that the Skyhook controller will lower the sprung body natural frequency transmissibility, while not affecting the unsprung mass natural frequency transmissibility, [9]. Next, it will be shown that the peak-to-peak sprung body acceleration response to a step input is relatively insensitive to the gain. Finally, this section will focus on the 1.34 Hz and 10.5 Hz sinusoidal responses, which take a closer look at the trends that are seen in transmissibility section.

5.1.1 Transmissibility Analysis

The Skyhook semiactive control law influences the sprung and unsprung mass 1.34 Hz response much more than the 10.5 Hz response, when compared to the passive transmissibility results. The Skyhook transmissibility plot, Figure 5.1-1, indicates that increasing the gain *G* decreases the sprung and unsprung body 1.34 Hz resonant peaks, but has no effect on the 10.5 Hz resonant frequency transmissibility. At 10.5 Hz, the choice of gain does not matter since the controller determines that the control force should be zero and hence we find the minimal damping at this frequency. In contrast, at

the sprung body resonant frequency of 1.34 Hz, increasing the Skyhook gain not only reduces the transmissibility but eventually causes the transmissibility to be less than one. Unlike the passive response, Skyhook control preserves the isolation at frequencies in between the resonant peaks. This phenomenon is discussed in detail by Ahmadian in [1]. Overall, we would expect, based on the transmissibility plots, that increasing the gain *G* would most significantly improve ride comfort and handling at the sprung body resonant frequency of 1.34 Hz, and have a minimal effect at the unsprung body resonant frequency of 10.5 Hz.

We can now analyze the relative transmissibility in Figure 5.1-2. Here we see that the rattle space decreases as the gain is increased. This decrease is very similar to the decrease that occurs as passive damping was increased in Figure 4.2. In a similar manner to the transmissibility plots in Figure 5.1-1, the rattle space is not reduced at 10.5 Hz, because Skyhook control does not attempt to reduce (or affect) the suspension rattle by modulating damping.

The acceleration power spectral density in Figure 5.1-3 follows similar trends with increasing *G* as does the transmissibility and rattle space discussed above. At 1.34 Hz, increasing the gain decreases the sprung mass resonant peak [9], but has a negligible effect on the 10.5 Hz response. These results suggest that increasing the Skyhook gain *G* will most significantly improve the ride comfort at 1.34 Hz.

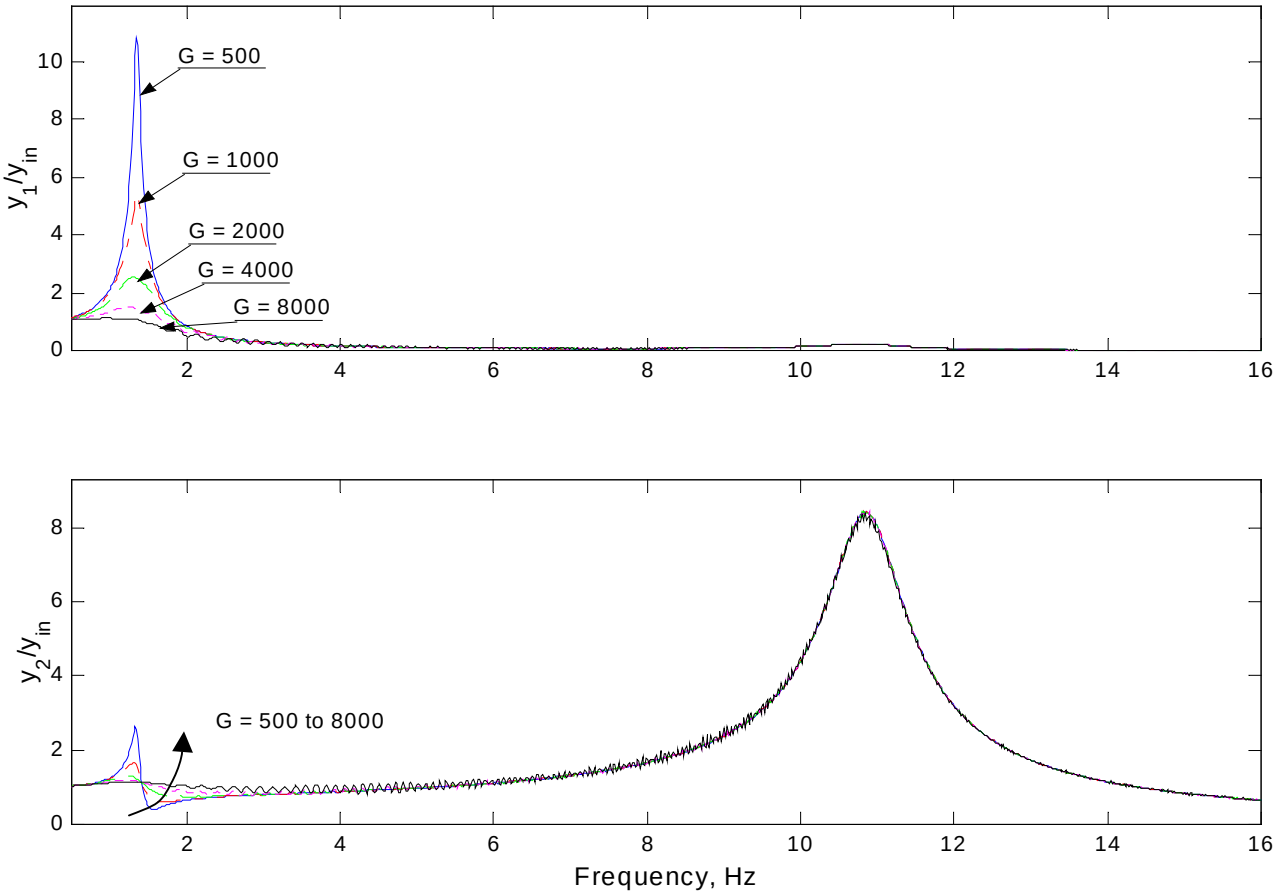

Figure 5.1-1 Transmissibility Plots of a Single Suspension under Skyhook Control. (y_1 : sprung mass displacement, y_2 : unsprung mass displacement, y_{in} : base displacement)

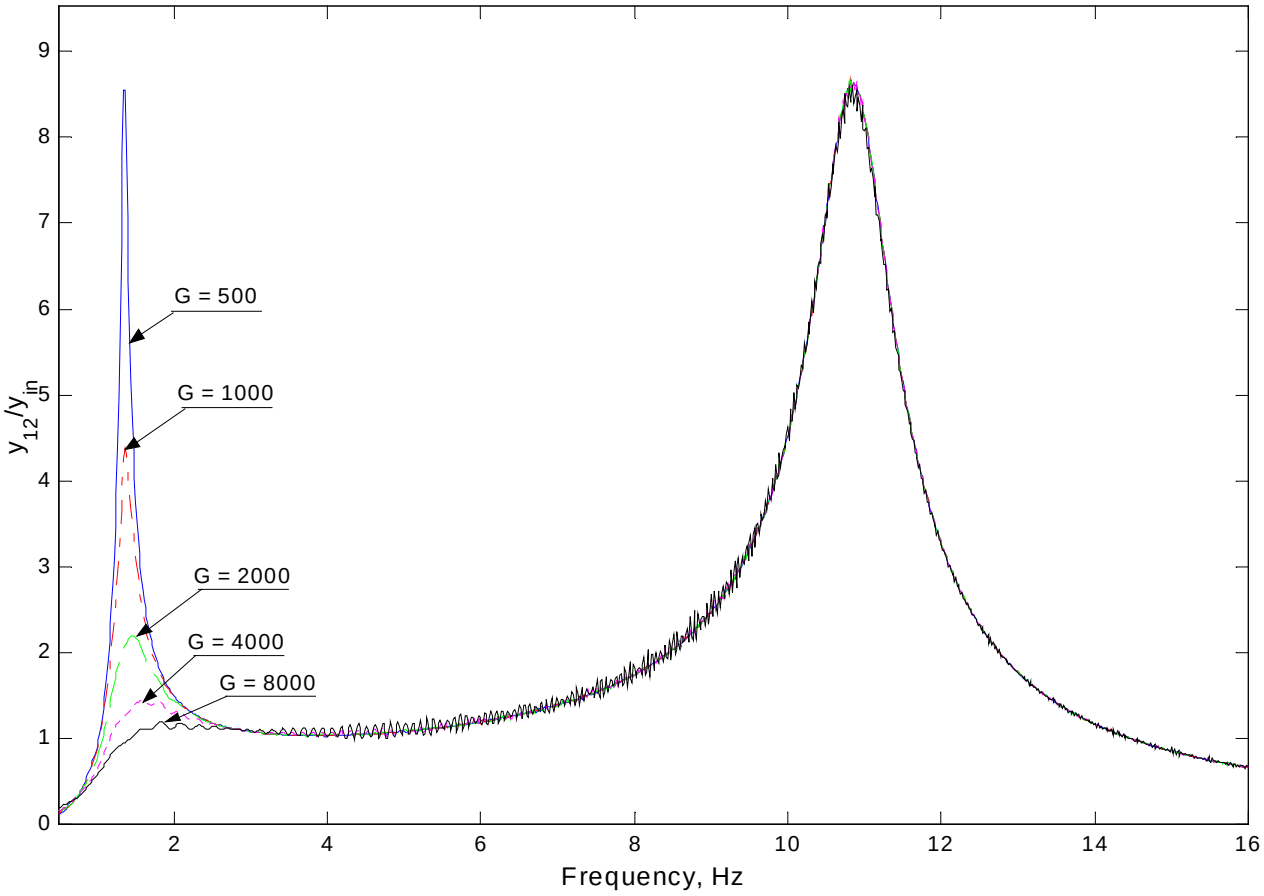

Figure 5.1-2 Relative Transmissibility of a Single Suspension under Skyhook Control.

(y_{12} : relative displacement, y_{in} : base displacement)

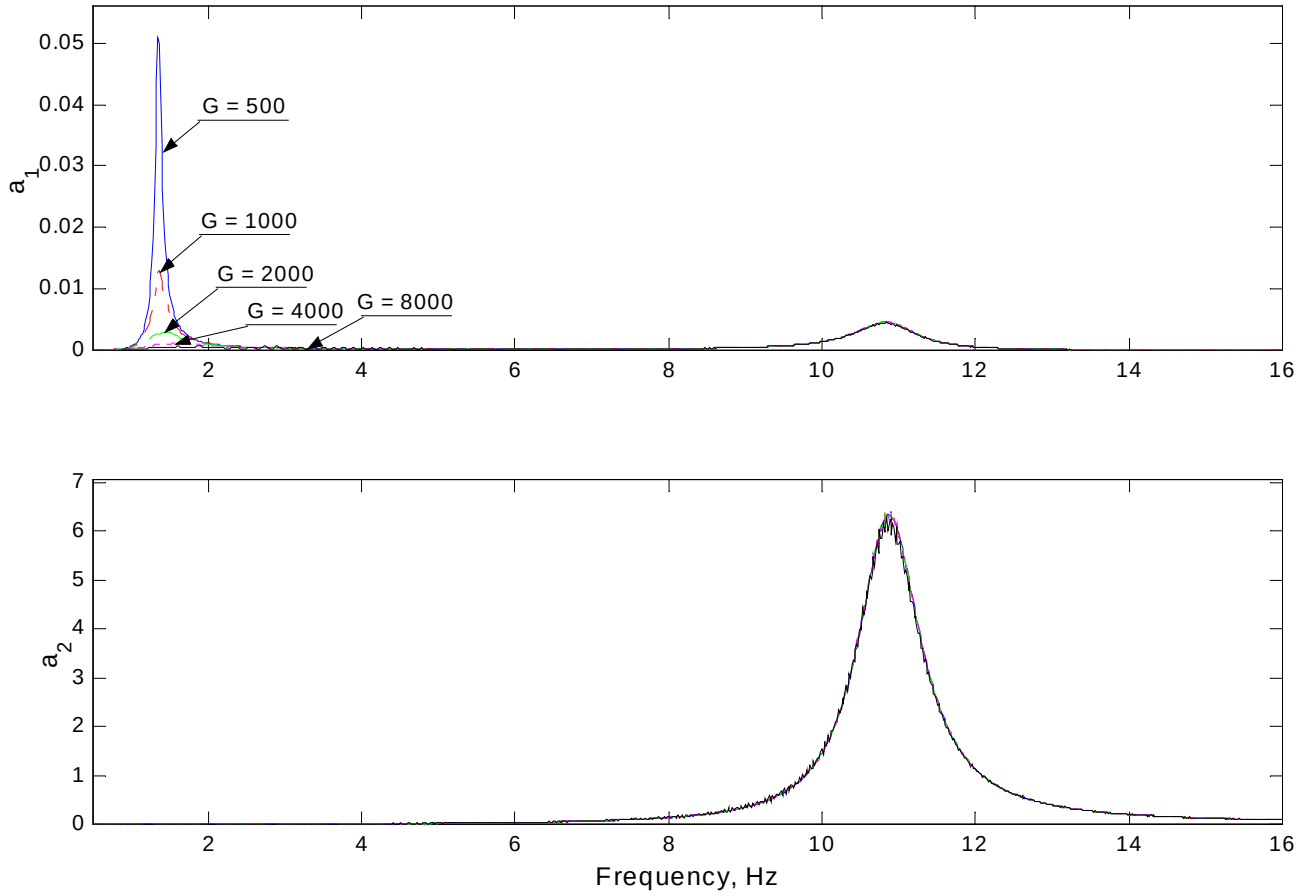

Figure 5.1-3 Acceleration Power Density Spectrum of a Single Suspension under Skyhook Control. (a_1: sprung mass acceleration power density, a_2: unsprung mass acceleration power density)

5.1.2 Transient Analysis

The tradeoffs involved in maximizing the Skyhook single suspension response performance to a step input can be seen in Figure 5.1-4. The transient response trade off that occurs as *G* changes from 500 N/m/s to 8000 N/m/s is between increasing the peak-to-peak jerk and decreasing the settling time, sprung and unsprung mass peak-to-peak displacements, and the sprung mass peak-to-peak acceleration. Over this gain range, the settling time reduces from 9 seconds to 0.623 seconds. The sprung and unsprung mass displacements decrease from 0.022 m to 0.001 m and from 0.015 m down to 0.012 m, respectively. In addition, the peak-to-peak acceleration is reduced from 3.13 m/s^2 to 2.73 m/s^2. The peak-to-peak jerk, however, increases from 146 m/s^3 to 230 m/s^3. Since we are assuming that jerk negatively impacts ride comfort, then an upper limit for jerk provides a practical limit on how much we should increase *G* in order to improve the other performance measures.

One advantage to using Skyhook control over passive dampers is the relative insensitivity of the sprung mass acceleration step response to the control gain, *G*, Figure 5.1-4. The Skyhook gain to acceleration relationship is more favorable for the ride performance than for passive dampers, as indicated by Figure 4.4. The explanation for this relative insensitivity to changes in gain is that the switch turns the damper off for the first 0.05 seconds of the solution and prevents the damper from transmitting the impact of the step to the body, as shown in Figure 5.1-5. The desired damper force is determined by the controller alone and, along with the current physical constraints, determines the actual damper force. With the damper off, the impact force is mainly transmitted by the spring, which has a constant spring constant. This means that, when the damper turns off, the choice of gain hardly matters since the impact force transmitted to the sprung body is primarily transmitted by the spring, which is not semiactive.

One might ask how well semiactive dampers can apply the desired force. We can see from Figure 5.1-5 that the damper force is approximately equal to the desired damper force when the damper is supposed to be on. However, there is a minimum damping coefficient and therefor we cannot get a zero damper force when the damper is moving.

This situation occurs during the first 0.05 seconds of the solution where the desired damper force is zero. Unfortunately, the zero damper force cannot be realized and we find that the actual damper force reaches a maximum magnitude of about 200 N.
One effect of the semiactive control law switch that should not be ignored is that the semiactive damper can create a large jerk when the switch turns the damper on or off. Jerk, for semiactive control Figure 5.1-6, can loosely be compared with that for passive dampers, Figure 4.7. We will find throughout the rest of this thesis that a characteristic feature of semiactive dampers is the spikes in sprung mass jerk response. One can refer to the Background Section in Chapter 2 for a brief review of past studies that have investigated this phenomenon.

The damper force/velocity characteristic gives a clear picture of defining the input/output relationship for the damper. Figure 4.7 contains four such plots; one each for the gains of 1000, 2000, 4000, and 8000. The filter that was used to converge the jerk calculation in Chapter 3 now introduces some interesting behavior, namely a hysteresis effect. In a close inspection, we find that, at times, we have positive damper forces when the damper velocity is negative. Figure 5.1-5, however, puts this inconsistency in perspective, by showing that it does not appear to be more than a minor logical inconvenience required to obtain a converged jerk solution that has some meaning.

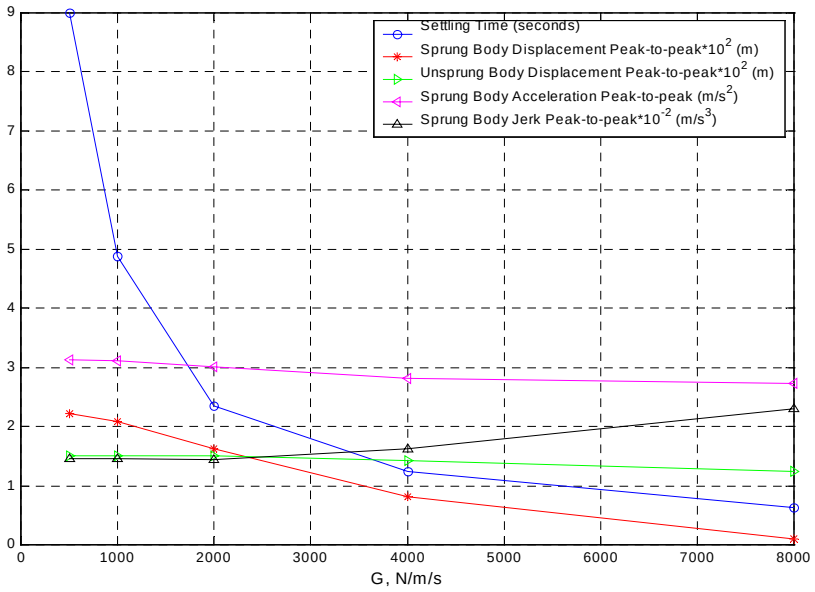

Figure 5.1-4 Effect of Varying *G* on the Peak-to-peak Step Response Performance Measures for a Single Suspension under Skyhook Control.

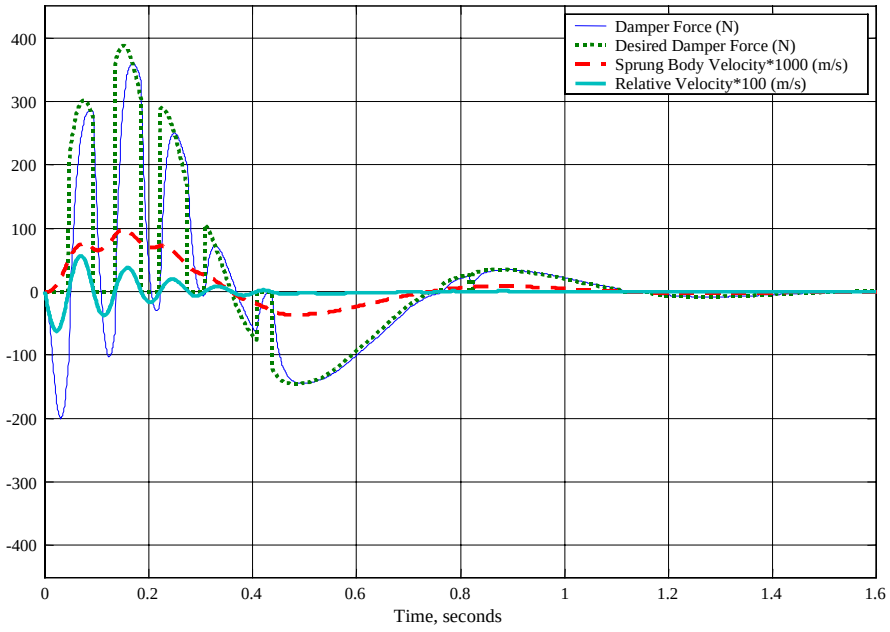

Figure 5.1-5 Step Response of a Single Suspension under Skyhook Control for *G* = 4000.

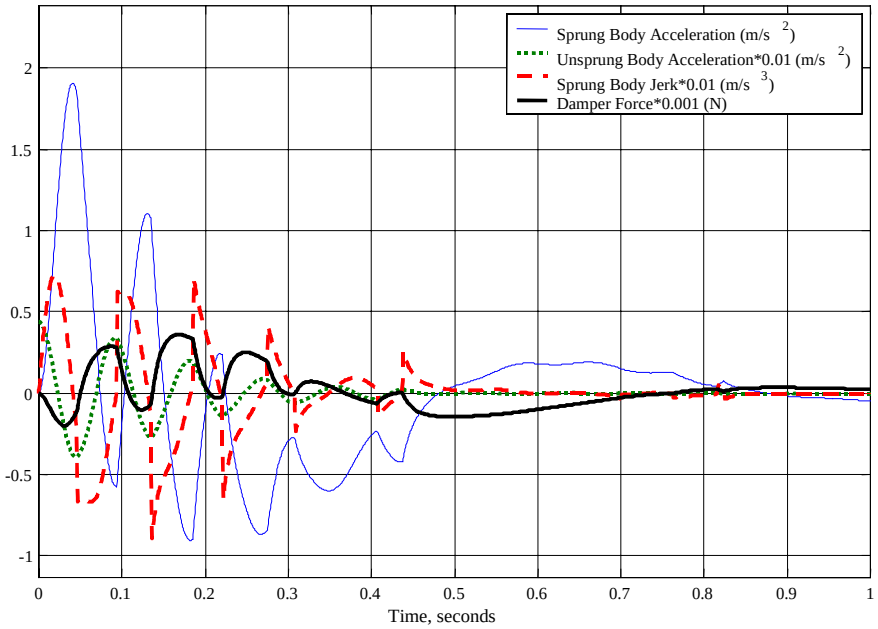

Figure 5.1-6 Step Response of a Single Suspension under Skyhook Control for $G = 4000$.

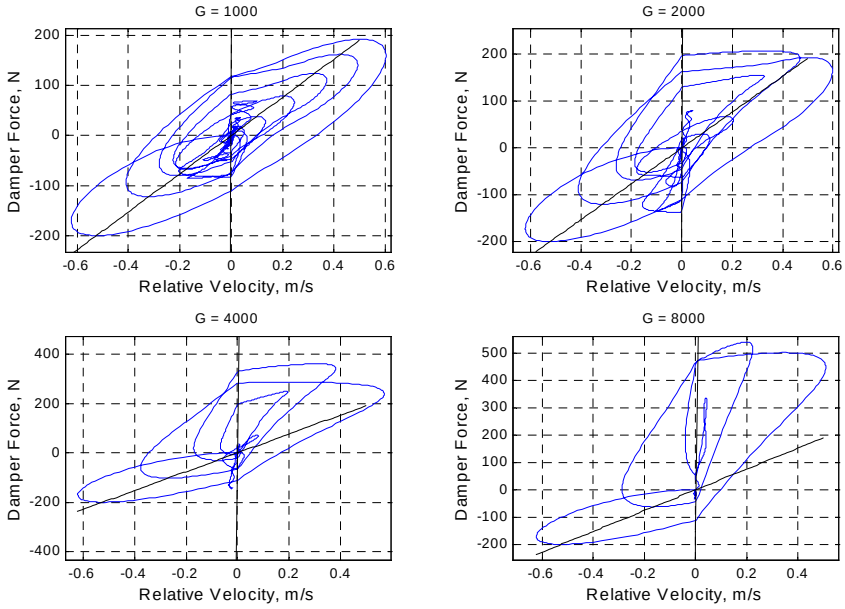

Figure 5.1-7 Comparison of the Force/Velocity Trajectory Step Responses for a Single Suspension under Skyhook Control.

5.1.3 Steady State Analysis

5.1.3.1 1.34 Hz Sinusoid Response

The peak-to-peak measure trade off created by increasing the gain is between jerk and the other performance measures, namely the body peak-to-peak displacements, and sprung mass peak-to-peak acceleration, as shown in Figure 5.1-8. The gain range, G = 500 to 8000 N/m/s, used for the steady state response analysis is the same as for the transient analysis. As the gain is increased, the sprung and unsprung peak-to-peak body displacements decrease from 0.249 m to 0.024 m and from 0.059 m to 0.033 m, respectively. In addition, the sprung mass peak-to-peak acceleration decreases from 17.7 m/s^2 to 2.12m/s^2. These decreases should benefit both the ride comfort and the handling. Jerk, however, increases from 150 m/s^3 to 286 m/s^3 as the gain is increased. This increase in jerk would significantly detract from the ride comfort. Similar to what was discussed earlier, when trying to improve the performance measures solely by the gain. Note, that these displacement and acceleration trends were also revealed in the transmissibility plots in Figures 5.1-1 to 5.1-3.

The RMS performance measures, as a function of the gain, show the same trends as does the peak-to-peak measures. The sprung and unsprung body RMS displacements decrease from 0.091 m to 0.009 m and from 0.021 m to 0.01 m. The sprung body RMS acceleration is reduced from 6.42 m/s^2 down to 0.684 m/s^2. The sprung body RMS jerk, however, increases from 51.3 m/s^3 up to 22.2 m/s^3. Again, we see the trade off between jerk and both the displacement and acceleration performance measures.

We can analyze the response further by looking at Figures 5.1-10 to 5.1-12. In Figure 5.1-10, the Skyhook steady state displacement response is nearly as smooth as the passive response, shown in Figure 4.10. The Skyhook acceleration response, however, is not quite as smooth as that in Figure 4.13, especially when the gain is increased. This roughness shows up as a relatively large jerk in the Skyhook response, depicted in Figure 5.1-12. In fact, we see a significant increase in the jerk peak-to-peak as the gain is increased from 4000 to 8000. It can also be seen that a periodic jerk step response is

superimposed on the sinusoidal jerk response. To get a better understanding of this response we can examine the damper operation in an example response for G = 4000.

The operation of the Skyhook controller during the 1.34 Hz sinusoidal base excitation is to turn the damper on and off with the desired damper force proportional, by *G*, to the body velocity, as seen in Figure 5.1-13. This on/off happens twice every cycle. Once to counter the positive velocity motion of the body and once to counter the negative velocity portion of the body during the body's sinusoidal oscillation. It turns out that the filter used in the damper model causes the damper to turn on and off relatively quickly two additional times for every 'on' damper switch. To keep our discussion focused we will consider this a noise in the actual switching of the damper. Every time the damper turns on or off the damper either grabs or lets go of the sprung body, which is being excited at its resonance frequency. This sudden change in damper force causes a quick change in acceleration of the sprung body, shown in Figure 5.1-14. Since jerk is the derivative of acceleration, a quick change in acceleration results in a large jerk. It is clear that the switching action required to implement the semiactive control laws causes a relatively large jerk in the sinusoidal response compared to the smoother passive response.

Another approach to better understanding the damper operation, as discussed before, is to analyze the damper force/velocity trajectory, which is shown in Figure 5.1-15. This figure reveals that with 1.34 Hz sinusoidal base excitation, increasing the gain tends to make the trajectory rotate counter-clockwise. The higher gain responses make more use of the greater damping coefficients. In addition, the maximum velocity decreases as the gain is increased.

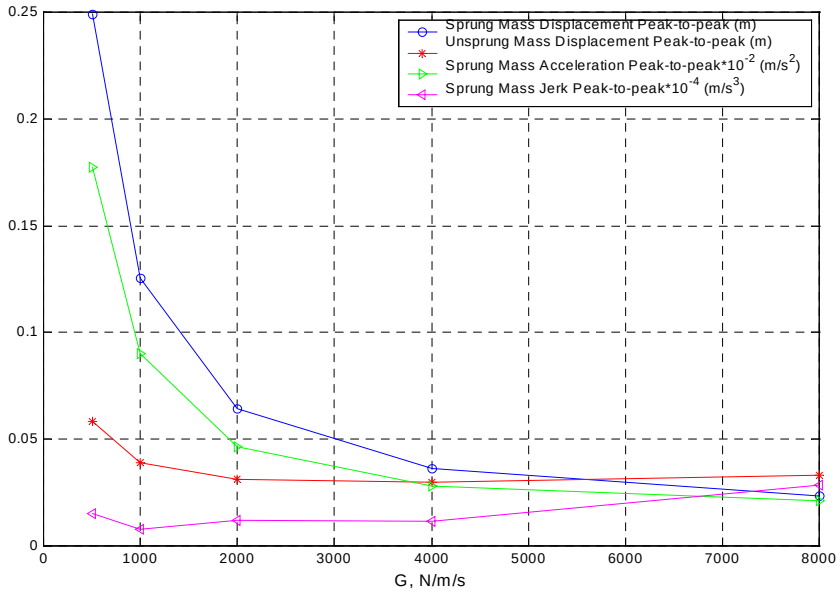

Figure 5.1-8 Effect of Varying *G* on the Peak-to-Peak Steady State Response Performance Measures for a Single Suspension under Skyhook Control. (1.34 Hz Sine Input).

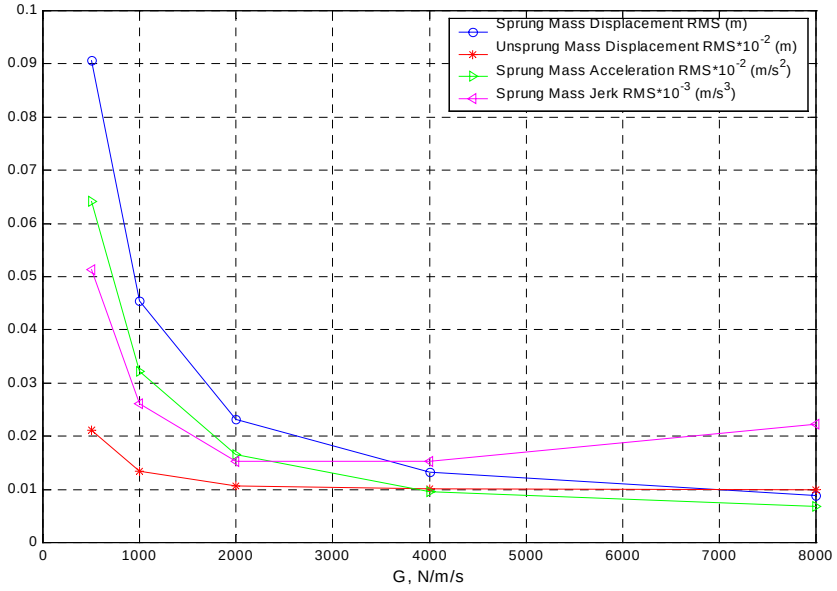

Figure 5.1-9 Effect of Varying *G* on the RMS Steady State Response Performance Measures for a Single Suspension under Skyhook Control. (1.34 Hz Sine Input).

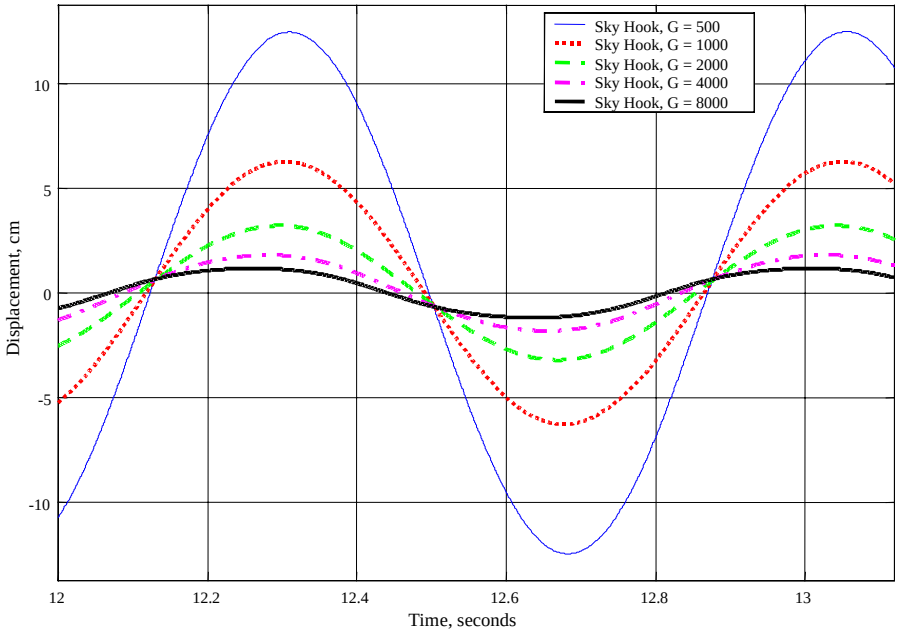

Figure 5.1-10 Effect of Varying *G* on the Displacement Amplitude of the Steady State Response for a Single Suspension under Skyhook Control. (1.34 Hz Sine Input).

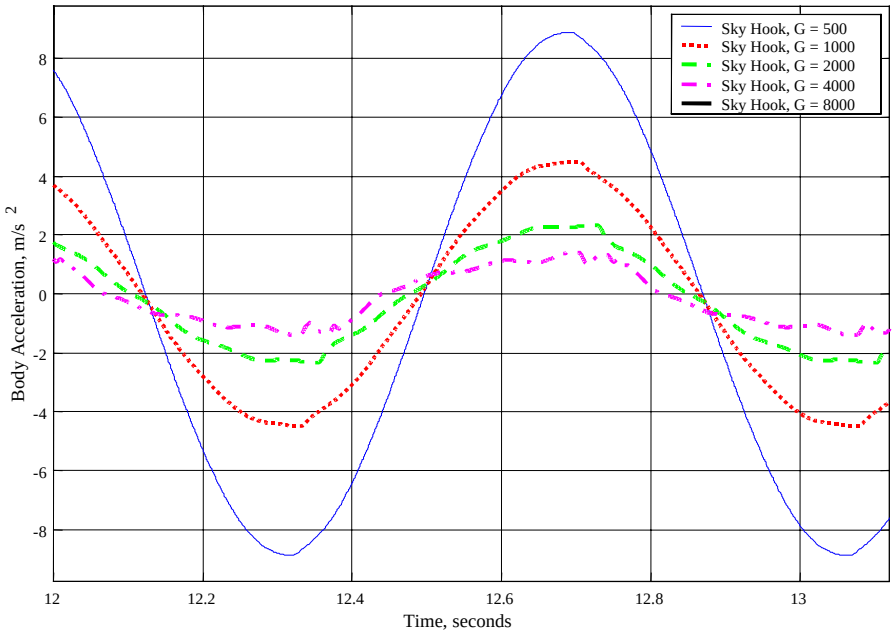

Figure 5.1-11 Effect of Varying *G* on the Displacement Amplitude of the Steady State Response for a Single Suspension under Skyhook Control. (1.34 Hz Sine Input).

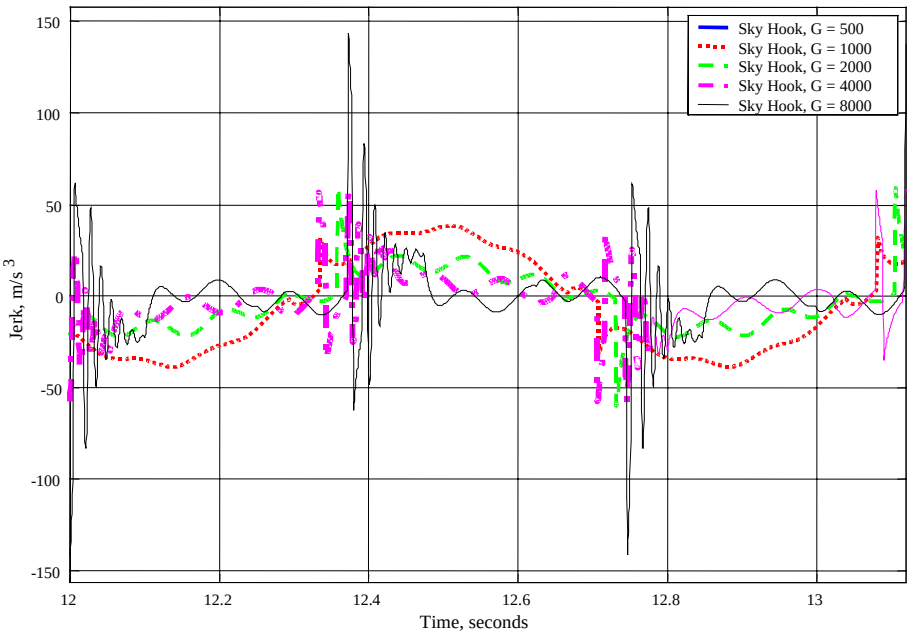

Figure 5.1-12 Effect of Varying *G* on the Displacement Amplitude of the Steady State Response for a Single Suspension under Skyhook Control. (1.34 Hz Sine Input).

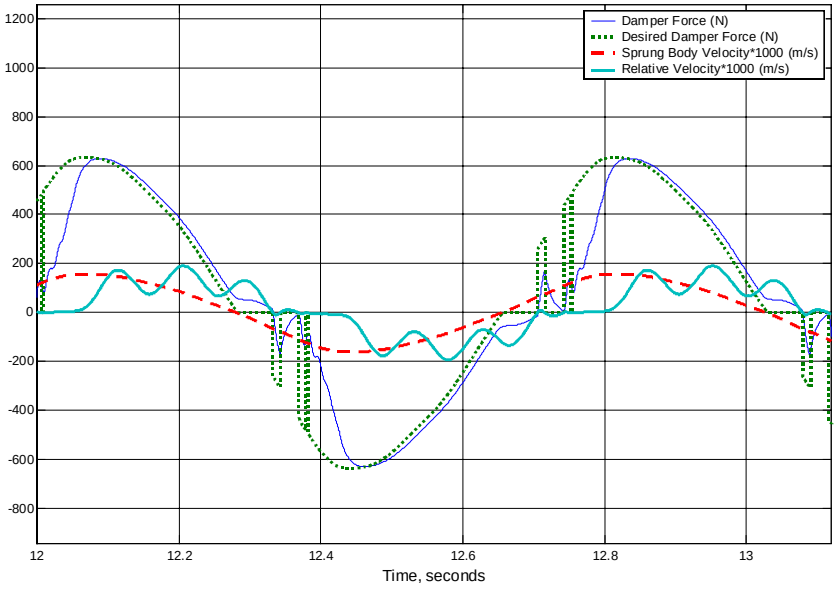

Figure 5.1-13 1.34 Hz Steady State Response of a Single Suspension under Skyhook Control for *G* = 4000.

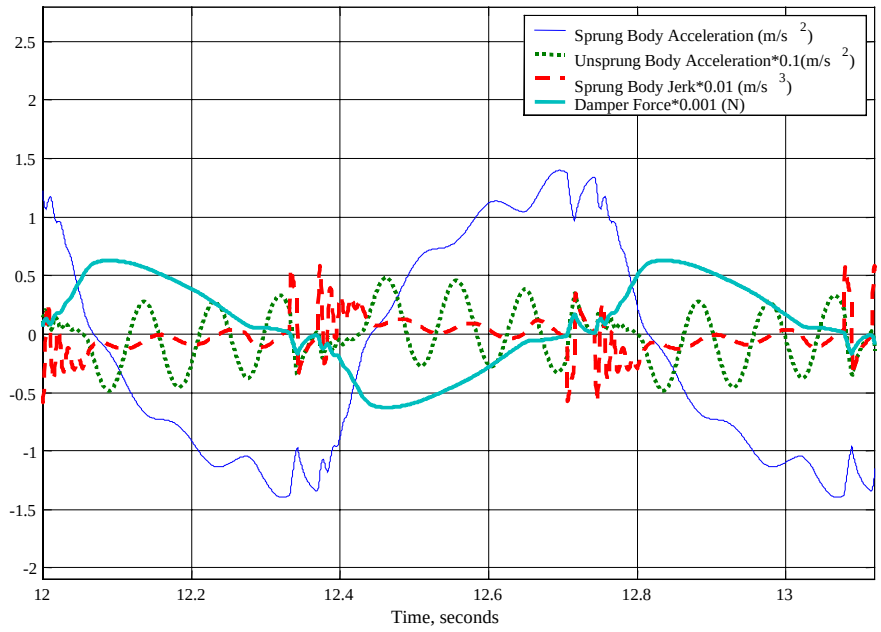

Figure 5.1-14 1.34 Hz Steady State Response of a Single Suspension under Skyhook Control for G = 4000.

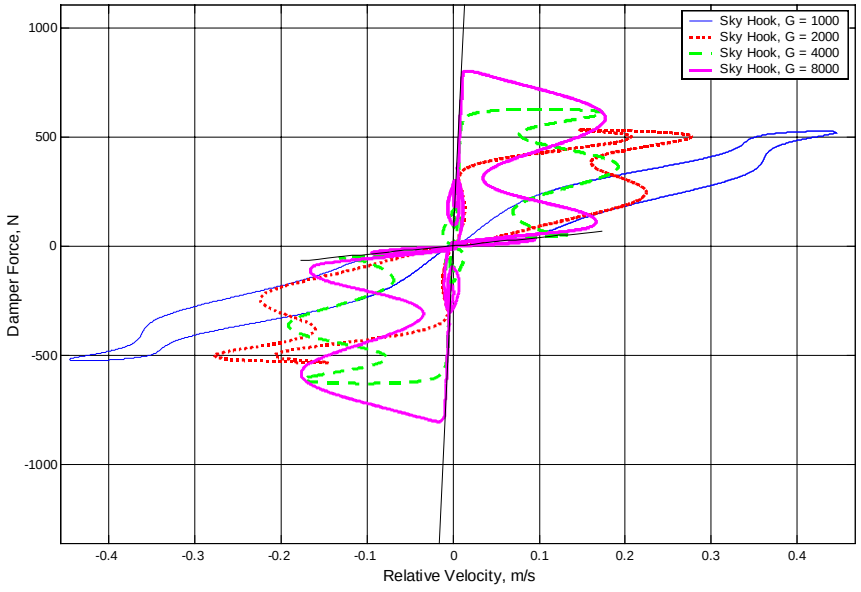

Figure 5.1-15 Comparison of the Damper Force/Velocity Trajectory 1.34 Hz Steady State Responses for a Single Suspension under Displacement Skyhook Control.

5.1.3.2 10.5 Hz Sinusoid Response

Changing the Skyhook gain has little to no effect on the quarter car response when the system is driven at the sprung body resonant frequency of 10.5 Hz, as shown in Figures 5.1-16 and 17. The transmissibility plots of Figures 5.1-1 to 5.1-3 had also shown that changing the Skyhook gain does not affect the performance near the unsprung body resonant frequency. By comparing Figure 4.14 with Figure 5.1-17, it is clear that Skyhook control, at 10.5 Hz, provides near zero damping regardless of the gain.

The performance measures, except for the jerk, are constant as a function of the gain, as indicated in Figure 5.1-16. The peak-to-peak sprung and unsprung displacement is fixed at 0.005 m and 0.177 m, respectively. The peak-to-peak acceleration is fixed at 22 m/s^2 and jerk decreases only slightly from 1450 m/s^3 to 1435 m/s^3. The RMS performance measures in Figure 5.1-17 show a similar pattern as the peak-to-peak measures. The sprung and unsprung body RMS displacement is fixed at 0.002 m and 0.063 m, respectively. The sprung mass acceleration is fixed at 7.77 m/s^2, while jerk decreases from 513 m/s^3 to 509 m/s^3. Except for slight decreases in jerk, increasing the gain has little effect on the Skyhook 10.5Hz response.

As shown in Figure 5.1-18, the 10.5 Hz Skyhook response is the minimal damping response because the desired damper force is nearly always less than the minimum damping force. For example, at 12.06 seconds, the desired damper force, 655 N, is the product of the sprung body velocity, 0.1637 m/s, and the gain, 4000 N/m/s. The actual damper force, however, as by calculated the product of the minimum damping coefficient, 381.9 N/m/s, and the relative velocity, 5.94 m/s is 2270 N. Note that the 1^{st} order filter, $\tau = 10$ msec, delays the output of the 2270 N damper force by about 10 msec. The relatively high damper velocity at the unsprung body resonant frequency causes the over reaction of the damper force. The off condition of the damper causes the jerk response, shown in Figure 5.1-19, to be much smoother than it was for the 1.34 Hz sinusoidal response.

Figure 5.1-20 clearly shows that the damper is not behaving as a classical linear viscous damper even though the Skyhook damping is practically equivalent to a 5% passive damping ratio. This deviation from the linear model is created by the filter delay. This delay is more pronounced compared with the period of the response, at the higher frequencies. Without the filter, however, we cannot easily calculate a converged jerk using the numerical simulation, as was discussed earlier in Chapter 3.

5.1.4 Skyhook Results Summary

The semiactive sprung body velocity based control force and the switch create single suspension dynamics that are significantly different from the passive results. Increasing Skyhook gain, *G*, will control the 1.34 Hz dynamics but will not affect the 10.5 Hz system dynamics. Another benefit of Skyhook is that the peak-to-peak sprung body acceleration does not increase when the gain is increased. These trends free us from the related constraints imposed by using a passive system, although we do not get the same 10.5 Hz control. The switching action, however, introduces a relatively large jerk, which must be weighed against the improvements of increasing the Skyhook gain. Crosby, Harwood, and Karnopp, in [9], refer to this phenomenon as a, “very discontinuous damper force.”

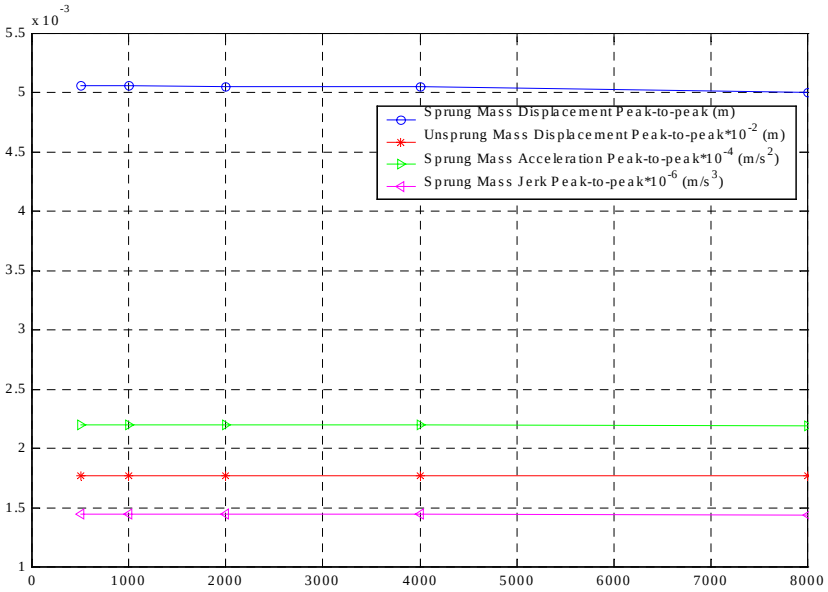

Figure 5.1-16 Effect of Varying *G* on the Peak-to-Peak Steady State Response Performance Measures for a Single Suspension under Skyhook Control. (10.5 Hz Sinusoidal Input).

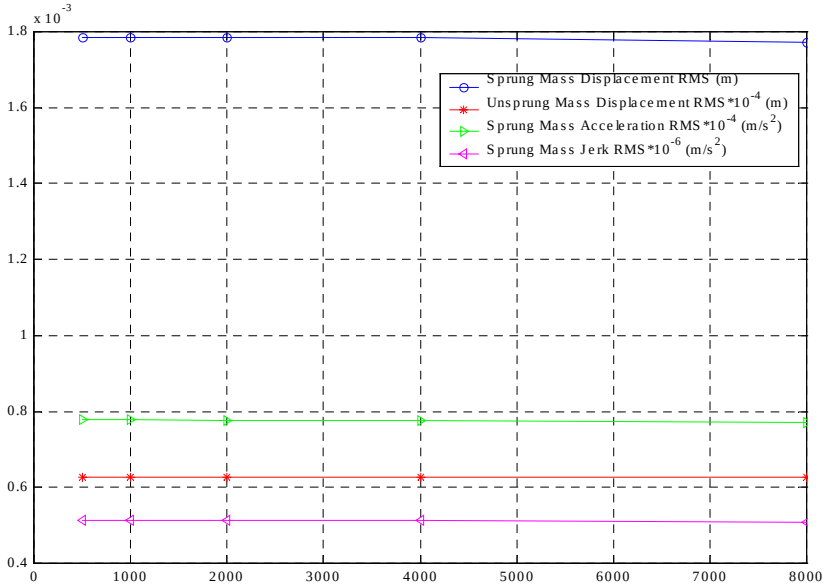

Figure 5.1-17 Effect of Varying *G* on the RMS Steady State Response Performance Measures for a Single Suspension under Skyhook Control. (10.5 Hz Sinusoidal Input).

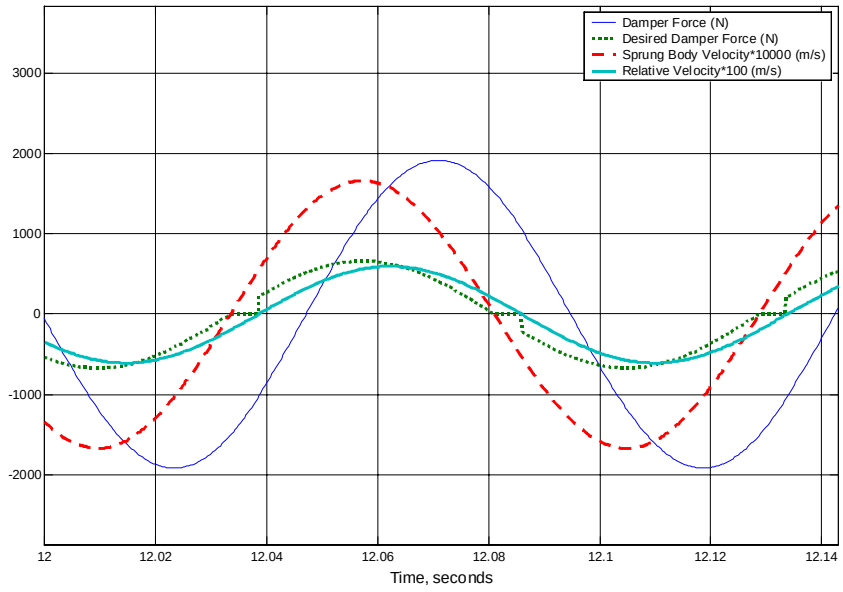

Figure 5.1-18 10.5 Hz Steady State Damper Force Response of a Single Suspension under Skyhook Control for *G* = 4000.

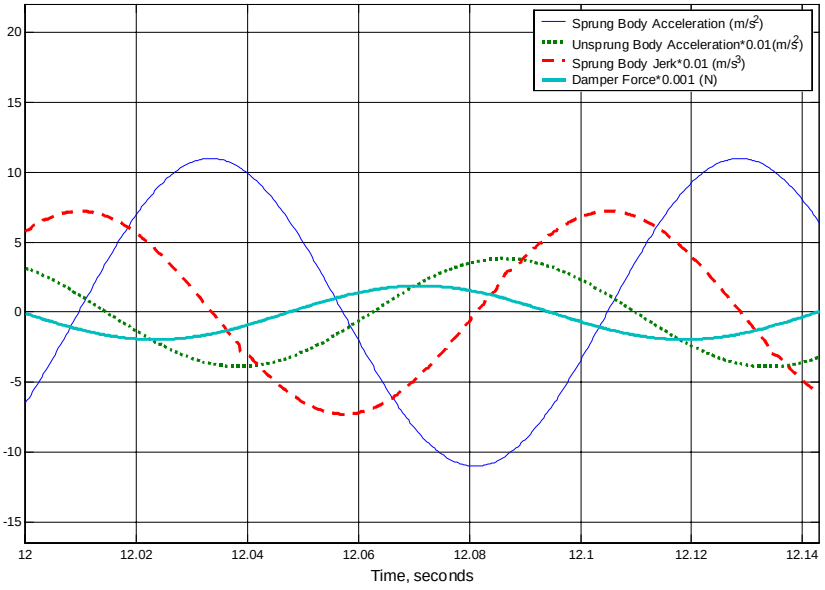

Figure 5.1-19 10.5 Hz Steady State Acceleration Response of a Single Suspension under Skyhook Control for G = 4000.

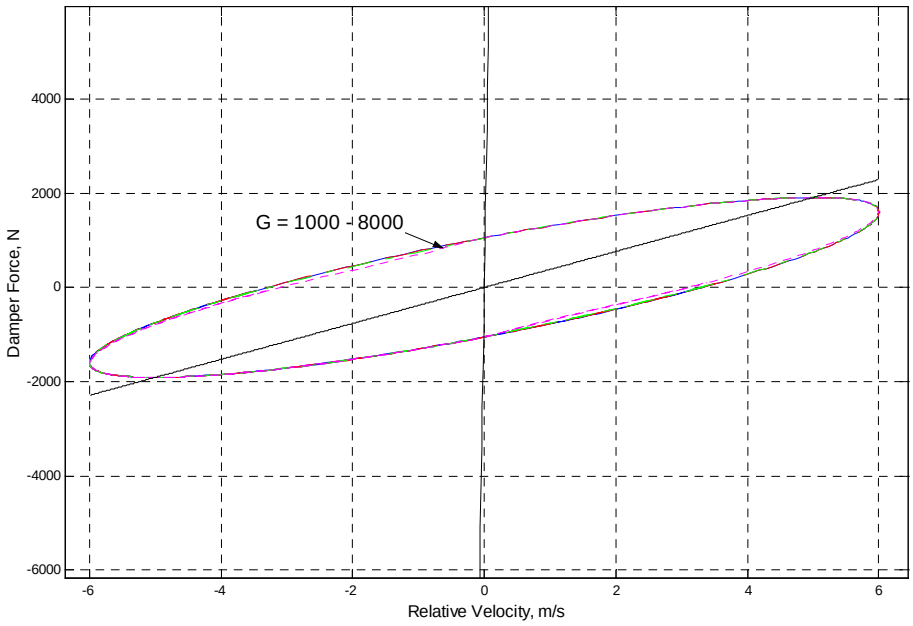

Figure 5.1-20 Comparison of the Damper Force/Velocity Trajectory 10.5 Hz Steady State Responses for a Single Suspension under Skyhook Control.

5.2 Hybrid Control Results

The Hybrid controller is designed to not only directly control the sprung mass, but to control the unsprung mass directly as well. This added control is attempted by utilizing unsprung body velocity feedback in addition to the Skyhook sprung body velocity feedback. The results presented in this section show that we can trade off the sprung mass natural frequency, 1.34 Hz, performance with the unsprung mass natural frequency, 10.5 Hz, performance [3].

5.2.1 Transmissibility Analysis

The Hybrid controller is capable of controlling both the sprung and unsprung body resonance peaks. The difference between the Skyhook and the Hybrid control is that the Hybrid now controls the unsprung mass resonance. This additional control is the result of combining Skyhook with Groundhook. The variable α is used to favor either Skyhook control or Groundhook control.

Alpha is the weighting factor that shifts the Hybrid control from a predominantly Skyhook control, $\alpha = 1$, to a Ground Hook control, $\alpha = 0$. A fractional α provides a blend between these two control laws, see the Hybrid description in Chapter 3. The effect of varying α on the transmissibility is shown in Figure 5.2-1. Lowering the weighting factor, to favor Groundhook, decreases the 10.5 Hz displacement resonance peaks at the expense of increasing the 1.34 Hz displacement resonance peaks. This trade off might increase the handling of the vehicle, at a 10.5 Hz base excitation, while diminishing the ride comfort and handling at a 1.34 Hz base excitation.

The effect of increasing α on the rattle space, or relative transmissibility, is to decrease the 1.34 Hz rattle space while increasing the 10.5 Hz rattle space, as shown in Figure 5.2-2. The invariable point is approximately 3 Hz. Below this frequency, the increasing α decreases the rattle space and above this frequency, increasing α increases the rattle space. This trend is distinctly different than the trends we saw in the passive study, as ζ was varied, and in the Skyhook study, as *G* was varied.

The acceleration is also significantly affected by varying α, as shown in Figure 5.2-3. Increasing α will decrease the 1.34 Hz sprung mass acceleration resonance peak but will increase the 10.5 Hz sprung and unsprung mass acceleration resonance peaks. This trade off would increase the ride comfort at 1.34 Hz but will decrease the ride comfort at 10.5 Hz. Increasing the weighting factor, α, has the net effect of favoring the 1.34 Hz performance at the expense of the 10.5 Hz performance. However, α is not the only Hybrid control variable.

Another variable in the Hybrid controller is the gain, *G*. Figure 5.2-4 shows that increasing *G* has a similar effect as that of increasing the damping in the passive case shown in Figure 4.3. Increasing *G* reduces the sprung and unsprung body resonant frequency displacement transmissibility. However, just as with the passive case, increasing *G* slightly increases the displacement transmissibility in between the resonant peaks. Overall, at the resonant frequencies, the ride comfort and vehicle handling should improve by increasing *G*.

The Hybrid response rattle space of Figure 5.2-5 follows a similar pattern as that of increasing the passive damping in the passive case shown in Figure 4.2. At 1.34 Hz and 10.5 Hz, increasing the *G* decreases the rattle space. The invariant point occurs at approximately 3 Hz. At this point the choice of gain does not affect the rattle space. The rattle space, as mentioned before is important because the suspension will need at least this much space to operate without interfering with other parts of the vehicle.

Just as with the displacement transmissibility and the rattle space, increasing *G*, as shown in Figure 5.2-6, has a similar effect as does increasing the passive damping shown in Figure 4.3. The sprung mass 1.34 Hz resonant peak is significantly decreased as *G* is increased. This decrease in acceleration should improve the ride comfort to a 1.34 Hz base excitation. Increasing G also reduces the 10.5 Hz sprung and unsprung acceleration. This reduction in acceleration should improve the ride comfort as well. Overall, increasing *G* should improve the ride comfort and the vehicle handling at both 1.34 Hz and 10.5 Hz.

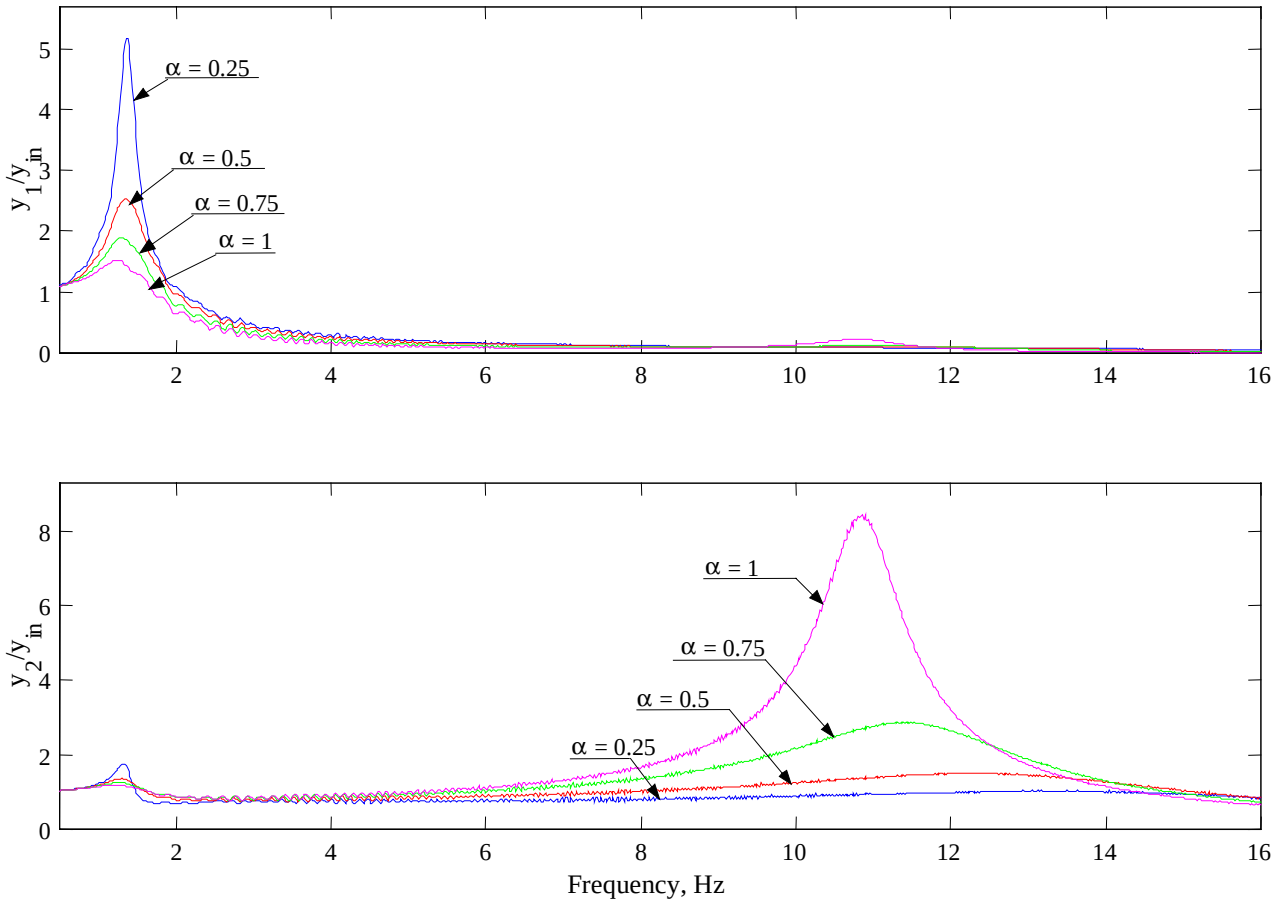

Figure 5.2-1 Transmissibility Plots of a Single Suspension under Hybrid Control with G = 4000. (y_1 : sprung mass displacement, y_2 : unsprung mass displacement, y_{in} : base displacement)

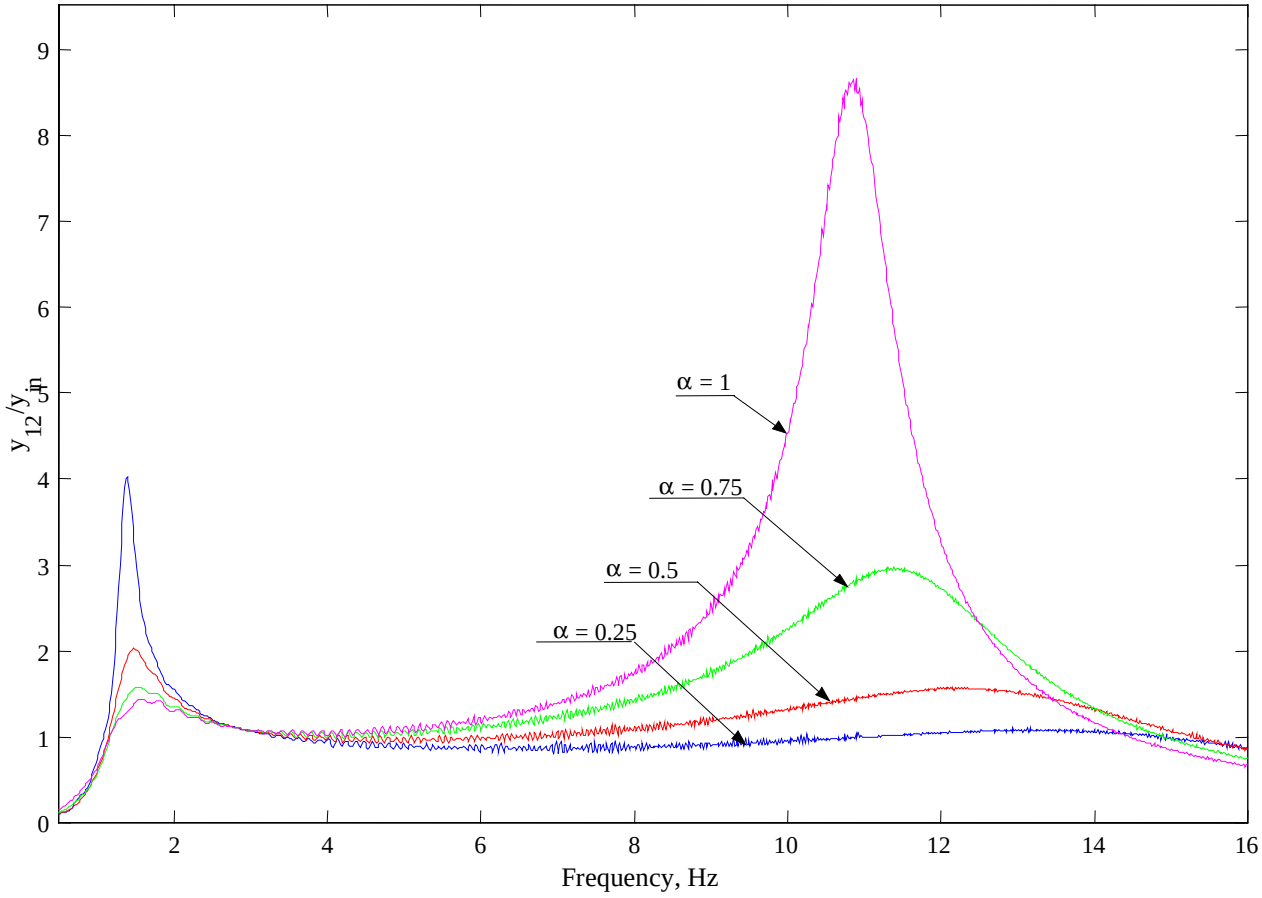

Figure 5.2-2 Relative Transmissibility of a Single Suspension under Hybrid Control for G = 4000. (y_{12} : relative displacement, y_{in} : base displacement)

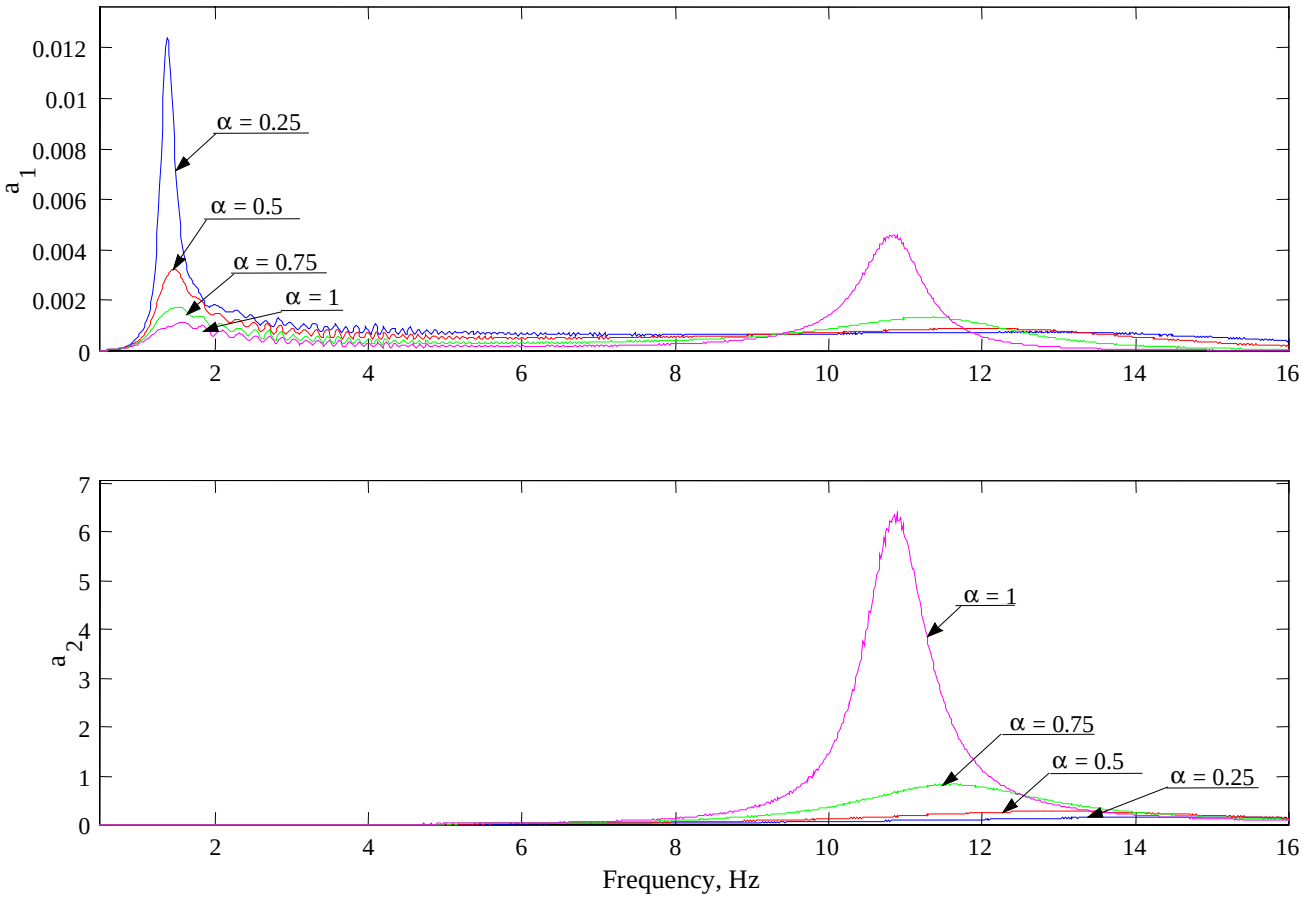

Figure 5.2-3 Acceleration Power Density Spectrum of a Single Suspension under Hybrid Control for G = 4000. (a_1: sprung mass acceleration power density, a_2: unsprung mass acceleration power density)

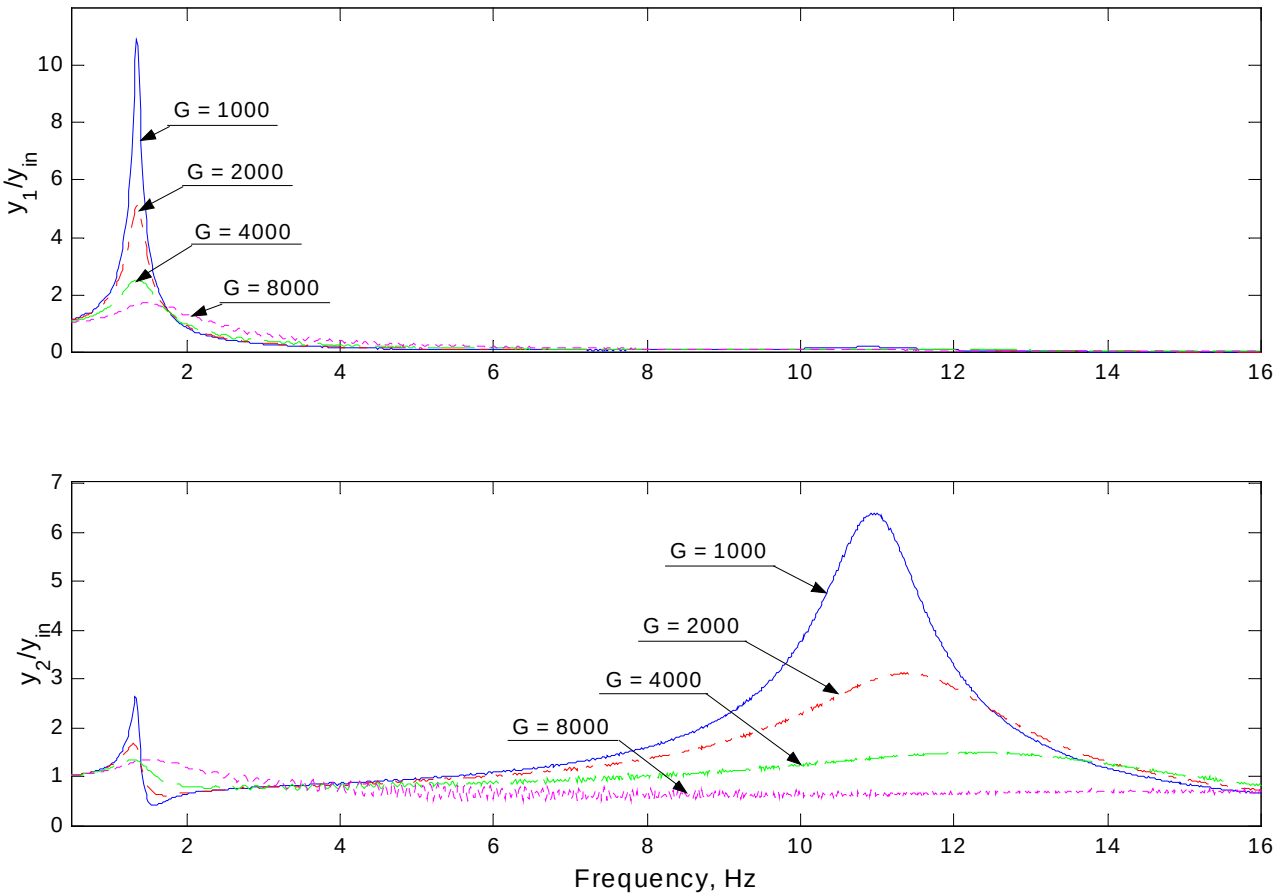

Figure 5.2-4 Transmissibility Plots of a Single Suspension under Hybrid Control with α = 4000. (y_1 : sprung mass displacement, y_2 : unsprung mass displacement, y_{in} : base displacement)

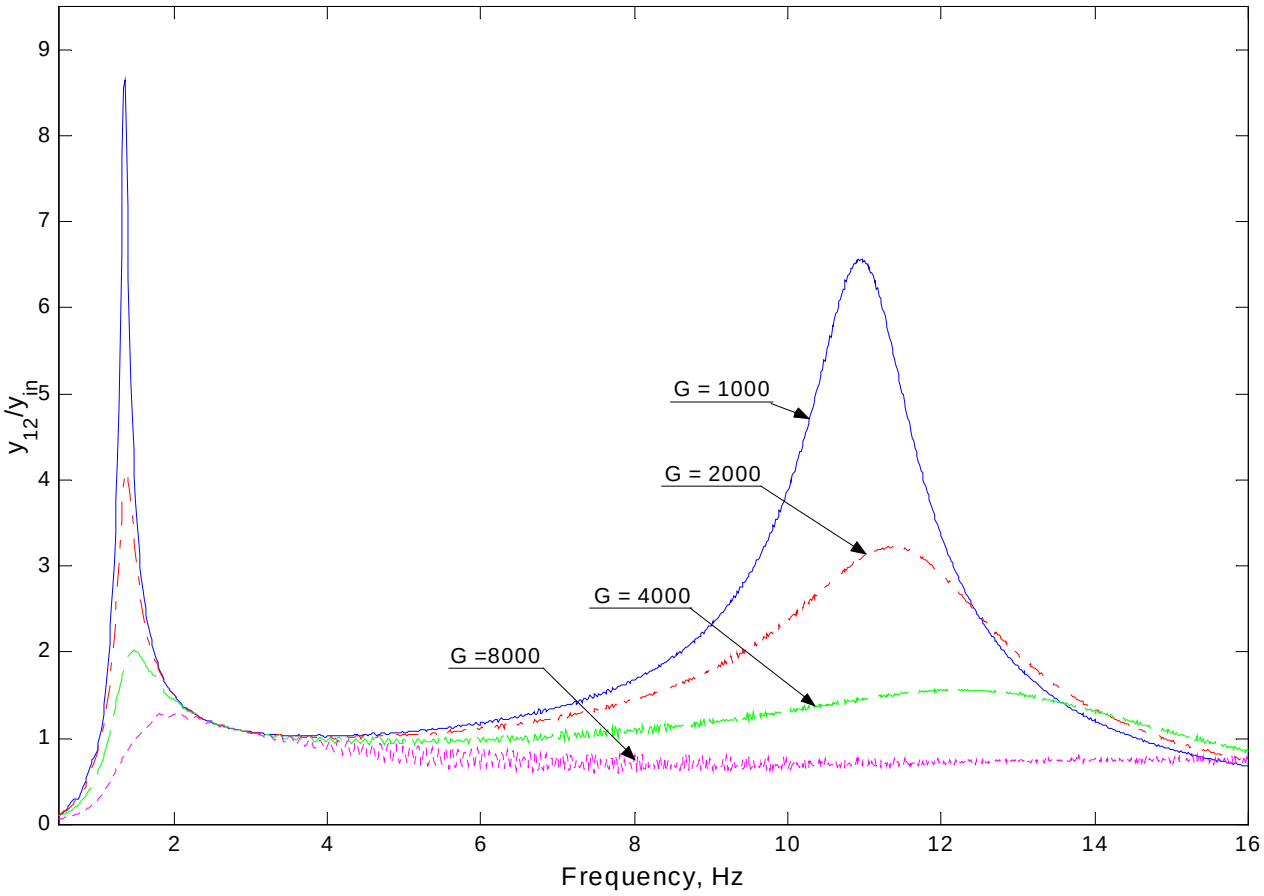

Figure 5.2-5 Relative Transmissibility of a Single Suspension under Hybrid Control for $\alpha = 4000$. (y_{12} : relative displacement, y_{in} : base displacement)

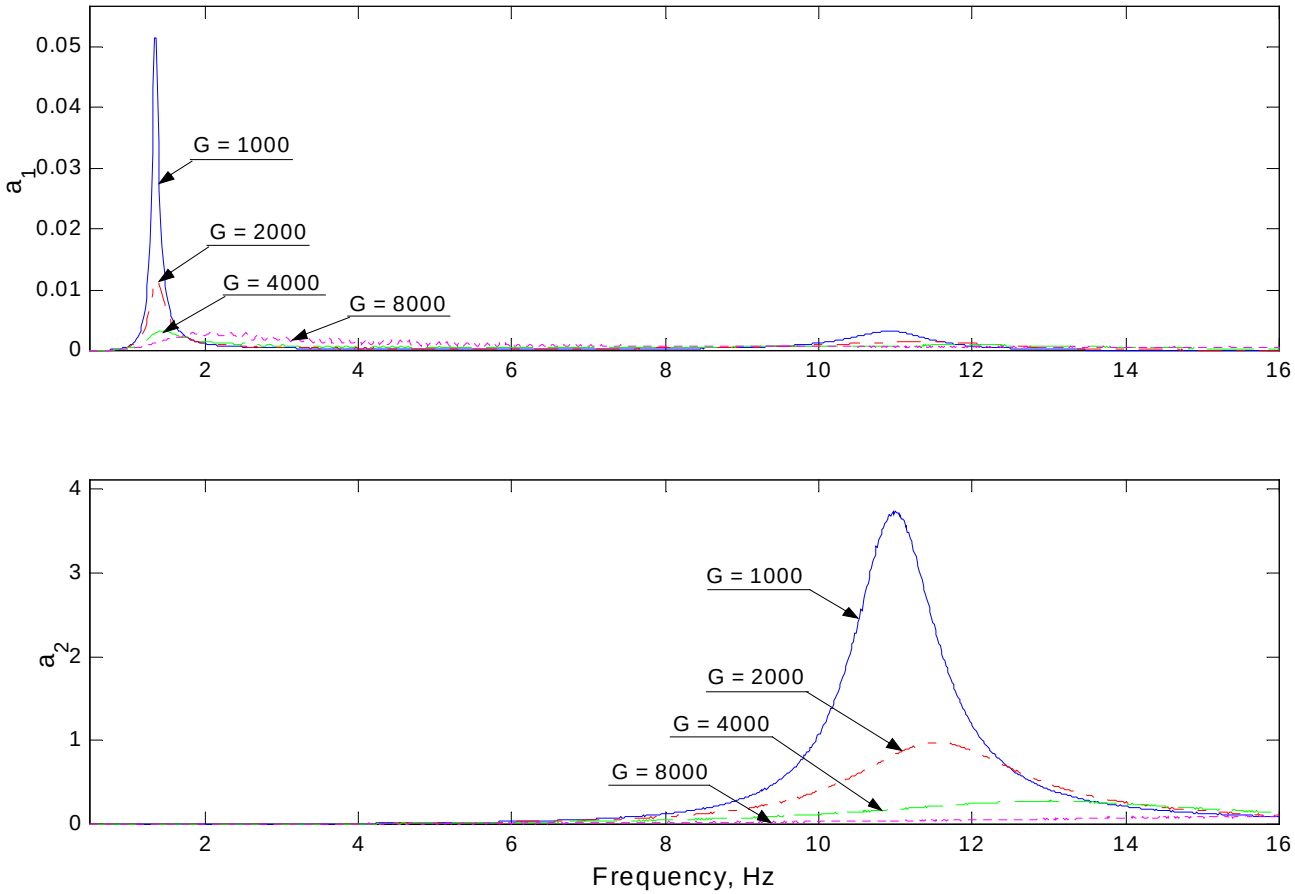

Figure 5.2-6 Acceleration Power Density Spectrum of a Single Suspension under Hybrid Control for $\alpha = 4000$. (a_1: sprung mass acceleration power density, a_2: unsprung mass acceleration power density)

5.2.2 Transient Analysis

A trade off occurs, when increasing α from 0.5 to 1, between increasing the unsprung mass peak-to-peak displacement and decreasing the settling time and the sprung mass peak-to-peak displacement, acceleration, and jerk, as shown in Figure 5.2-7. First, over the lower gain range of α = 0.25 to 0.5, the unsprung mass peak-to-peak displacement decreases from 0.0045 m to 0.0032 m and then, over the upper gain range of α = 0.5 to α = 1, the displacement increases to 0.0143 m. The increase in unsprung mass displacement would decrease the transient handling ability of the vehicle. Over the full simulated gain range of α = 0.25 to 1, settling time decreases from 4.5 seconds to 1.2 seconds which should improve ride comfort. Over the same gain range, sprung mass peak-to-peak displacement decreases from 0.0197 m to 0.0081 m, peak-to-peak acceleration decreases from 4.21 m/s^2 to 2.81 m/s^2, and peak-to-peak jerk decreases from 364 m/s^3 to 162 m/s^3. These performance measure decreases should cause ride comfort to improve. In sum, increasing α beyond 0.5 will decrease the vehicle handling and improve the ride comfort.

Increasing *G* of the Hybrid controller, see Figure 5.2-8, has a similar effect as increasing the passive damping, as shown in Figure 4.4. As *G* is increased from 1000 to 8000, the settling time and the sprung and unsprung body peak-to-peak displacements decrease while the peak-to-peak acceleration and jerk increase. Over this gain range, the settling time decreases from 9 seconds to 0.86 seconds, which should improve the ride comfort. The sprung and unsprung peak-to-peak displacement decreases from 0.0225 m down to 0.0065 m and from 0.0139 m down to 0.0028 m, respectively. This decrease should also improve ride comfort as well as vehicle handling. However, the acceleration and jerk increase from 3.11 m/s^2 up to 4.50 m/s^2 and from 155 m/s^3 up to 491 m/s^3, respectively. These increases should detract from ride comfort. Overall, increasing the gain, G, would diminish the ride comfort, but should improve the vehicle handling.

The transient behavior of the Hybrid controller can be studied further by examining Figure 5.2-9. During the Hybrid response, as shown in Figure 5.2-9, the actual damper force is approximately equal to the desired damper force. One reason for the similarity in

the actual and desired damper force is that the desired damper force usually has the same sign as the damper velocity (relative velocity). Since the damper velocity direction is consistent with the desired damper force direction, the switches do not intercede in a way that turns the damper force to zero.

We can explain why the damper is always on by using the Hybrid switch equations given in Chapter 3. For this example, we will concentrate on the first ½ cycle of the transient response. During this period of the response, the relative velocity, v_{12}, is of the opposite sign as the sprung body velocity, v_1, and their product is therefor negative. According to equation (3.9), the Skyhook component of the desired damper force is zero. In addition, the product of the relative velocity, v_{12}, and the unsprung velocity, v_2, is negative. However, according to equation (3.9), the Groundhook component desired force is nonzero. Therefore, the total desired damper force is nonzero. This type of independent switching results in the transient response actual damper force approximating the desired damper force.

In the previous Skyhook section, we saw that the switch was responsible for the jerk spikes. Figure 5.2-10 shows that the spiky transient jerk response is more characteristic of the Skyhook response, as shown in Figure 5.1-6 than that of the passive response, see Figure 4.6. Although, the cause of the jerk spikes in the response is not clear from Figure 5.2-10, we might expect that it is the nonlinear switching which creates this jerk. Studying the Hybrid sinusoidal responses in the next section will further reveal the existence of jerk spikes under Hybrid control.

However, before the Hybrid sinusoidal response is studied, notice that the damper force/velocity trajectory reveals, once again, the interesting effect that the use of the filter has on the response, Figures 5.2-11 and 12. However, the sense of time is lost in these trajectories. To put the filter delay in perspective, we should consider the magnitude of the time constant, $\tau = 0.010$ msec, and the relatively small delay of the damper force in the transient response in Figure 5.2-8. The delay does not appear to be overwhelmingly concerning considering that the filter is being used to converge the jerk calculation.

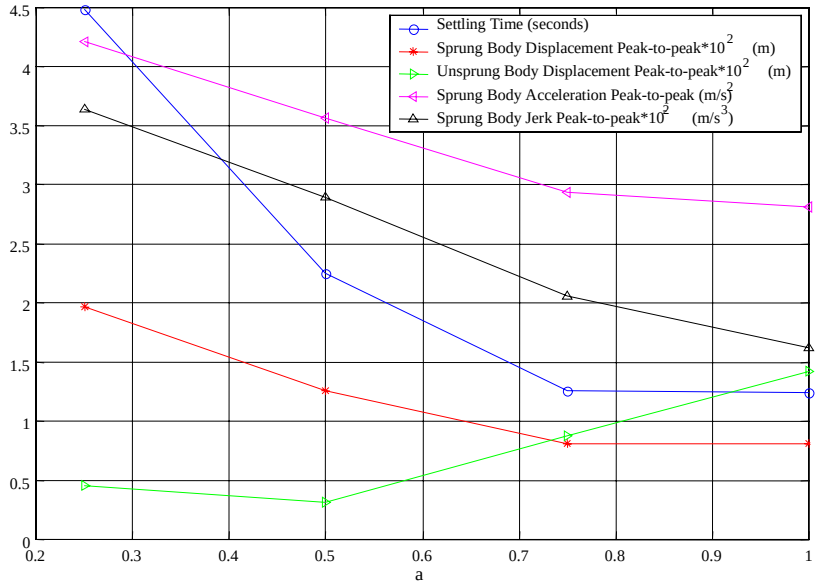

Figure 5.2-7 Effect of Varying α on the Peak-to-peak Step Response Performance Measures for a Single Suspension under Hybrid Control for G = 4000.

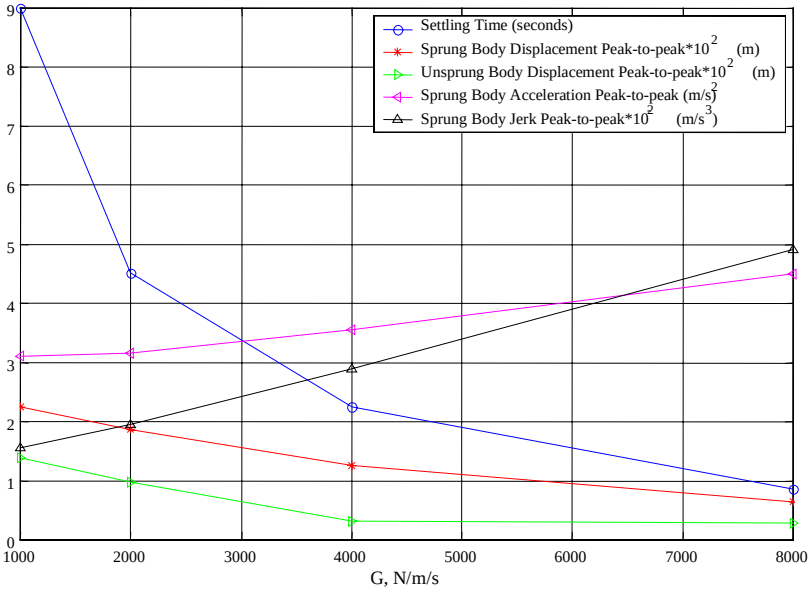

Figure 5.2-8 Effect of Varying G on the Peak-to-peak Step Response Performance Measures for a Single Suspension under Hybrid Control for α = 0.5.

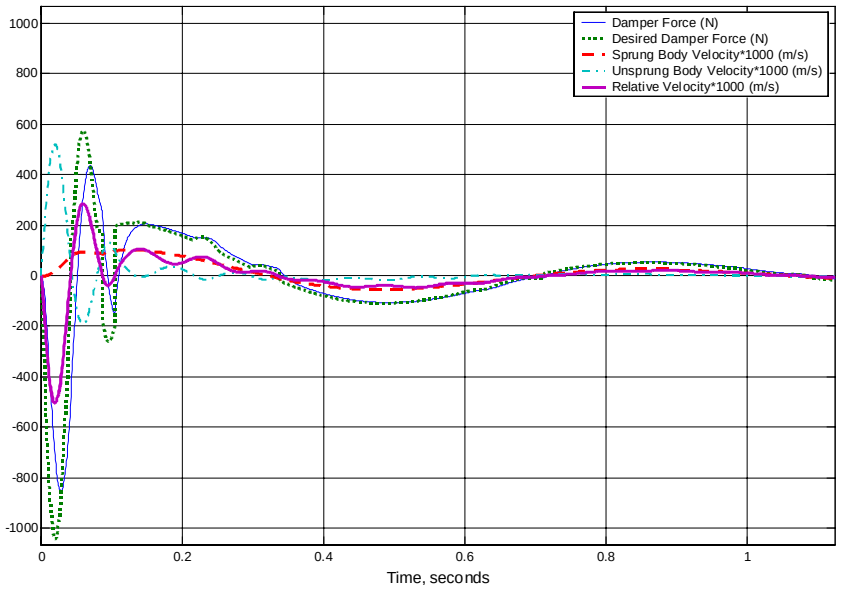

Figure 5.2-9 Step Response of a Single Suspension under Hybrid Control for $G = 4000$ and $\alpha = 0.5$.

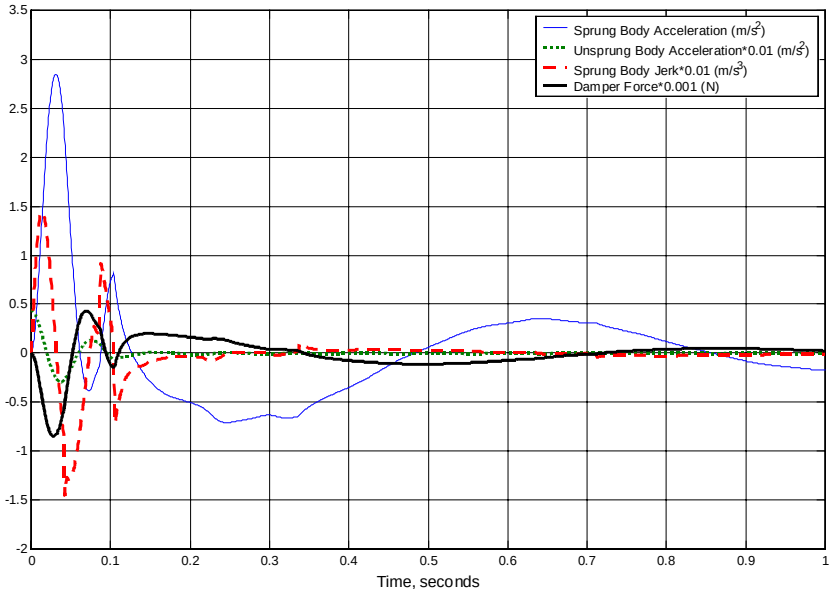

Figure 5.2-10 Step Response of a Single Suspension under Hybrid Control for $G = 4000$ and $\alpha = 0.5$.

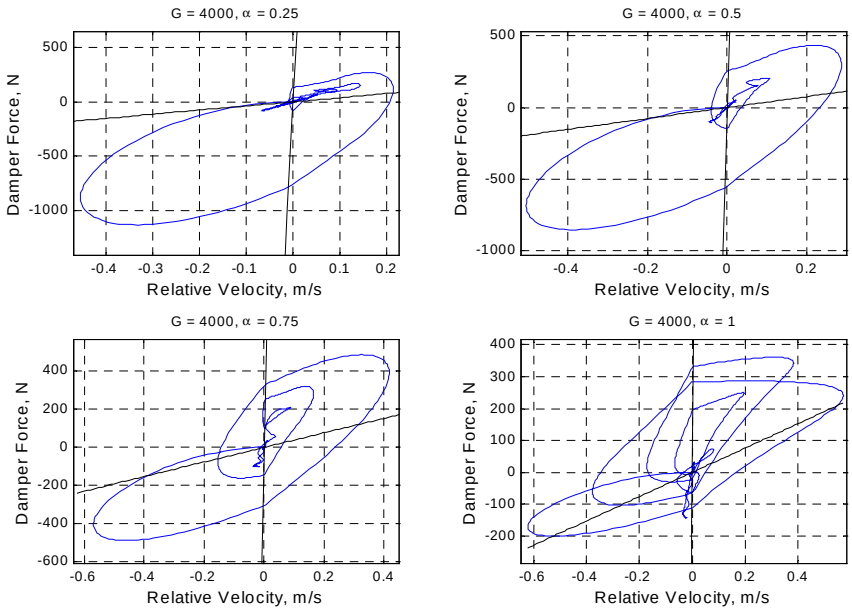

Figure 5.2-11 Comparison of the Force/Velocity Trajectory Step Responses for a Single Suspension under Hybrid Control for G = 4000.

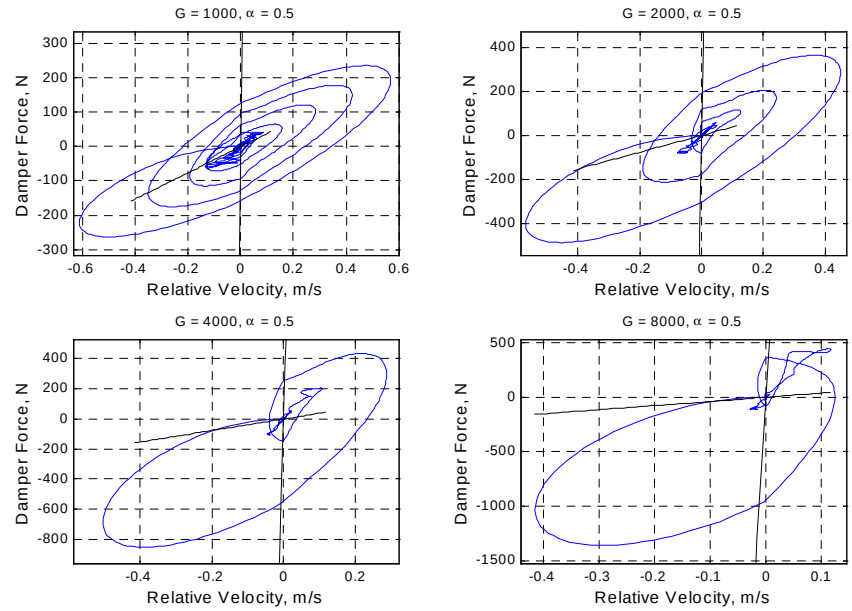

Figure 5.2-12 Comparison of the Force/Velocity Trajectory Step Responses for a Single Suspension under Hybrid Control for α = 0.5.

5.2.3 Steady State Analysis

5.2.3.1 1.34 Hz Sinusoid Response

Increasing α from 0.25 to 0.5 decreases the sprung and unsprung mass peak-to-peak displacement from 0.120 m down to 0.0362 m and from 0.0418 m down to 0.0300 m, respectively, as shown in Figure 5.3-13. Over the same gain range, the sprung mass acceleration decreases from 9.24 m/s^2 down to 2.79 m/s^2. The jerk decreases by only about 3%. Increasing α from 0.25 to 0.5 should improve the ride comfort and vehicle handling for G = 4000.

Increasing α from 0.5 to 0.75 decreases the sprung mass peak-to-peak displacement and acceleration from 0.0631 m down to 0.0458 m and from 4.88 m/s^2 down to 3.36 m/s^2, respectively, as shown in Figure 5.3-13. Over the same gain range, the sprung mass jerk decreases from 161 m/s^3 down to 70 m/s^3. The unsprung mass displacement does not decrease over this gain range. Increasing α from 0.5 to 0.75 should improve the ride comfort for G = 4000.

Increasing α from 0.75 to 1, full Skyhook, creates a trade off between increasing the jerk and decreasing the sprung and unsprung body peak-to-peak displacement and acceleration, as shown in Figure 5.2-13. The sprung mass displacement and acceleration decrease from 0.0458 m down to 0.0362 m and from 3.36 m/s^2 down to 2.79 m/s^2, respectively. Jerk, however, increases from 70 m/s^3 up to 116 m/s^3. Just how these changes will impact the ride comfort is not clear since two of the ride comfort measures decrease, the sprung mass displacement and the acceleration, and one of the ride comfort measures increases, the jerk.

A similar trade off occurs with the RMS performance measures, see Figure 5.3-14, for the 0.75 to 1 α range. The RMS jerk increases from 13.1 m/s^3 to 15.2 m/s^3 while the other performance measures decrease. The sprung and unsprung mass RMS displacement decreases from 0.0165 m down to 0.0132 m and from 0.0107 m down to 0.0101 m, respectively. The sprung mass acceleration decreases from 1.19 m/s^2 down to

0.96 m/s^2. Although it is clear that the unsprung mass displacement decrease would improve the vehicle handling, it is not clear how the ride comfort would be affected.

We can also affect the single suspension performance under Hybrid control by varying the second *G*, as shown in Figure 5.3-15. For this comparison, α = 0.5 was chosen to equally weight the Skyhook and the Groundhook component. When we vary G from 1000 to 8000, we find that all of the performance measures decrease except for the jerk. The sprung and unsprung mass peak-to-peak displacements decrease from 0.249 m down to 0.0395 m and from 0.0586 m down to 0.0323 m. In addition, the sprung mass peak-to-peak acceleration decreases from 17.8 m/s^2 down to 2.96 m/s^2. The jerk is not so well behaved as it reaches a maximum of 161 m/s^3 at *G* = 4000 and reaches a minimum of 57 m/s^3 at *G* = 8000. For α = 0.5, increasing the gain, *G*, from 4000 to 8000 improves both the ride comfort and the vehicle handling.

Determining the effect of increasing *G* on the RMS performance is easy since all of the RMS performance measures decrease over the gain range of 1000 to 8000, as shown in Figure 5.3-16. The sprung and unsprung mass RMS displacements decrease from 0.0905 m down to 0.0141 m and from 0.0212 m down to 0.0114 m, respectively. The sprung body acceleration and jerk decrease from 6.42 m/s^2 down to 1.06 m/s^2 and from 51.4 m/s^3 down to 13.6 m/s^3, respectively. It is clear that increasing the gain improves both the ride comfort and the vehicle handling at α = 0.5.

We can try to gain some insight into the reason for the above relationships by examining the operation of the Hybrid controller at 1.34 Hz is seen in Figures 5.2-17. For example, briefly examining this plot reveals that the output is not a nice, smooth version of the input sinusoid wave. The most obvious cause of the rough response is the quick sign reversal of the desired and actual damper force. In addition, this reversal occurs when the damper force is large. This occurs twice every period; once between 12.2 and 12.4 seconds and once between 12.6 and 12.8 seconds. This type of behavior is possible since even at relatively low damper velocities the damping coefficient can be quite large. When the velocity across the damper changes sign, at approximately 12.7 seconds, the

desired damper force changes from -659 N to +660 N. This sharp change in the damper force direction coincides with a sharp change in the body acceleration causing a large jerk, Figure 5.3-18.

Another interesting system feature is the saturation of the damper force at the C_{on} and C_{off} line on the damper force/velocity characteristic, as shown in Figure 3.1. The damper force/velocity trajectory is superimposed on this characteristic in Figure 5.2-19. Here we can see the input/output relationship required of the damper under Hybrid control. Notice that there are relatively sharp changes in trajectory direction near the saturation lines. These sharp changes can also contribute to nonsmooth responses.

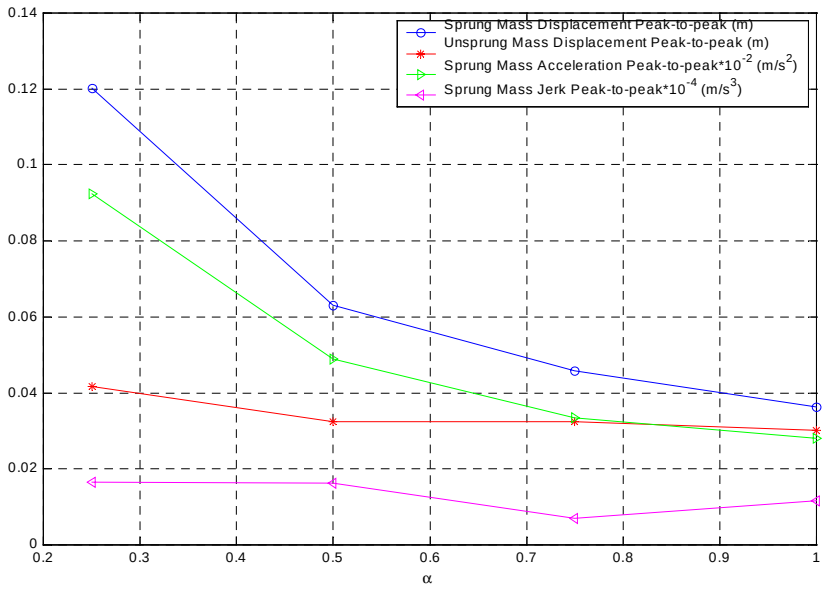

Figure 5.2-13 Effect of Varying α on the Peak-to-peak Steady State Response Performance Measures for a Single Suspension under Hybrid Control for G = 4000. (1.34 Hz Sinusoidal Input)

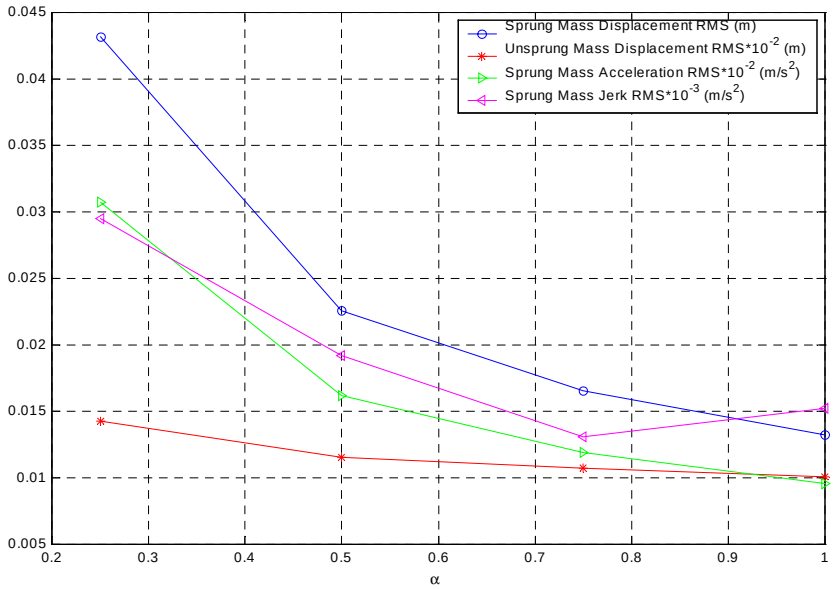

Figure 5.2-14 Effect of Varying α on the RMS Steady State Response Performance Measures for a Single Suspension under Hybrid Control for G = 4000. (1.34 Hz Sinusoidal Input)

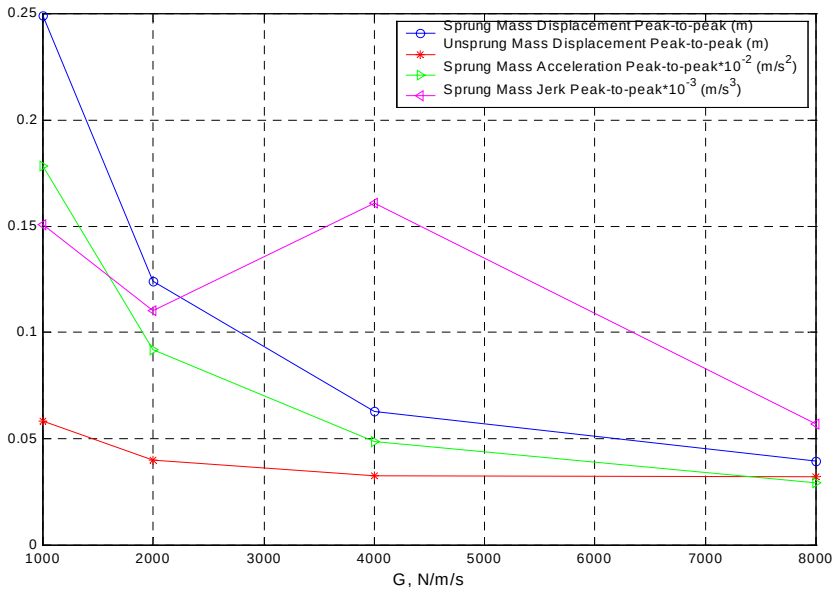

Figure 5.2-15 Effect of Varying G on the Peak-to-peak Steady State Response Performance Measures for a Single Suspension under Hybrid Control for α = 0.5. (1.34 Hz Sinusoidal Input)

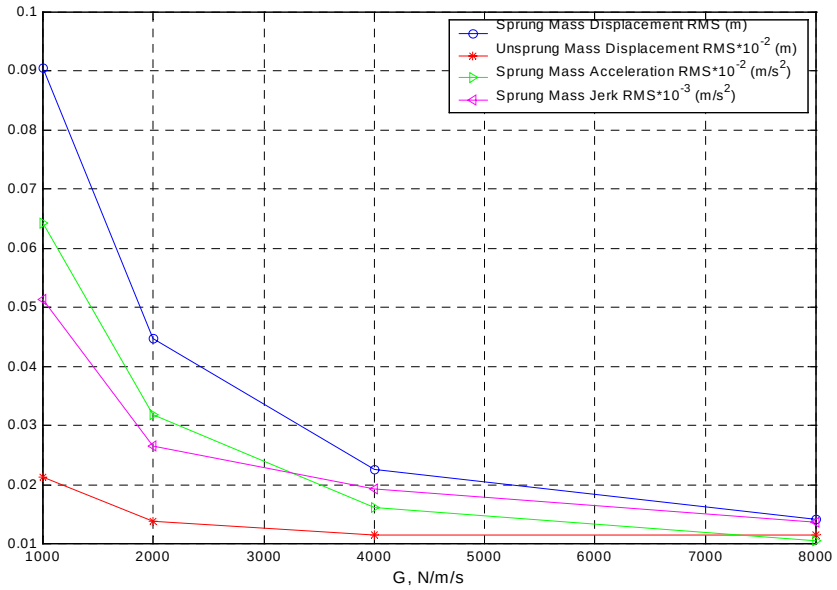

Figure 5.2-16 Effect of Varying *G* on the RMS Steady State Response Performance Measures for a Single Suspension under Hybrid Control for $\alpha = 0.5$. (1.34 Hz Sinusoidal Input)

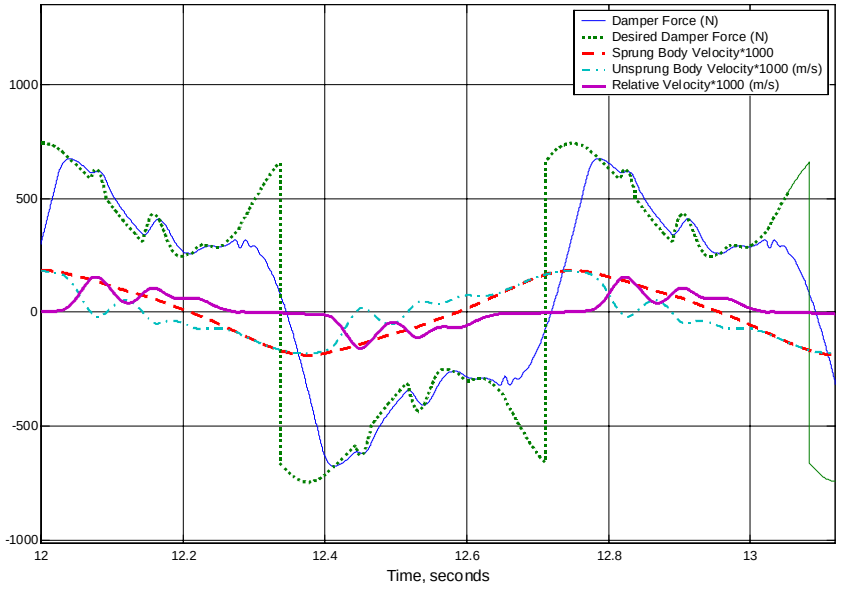

Figure 5.2-17 Steady State Response of a Single Suspension under Hybrid Control for $G = 8000$ and $\alpha = 0.5$. (1.34 Hz Sinusoidal Input)

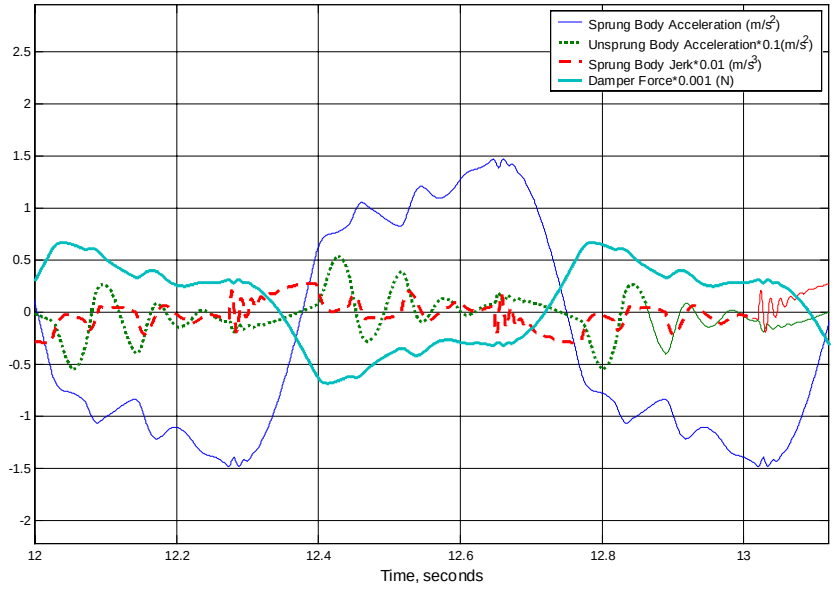

Figure 5.2-18 Steady State Response of a Single Suspension under Hybrid Control for G = 8000 and α = 0.5. (1.34 Hz Sinusoidal Input)

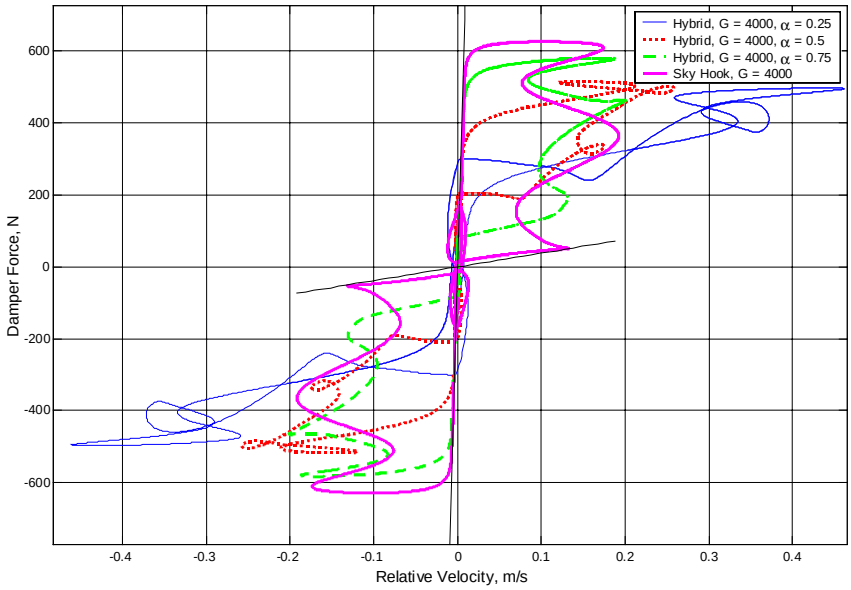

Figure 5.2-19 Comparison of the Force/Velocity Trajectory Step Responses for a Single Suspension under Hybrid Control for G = 4000. (1.34 Hz Sinusoidal Input)

5.2.3.2 10.5 Hz Sinusoid Response

Figures 5.2-20 and 21 clearly show the difference between a Hybrid controller and a Skyhook controller. When α is raised from 0.75 (Hybrid control), to 1 (Skyhook) control, the peak-to-peak and RMS performance measures at the unsprung resonant frequency, 10.5 Hz, increase. This increase occurs since the unsprung control component of Hybrid, that is Groundhook, is eliminated. In order to regain further control at this gain, G = 4000, we can decrease α which will increase the weighting on the Groundhook component. By increasing α, we reduce the ride comfort and the vehicle handling.

Increasing G causes the opposite performance measure trends, as shown in Figures 5.2-22 and 23, as does increasing α, as shown in Figures 5.2-20 and 21. Increasing G, for α = 0.5, causes all of the dynamic measures to decrease. Increasing G has the same effect as increasing the passive damping in the passive case, see Figure 4.13. Overall, raising G should improve the ride comfort and handling.

An example time trace of the Hybrid operation at 10.5 Hz reveals that the response is very smooth, as shown in Figure 5.2-24. It is interesting that the Groundhook component is always on and possibly expected since the unsprung body is very active at its resonant frequency. The Groundhook component is always on because the relative velocity and the unsprung mass velocity are always of the opposite sign. In addition, the Skyhook component is on for approximately ¾ of the time. The end result is that the sprung mass acceleration and jerk do not exhibit the excessive number of spikes, as shown in Figure 5.2-25, that were observed for the 1.34 Hz case, as shown in Figure 5.2-14. This smoother response might result in a smoother ride for the vehicle occupants.

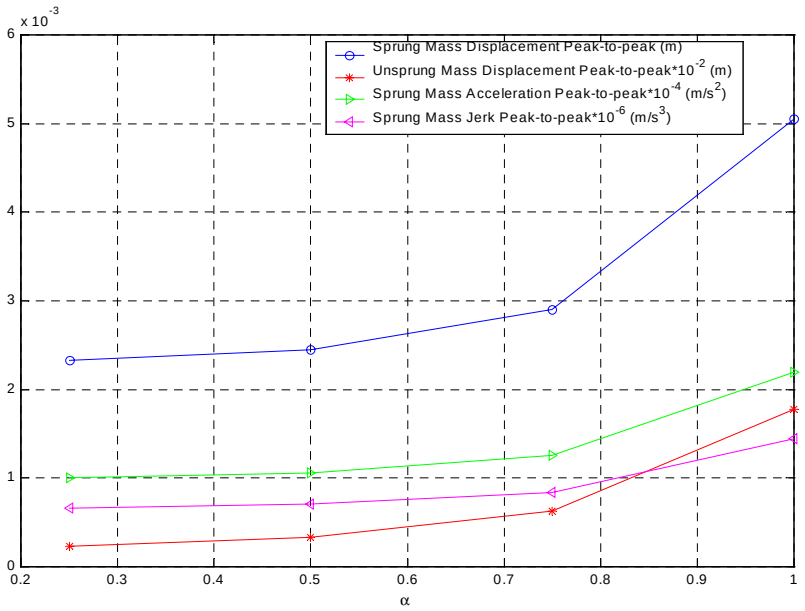

Figure 5.2-20 Effect of Varying α on the Peak-to-peak Steady State Response Performance Measures for a Single Suspension under Hybrid Control for G = 4000. (10.5Hz Sinusoidal Input)

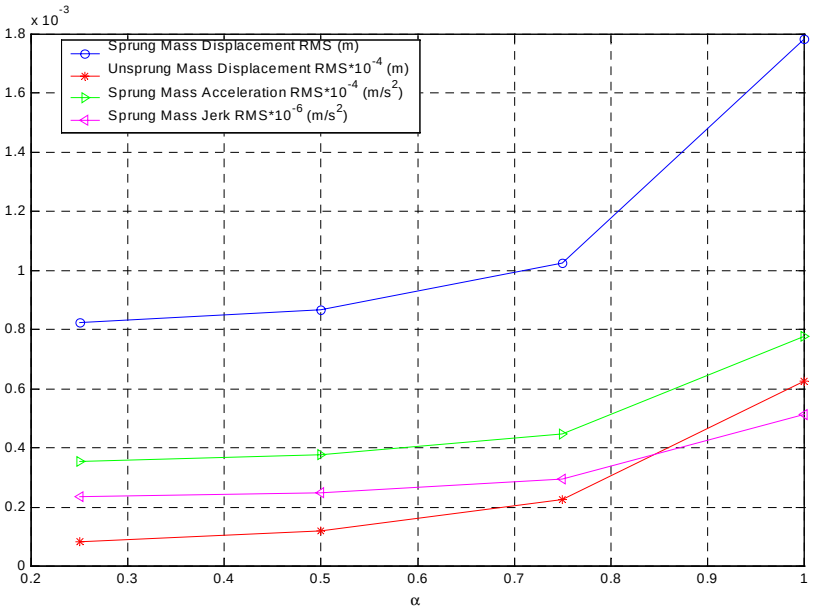

Figure 5.2-21 Effect of Varying α on the RMS Steady State Response Performance Measures for a Single Suspension under Hybrid Control for G = 4000. (10.5 Hz Sinusoidal Input)

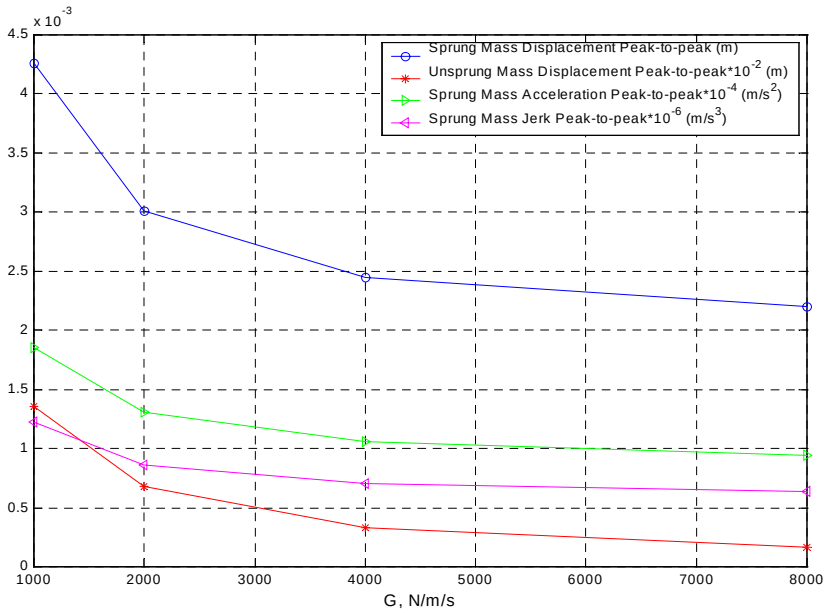

Figure 5.2-22 Effect of Varying *G* on the Peak-to-peak Steady State Response Performance Measures for a Single Suspension under Hybrid Control for $\alpha = 0.5$. (10.5 Hz Sinusoidal Input)

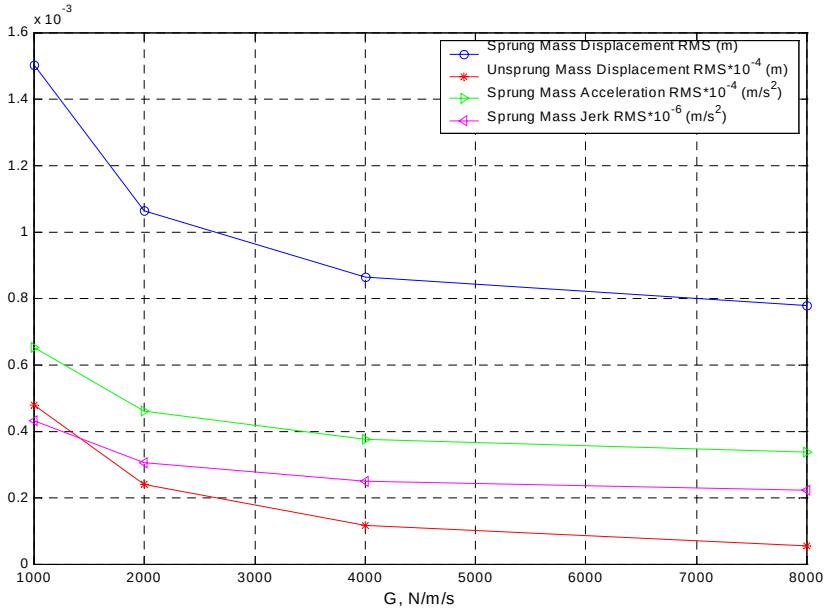

Figure 5.2-23 Effect of Varying *G* on the RMS Steady State Response Performance Measures for a Single Suspension under Hybrid Control for $\alpha = 0.5$. (10.5 Hz Sinusoidal Input)

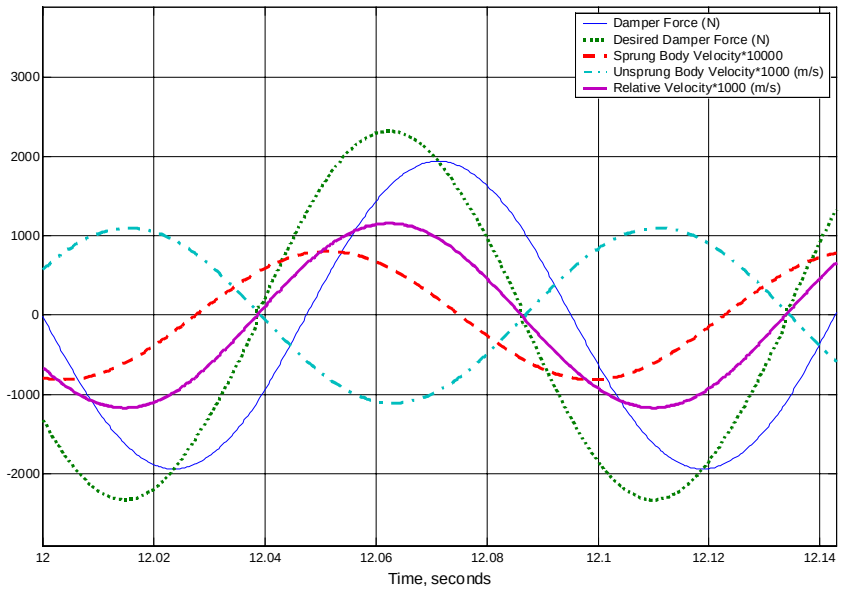

Figure 5.2-24 Steady State Response of a Single Suspension under Hybrid Control for G = 4000 and α = 0.5. (10.5 Hz Sinusoidal Input)

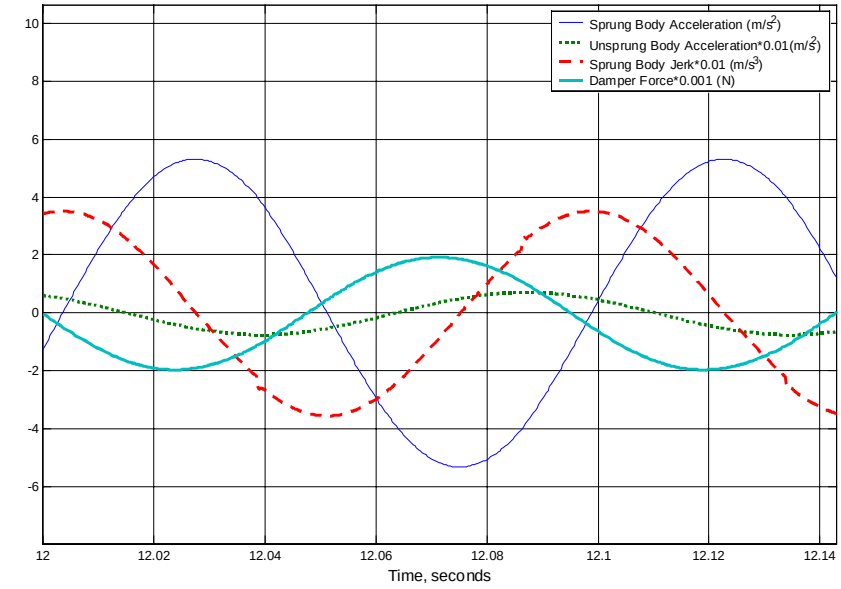

Figure 5.2-25 Steady State Response of a Single Suspension under Hybrid Control for G = 4000 and α = 0.5. (10.5 Hz Sinusoidal Input)

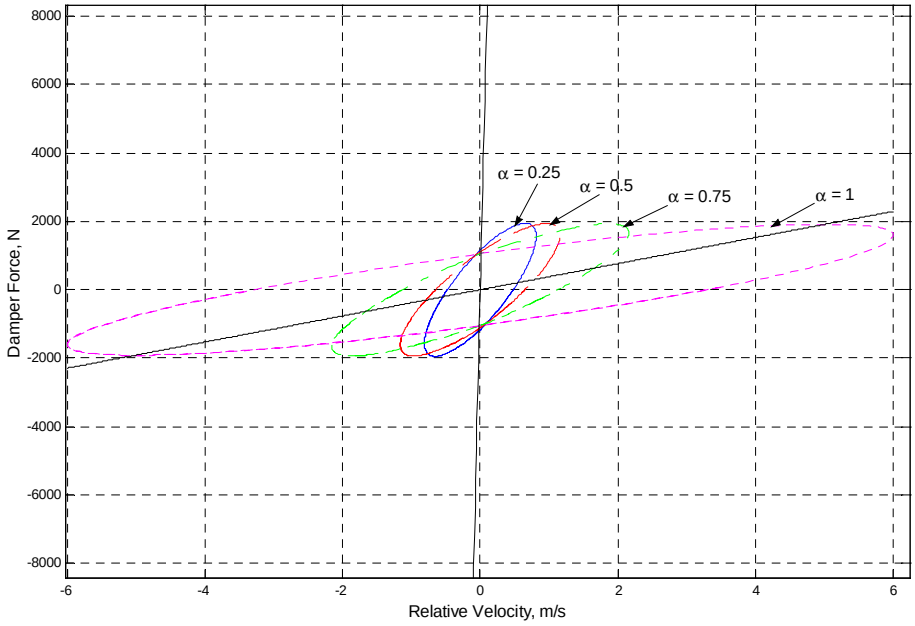

Figure 5.2-26 Comparison of the Force/Velocity Trajectory Step Responses for a Single Suspension under Hybrid Control for *G* = 4000. (10.5 Hz Sinusoidal Input)

5.2.4 Hybrid Results Summary

There are four main trade offs to recognize when dealing with the Hybrid controller.

1) The first trade off exists between improving the 1.34 Hz performance at the expense of the 10.5 Hz performance. This first trade off is seen in the Hybrid frequency spectrum results, as shown in Figure 5.2-1 and occurs when α is increased.

2) The second trade off is between improving the 1.34 Hz response and increasing the unsprung mass transient displacement response, as shown in Figure 5.2-7. This trade off occurs when α is increased.

3) The third trade off is between improving the 1.34 Hz and 10.5 Hz displacement and acceleration response and increasing the 1.34 Hz jerk, as shown in Figure 5.2.5 and 5.2.22. This trade off occurs when *G* is increased.

4) The fourth trade off is between improving the 1.34 Hz and 10.5 Hz response and increasing the acceleration and jerk of the transient response, as shown in Figure 5.2.15, 5.2.22, and 5.2.8. This trade off occurs when *G* is increased.

By varying both α and *G* we can affect the single suspension performance in a way not possible with either passive or Skyhook control.

5.3 Displacement Skyhook Control Results

The general behavior of the Displacement Skyhook law is the same as the velocity based Skyhook law. It is however a different control law with a different combination of performance values and is therefor worth comparing to the passive case at the end of this chapter. The difference in the equations of Displacement Skyhook from Skyhook is the replacement of the sprung mass velocity, v_1, with the sprung mass displacement, x_1. In this section, we will analyze the ability of Displacement Skyhook to control the behavior of the single suspension subjected to the selected test inputs.

5.3.1 Transmissibility Analysis

The Displacement Skyhook transmissibility is very similar to the Skyhook control law of Section 5.2. We can see that just as before, increasing the gain decreases the sprung mass resonant frequency, 1.34 Hz, peaks for both the sprung and unsprung mass, as shown in Figure 5.3-1. These decreases should have the effect of increasing both the ride comfort and the vehicle handling at a 1.34 Hz base excitation. In addition, changing the gain has no effect on the behavior of the unsprung resonant frequency, 10.5 Hz, peaks, for either the sprung or unsprung masses. We can not alter the ride comfort or the vehicle handling at 10.5 Hz. Even the isolation at the frequencies in between 1.34 Hz and 10.5 Hz is preserved as the gain is increased.

The relative displacement, or rattle space, also shows the same trend under Displacement Skyhook control as it did under Skyhook control. We find that increasing the gain decreases the 1.34 Hz rattle space resonant peak. This means that the suspension would take up less room, at 1.34 Hz, if the greater gains were used. Under the Displacement Skyhook control law, we still find that changes in the gain have no effect on the 10.5 Hz rattle space, which is relatively large.

The last frequency spectrum measure that we will analyze here, the acceleration power density spectrum also responds similarly to increases in the gain. As the gain is increased, the sprung mass resonant peak is reduced at 1.34 Hz. Again, the 10.5 Hz peak is not affected. The ride comfort should improve at 1.34 Hz but not at 10.5 Hz.

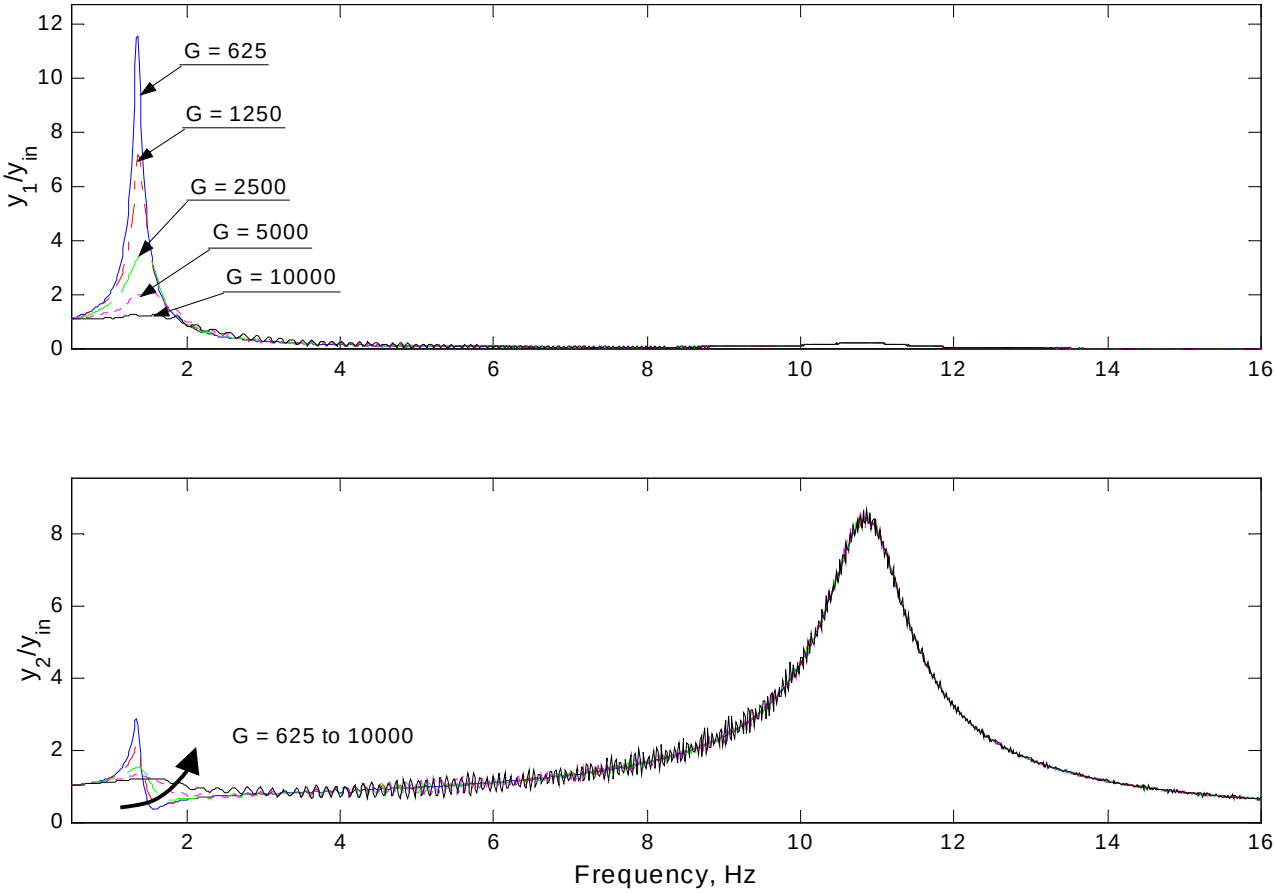

Figure 5.3-1 Transmissibility Plots of a Single Suspension under Displacement Skyhook Control. (y_1 : sprung mass displacement, y_2 : unsprung mass displacement, y_{in} : base displacement)

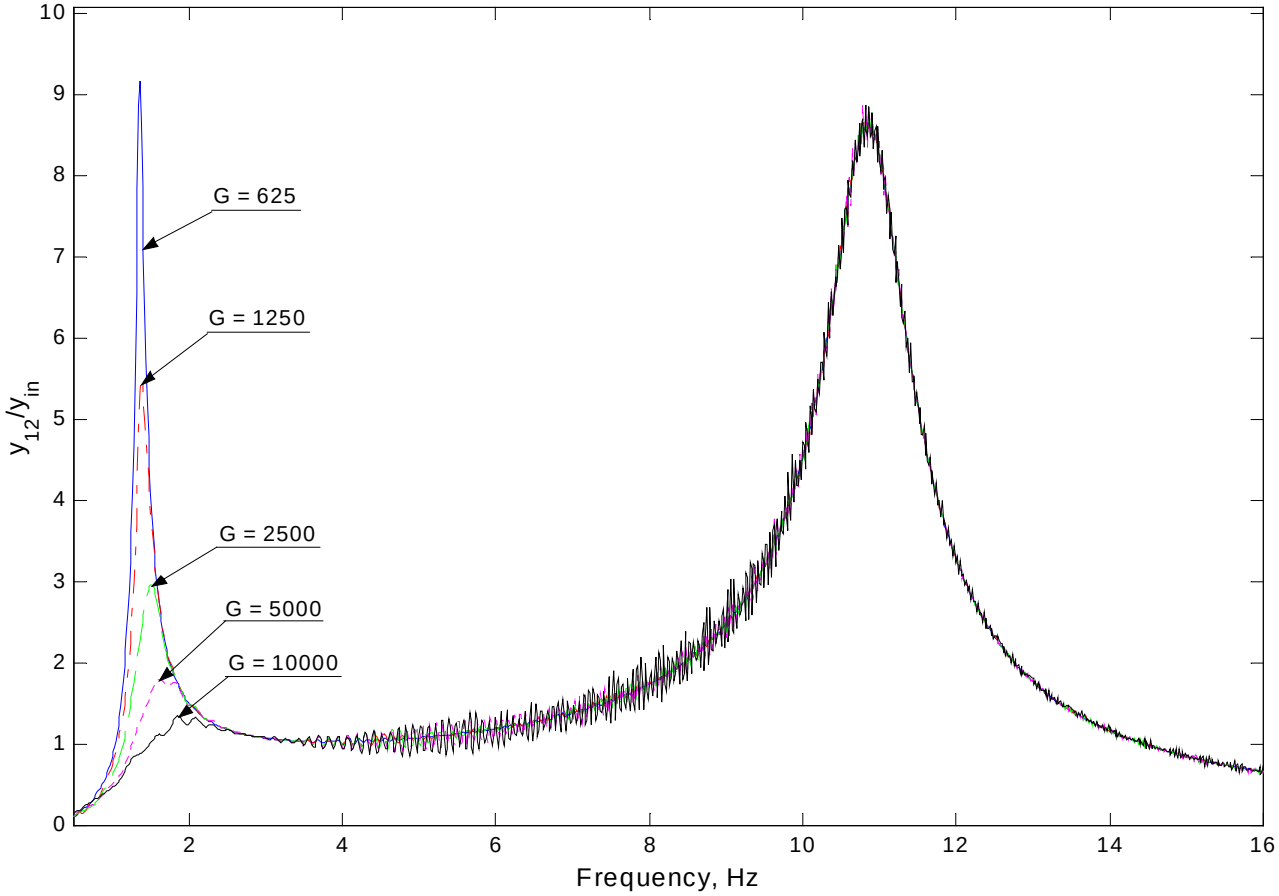

Figure 5.3-2 Relative Transmissibility of a Single Suspension under Displacement Skyhook Control. (y_{12} : relative displacement, y_{in} : base displacement)

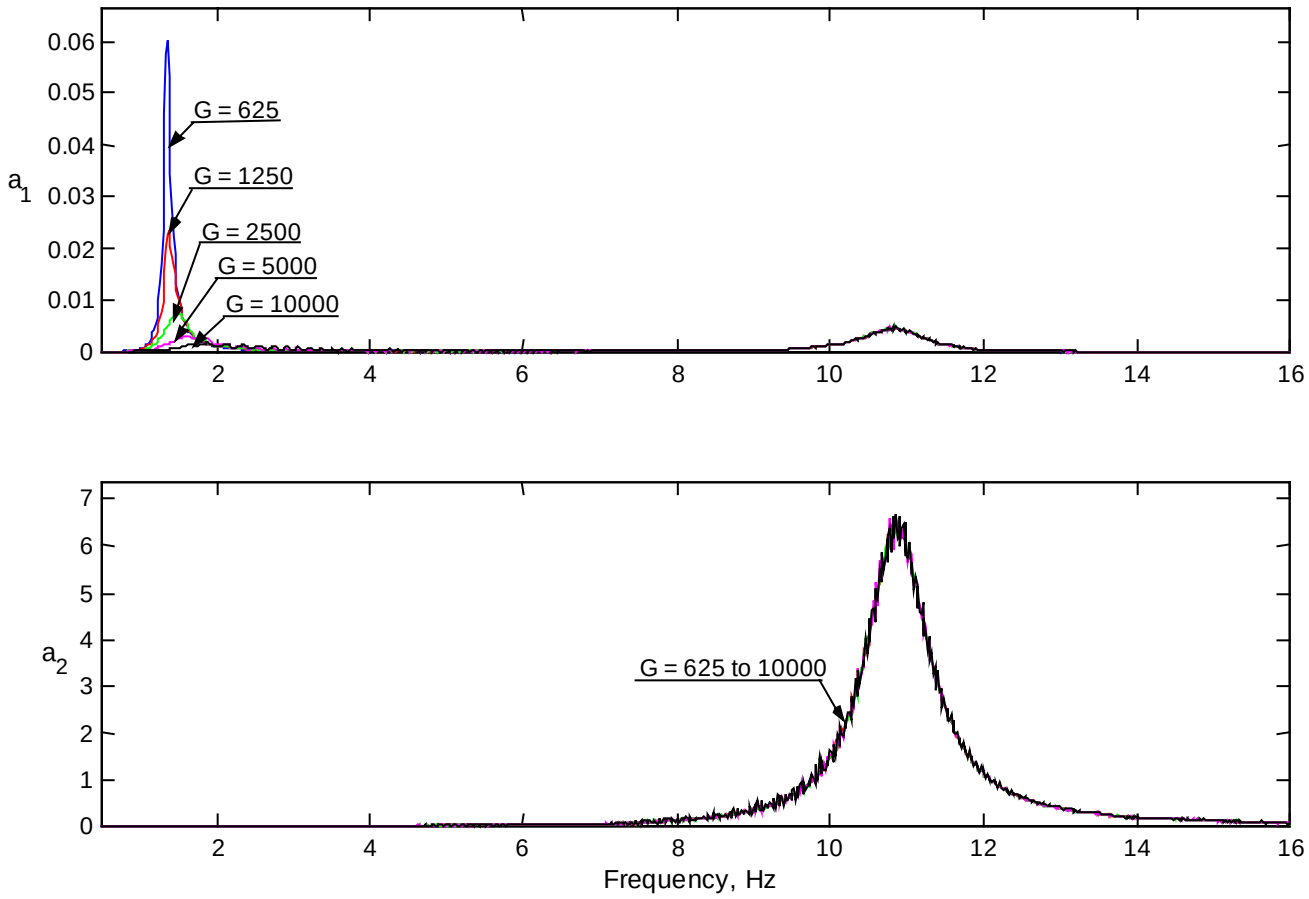

Figure 5.3-3 Acceleration Power Density Spectrum of a Single Suspension under Displacement Skyhook Control. (a_1: sprung mass acceleration power density, a_2: unsprung mass acceleration power density)

5.3.2 Transient Analysis

The only calculated step response measure that increases, as the gain is increased from G = 625 to G = 10,000, is the peak-to-peak jerk, as shown in Figure 5.3-4. This increase would detract from the ride comfort. However, increasing the gain, over the stated range, decreases the other performance measures. The settling time decreases from 9 to 0.31 seconds, the sprung and unsprung peak-to-peak displacement decrease from 0.0223 m to 0.0004 m and from 0.0151 m to 0.0119 m, respectively, and the sprung mass peak-to-peak acceleration decreases from 3.13 m/s^2 down to 2.75 m/s^2. These improvements in the performance measures, as the gain is raised, indicate that the ride comfort and the vehicle handling will improve. In total, when selecting a gain for the Displacement Skyhook, one would need to balance the increase in jerk with the decrease in the rest of the performance measures.

Note: Although it appears that we could increase the gain further in an effort to improve the step response, greater gains were not tested since the peak-to-peak 1.34 Hz acceleration and jerk at G = 10,000 are already significantly greater than the same measures selected for the Skyhook case later in Section 5.5)

One might ask, 'Why doesn't the acceleration increase when the gain is increased?' After all, when the passive damping was increased, the acceleration step response increased. The answer is the same as it was for the Skyhook results. Figure 5.3-5 shows that the desired damper force is zero during the first 0.045 seconds of the response. The damper turns off at this time regardless of the gain and limits the step input impact that gets transmitted to the sprung body. In the passive case, the large acceleration occurred at the beginning of the solution. Under Displacement Skyhook and Skyhook control, whatever impact does get transmitted to the sprung body is mainly transmitted by the spring.

Figure 5.3-4 also reveals the operation of the damper. Whenever the relative velocity and the sprung body position are of the opposite sign, the Displacement Skyhook controller

switch turns the damper off. This on/off type response is typical of the Skyhook type controllers. Every on/off of the switch causes a jerk, which can be seen in Figure 5.3-6.

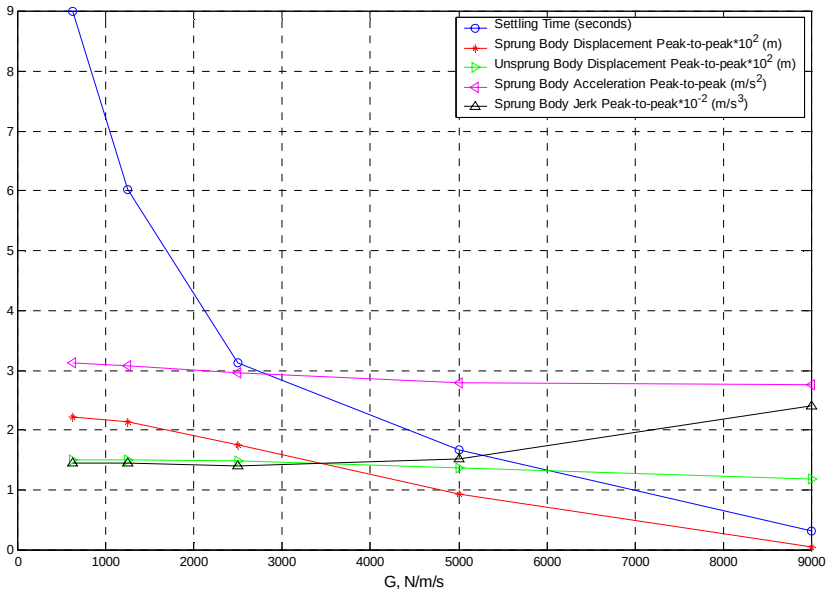

Figure 5.3-4 Effect of Varying *G* on the Peak-to-peak Step Response Performance Measures for a Single Suspension under Displacement Skyhook Control.

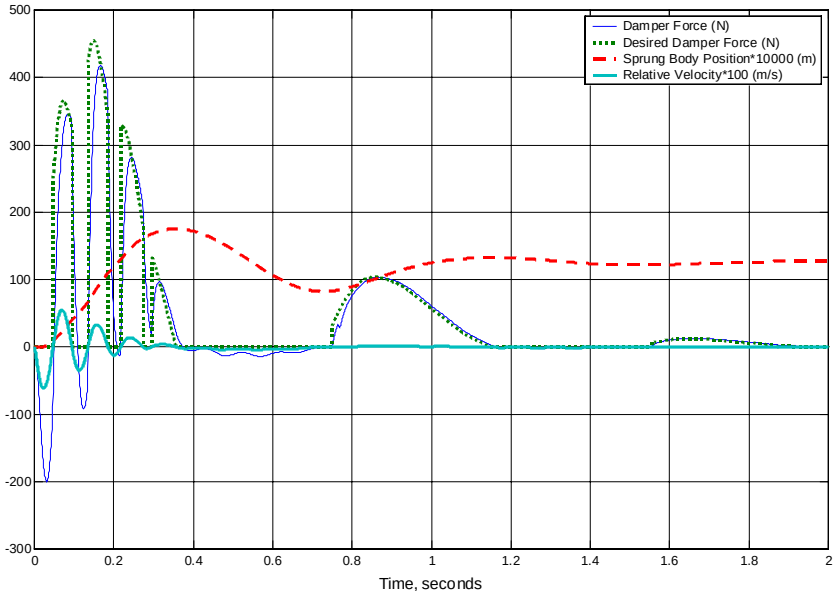

Figure 5.3-5 Step Response of a Single Suspension under Displacement Skyhook Control for G = 5000.

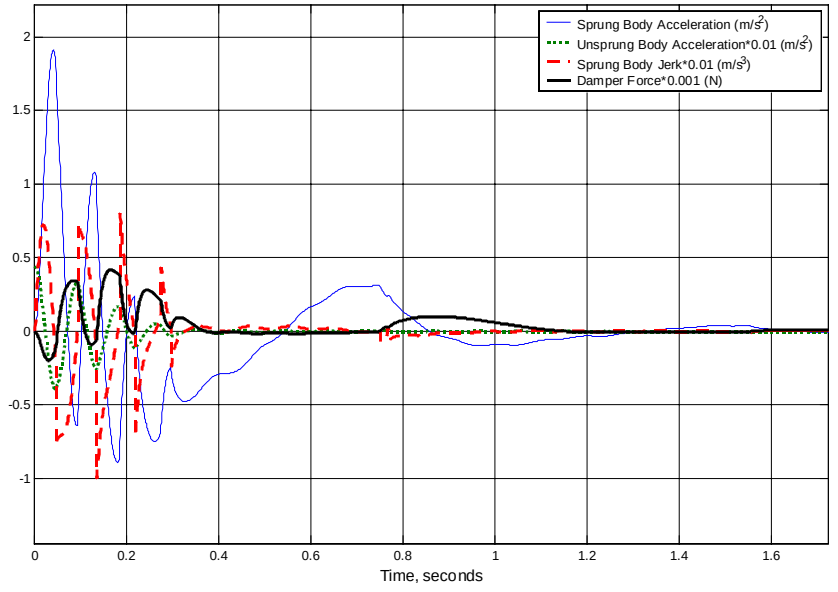

Figure 5.3-6 Step Response of a Single Suspension under Displacement Skyhook for G = 5000.

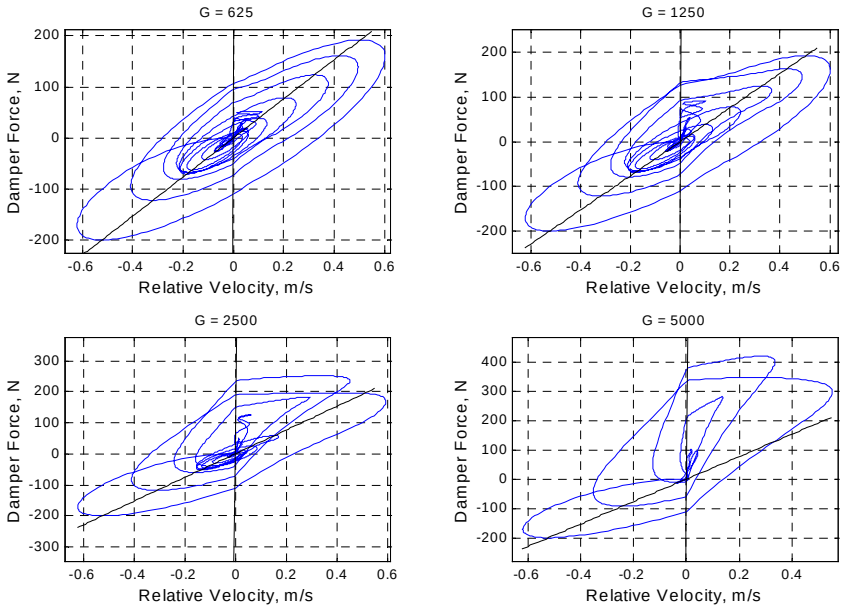

Figure 5.3-7 Comparison of the Force/Velocity Trajectory Step Responses for a Single Suspension under Displacement Skyhook Control.

5.3.3 Steady State Analysis

5.3.3.1 1.34 Hz Sinusoid Response

Again, as with the Skyhook results, increasing the gain creates a trade off at 1.34 Hz between reducing the sprung and unsprung peak-to-peak displacements and the sprung mass peak-to-peak acceleration. Over the gain range of G = 625 to 9,000, the jerk increases from 324 m/s^3 up to 648 m/s^3. This jerk increase would detract from the ride quality. On the other hand, increasing the gain decreases the sprung mass peak-to-peak displacement and peak-to-peak acceleration from 0.272 m down to 0.0329 m and from 19.2 m/s^2 down to 3.43 m/s^2 (with a minimum of 3.32 m/s^2 at G = 5000), respectively. These decreases should improve the ride comfort. Finally, over the simulated gain range, the unsprung mass peak-to-peak displacement decreases from 0.701 m to .039 m; a decrease that will improve the vehicle handling. Overall, increasing the gain during a 1.34 Hz excitation of the base sacrifices jerk performance for displacement and acceleration performance.

The RMS trends for the Displacement Skyhook 1.34 Hz sinusoidal response show the same pattern as does the Skyhook 1.34 Hz sinusoidal response. The jerk decreases from 57.4 m/s^3 at G = 625 down to a minimum of 28.6 m/s^3 at G = 2500 and then back up to 54.9 m/s^3 at G = 9000. As before, we will consider lower levels of jerk beneficial to ride comfort. Over this same gain range, the sprung mass RMS displacement and RMS acceleration decrease from 0.0987 m to 0.0123 m and from 7 m/s^2 to 1.0 m/s^2, respectively which should improve the ride comfort. The unsprung mass RMS displacement decreases from 0.0245 m to 0.0108 m. Increasing the gain from 625 to 9000 will improve the ride comfort measures, except for the jerk, and improve the vehicle handling.

The unique performances of the Skyhook laws are a consequence of the damper's semiactive operation. As with Skyhook, Displacement Skyhook causes the damper to turn on and off repeatedly when the single suspension is base excited by a 1.34 Hz sinusoidal displacement. This time, however, the sign of the sprung mass displacement helps to determine whether the damper is on or off. Looking at Figure 5.3-10, we see that

every time that the sprung body displacement is positive, the relative velocity is positive as well and the damper turns on. When the single suspension is base excited by a 1.34 Hz displacement sinusoid, under Displacement Skyhook control, the damper force exhibits a saw tooth pattern characteristic of the Skyhook laws. Based on our understanding of dynamics and Figure 5.3-11, we can see that the sudden turning on of the damper creates a relatively quick change in sprung mass acceleration and a jerk spike. We can also see that the sharp turning on of the damper coincides with the periodic start of a ringing oscillation in the sprung and unsprung mass acceleration. Overall, the saw tooth pattern creates a much more noisy response than does the linear passive damper.

Another way to look at the similarities between the Displacement Skyhook and Skyhook controlled semiactive damper operation is through examining the damper force/velocity trajectory, as shown in Figure 5.1-12. This trajectory shows how the damper characteristic maximum and minimum force lines saturate the damper force. In other words, the damper force is bound to region A and B of the damper characteristic, see Figure 3.1. We can see that increasing the Displacement Skyhook gain will decrease the maximum relative velocity (damper velocity) and increase the maximum required damper force.

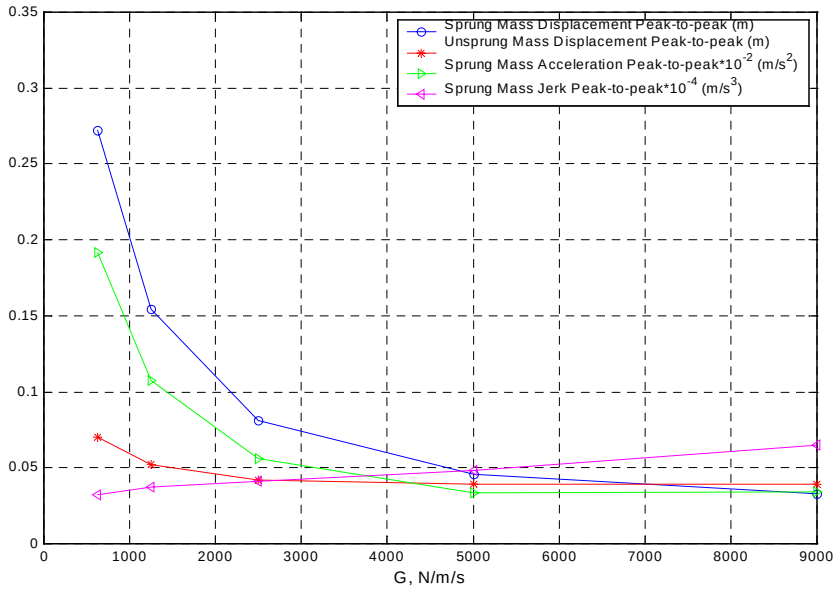

Figure 5.3-8 Effect of Varying *G* on the Peak-to-Peak Steady State Response Performance Measures for a Single Suspension under Displacement Skyhook Control. (1.34 Hz Sine Input).

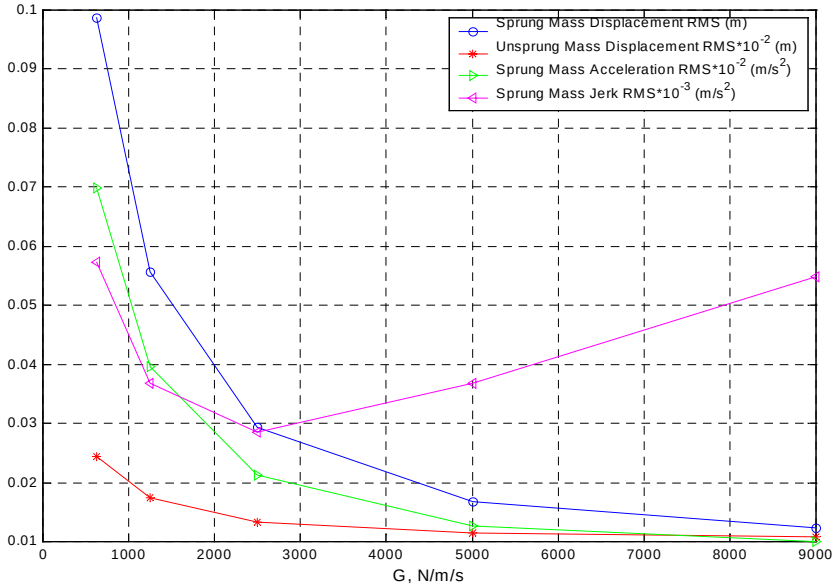

Figure 5.3-9 Effect of Varying *G* on the RMS Steady State Response Performance Measures for a Single Suspension under Displacement Skyhook Control. (1.34 Hz Sine Input).

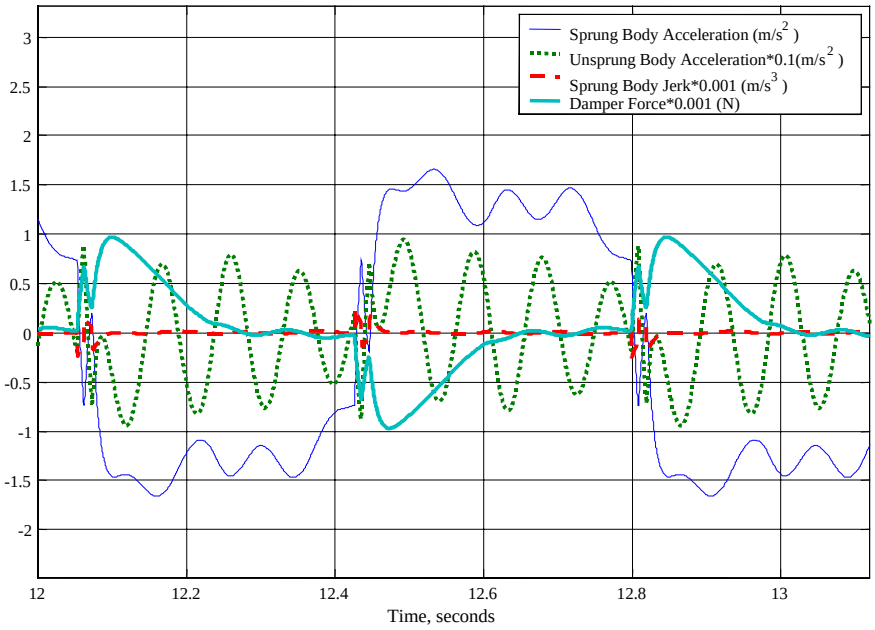

Figure 5.3-10 1.34 Hz Steady State Response of a Single Suspension under Displacement Skyhook Control for G = 5000.

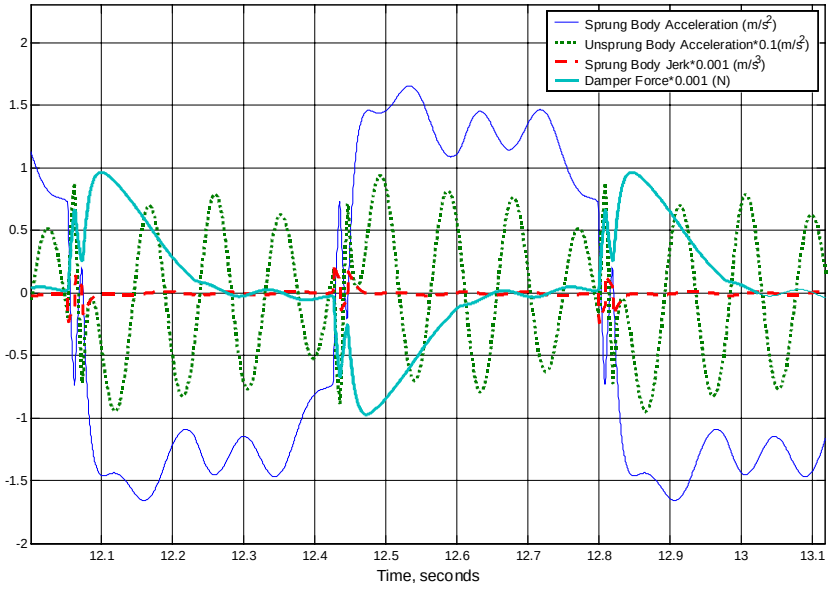

Figure 5.3-11 1.34 Hz Steady State Response of a Single Suspension under Displacement Skyhook Control for G = 5000.

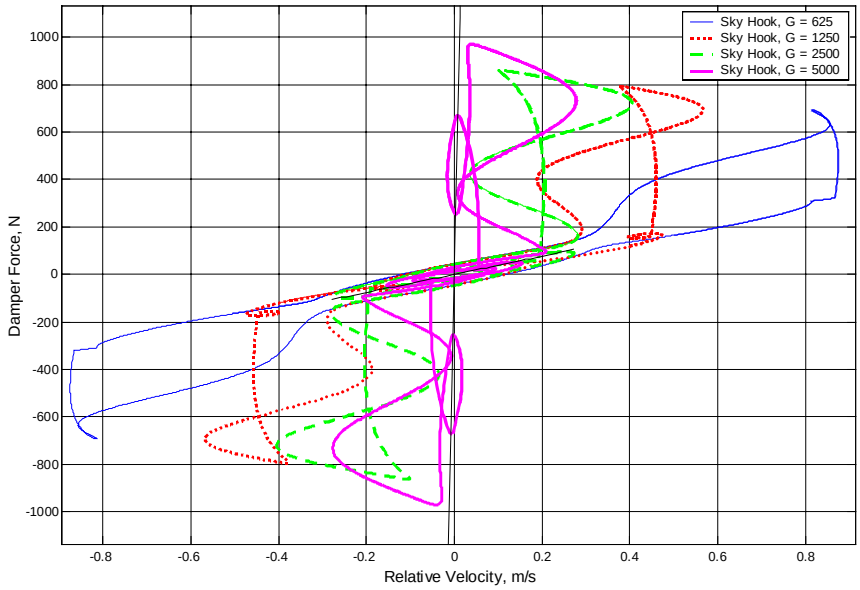

Figure 5.3-12 Comparison of the Damper Force/Velocity Trajectory 1.34 Hz Steady State Responses for a Single Suspension under Displacement Skyhook Control.

5.3.3.2 10.5 Hz Sinusoid Response

As expected, after studying the transmissibility plots in Figure 5.3-1, changing the gain has no effect on the 10.5 Hz sinusoidal response. The sprung mass peak-to-peak displacement and acceleration are fixed at 0.0051 m and 22 m/s^2 respectively. The unsprung mass peak-to-peak displacement is fixed at 0.177 m and the sprung mass jerk is fixed at 1450 m/s^3. The RMS performance measures are also not affected by changing the gain. The sprung mass RMS displacement and RMS acceleration are a constant 0.0018 m and 7.77 m/s^2 respectively. The sprung mass RMS jerk is 513 m/s^3 and the unsprung mass RMS displacement is 0.0627 m. The changing the gain will not improve the ride comfort or the vehicle handling when the suspension is subjected to a 10.5 Hz base excitation.

Changing the gain will not affect the performance at 10.5 Hz because the Displacement Skyhook controller requests forces which are below the minimum damper force

saturation line, C_{off} for any given v_{12}. In Figure 5.3-15, the desired damper force magnitude is always less than the actual damper force magnitude. The damper is moving too fast at 5% damping to allow for lower actual damper forces. Due to the damper design and MR fluid used, the damping coefficient can not be reduced below 5%. The combination of the minimum damping coefficient and the relatively fast moving damper at 10.5Hz eliminates the Displacement Skyhook controllers ability to impose its requested force on the damper.

Figure 5.3-16 shows us that because the semiactive damper is providing a smooth damper force, the sprung mass acceleration is smooth. We are assuming that the ride comfort will be more acceptable if the acceleration response is smooth rather than rough and full of spikes. The smooth response is also shown in Figure 5.3-17. Here we see that the damper is nearly always off. As it turns out, the circular nature of this damper force/velocity trajectory is caused by the filter delay; without the filter, the damper exhibits nearly pure linear 5% passive damping. Remember, changing the gain does not affect the response, therefor, all of the response lines fall on top of each other.

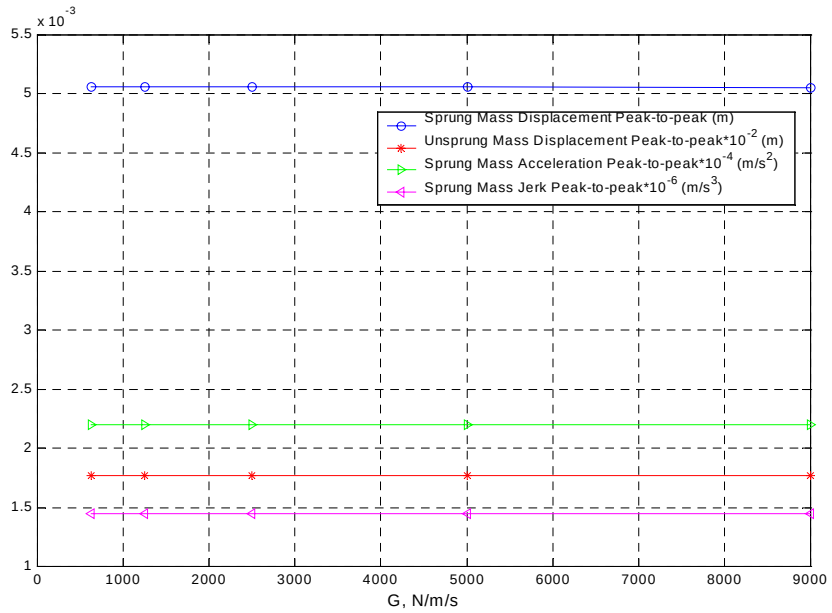

Figure 5.3-13 Effect of Varying *G* on the Peak-to-Peak Steady State Response Performance Measures for a Single Suspension under Displacement Skyhook Control. (10.5 Hz Sinusoidal Input).

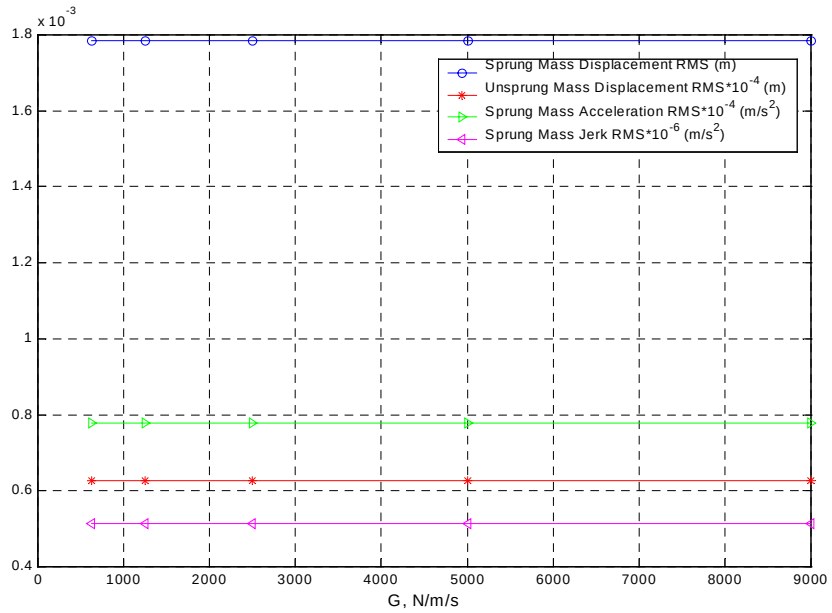

Figure 5.3-14 Effect of Varying *G* on the RMS Steady State Response Performance Measures for a Single Suspension under Displacement Skyhook Control. (10.5 Hz Sinusoidal Input).

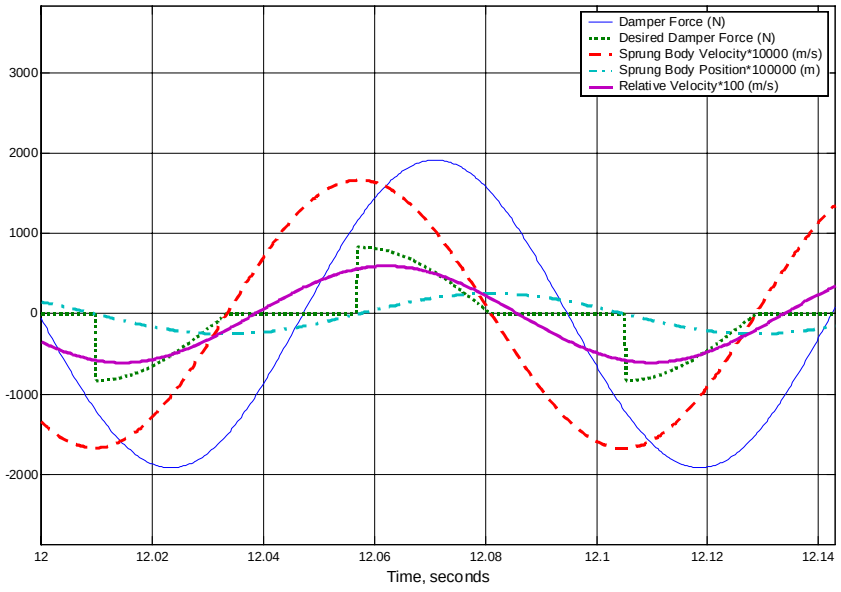

Figure 5.3-15 10.5 Hz Steady State Response of a Single Suspension under Displacement Skyhook Control for *G* = 5000.

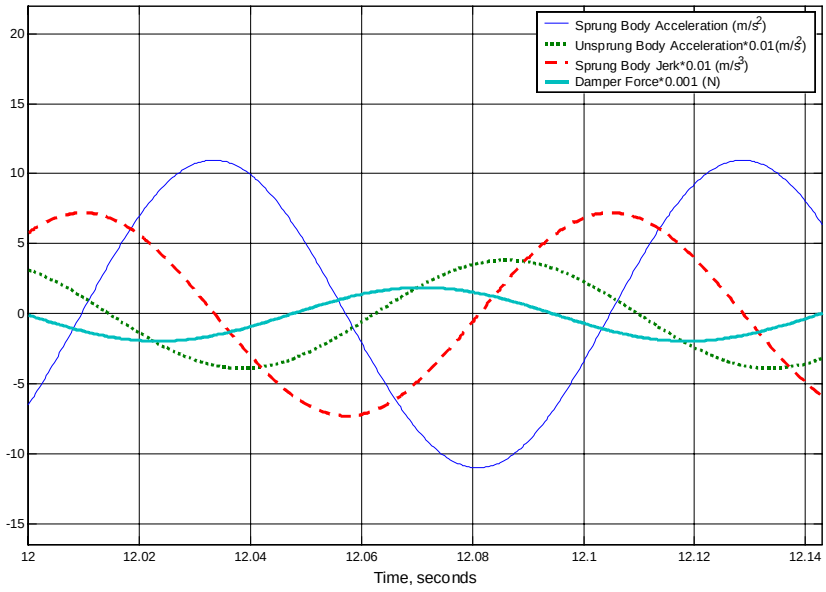

Figure 5.3-16 10.5 Hz Steady State Response of a Single Suspension under Displacement Skyhook Control for G = 5000.

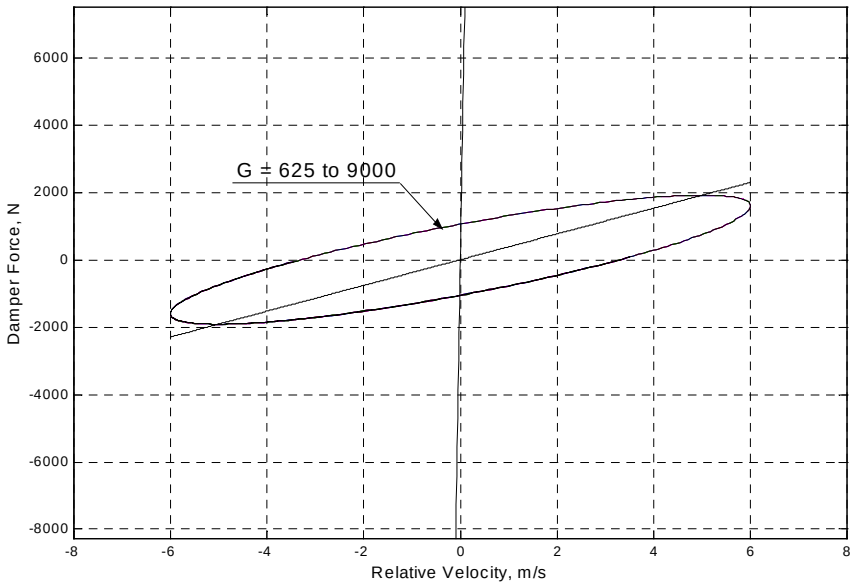

Figure 5.3-17 Comparison of the Damper Force/Velocity Trajectory 10.5 Hz Steady State Responses for a Single Suspension under Displacement Skyhook Control.

5.3.4 Displacement Skyhook Summary

The Displacement Skyhook results show similar trends as does the Skyhook results. Increasing the Displacement Skyhook gain will improve the step response sprung and unsprung mass peak-to-peak displacement and acceleration. However, the peak-to-peak jerk will increase. By increasing the Displacement Skyhook gain, we can also improve the all of the 1.34 Hz sinusoid response peak-to-peak and RMS dynamic measures, except for the jerk. However, changing the gain at 10.5 Hz does not affect the response. These are the same trends as the Skyhook trends. Section 5.5 gives performance comparisons between the two control laws.

5.4 Displacement Hybrid Control Results

5.4.1 Transmissibility Analysis

Increasing the Displacement Hybrid gain α has a similar effect on the single suspension performance as does increasing the Hybrid gain α. However, in the Displacement case, when α is increased from 0.25 to 1, the unsprung resonant frequency changes from 14 Hz to 10.5 Hz, as shown in Figure 5.4-1. Now, we have to be careful in how we interpret the unsprung resonant frequency results. The maximum response for each particular α at 10.5 Hz is not the same as the maximum in the local area. For example, claiming that $G = 5000$ and $\alpha = 0.25$ provides an unsprung resonance transmissibility of less than 2 would be incorrect as the true value is closer to 2. The effect of increasing the Groundhook component is to stiffen the tire. Apparently, this is caused by the displacement dependence of the Displacement Hybrid control switch.

When α is increased, the sprung and unsprung 1.34 Hz resonant transmissibility peaks decrease in amplitude, as shown in Figure 5.4-2. This effect should improve both ride comfort and vehicle handling at a suspension base excitation of 1.34 Hz. However, increasing α also increases the unsprung resonant transmissibility amplitude. This increase would detract from ride handling at a 10.5 Hz base excitation.

The rattle space is also affected by increases in α. As might be expected from the above results, increasing α decreases the 1.34 Hz rattle space and increases the 10.5 Hz rattle

space, as shown Figure 5.4-3. Again, a greater rattle space simply means that more space must be allotted to the suspension so that the moving parts involved do not interfere with any other surrounding parts.

As with the other control laws, the acceleration is another important measure in characterizing the suspension performance. We find that increasing α from 0.75 to 1 will significantly decrease the sprung body acceleration power density at a 1.34 Hz base excitation but will increase the acceleration power density at 10.5 Hz, as shown in Figure 5.4-3. Interestingly, increasing α from 0.25 to 0.75 has only a relatively slight effect on the sprung mass 10.5 Hz acceleration power amplitude peak. However, as with the displacement transmissibility, the unsprung resonant frequency increases.

Increasing the Displacement Hybrid gain, *G*, also has a similar effect as increasing the Hybrid gain, *G*. Increasing *G* over the range of 625 to 5000 reduces the sprung and unsprung mass 1.34 Hz displacement transmissibility, see Figure 5.4-4. This decrease should benefit both the ride comfort and the vehicle handling at a 1.34 Hz base excitation. In addition, increasing the gain reduces the 10.5 Hz sprung and unsprung mass displacement transmissibility. This displacement reduction should also improve both the ride comfort and the vehicle handling.

The rattle space is also reduced over the entire frequency spectrum, except at the invariant point, which occurs at approximately 3 Hz, as shown in Figure 5.4-5. Also, the last transmissibility performance measure that we are using, the acceleration power density, improves as the gain, *G*, is increased, as shown in Figure 5.4-6. The sprung mass 1.34 Hz and the unsprung mass 10.5 Hz resonant peaks improve the most with an increase in the gain, over the range of 625 to 5000. In sum, the greater gains will result in improved ride comfort and vehicle handling.

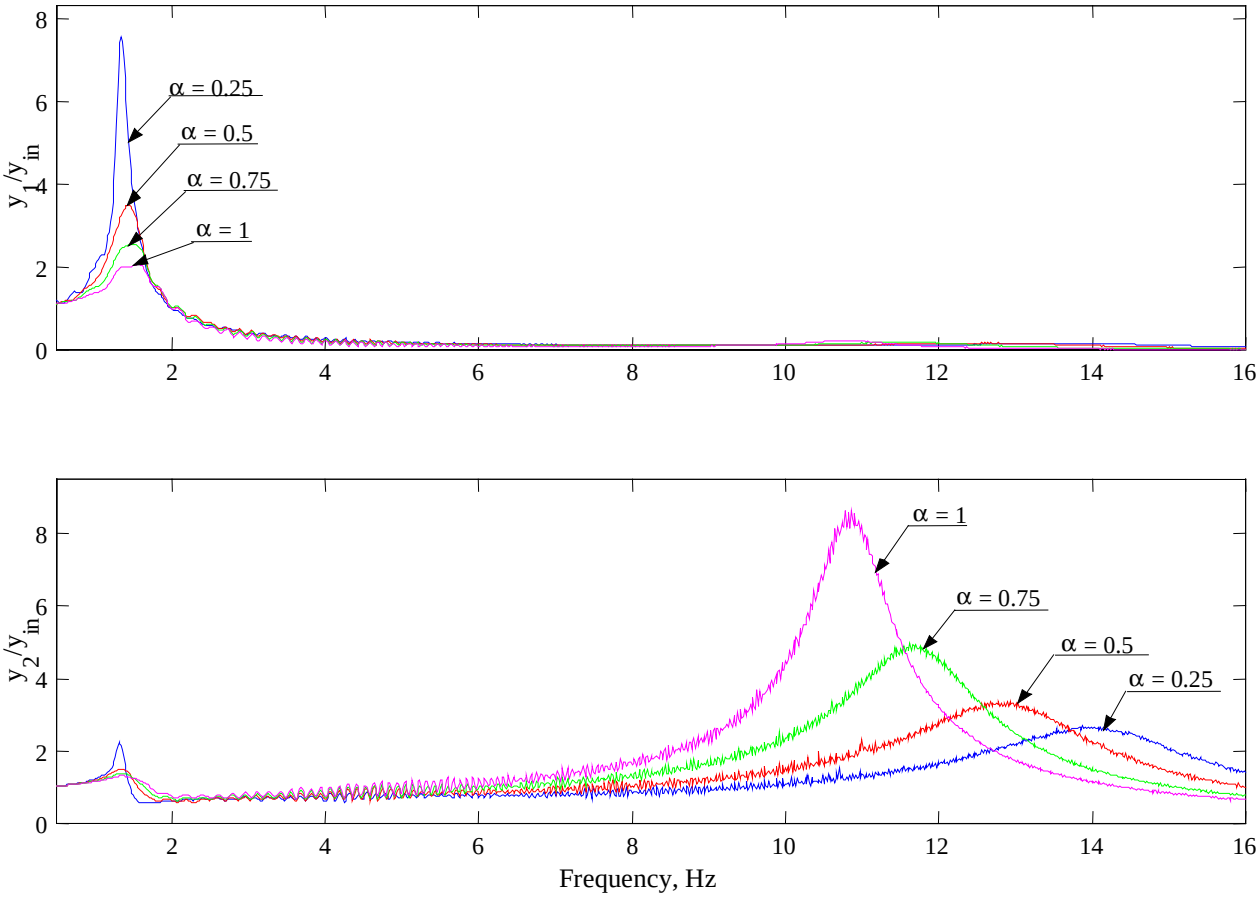

Figure 5.4-1 Transmissibility Plots of a Single Suspension under Displacement Hybrid Control with G = 5000. (y_1 : sprung mass displacement, y_2 : unsprung mass displacement, y_{in} : base displacement)

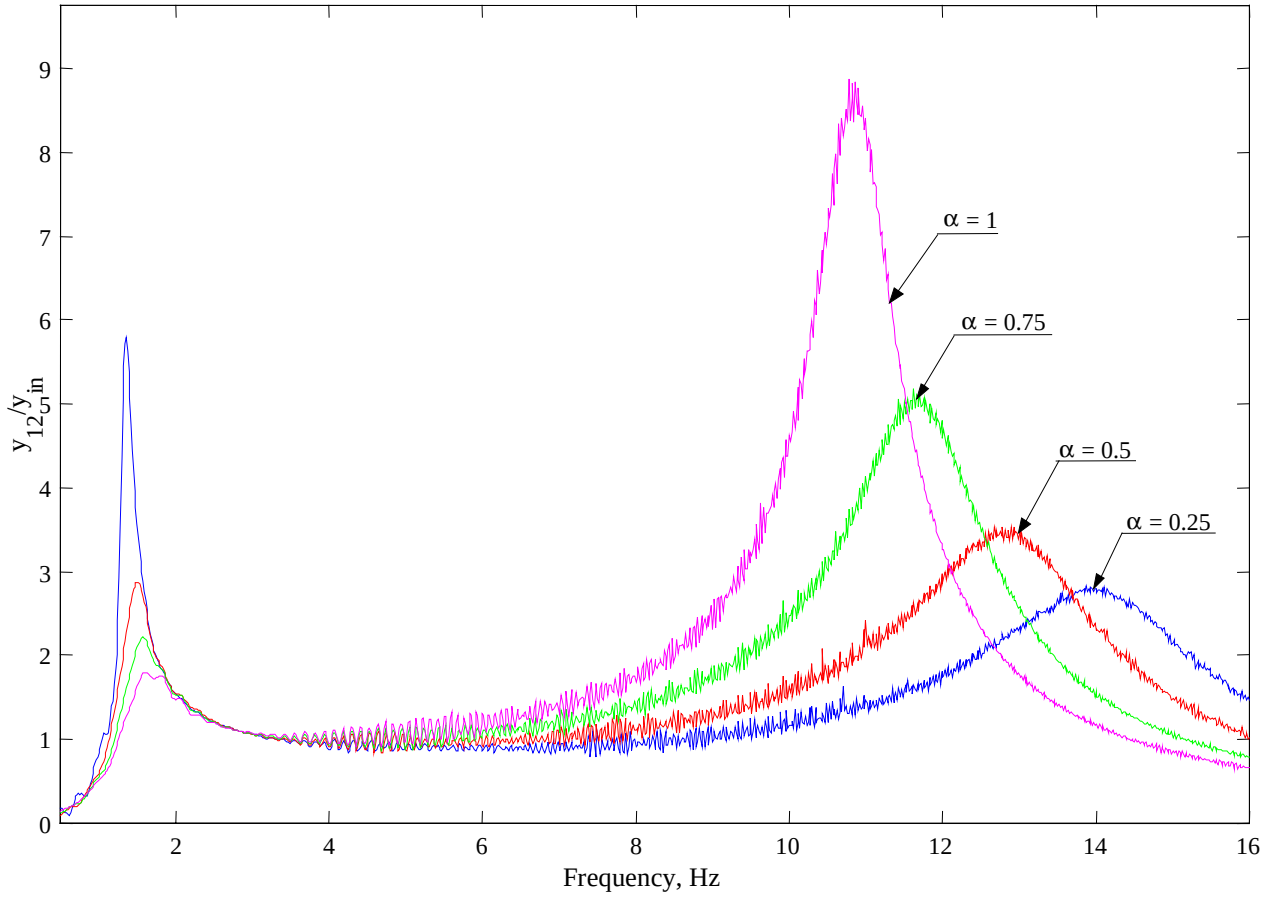

Figure 5.4-2 Relative Transmissibility of a Single Suspension under Displacement Hybrid Control for G = 5000. (y_{12} : relative displacement, y_{in} : base displacement)

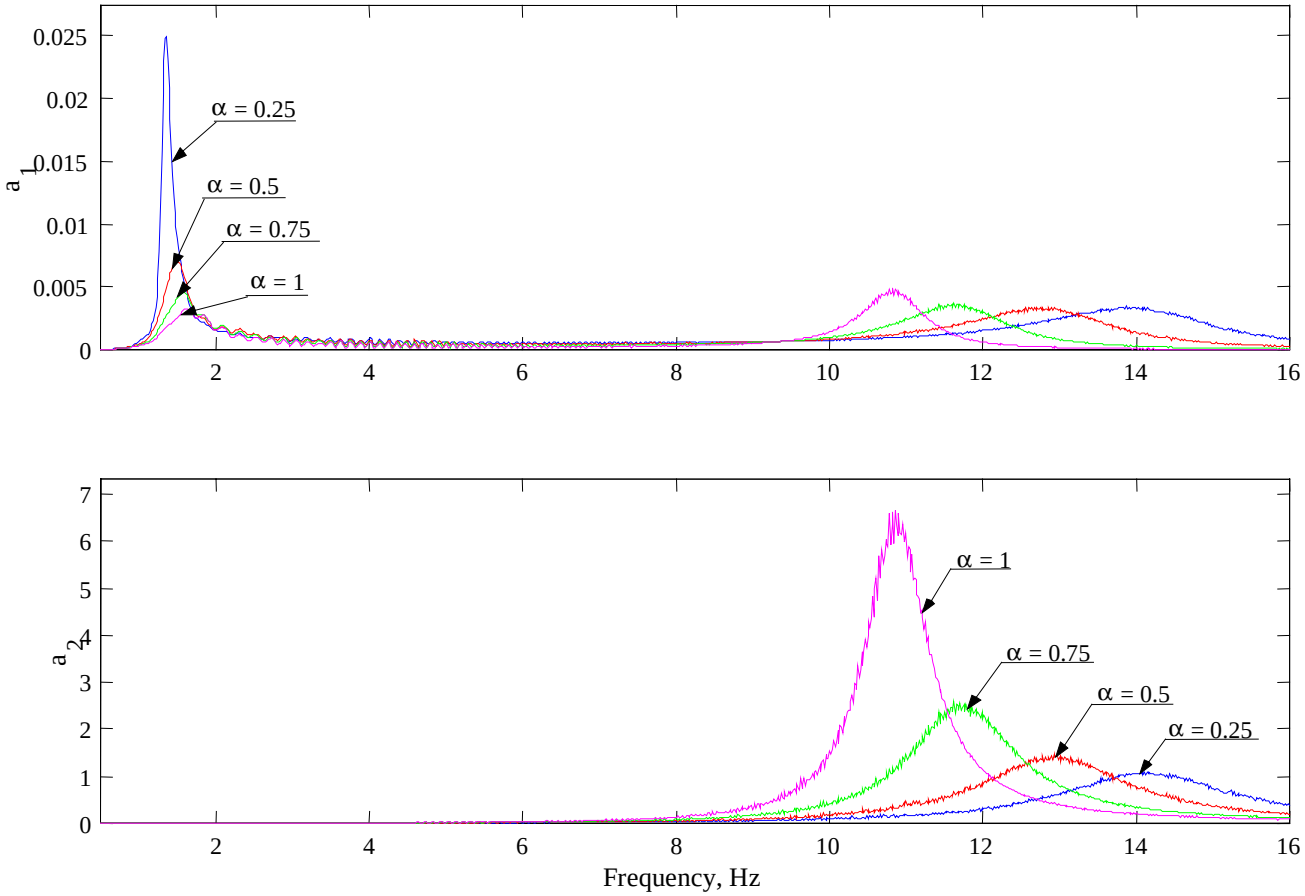

Figure 5.4-3 Acceleration Power Density Spectrum of a Single Suspension under Displacement Hybrid Control for G = 5000. (a_1: sprung mass acceleration power density, a_2: unsprung mass acceleration power density)

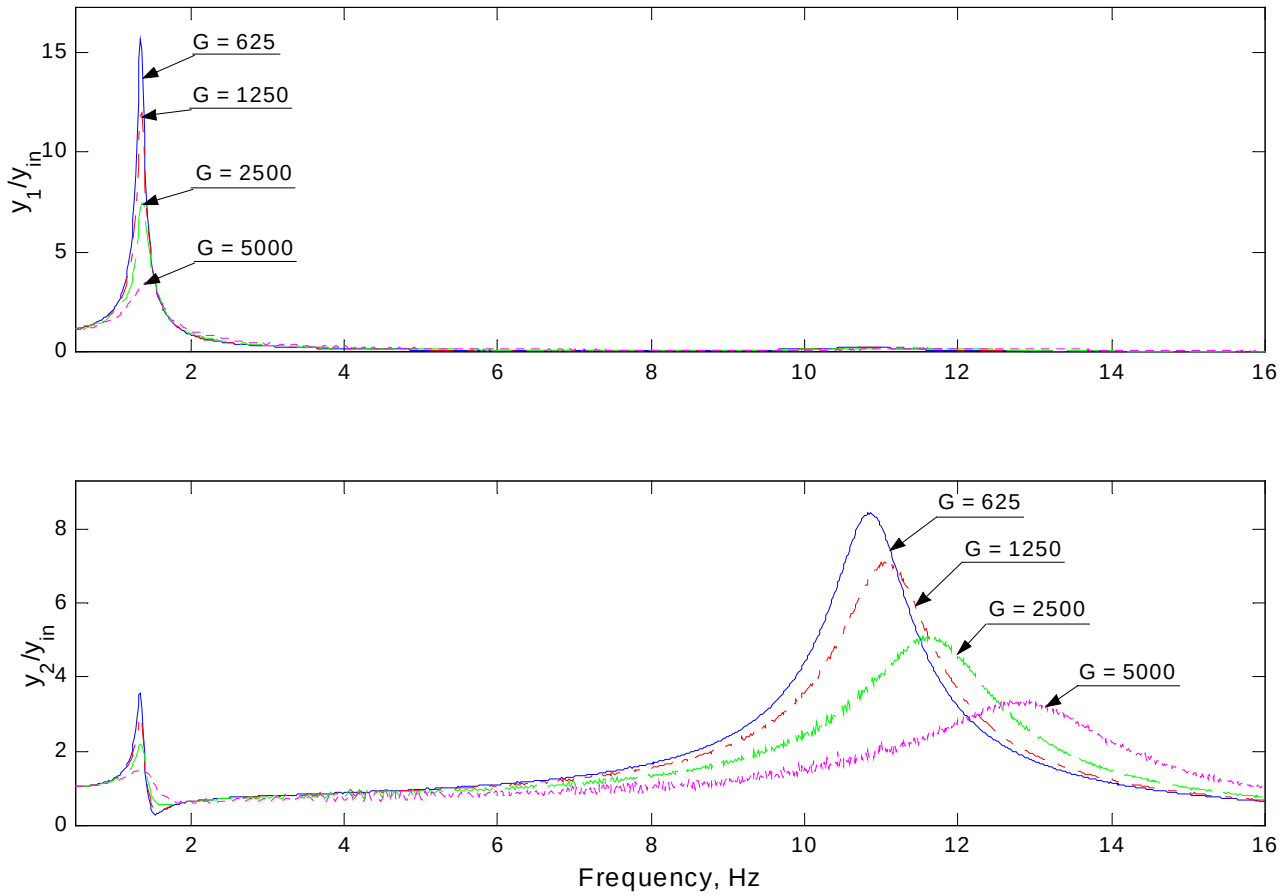

Figure 5.4-4 Transmissibility Plots of a Single Suspension under Displacement Hybrid Control with α = 5000. (y_1 : sprung mass displacement, y_2 : unsprung mass displacement, y_{in} : base displacement)

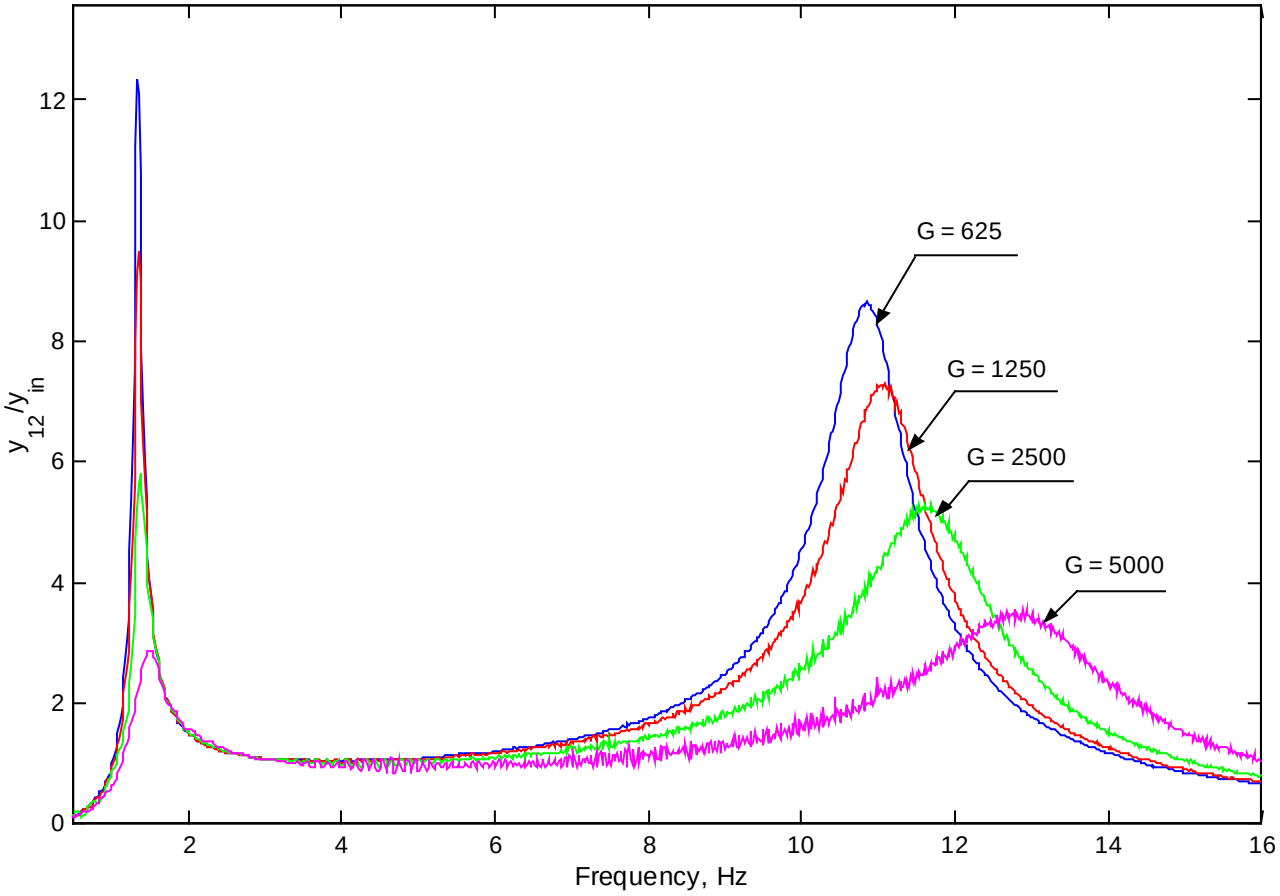

Figure 5.4-5 Relative Transmissibility of a Single Suspension under Displacement Hybrid Control for α = 5000. (y_{12} : relative displacement, y_{in} : base displacement)

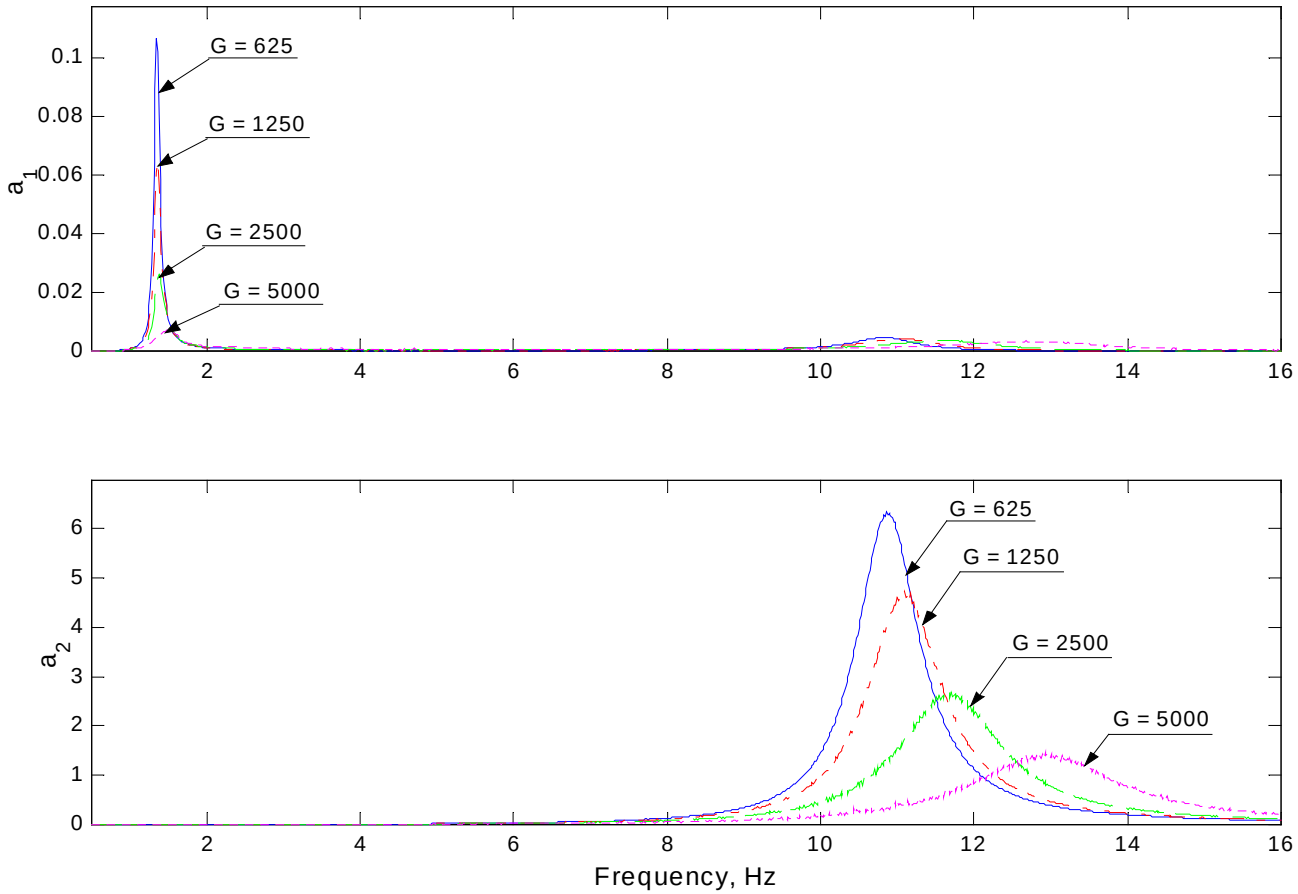

Figure 5.4-6 Acceleration Power Density Spectrum of a Single Suspension under Displacement Hybrid Control for α = 5000. (a_1: sprung mass acceleration power density, a_2: unsprung mass acceleration power density)

5.4.2 Transient Analysis

Increasing α will decrease the settling time, body position and acceleration, and even the jerk peak-to-peak, Figure 5.4-7. However, the tire position peak-to-peak increases. This is expected since we increasingly lose the Ground Hook control. These measures can be examined individually in Figures 5.4-13 through 16. The effect of increasing G is to decrease the settling time, body position, and tire position peak-to-peak measures. However, the body acceleration and the jerk increase, see Figure 5.4-8.

The Hybrid controller, as stated before, has 2 switches; one each for turning on and off the Skyhook and Groundhook components. For the displacement case, a switch is also added to zero impossible forces. Let's look at how this control law operates. During the initial phase of the step response the body position and velocity are positive, however, the damper velocity is negative and so the controller turns the damper off. This happens again around 0.5 seconds and beyond approximately 1 second. This on and off behavior is able to control the quarter car but at the same time causes jerk spikes in the solution, as shown in Figure 5.4-10.

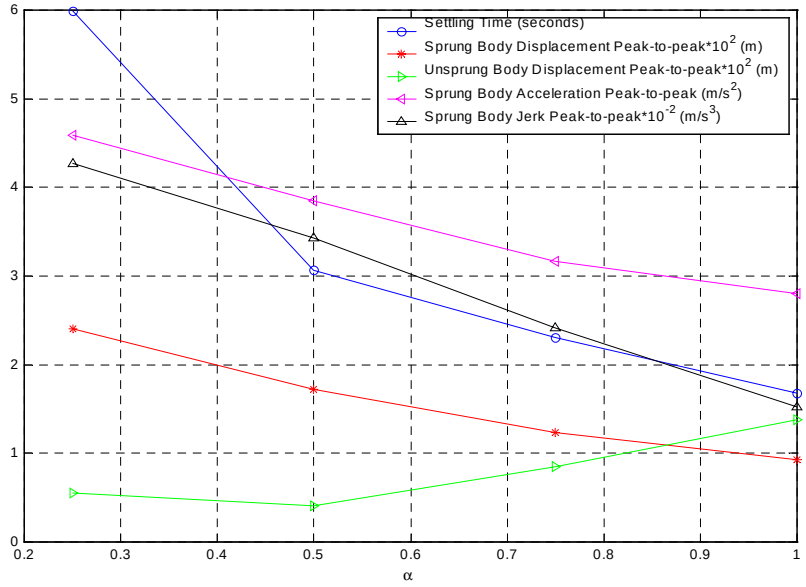

Figure 5.4-7 Effect of Varying α on the Peak-to-peak Step Response Performance Measures for a Single Suspension under Displacement Hybrid Control for G = 5000.

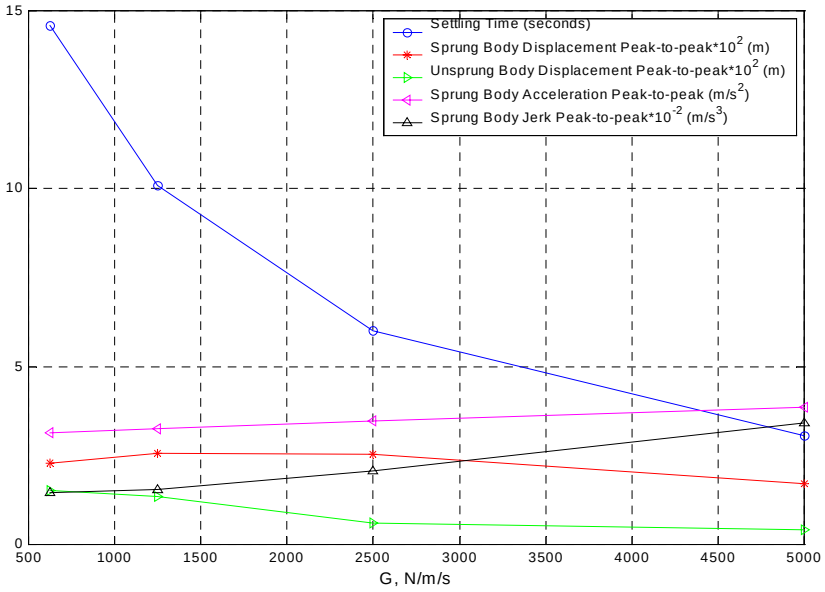

Figure 5.4-8 Effect of Varying *G* on the Peak-to-peak Step Response Performance Measures for a Single Suspension under Displacement Hybrid Control for $\alpha = 0.5$.

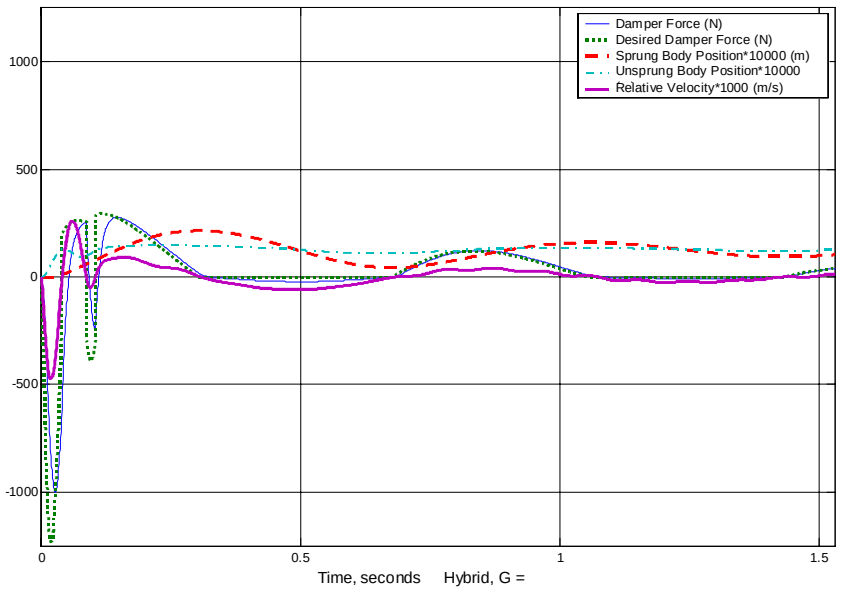

Figure 5.4-9 Step Response of a Single Suspension under Displacement Hybrid Control for $G = 5000$ and $\alpha = 0.5$.

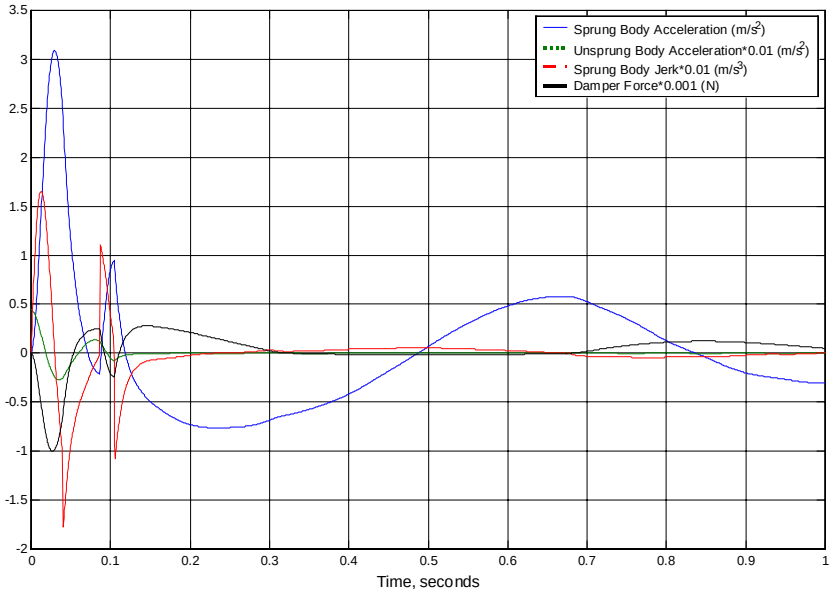

Figure 5.4-10 Step Response of a Single Suspension under Displacement Hybrid Control for G = 5000 and α = 0.5.

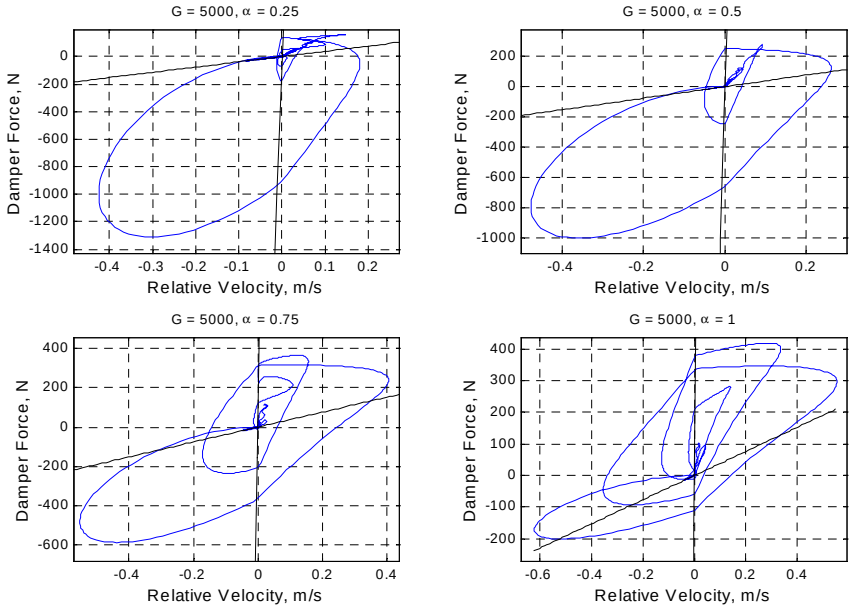

Figure 5.4-11 Comparison of the Force/Velocity Trajectory Step Responses for a Single Suspension under Displacement Hybrid Control for G = 4000.

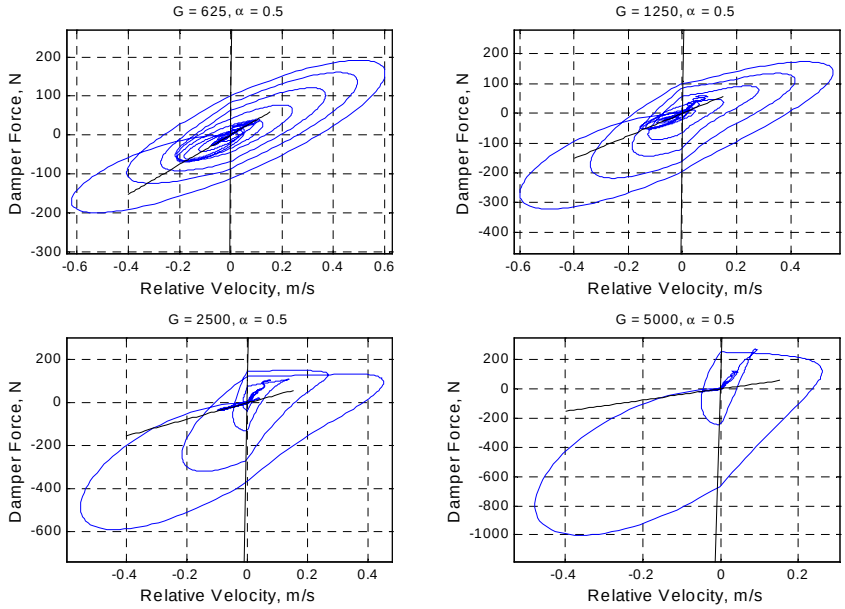

Figure 5.4-12 Comparison of the Force/Velocity Trajectory Step Responses for a Single Suspension under Displacement Hybrid Control for α = 0.5.

5.4.3 Steady State Analysis

5.4.3.1 1.34 Hz Sinusoid Response

Weighting the Displacement Hybrid control law towards Displacement Skyhook, by increasing α, trades an increase in sprung body peak-to-peak jerk for decreases in sprung and unsprung body peak-to-peak displacements as well as a decrease in the sprung body peak-to-peak acceleration, Figure 5.4-13. Over the gain range of α = 0.25 to 1, the sprung and unsprung mass displacements decrease from 0.155 m down to 0.046 m and from 0.0518 m down to 0.0391 m, respectively. These displacement decreases should improve the ride comfort and the vehicle handling. The sprung mass acceleration decreases by 10.8 m/s^2 down to 3.32 m/s^2 while jerk increases from 374 m/s^3 up to 482 m/s^3. The acceleration decrease would benefit ride comfort while the jerk increase would detract from ride comfort. Overall, increasing α would improve vehicle handling and alter ride comfort depending on how a rider values displacement, acceleration, and jerk.

Increasing the Displacement Hybrid gain α also decreases all of the RMS dynamic measures, except for jerk, as shown in Figure 5.4-14. Over the range of α = 0.25 to 1, the sprung and unsprung mass RMS displacements decrease from 0.0557 m down to 0.0168 m and from 0.0174 m down to 0.0114 m, respectively. The sprung mass RMS acceleration decreases from 4 m/s^2 down to 1.26 m/s^2. The RMS jerk dips down from 36.8 m/s^3 to 28.7 m/s^3 over α = 0.25 to 0.5 and then increases to 37.2 m/s^3 at α = 0.75 before dipping to 36.8 m/s^3 at α = 1. For the most part, increasing α improves the ride comfort and the vehicle handling, although, the jerk is not necessarily improved.

Increasing *G*, over the gain range of 625 to 9000, will decrease all of the performance measures, except, of course, the peak-to-peak jerk, as shown in Figure 5.4-15. The sprung and unsprung body peak-to-peak accelerations are decreased from 0.4 m to 0.0499 m and from 0.0889 m to 0.0391 m, respectively. In addition, the sprung body peak-to-peak acceleration decreases from 28.5 m/s^2 down to 3.53 m/s^2. The peak-to-peak jerk, however, increases, from 247 m/s^3 up to 608 m/s^3. In sum, we find that increasing the gain improves the vehicle handling and, according to the displacement and acceleration,

improves the ride comfort. Although, the increasing jerk measure detracts from the ride comfort.

We can also take a brief look at how the RMS performance measures are affected by increasing the gain. All of the RMS performance measures shown in Figure 5.4-16 decrease as the gain is increased from G = 625 to 9000, except for the RMS jerk, which increases between G = 5000 and G = 9000. The sprung and unsprung RMS displacements decrease from 0.147 m to 0.0182 m and from 0.0323 m down to 0.0116 m, respectively. The sprung body acceleration decreases from 10.4 m/s^2 and from 1.36 m/s^2. The RMS jerk decreases from 83.1 m/s^3 down to 28.7 m/s^3 at G = 5000 and then increases to 43.4 m/s^3 by G = 9000.

The performance measures discussed above are the result of a slightly different control mechanism than that of Hybrid control. Comparing the definition of Displacement Hybrid, equation (3.11), to the Hybrid equation, (3.9), we find that the Displacement Hybrid switch is operated, in part, by the sprung body position as opposed to the sprung body velocity. The end effect, at G = 5000 and α = 0.5, is that the Displacement Hybrid damper force has a sawtooth pattern similar to that of Skyhook, see Figure 5.4-17. For example, at 12.8 seconds, the damper force increases from near zero to approximately 800 N in less than a tenth of a second. This sharp increase in the damper force creates a quick change in acceleration and, consequently, a spike in the jerk.

Another way, as mentioned for the other cases, to examine the damper by looking at the damper force/velocity trajectory, as shown in Figure 5.4-18. The damper force/velocity relationship clearly shows that the minimum and maximum force lines are saturating the damper forces. Within this available damping envelope, as α is increased, the maximum damping force increases for the same velocity. In other words, there is more activity in the higher damping coefficient region for greater α. This increased damping is associated with the decrease in the sprung and unsprung mass displacements and the decrease in acceleration that occurs as α is increased, as shown in Figure 5.4-13.

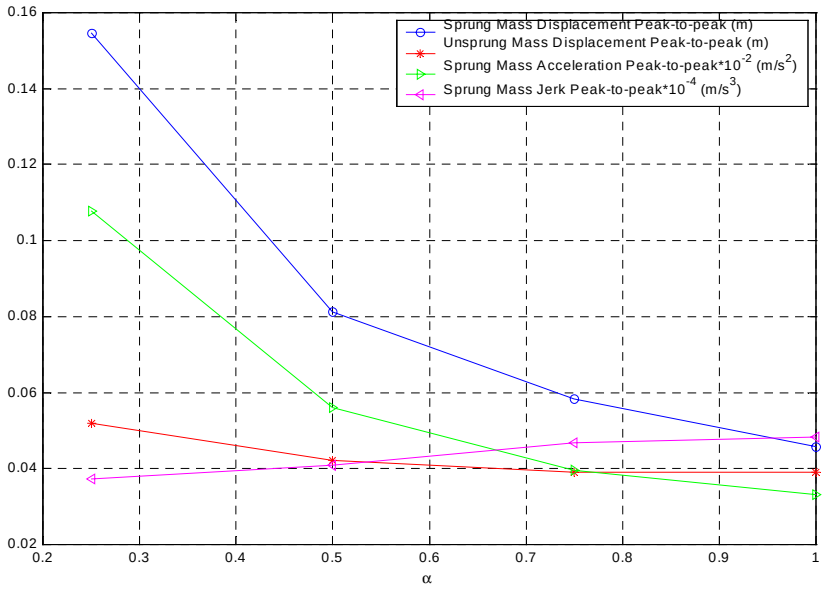

Figure 5.4-13 Effect of Varying α on the Peak-to-peak Steady State Response Performance Measures for a Single Suspension under Displacement Hybrid Control for G = 5000. (1.34 Hz Sinusoidal Input)

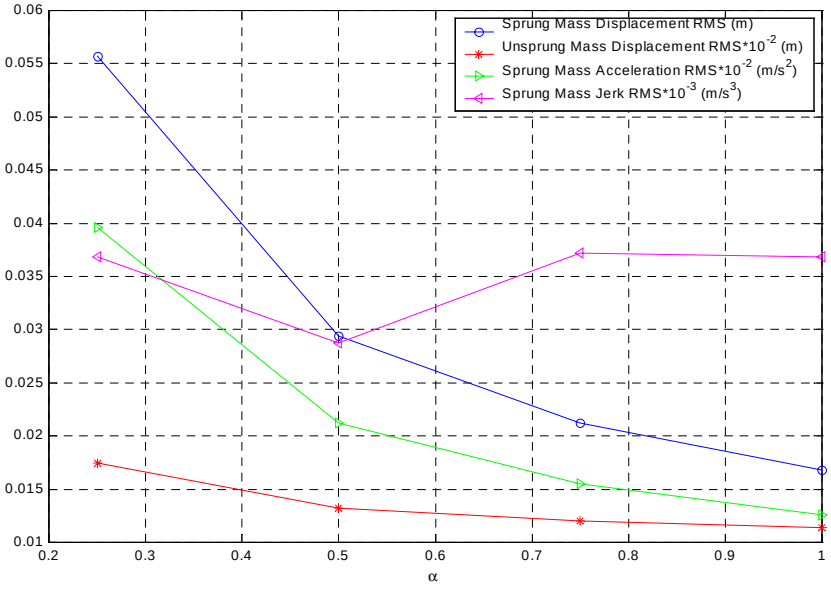

Figure 5.4-14 Effect of Varying α on the RMS Steady State Response Performance Measures for a Single Suspension under Displacement Hybrid Control for G = 5000. (1.34 Hz Sinusoidal Input)

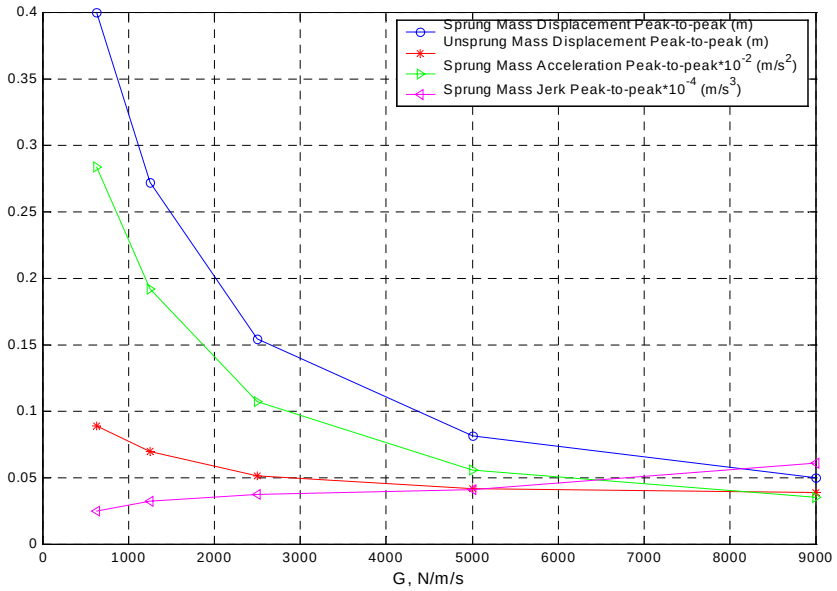

Figure 5.4-15 Effect of Varying *G* on the Peak-to-peak Steady State Response Performance Measures for a Single Suspension under Displacement Hybrid Control for $\alpha = 0.5$. (1.34 Hz Sinusoidal Input)

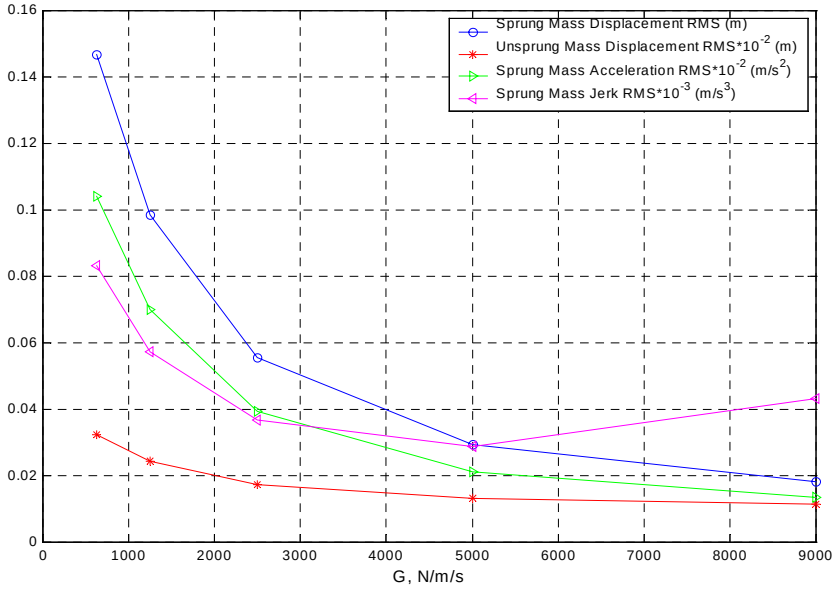

Figure 5.4-16 Effect of Varying *G* on the RMS Steady State Response Performance Measures for a Single Suspension under Displacement Hybrid Control for $\alpha = 0.5$. (1.34 Hz Sinusoidal Input)

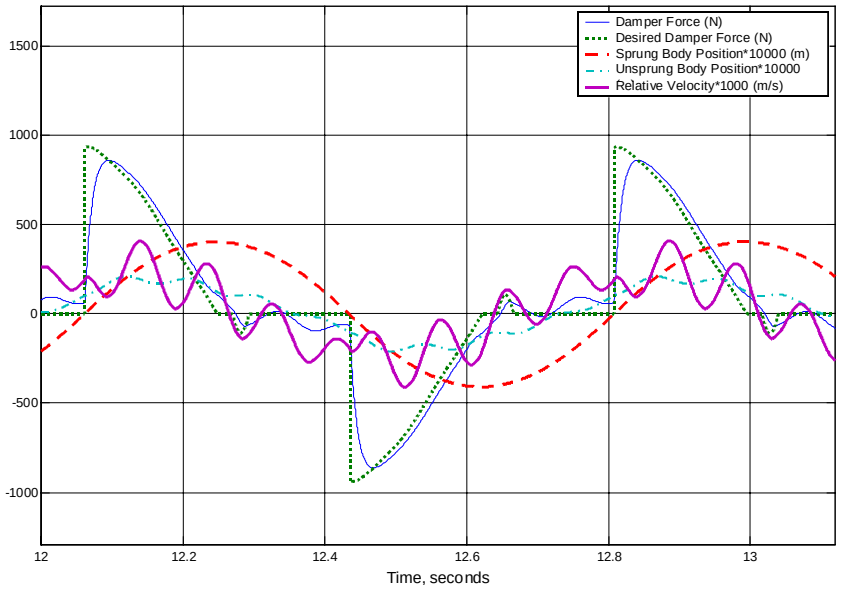

Figure 5.4-17 Steady State Response of a Single Suspension under Displacement Hybrid Control for G = 5000 and α = 0.5. (1.34 Hz Sinusoidal Input)

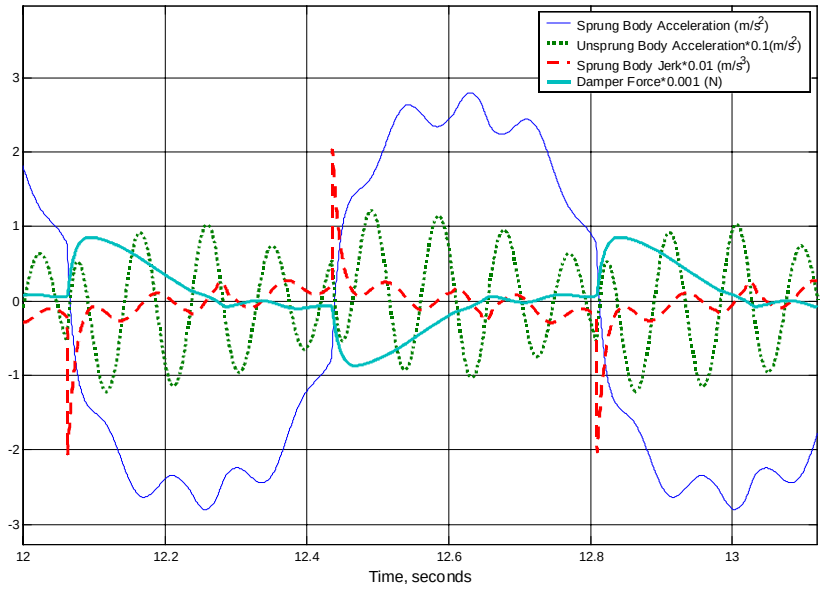

Figure 5.4-18 Steady State Response of a Single Suspension under Displacement Hybrid Control for G = 5000 and α = 0.5. (1.34 Hz Sinusoidal Input)

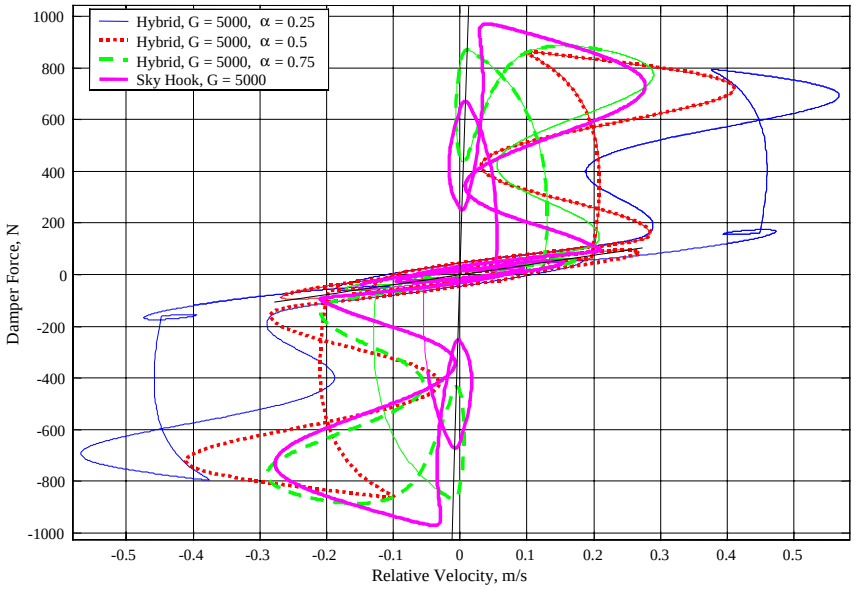

Figure 5.4-19 Comparison of the Force/Velocity Trajectory Steady State Responses for a Single Suspension under Displacement Hybrid Control for *G* = 5000. (1.34 Hz Sinusoidal Input)

5.4.3.2 10.5 Hz Sinusoid Response

As was the case with the Hybrid results, increasing the Displacement Hybrid gain, α, at 10.5 Hz increases all of the performance measures except for the jerk, which decreases, as shown in Figure 5.4-21. Increasing α from 0.25 to 1 increases the sprung and unsprung mass peak-to-peak displacements from 0.0026 m to 0.0051 m and from 0.0294 m to 0.177 m, respectively. In addition, the sprung mass peak-to-peak acceleration increases from 13.1 m/s^2 to 22 m/s^2. However, the sprung mass peak-to-peak jerk decreases from 1800 m/s^3 down to 1450 m/s^3. Increasing α to full Skyhook adversely affects the vehicle handling and the ride comfort, except for the effect of the increased jerk on the ride comfort.

However, all of the RMS performance measures, even the RMS jerk, increase as we increase α at G = 5000, as shown in Figure 5.4-22. The sprung and unsprung mass RMS displacements increase from 0.0009 m to 0.0018 m and from 0.0105 m to 0.0627 m respectively. The sprung mass RMS acceleration increases from 4.04 m/s^2 to 7.77 m/s^2 while the RMS jerk increases from 334 m/s^3 to 513 m/s^3. All of these increases will detract from the ride comfort and vehicle handling at a base excitation of 10.5Hz.

Increasing the Displacement Hybrid G primarily has the opposite effect on the performance measures as does increasing α, as shown in Figure 5.4-23. Increasing G, over the range of G = 625 to 9000, decreases most of the peak-to-peak performance measures, except for the jerk. The sprung and unsprung mass peak-to-peak displacements are reduced from 0.0051 m to 0.0025 m and from 0.177 m to 0.0236 m, respectively. These displacement decreases should improve the ride quality and the vehicle handling. The peak-to-peak acceleration is reduced from 22 m/s^2 down to 12.9 m/s^2 which should improve the ride comfort. Finally, the peak-to-peak jerk increases from 1450 m/s^3 up to 1869 m/s^3. Overall, increasing G, for α = 0.5, should improve the vehicle handling while the decreases in displacement and acceleration should improve the ride comfort.

All of the 10.5 Hz Displacement Hybrid RMS performance measures decrease over the gain range of G = 625 to 9000, as shown in Figure 5.4-24. The sprung and unsprung mass RMS displacements decrease from 0.0018 m to 0.0009 m and from 0.0627 m to 0.0085 m, respectively. In addition, the sprung mass RMS acceleration and jerk decrease from 7.77 m/s^2 to 3.90 m/s^2 and from 513 m/s^3 to 337 m/s^3, respectively. The decrease in sprung mass RMS displacement, acceleration, and jerk should all benefit the ride comfort. The vehicle handling should also improve due to the decrease in the sprung mass RMS displacement.

As was seen in the previous semiactive control results, Figure 5.4-25 reveals the origin of the jerk spike. At approximately 12.06 seconds, the desired damper force changes from just over zero to almost 4000 N. The turning on of the Groundhook creates the abrupt increase in the damper force. Groundhook turns on at this point as the unsprung mass velocity sign turns negative while the relative velocity is positive, equation (3.11). Figure 5.4-26 shows that this abrupt change in damper force causes a spike in the jerk. However, the rest of the damper force time trace is smooth and results in a relatively smooth acceleration. This smoothness is interpreted here as being more beneficial than times of abrupt acceleration changes.

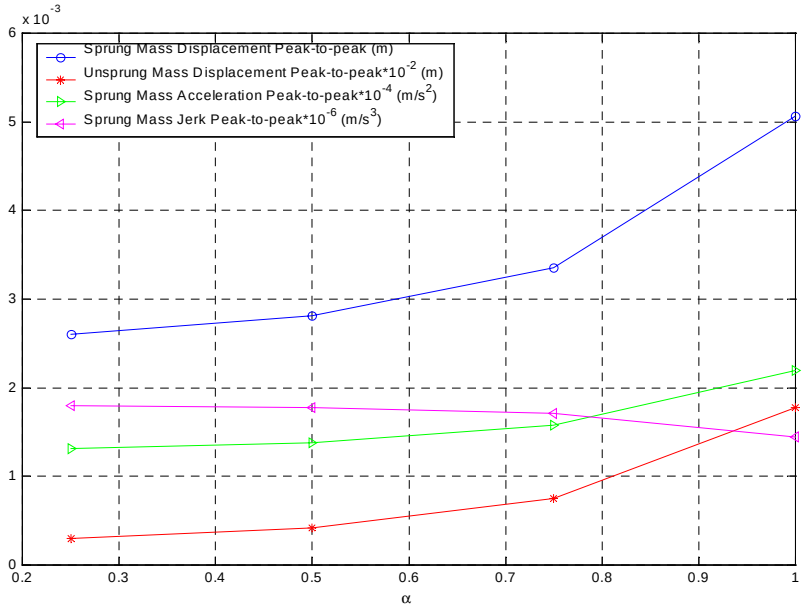

Figure 5.4-20 Effect of Varying α on the Peak-to-peak Steady State Response Performance Measures for a Single Suspension under Displacement Hybrid Control for G = 5000. (10.5 Hz Sinusoidal Input)

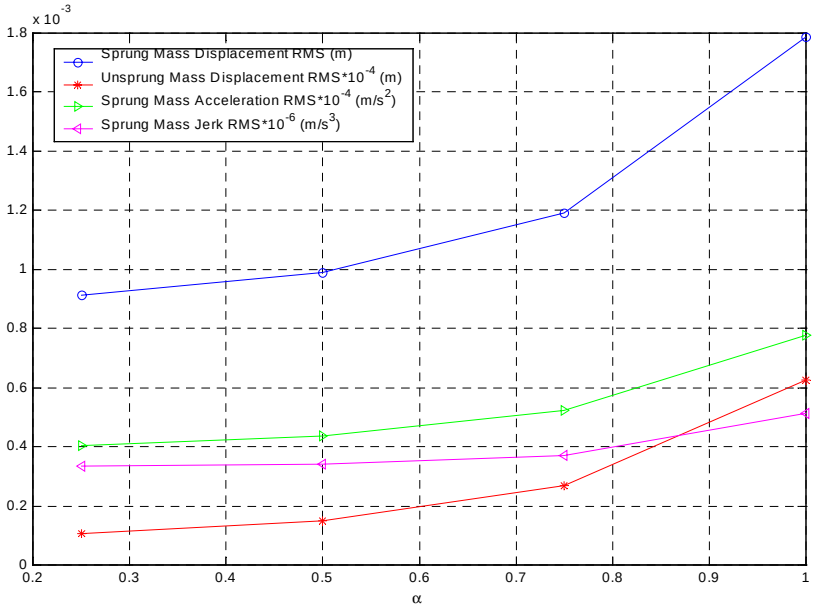

Figure 5.4-21 Effect of Varying α on the RMS Steady State Response Performance Measures for a Single Suspension under Displacement Hybrid Control for G = 5000. (10.5 Hz Sinusoidal Input)

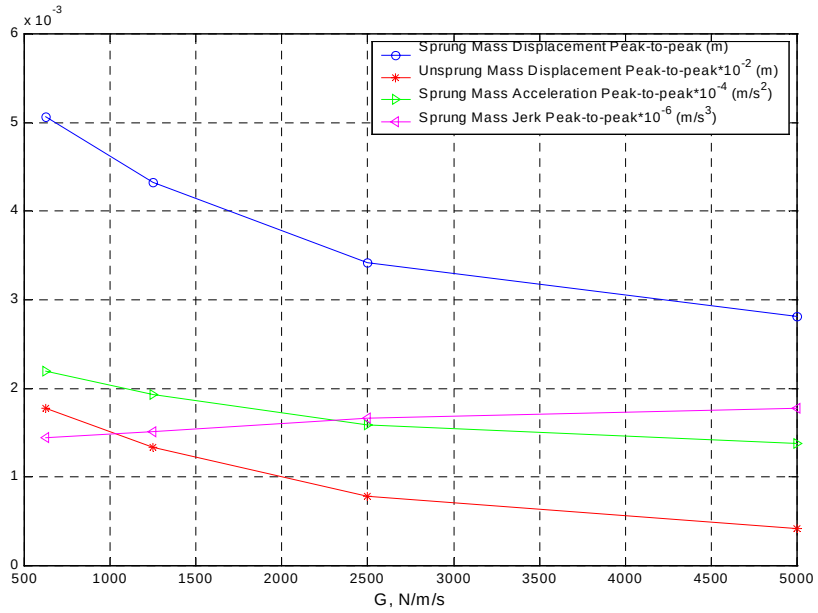

Figure 5.4-22 Effect of Varying *G* on the Peak-to-peak Steady State Response Performance Measures for a Single Suspension under Displacement Hybrid Control for $\alpha = 0.5$. (10.5 Hz Sinusoidal Input)

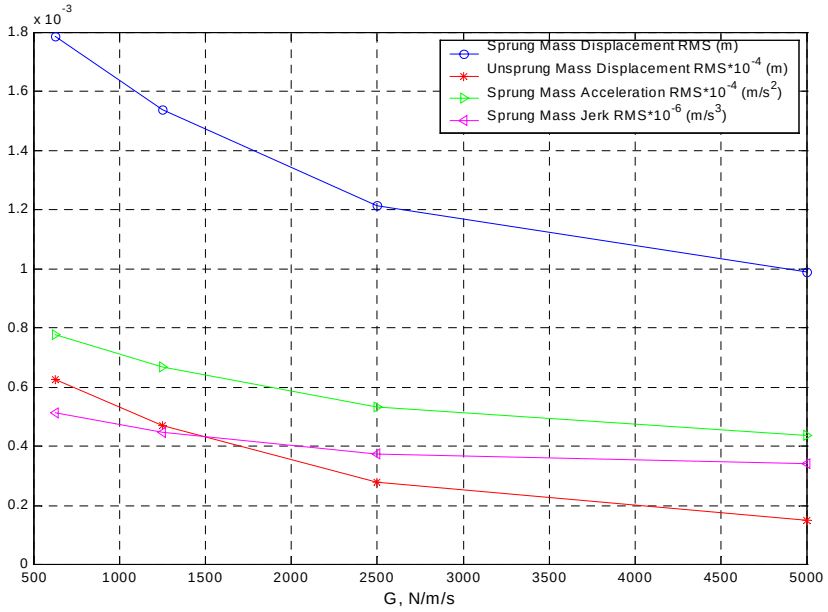

Figure 5.4-23 Effect of Varying *G* on the RMS Steady State Response Performance Measures for a Single Suspension under Displacement Hybrid Control for $\alpha = 0.5$. (10.5 Hz Sinusoidal Input)

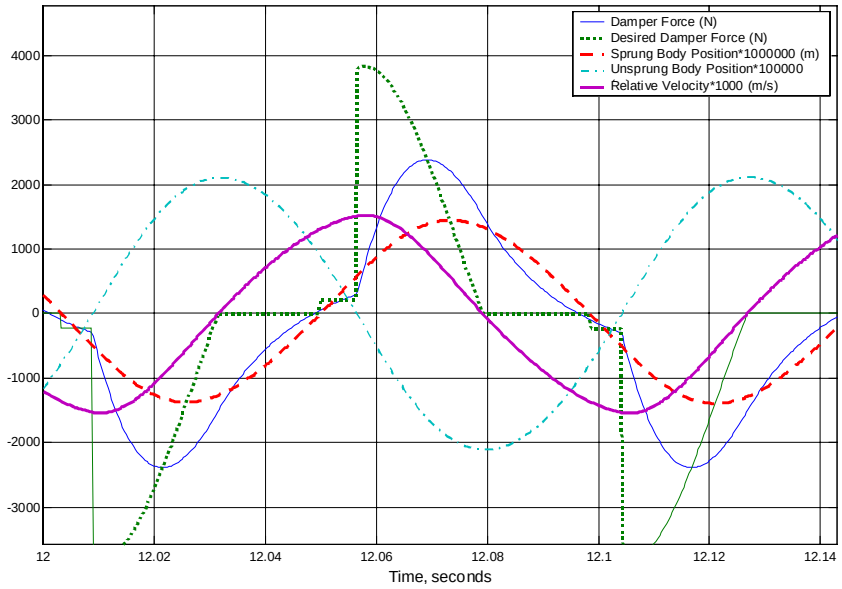

Figure 5.4-24 Steady State Response of a Single Suspension under Displacement Hybrid Control for $G = 5000$ and $\alpha = 0.5$. (10.5 Hz Sinusoidal Input)

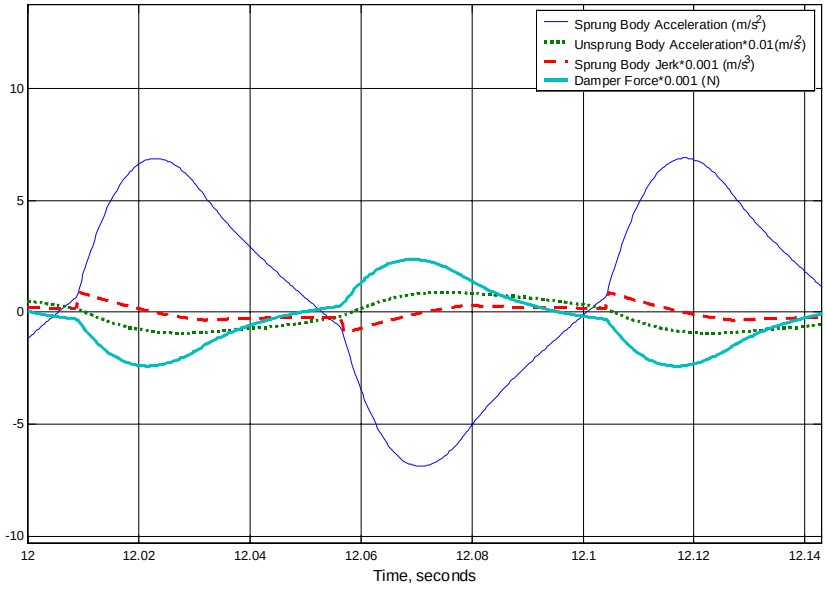

Figure 5.4-25 Steady State Response of a Single Suspension under Displacement Hybrid Control for $G = 5000$ and $\alpha = 0.5$. (10.5 Hz Sinusoidal Input)

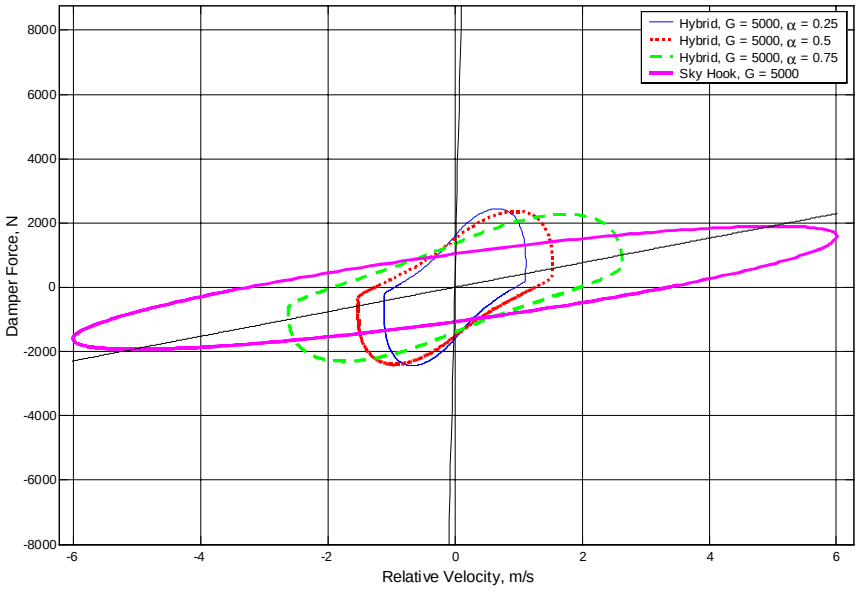

Figure 5.4-26 Comparison of the Force/Velocity Trajectory Step Responses for a Single Suspension under Displacement Hybrid Control for G = 5000.
(10.5 Hz Sinusoidal Input)

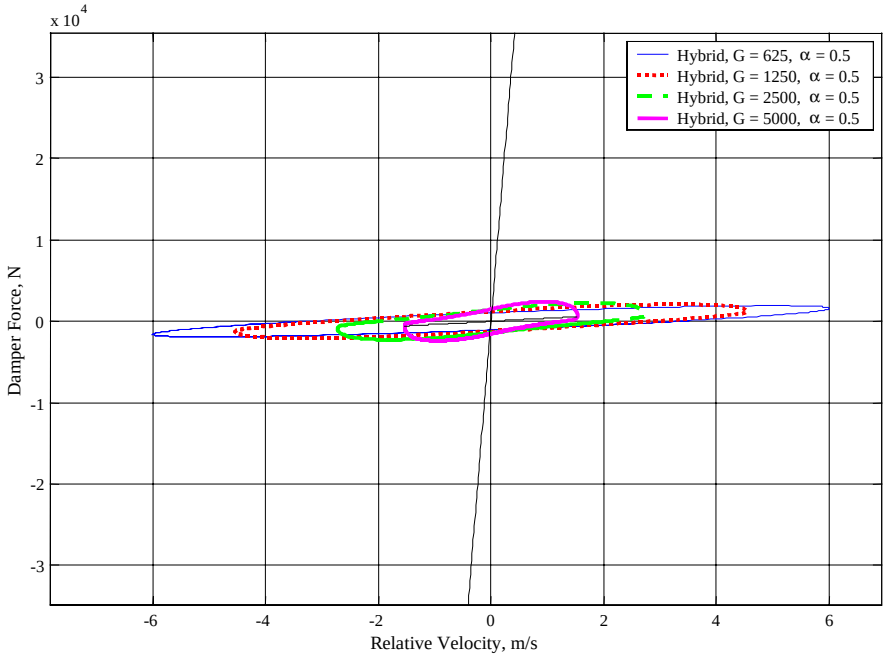

Figure 5.4-27 Comparison of the Force/Velocity Trajectory Step Responses for a Single Suspension under Displacement Hybrid Control for α = 0.5.
(10.5 Hz Sinusoidal Input)

5.4.4 Summary of Displacement Hybrid Results

Displacement Hybrid shows many of the same trends as Hybrid. One noticeable difference, however, is that the unsprung natural frequency increases as the *G* increases. This natural frequency increase is similar to the increase that would occur if the tire stiffness were increased. Apparently, this is caused by the displacement dependence of the Displacement Hybrid switches.

5.5 Comparison of Control Laws

The performance measure results of various selected control law cases are compared in this section. Representative results for each controller were chosen based on how well they performed. For example, Skyhook (G = 2000) was chosen over Skyhook (G = 1000) because using the greater gain resulted in a better performance, for the most part. However, Skyhook (G = 8000) was not chosen because its jerk is greater than that of (G = 4000) and the jerk associated with (G =4000) is already significantly greater than the passive case jerk. Certainly other cases could be selected and so this is not an all inclusive determination of which control law is better than the other, but a helpful comparison for revealing some of the possibilities that each controller offers. The following sections compare the individual controllers.

5.5.1 Comparison of Passive with Skyhook

In this section we find that using Skyhook eliminates a limiting trade off that exists with passive dampers [14]. In addition, we look at the Skyhook limitation of controlling the unsprung mass as well as the jerk that occurs due to Skyhook control.

An advantage of Skyhook is shown in Figure 5.5-1a, where all of the step response performance measures are improved by increasing the gain from G = 2000 to G = 4000, except for jerk, which is still much lower than the passive case jerk. This is important because increasing the gain also improves the 1.34 Hz sinusoid response by lowering the sprung mass peak-to-peak displacement and acceleration, as shown in Figures 5.5-2a and 5.5-3a. Practically, in this gain range, there is no trade off between the step response and the 1.34 Hz sinusoid response. This lack of trade off is unlike the trade off that does occur when the passive damping is increased, which causes both acceleration and jerk to increase because of the larger forces that are transmitted to the sprung mass by a more resistive damper.

There are, however, some disadvantages to using Skyhook. First, the unsprung mass step response displacement is large compared with that of the passive case. Although increasing the gain tends to improve the unsprung body displacement, doing outside of

this gain range will increase the sprung body 1.34 Hz jerk significantly, as shown in Figure 5.1-12; for the jerk associated with G = 8000. The second disadvantage of Skyhook is that both its peak-to-peak and RMS 1.34Hz response jerk are greater for the passive case dampers, as shown in Figures 5.5-2a and 5.5-3a. Lastly, the 10.5 Hz Skyhook sprung and unsprung responses are much greater than for passive dampers, as indicated in Figures 5.5-4a and 5.5-5a.

Overall, we find that Skyhook can control the sprung body step response and 1.34 Hz sinusoid response fairly well, although it does not always directly control the unsprung mass as well as a passive damper.

5.5.2 Comparison of Passive with Hybrid

The Hybrid control is designed to directly control the unsprung mass dynamics as well as the sprung body dynamics. The end result is that Hybrid control improves several step and 1.34 Hz response measures, compared to the passive (40%) case, at the expense of the 10.5Hz performance and increased 1.34 Hz jerk.

As shown in Figure 5.5-1, an advantage of Hybrid (G = 8000, α = 0.75) compared to passive (40%) is the lower step response settling time and sprung and unsprung peak-to-peak body displacements, for approximately the same peak-to-peak acceleration and jerk as passive dampers. The 1.34 Hz sprung body peak-to-peak and RMS displacements and acceleration are lower for passive dampers, for a similar unsprung body displacement.

These results indicate that there are some areas where passive dampers appear to perform better than Hybrid. First, as shown in Figure 5.5-2b, the Hybrid (G = 8000, α = 0.75) 1.34 Hz peak-to-peak jerk is significantly greater than for passive (40%) for the gains that provide similar Hybrid and passive step response sprung body acceleration and jerk.

Second, for the same gains, the Hybrid 10.5 Hz (G = 8000, α = 0.75) performance measures are greater than passive (40%) measures, except for sprung body peak-to-peak displacement as indicated by, as shown in Figures 5.5-4b and 5.5-5b.

Overall, Hybrid (G = 8000, α = 0.75) provides improved performance over passive (40%) in some areas, such as step response settling time and displacements, as well as 1.34 Hz sprung body performance, but at the expense of a poorer 10.5Hz performance and larger 1.34 Hz peak-to-peak jerk.

5.5.3 Comparison of Skyhook with Hybrid

The results shown in Figure 5.5-1 and 5.5-2 indicate that Skyhook does not cause a trade off between the step and 1.34 Hz response, as is the case for Hybrid control. The Hybrid control 10.5 Hz performance, however, is superior to that for the Skyhook.

In Section 5.5-1c it was discussed that Skyhook control does not trade off between the step and 1.34 Hz response, except for jerk, as does passive damping. Hybrid control, however, does cause a trade off between the step and 1.34 Hz response. To explain this trade off, it is worth noting that increasing the Hybrid G, for α = 0.75 increases the step response acceleration and jerk, as shown in Figure 5.5-1c. Increasing the Skyhook G, however, does not increase the step response acceleration and jerk. Increasing the gain is desirable because it improves a number of other performance measures. For example, increasing the gain reduces the 1.34 Hz sprung body peak-to-peak and RMS displacement for both Skyhook and Hybrid (α = 0.75), as shown in Figures 5.5-2c and 5.5-3c.

An advantage of Hybrid (G = 8000, α = 0.75) over Skyhook (G = 4000) is that Hybrid produces a much better performance at 10.5 Hz. Figures 5.5-4c and 5.5-5c clearly show that the Hybrid 10.5 Hz unsprung body peak-to-peak and RMS displacement as well as the sprung body peak-to-peak and RMS acceleration and jerk are much lower than for Skyhook. After all, Hybrid control is configured such that it can directly resist the motion of the unsprung mass and reduce the unsprung mass resonance. Since both the sprung and unsprung bodies are connected together by the suspension, reducing the unsprung body resonance reduces the suspension forces and therefore, the force transmitted to the sprung body. The end result is a smoother ride!

In summary, Skyhook control allows one to increase the gain to improve the performance of both the step and 1.34 Hz response; while a similar increase in the gain for Hybrid control ($\alpha = 0.75$) will increase the step response sprung body peak-to-peak acceleration, possibly causing a less desirable ride comfort in a vehicle. Increasing the Hybrid ($\alpha = 0.75$) gain, however, will improve the 10.5 Hz response as compared with Skyhook control; therefore, offering less wheel hop and a better handling of the vehicle.

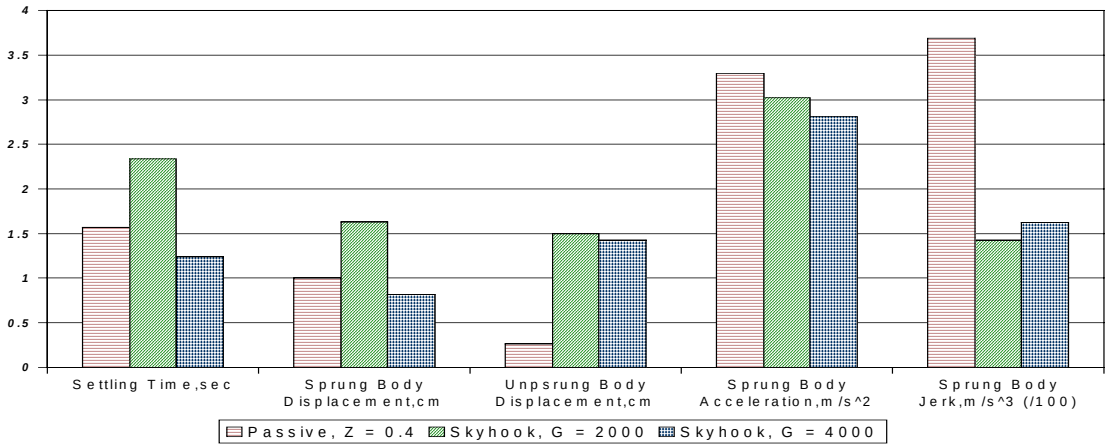

(a)

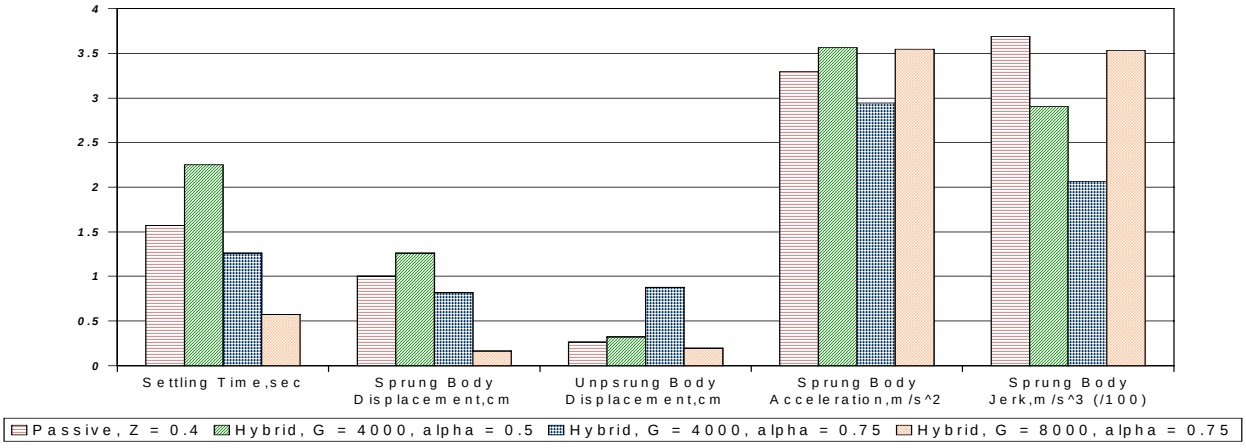

(b)

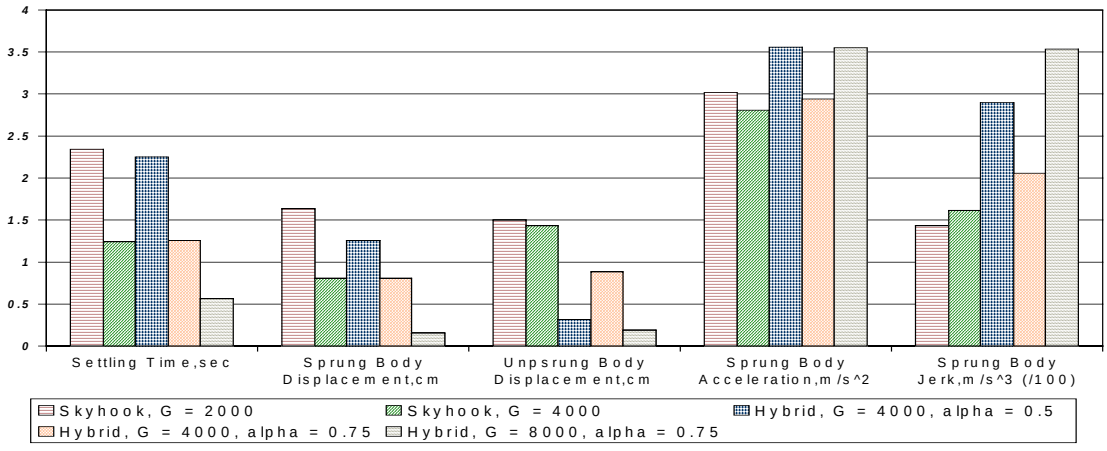

(c)

Figure 5.5-1 Comparison of Transient Peak-to-Peak Responses between Various Traditional Control Methods for a step Input.

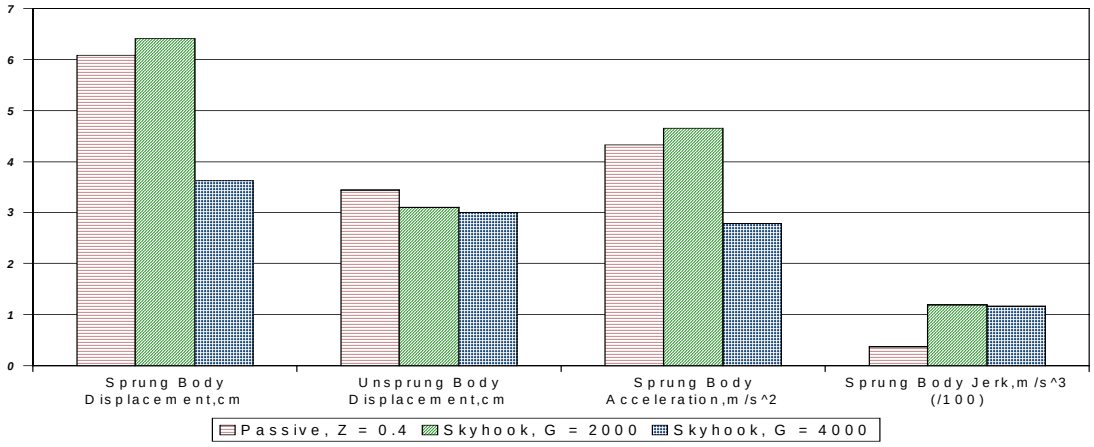

(a)

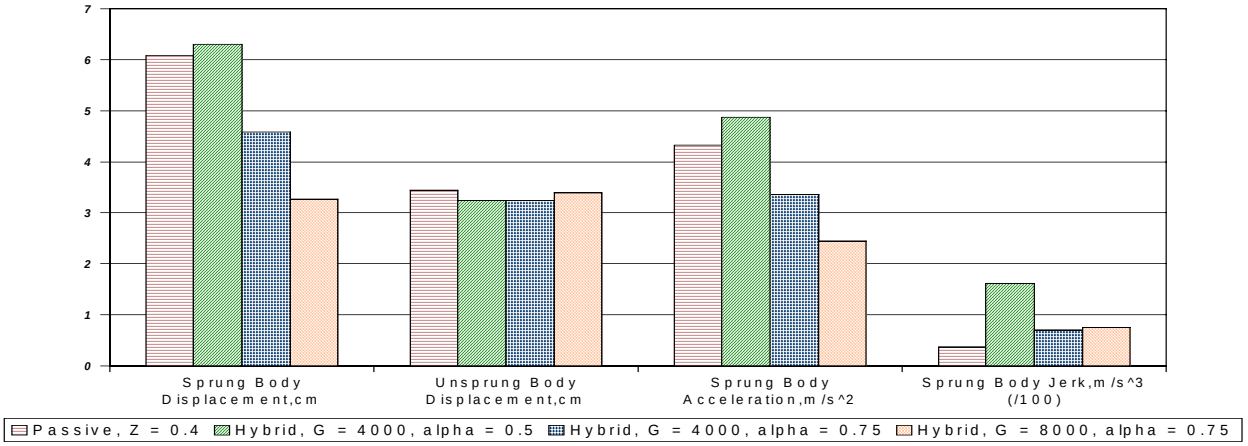

(b)

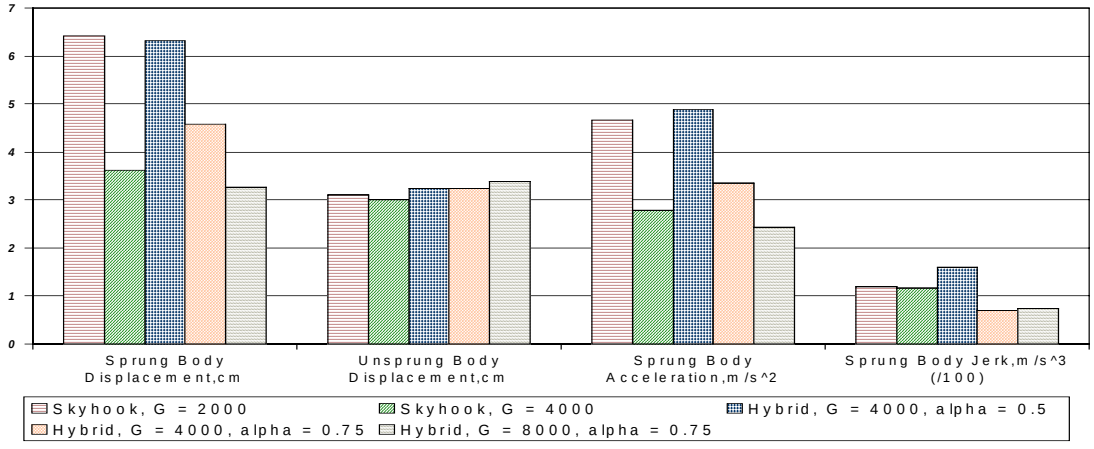

(c)

Figure 5.5-2 Comparison of Steady State Peak-to-Peak Responses between Various Control Methods. (1.34Hz Sinusoid Input)

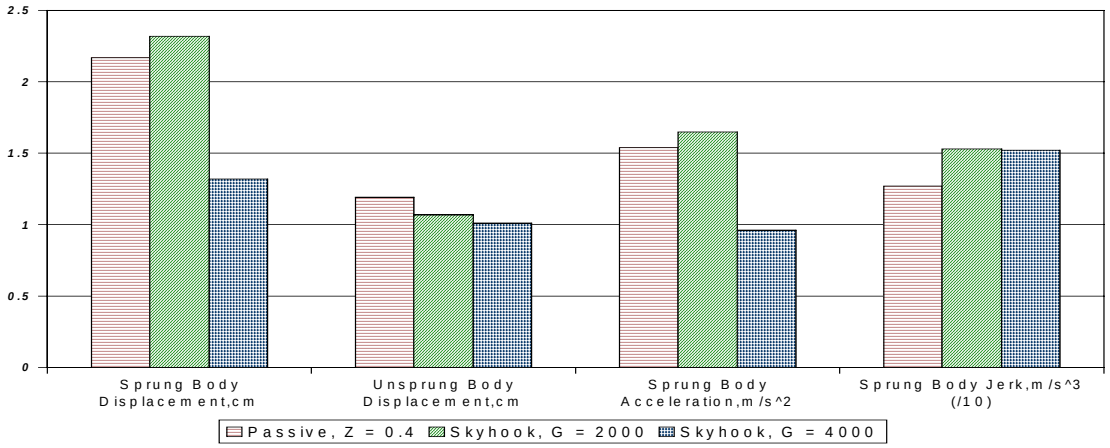

(a)

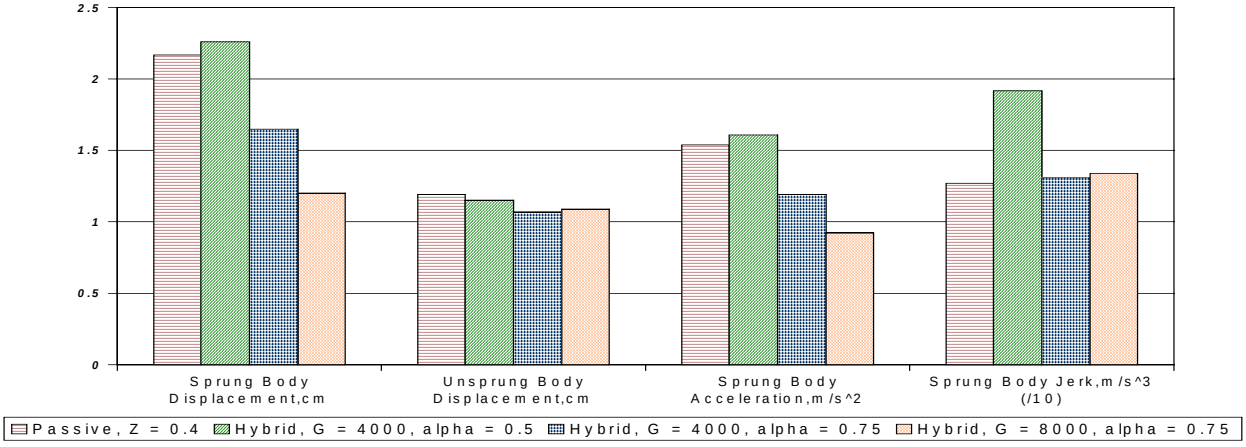

(b)

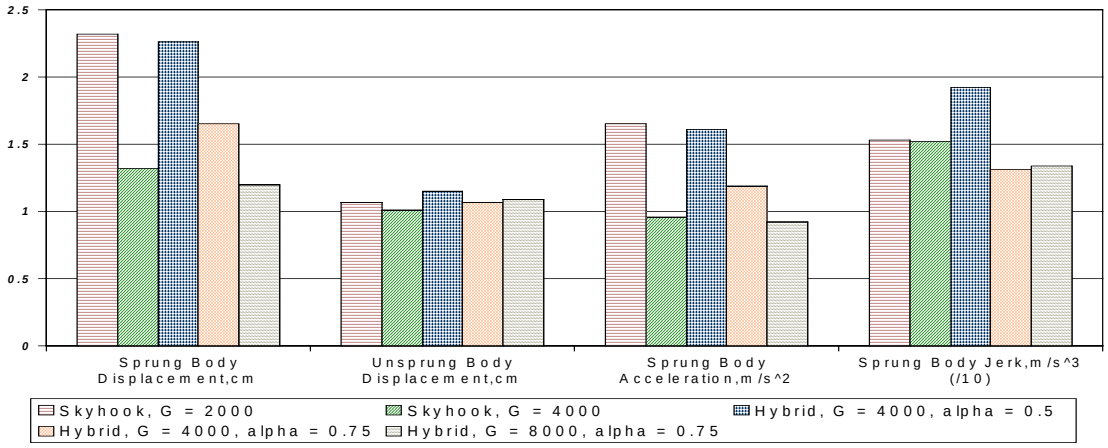

(c)

Figure 5.5-3 Comparison of Steady State RMS Responses between Various Control Methods. (1.34Hz Sinusoid Input)

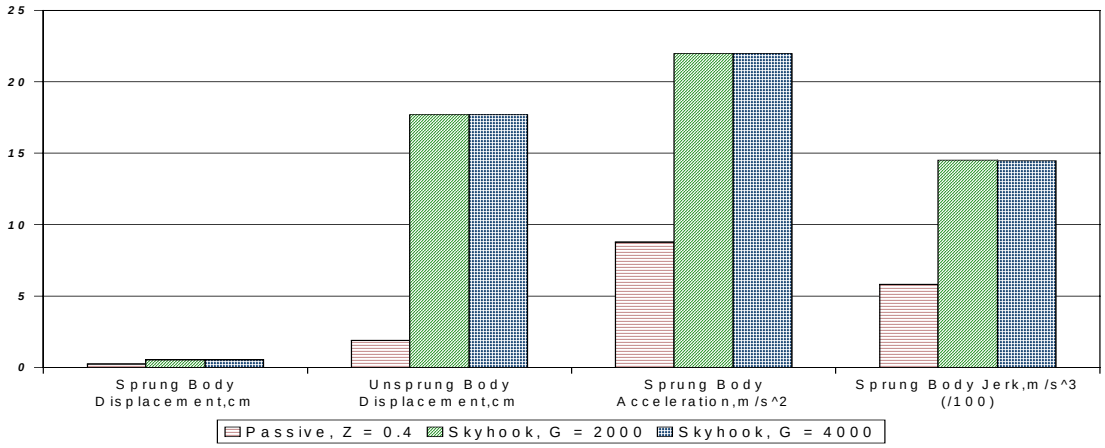

(a)

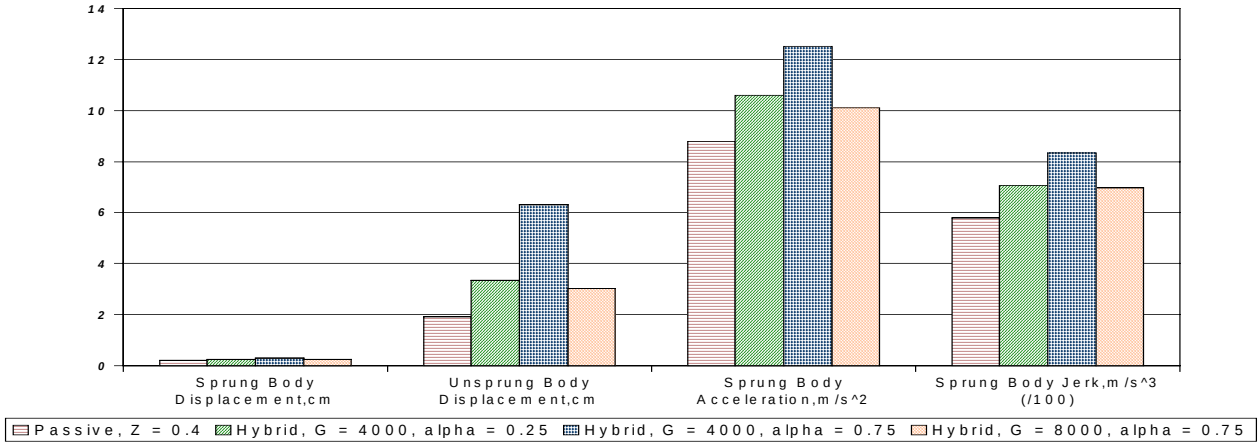

(b)

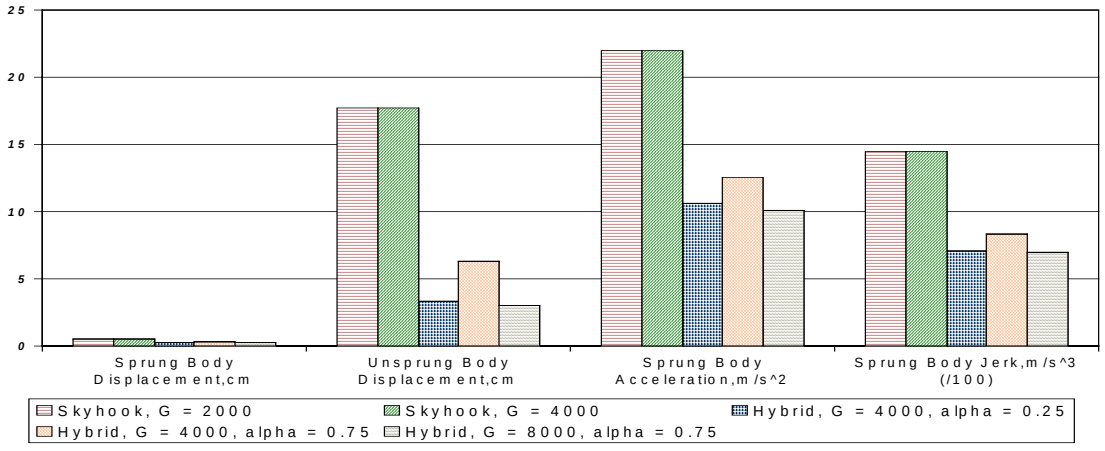

(c)

Figure 5.5-4 Comparison of Steady State peak-to-peak Responses between Various Control Methods. (10.5Hz Sinusoid Input)

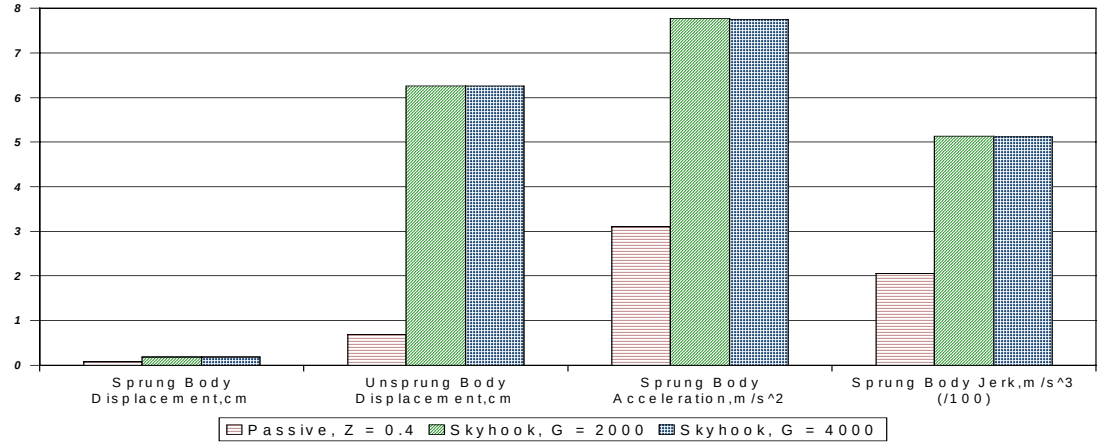

(a)

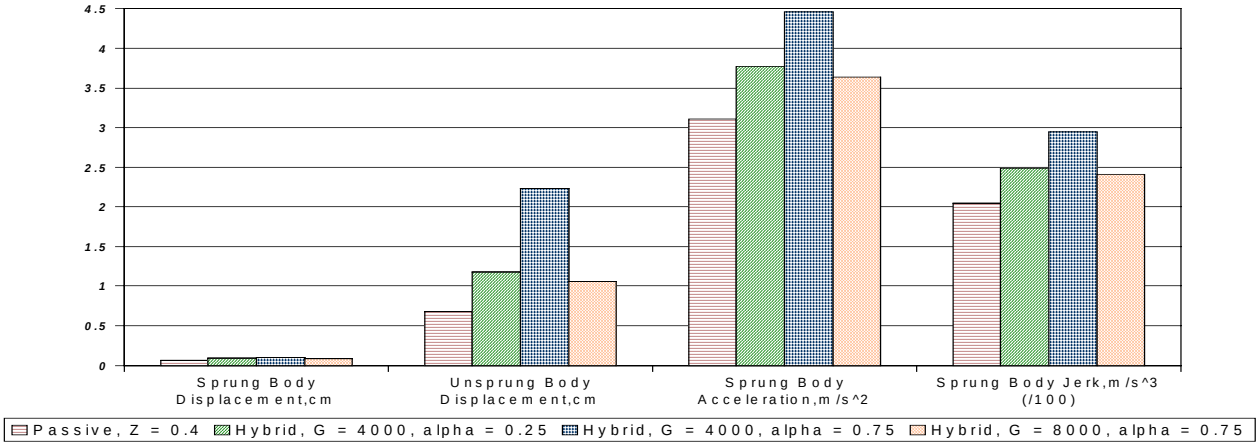

(b)

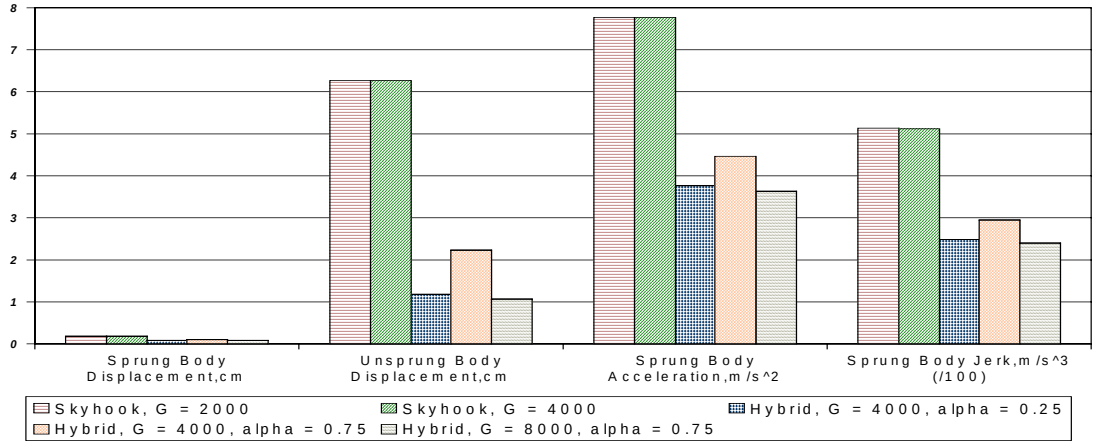

(c)

Figure 5.5-5 Comparison of Steady State RMS Responses between Various Control Methods. (10.5Hz Sinusoid Input)

5.5.4 Comparison of Passive with Displacement Skyhook

When we compare the Displacement Skyhook (G = 5000) with passive damping (40%) results, shown in Figures 5.5-6 to 5.5-10, we observe that the elimination of the step/1.34 Hz response trade off, discussed in section 5.5-1a, still exists. Unlike passive dampers, Displacement Skyhook (α = 0.75) does not make a trade off between the step and 1.34 Hz response, except for the step response peak-to-peak jerk, which is lower than the passive jerk as shown in Figure 5.5-6a. Practically, increasing the Displacement Skyhook gain, G, will improve both the step and 1.34 Hz response. Increasing the passive damping ratio, ζ, increases the step response acceleration and jerk, which is already significantly greater than the Displacement Skyhook step response jerk. The trade off relationship is nearly identical to the one that exists between passive and Skyhook, see Section 5.5-1a. [14] ([14] mentions a similar trade off with overshoot)

There are several disadvantages when using Displacement Skyhook, as compared to passive damping. The most noticeable disadvantage is that increasing the gain does not reduce the 10.5 Hz performance measures at all and they are much greater than those for passive damping, as shown in Figures 5.5-9a and 5.5-10a. Second, for Displacement Skyhook (G = 5000), the step response of the unsprung mass peak-to-peak displacement is much greater than for passive damping, as indicated in Figure 5.5-6a. Lastly, the 1.34 Hz and 10.5 Hz peak-to-peak and RMS jerk are much larger than that of passive damping, as shown in Figures 5.5.7a – 5.5.10a.

Overall, the advantage of Displacement Skyhook over passive is the elimination of the trade off in performance between the step and 1.34 Hz response. The disadvantages of Displacement are,

1) The inability to improve the performance at 10.5 Hz by increasing the Displacement Skyhook gain
2) The relatively large jerk at 1.34 Hz and 10.5 Hz.
3) The large step response unsprung body displacement

5.5.5 Comparison of Passive with Displacement Hybrid

In this section we find that the data does not look good for Displacement Hybrid (G = 5000, α = 0.75). This control law has a number of disadvantages that would limit its application in most vehicles, as well in most other systems.

According to this data, it is difficult to find any advantage to using Displacement Hybrid (G = 5000, α = 0.75). Although most performances measures improve as the gain is increased, as shown in Figure 5.5-6b and 5.5-7b, the step response settling time, and the sprung and unsprung peak-to-peak displacement are significantly greater than the same measures for passive damping, as shown in Figure 5.5-6b. Increasing the gain further may not be an option because the 1.34 Hz and 10.5 Hz peak-to-peak jerk is already much greater than for passive dampers, and increasing the gain would just further increase jerk, as depicted in Figures 5.5-7b and 5.5-9b. Additionally, the 10.5 Hz performance measures are much larger than for the passive damping, as indicated in Figure 5.5-9b and 5.5-10b.

In summary, it appears that passive control is better in almost all respects than the Displacement Hybrid (G = 5000, α = 0.75) control.

5.5.6 Comparison of Displacement Skyhook with Displacement Hybrid

In this section, Displacement Hybrid (G = 5000, α = 0.75) better controls the system at a base excitation of 10.5 Hz (the unsprung natural frequency) and better controls the unsprung mass step response displacement. However, there are a number of performance measures that are lower for Displacement Skyhook control.

One advantage of Hybrid over Skyhook is the ability to control the 10.5 Hz (unsprung mass natural frequency) response. Increasing the Displacement Skyhook gain does not affect the 10.5 Hz response, however increasing the Displacement Hybrid (α = 0.75) gain, G, does improve the 10.5 Hz performance, as shown in Figures 5.5-9c and 5.5-10c. In fact, for these selected cases, the Displacement Hybrid (G = 5000, α = 0.75) 10.5 Hz

performance is significantly better than that of the Displacement Skyhook (G = 5000) performance.

Another advantage of Displacement Hybrid (G = 5000, α = 0.75) over Displacement Skyhook (G = 5000) is the lower step response unsprung body peak-to-peak displacement, see Figure 5.5-6c. However, this improvement comes at a cost of greater settling time and sprung mass peak-to-peak displacement and acceleration. The other cost of Displacement Hybrid (G = 5000, α = 0.75) is that the sprung mass 1.34 Hz peak-to-peak and RMS are also greater, see Figures 5.5-7c and 5.5-8c.

Overall, we see that the results are mixed when it comes to trying to determine whether Displacement Hybrid (G = 5000, α = 0.75) or Displacement Skyhook (α = 0.75) is better. Displacement Hybrid performs better at 10.5 Hz and does a better job of keeping the unsprung mass step response displacement down. However, for this case, Displacement Skyhook is more favorable to Displacement Hybrid.

Having investigated each control law simulated in this study, we are now ready to compare the more traditional laws with the alternative laws presented in this report.

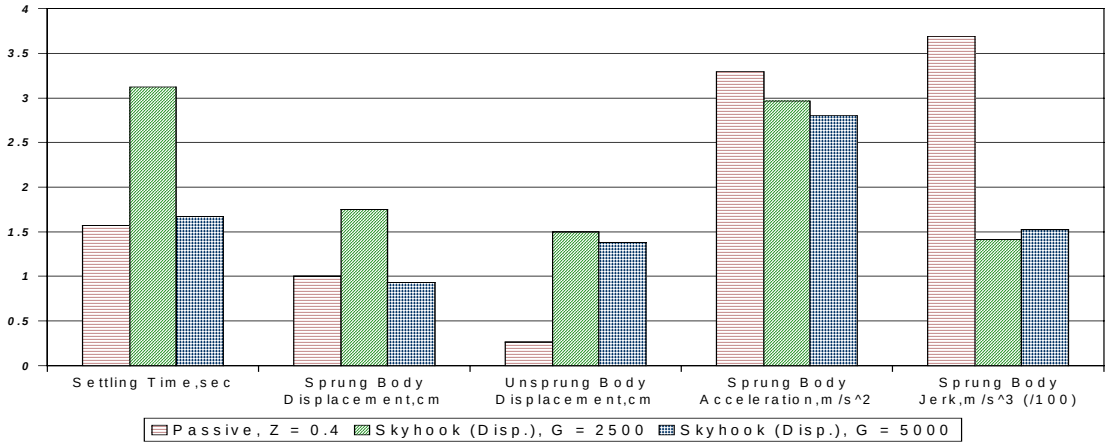

(a)

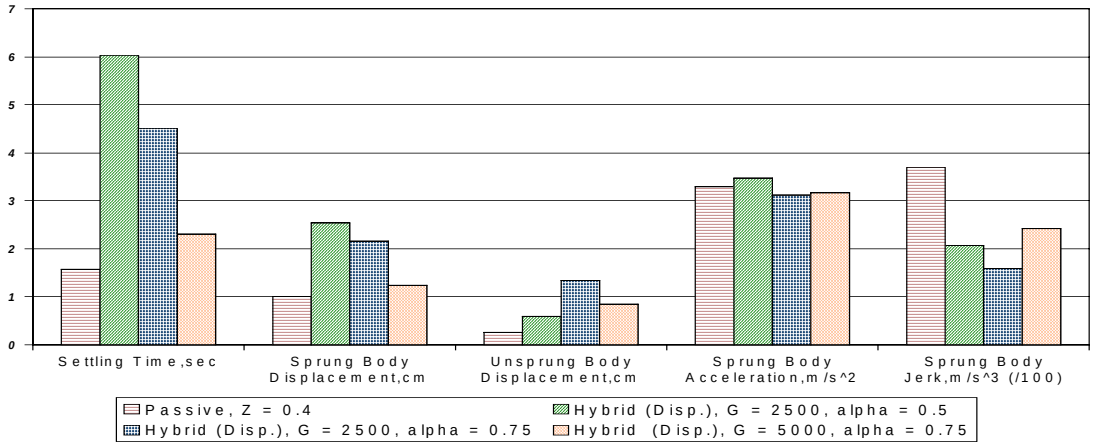

(b)

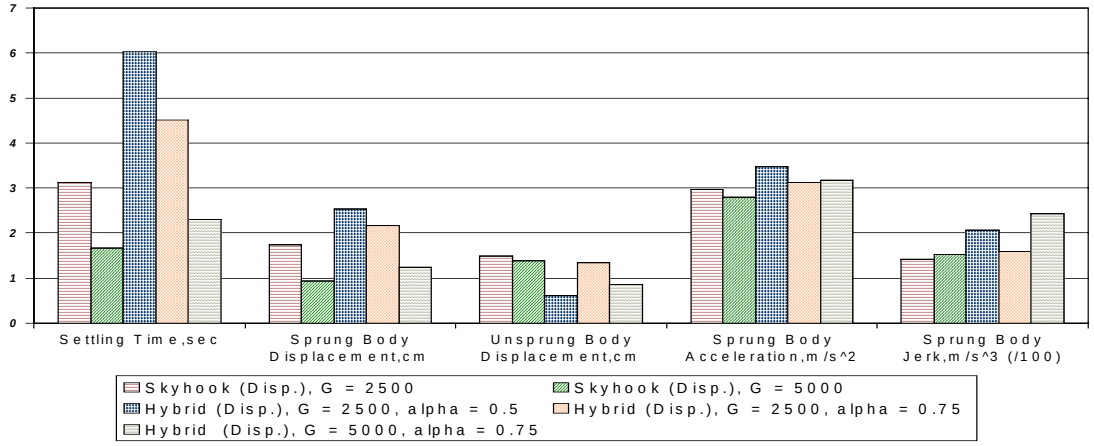

(c)

Figure 5.5-6 Comparison of Transient Peak-to-Peak Responses between Various Displacement Control Methods for a Step Input.

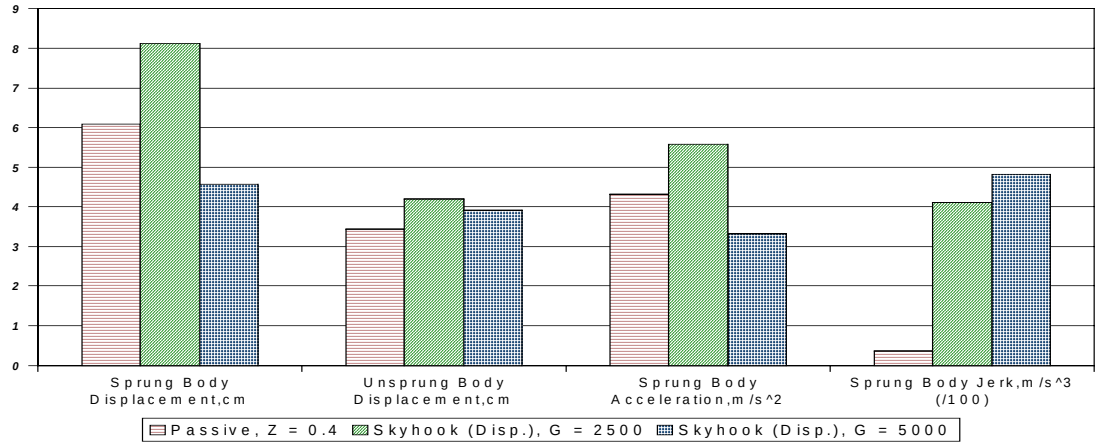

(a)

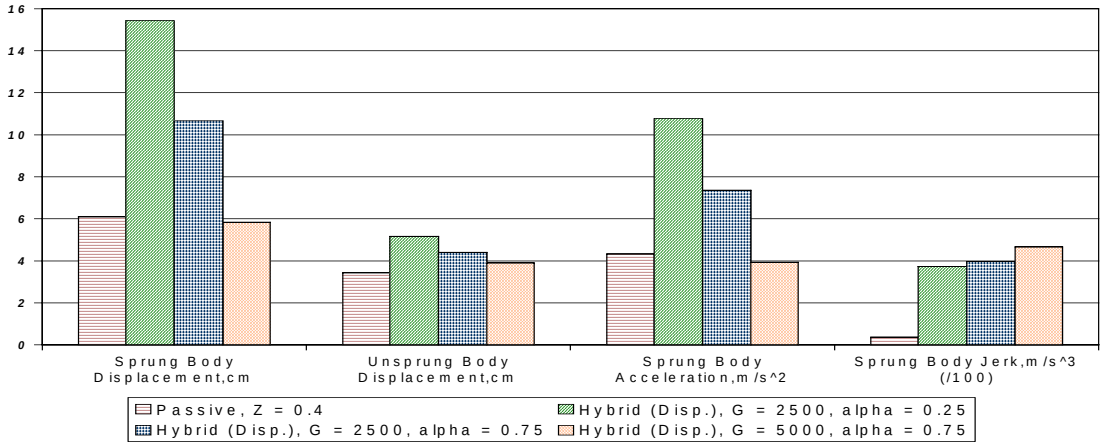

(b)

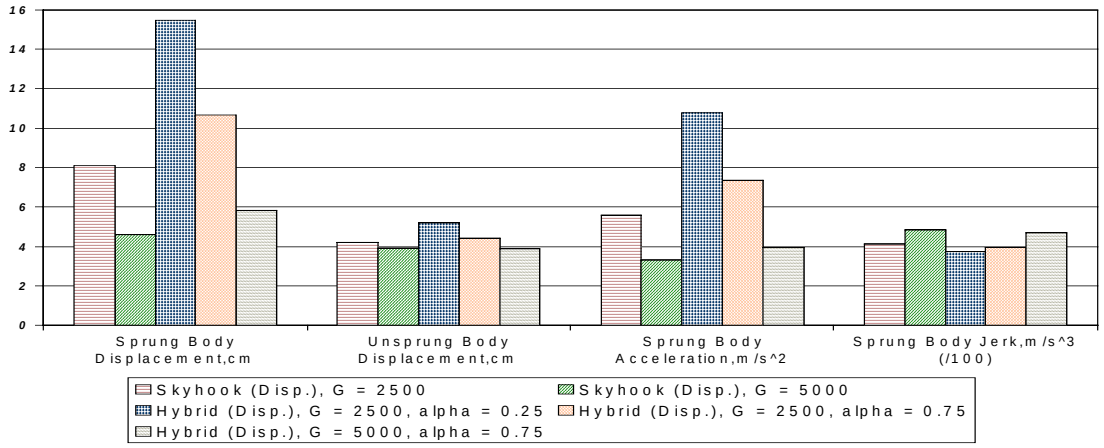

(c)

Figure 5.5-7 Comparison of Steady State Peak-to-Peak Responses between Various Displacement Control Methods. (1.34Hz Sinusoid Input)

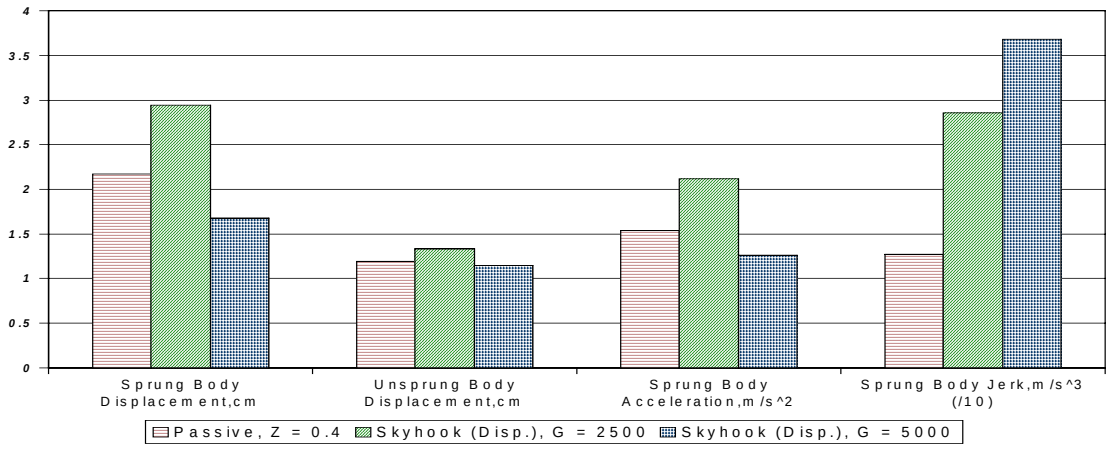

(a)

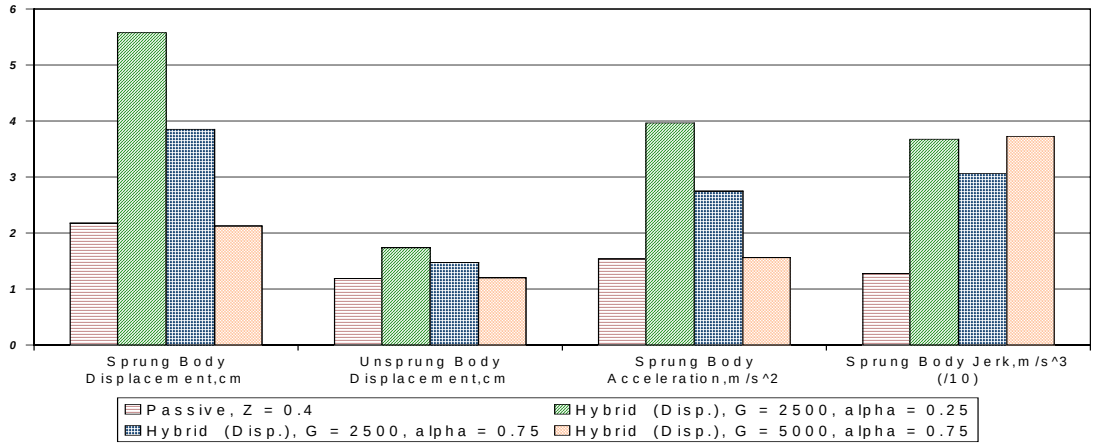

(b)

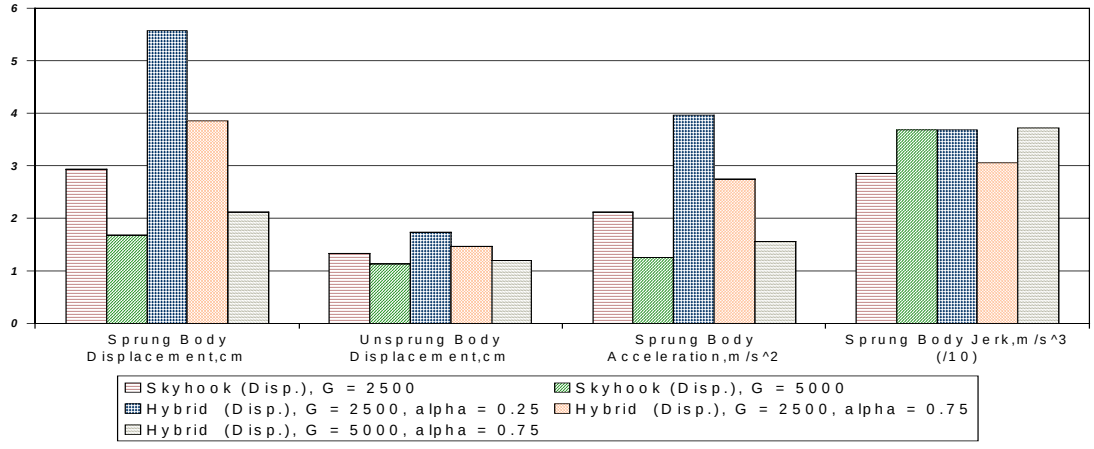

(c)

Figure 5.5-8 Comparison of Steady State RMS Responses between Various Displacement Control Methods. (1.34Hz Sinusoid Input)

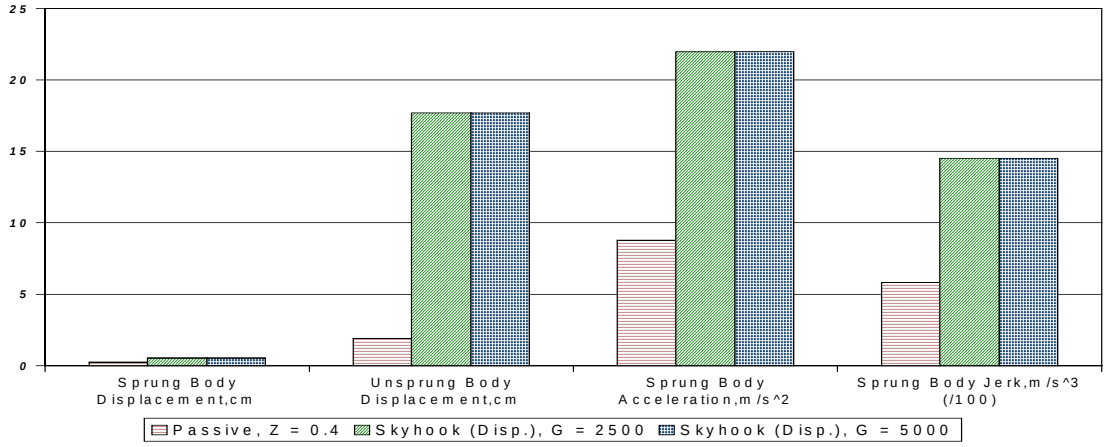

(a)

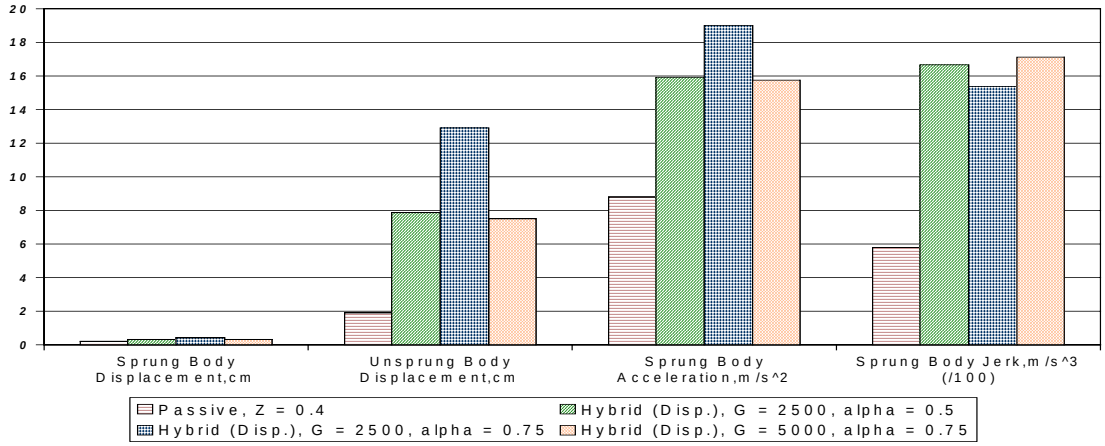

(b)

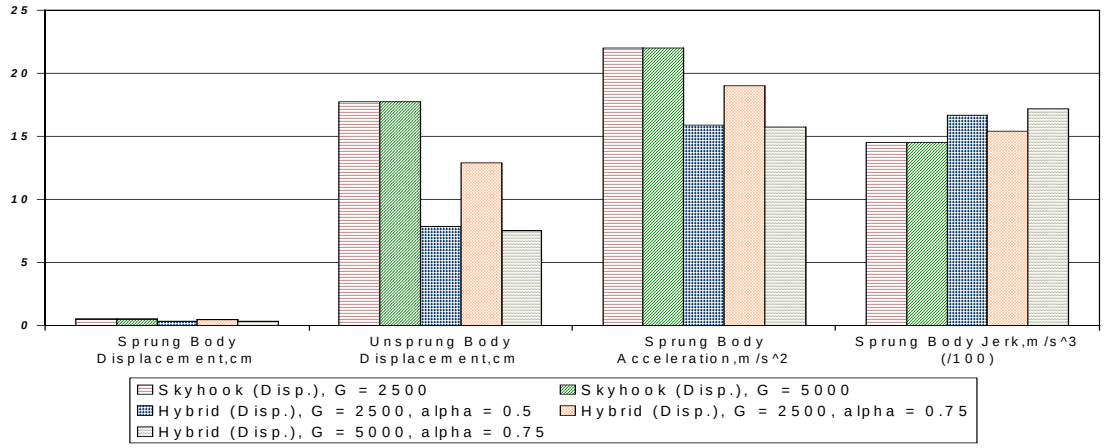

(c)

Figure 5.5-9 Comparison of Steady State peak-to-peak Responses between Various Displacement Control Methods. (10.5Hz Sinusoid Input)

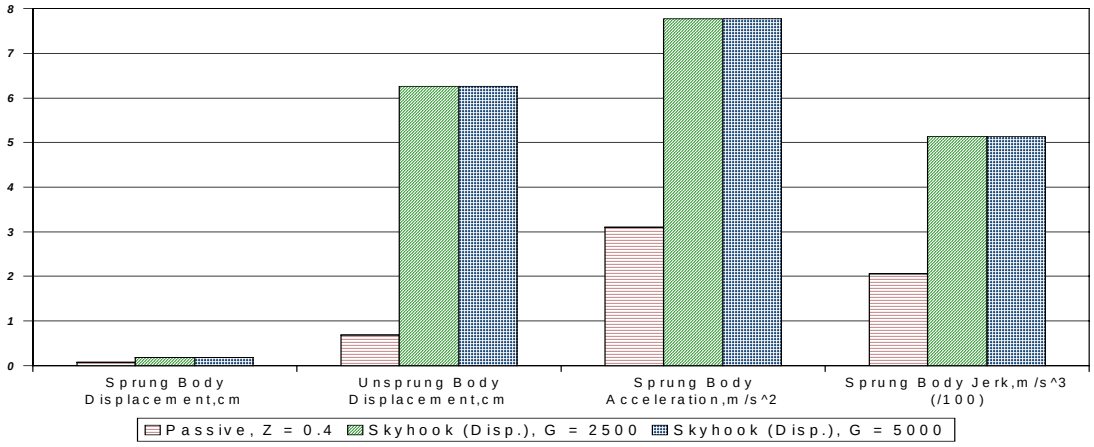

(a)

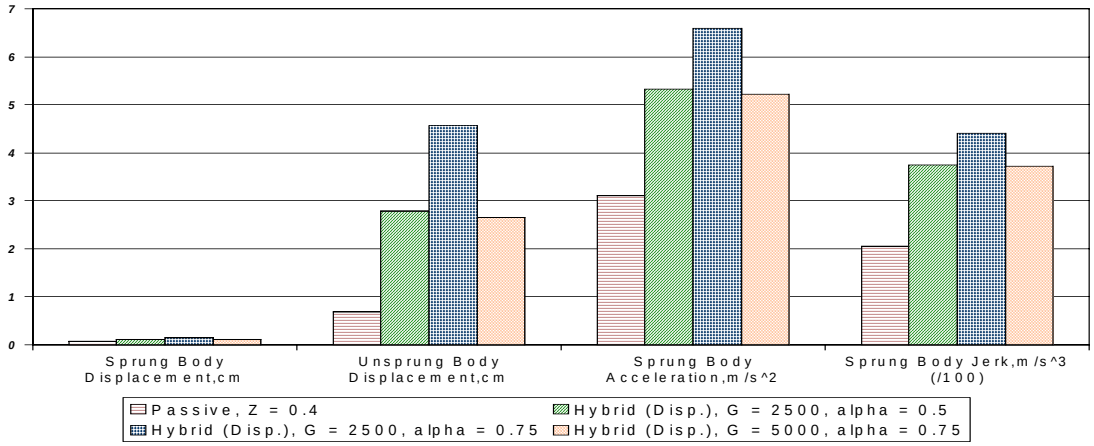

(b)

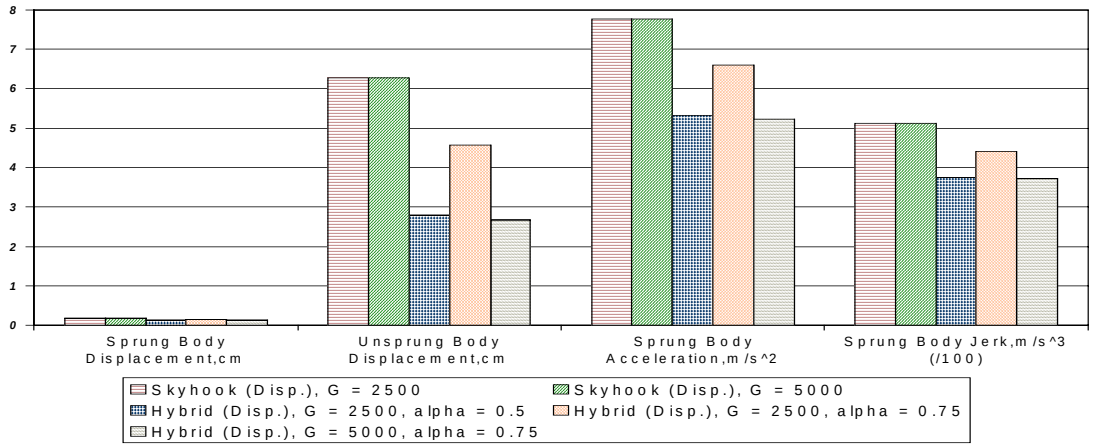

(c)

Figure 5.5-10 Comparison of Steady State RMS Responses between Various Displacement Control Methods. (10.5Hz Sinusoid Input)

5.5.7 Displacement Skyhook verses Skyhook

For this comparison, we will consider each input case separately; they are the step, 1.34 Hz, and 10.5 Hz inputs. We will find that Skyhook (G = 4000) performs better than Displacement Skyhook (G = 5000) for the step and 1.34Hz inputs, but both laws produce the same results at 10.5 Hz.

1. For the step response, we find that Displacement Skyhook is associated with a greater settling time and a greater sprung mass peak-to-peak displacement, for practically the same sprung mass acceleration and unsprung mass displacement, see Figure 5.5-11a. In general, it appears that the Displacement Skyhook is just not applying as much damping as the Skyhook law.

2. For the 1.34 Hz response, all of the selected performance measures are worse for Displacement Skyhook than they are for Skyhook, as shown in Figures 5.5-12a. For example, the Displacement Skyhook sprung body peak-to-peak displacement is 27.8% greater and the jerk is 300% greater. The 1.34 Hz RMS measures tell the same story, see Figure 5.5-13a.

3. For the 10.5 Hz response, Displacement Skyhook and Skyhook produce exactly the same results, as shown in Figures 5.5-14a and 5.5-15a. Both laws react the same to the 10.5 Hz input; they are both primarily off as the unsprung mass resonates, see Figures 5.1-20a and 5.3-17a.

Overall, these results indicate that Displacement Skyhook does not perform as well as the Skyhook law for the step and 1.34 Hz input. However, for the 10.5 Hz input, both laws produce exactly the same results.

5.5.8 Displacement Hybrid verses Hybrid

In this section a comparison is made between Displacement Hybrid (G = 5000, α = 0.75) law and the Hybrid (G = 8000, α = 0.75). We will see that this data suggests that the Hybrid law is better able to control the system.

1. For the step input, the Displacement Hybrid produces a greater settling time and sprung and unsprung displacement, as shown in Figure 5.5-11b. However, the Displacement Hybrid is also associated with a lower sprung body peak-to-peak acceleration and jerk.

2. For the 1.34 Hz input, the Displacement Hybrid is associated with greater displacements, accelerations, and jerk measures, see Figure 5.5-12b. For example, the Displacement Hybrid sprung body displacement is greater by 76% and the peak-to-peak jerk is greater by 571%. The RMS measures are also greater; the Displacement Hybrid sprung body displacement is greater by 75% and the jerk is greater by 185%.

3. For the 10.5 Hz input, the Displacement Hybrid performance measures are again greater than the Hybrid measures. For example, the Displacement Hybrid unsprung mass peak-to-peak displacement is greater by 150%. For the RMS measures, the same displacement measure is greater by 145%.

These results indicate that the Displacement Hybrid control law does not control the system as well as the Hybrid control. All of the measures for the Displacement version are greater.

5.5.9 Comparison Summary

There are several key points that these results show. They are,

5.5.9.1 Traditional Control

1. Skyhook control can be used to reduce a number of step and 1.34 Hz response measure while providing a lower step response acceleration and jerk than passive damping. Changing Skyhook control gain, however, will not affect the 10.5 Hz performance.

2. For the unsprung mass displacement, the hybrid control law has the ability to improve a number of performance measures for the 10.5 Hz base excitation case.

3. Compared with passive damping, the Skyhook and Hybrid control cases that were considered here cause larger peak-to-peak and RMS jerk at the sprung and unsprung resonance frequencies (i.e., 1.34 Hz and 10.5 Hz, respectively). The peak-to-peak jerk for Skyhook control due to a step input, however, is smaller than for that for passive damping.

5.5.9.2 Alternative Control

4. The Displacement Skyhook and Hybrid control methods are similar to velocity-based Skyhook and Hybrid controls, in that they both show the same trends as the control gains change.

5. The Displacement control methods cause larger jerk than the conventional velocity-based Skyhook and Hybrid controls.

6. Overall, the results indicate that the Displacement control methods do not offer any advantages over velocity-based Skyhook and Hybrid control methods.

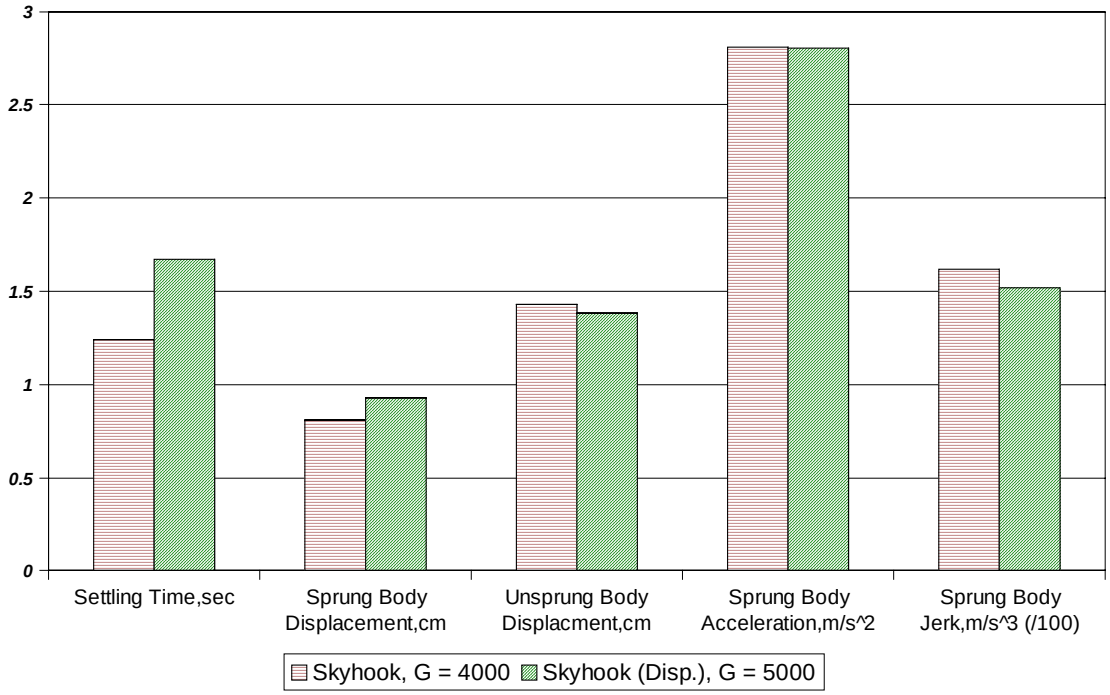

(a)

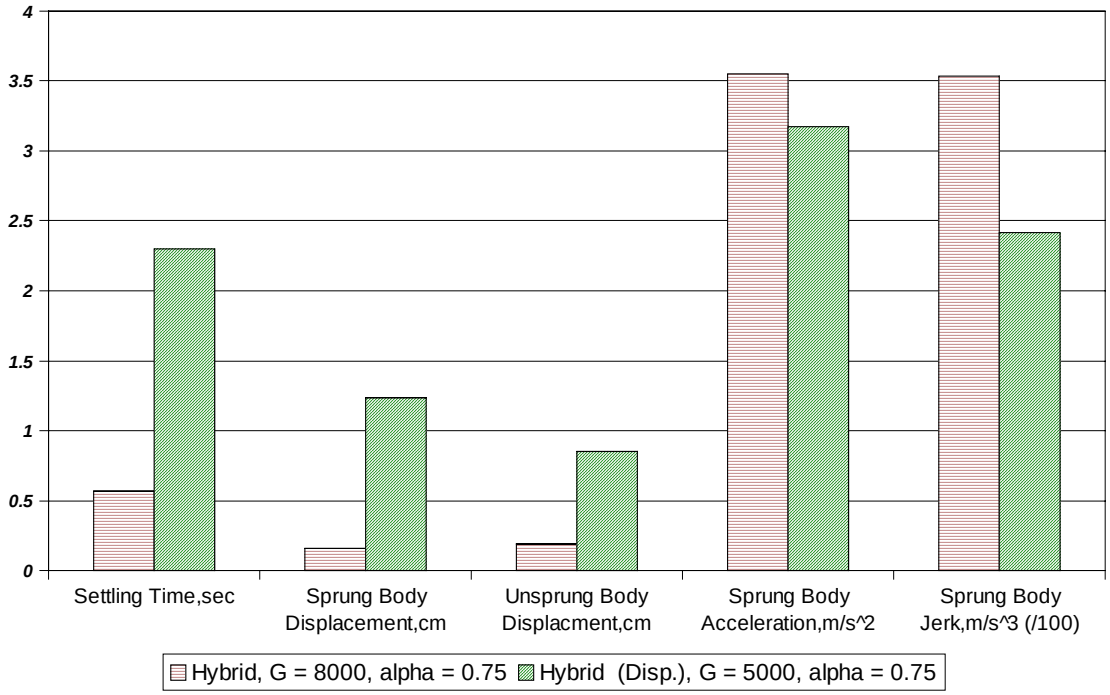

(b)

Figure 5.5-11 Comparison of Transient Peak-to-Peak Responses between Conventional Control Methods and Displacement Control Methods for a Step Input.

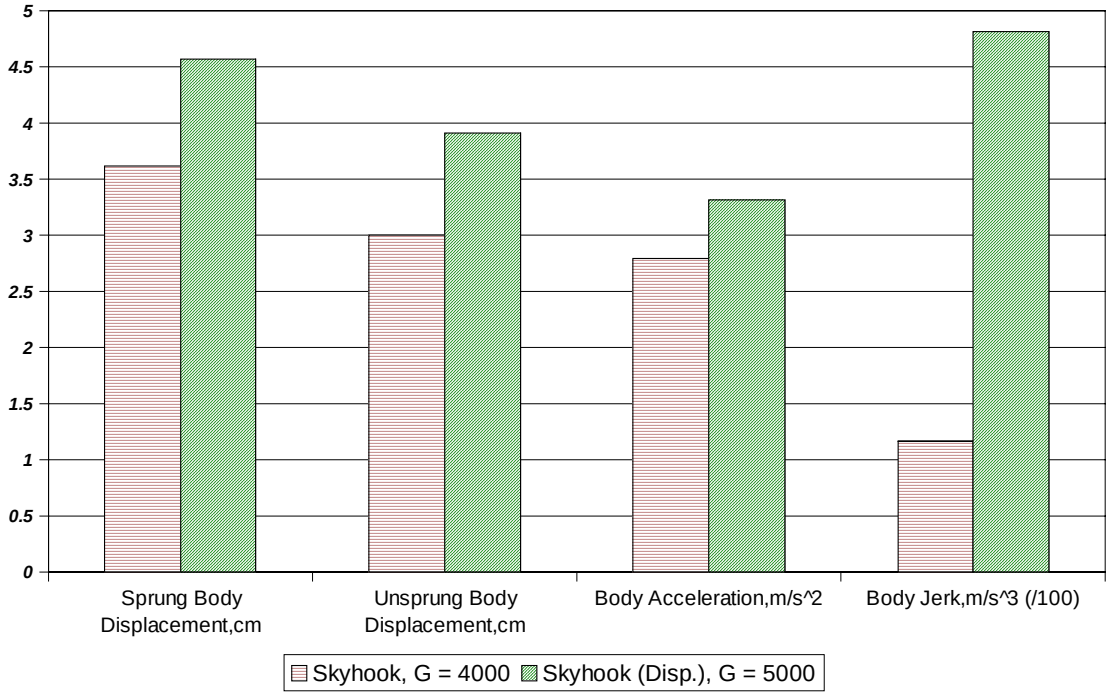

(a)

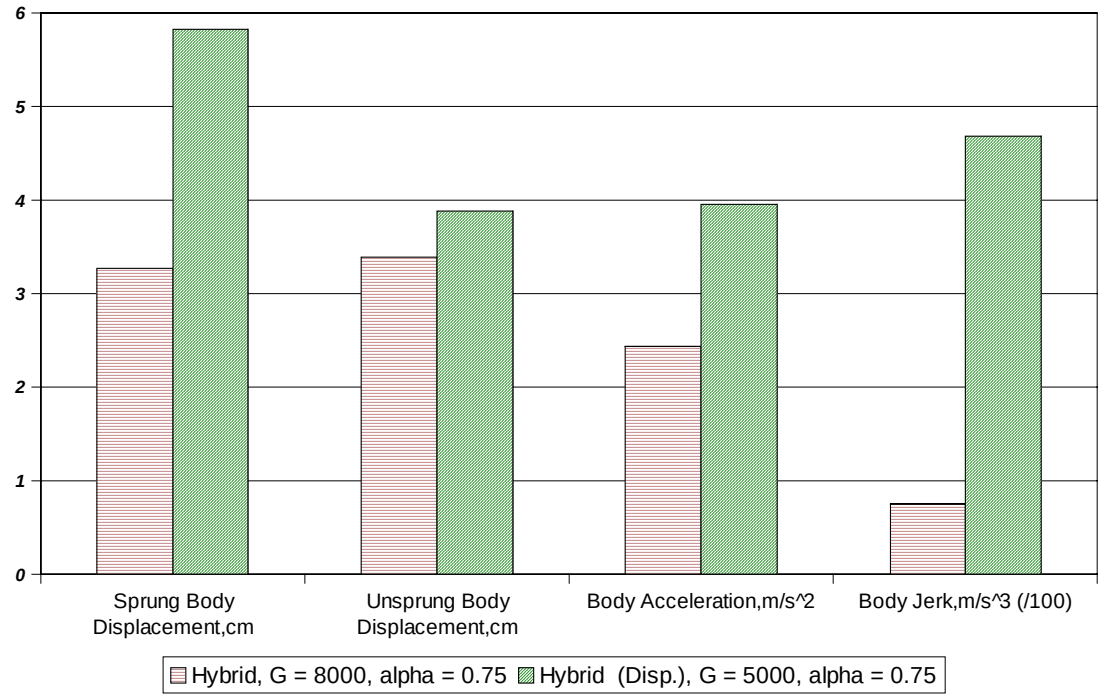

(b)

Figure 5.5-12 Comparison of Steady State Peak-to-Peak Responses between Conventional Control Methods and Displacement Control Methods. (1.34Hz Sinusoid Input)

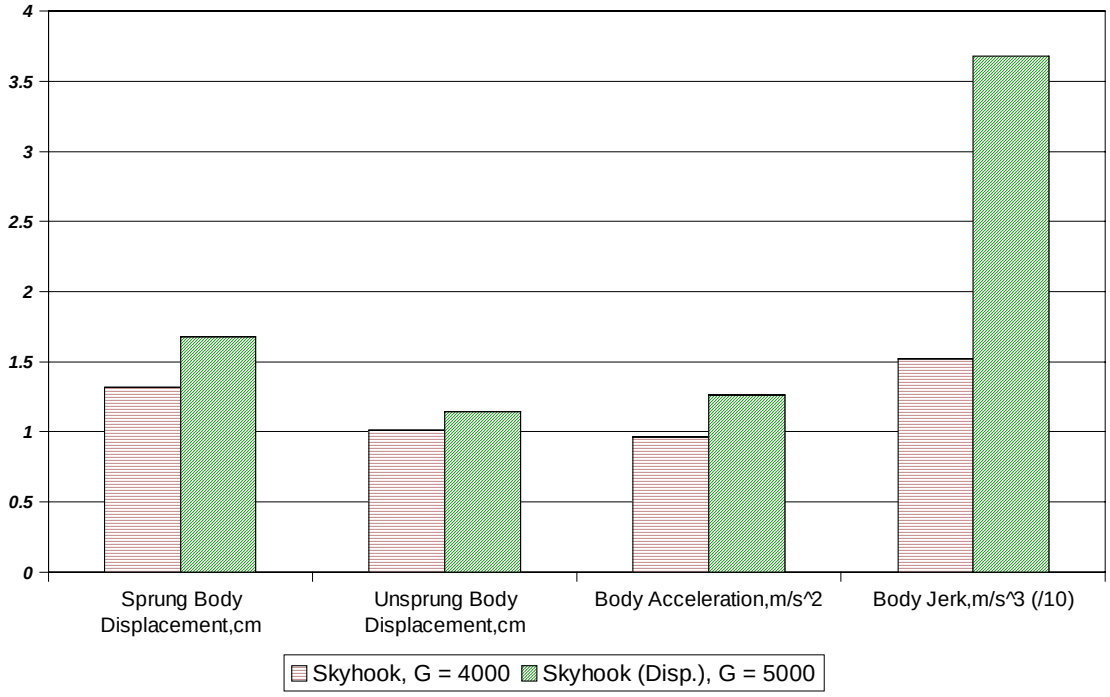

(a)

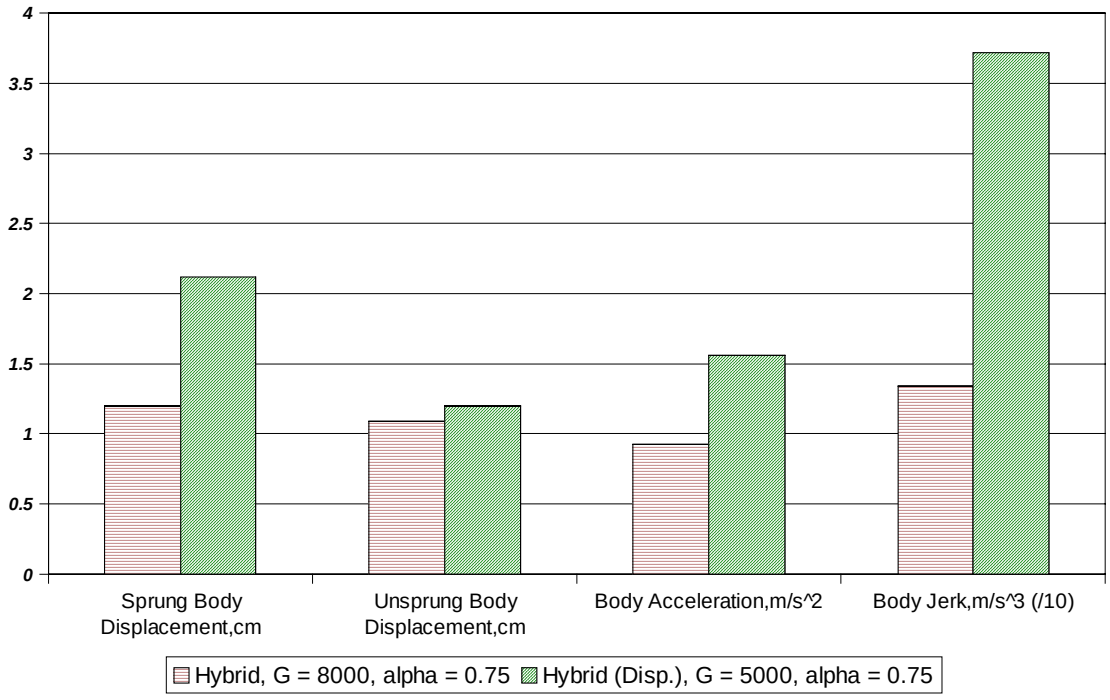

(b)

Figure 5.5-13 Comparison of Steady State RMS Responses between Conventional Control Methods and Displacement Control Methods. (1.34Hz Sinusoid Input)

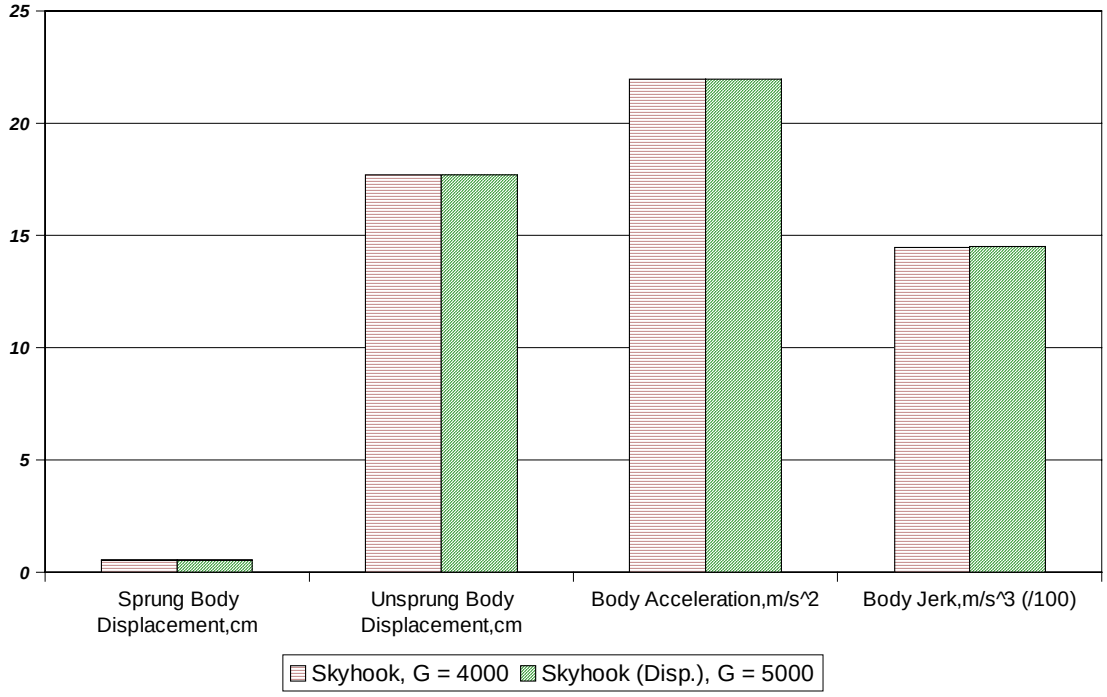

(a)

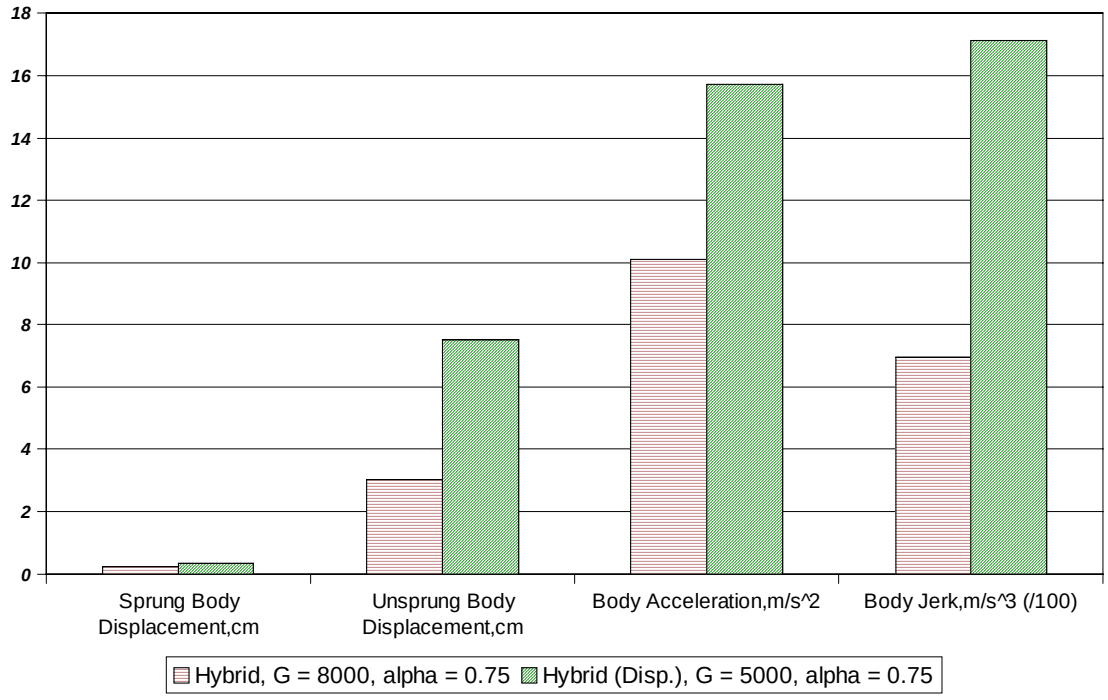

(b)

Figure 5.5-14 Comparison of Steady State peak-to-peak Responses between Conventional Control Methods and Displacement Control Methods. (10.5Hz Sinusoid Input)

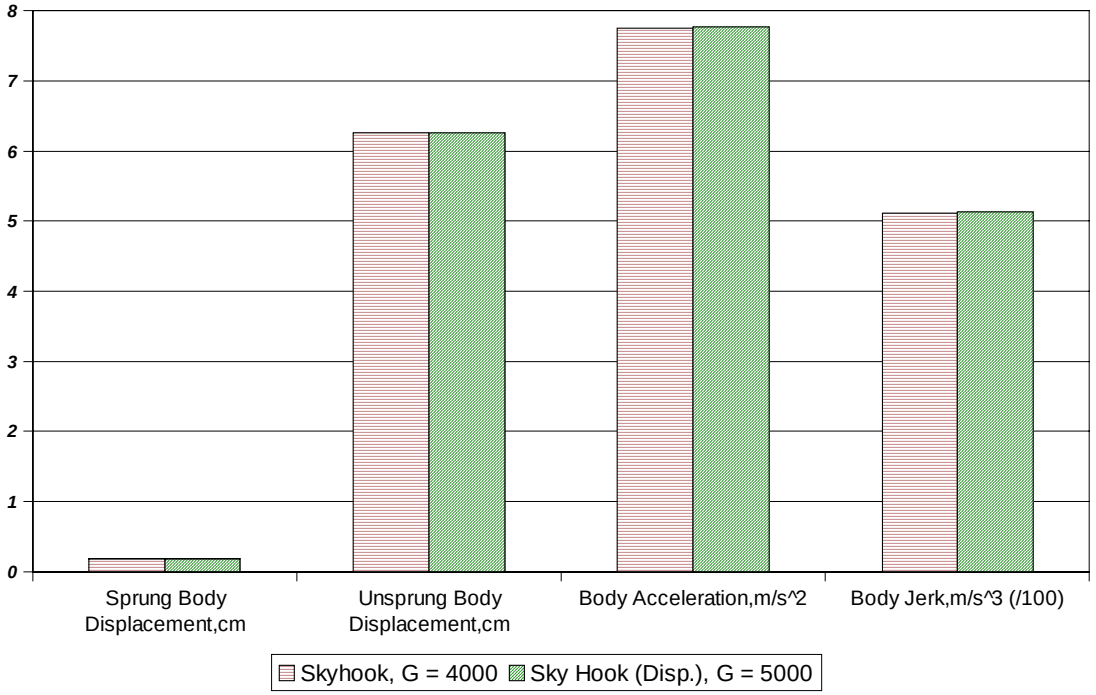

(a)

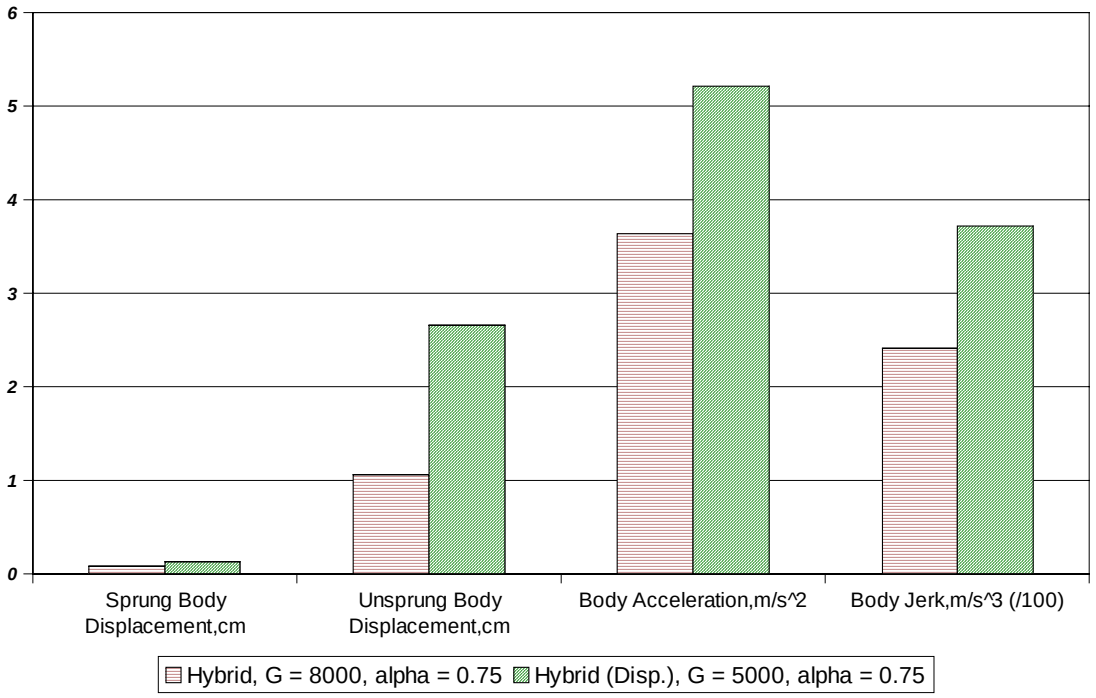

(b)

Figure 5.5-15 Comparison of Steady State RMS Responses between Conventional Control Methods and Displacement Control Methods. (10.5Hz Sinusoid Input)

6.1 Semiactive Results Summary

Completing this chapter accomplishes the main objectives of this study. The main objectives were to simulate a single suspension system with Skyhook and Hybrid control, introduce and simulate alternative control methods, and use a bounded force model to evaluate the effectiveness of each control method.

To meet the first objective, this chapter presented the simulation results for a single suspension model with Skyhook and Hybrid controls, and subjected to chirp input, step input, 1.34 Hz sinusoid, and 10.5 Hz pure tone inputs. To meet the second objective, this chapter also presents the simulated results of the same single suspension with alternative control methods; namely, Displacement Skyhook and Displacement Hybrid. Finally, the third objective was met by using the bounded force model presented in Chapter 3 for the results.

Chapter 6
Conclusions

6.1 Overview

This study presents single suspension simulations using a passive and semiactive damper, and discusses and compares the results. The semiactive single suspension simulations were carried out using a bounded force MR damper model with semiactive controllers. For each group of semiactive controller results, a brief discussion of the damper requirements was given. Then, two previously presented controller methods, Skyhook and Hybrid, were compared to the passive control case. Additionally, two more control methods, displacement Skyhook and displacement Hybrid, were compared to passive damping and to the other control methods mentioned earlier.

The single suspension model incorporates a bounded time-varying model of semiactive dampers which allows us to model the true dynamic characteristics of such dampers when used with various control methods. Other time-varying and nonlinear effects of the suspension are neglected. The parameters that were used for the model were based on actual experimental data from other studies at the Advanced Vehicle Dynamics Laboratory of Virginia Tech.

To verify the accuracy of the simulations, the results for passive damping were calculated using the SIMULINK model, were compared with results for a linear passive damper. To check the damper model and controllers, the results were analyzed to see if they behaved in a way indicated by the intended equations. Finally, the semiactive force/velocity trajectory results, for the Skyhook case, were compared to experimental results. This comparison shows that the model does not predict the magnitudes of the results, but that the behavior of the computer simulation was similar enough to the experimental results to proceed with the study.

The results were presented one controller at a time. For each controller the frequency response, step response and the 1.34Hz and 10.5Hz steady state responses were analyzed. Then comparisons were made between the more conventional control methods and the alternative control laws. For all discussions, the importance of the trends was explained in terms of ride comfort and vehicle handling to determine the effect that the control methods had on the performance of the semiactive damper in controlling the single suspension.

6.2 Recommendations for Future Studies

There are several issues that are not addressed in this report. They are,

1) the optimization of the solution (valuing of each performance measure),
2) a more detailed modeling of the spring, damper, and actuator, and
3) an in-vehicle ride assessment.

Recommendations for future research in each of the above areas will be explained in more detail next.

First, the solutions presented in this study were selected on a general understanding of what constitutes a good performance, such as a lower settling time is better than a greater settling time. In reality however, there exists tradeoffs between the various performance measures, such as between peak-to-peak body position and jerk. An optimization routine may be used to determine which solution offers the best performance in a specific vehicle condition. A greater understanding is needed of the relative value of each performance measure before a meaningful optimization can be used to maximize ride performance.

Second, the spring model was taken as a simple linear spring whereas the spring used may exhibit certain nonlinear behavior. Furthermore, the MR damper is actually more complicated than modeled here. This includes for instance the spring effect due to the damper gas charge, internal friction, and the bilinear damping characteristic, as shown in Figure 2.1. Future studies may consider using a more complete model of the damper to capture a more accurate representation of the damper characteristics in the model. The

complexities due to such damper models however, must be evaluated against the benefits that will be gained, for each specific case [Ahmadian].

Third, the man-machine interaction is quite critical to truly assessing the benefits of any vehicle system, including semiactive suspensions. Therefor, before any production decision is made on any type of suspension, it must be fully tested on the vehicle; as is commonly practices with the original equipment manufacturers. One such study at the Advanced Vehicle Dynamics Laboratory (AVDL) is described by Simon [29]. [Ahmadian]

References

1 Ahmadian, M., “On the Isolation Properties of Semiactive Dampers”, *Journal of Vibration and Control*, 5, pp. 217-232, 1999.

2. Ahmadian, M, “Ride Evaluation of a Class 8 Truck with Semiactive Suspensions”, *Advanced Automotive Technologies*, ASME, DSC-Vol. 52, pp. 21-28, 1993.

3. Ahmadian, M. and Pare, C., “A Quarter-Car Experimental Analysis of Alternative Semiactive Control Methods*”, Journal of Intelligent Material Systems and Structures*, 11 (8), pp. 604-612 August 2000.

4. Ahmadian, M., Reichert, B., and Song, X., “System Non-linearities Induced by Skyhook Dampers”, *Journal of Shock and Vibration*, 8 (2), pp. 95-104, 2001.

5. Ahmadian, M., Reichart, B., Song, X., and Southward, S., “No-Jerk Semi-Active Skyhook Control Method and Apparatus”, United States Patent # 6,115,658, January 1999.

6. Beer, F. P. and Johnston, E. R., Vector Mechanics for Engineers, fifth edition, McGraw Hill, New York, 1998.

7. Carlson, J. D., "Magnetorheological Fluid Actuators", Adaptronics and Smart Materials, H. Janocha, ed., Springer Verlag, Berlin, pp. 180-195, 1999.

8. Carter, A., “Transient Motion Control of Passive and Semiactive Damping

9. Crosby, M. J., Harwood, R. A., and Karnopp, D., “Vibration Control Using Semi-Active Force Generators”, Lord Library of Technical Articles, LL-7004, 1973.

10. Dorf, R. C. and Bishop, R. H., Modern Control Systems, eighth edition, Addison Wesley, California, 1998.

11. Franklin, G. F., Powell, J. D., and Workman, Michael, Digital Control of Dynamic Systems, third edition, Addison Wesley, California, 1998.

12. Goncalves, F., “Dynamic Analysis of Semiactive Control Techniques for Vehicle Applications”, Master of Science Thesis, Virginia Polytechnic and State University, Blacksburg, Virginia, 2001.

13. Inman, D. J., Engineering Vibration, second edition, Prentice Hall, New Jersey, 2001.

14. Ivers, D. E. and Miller, L. R., “Experimental Comparison of Passive, Semi-active On/Off, and Semi-Active Continuous Suspensions”, *SAE Technical Paper Series*, 892484, 1989.

15. Jolly, M. R., Bender, J.W., and Carlson, J. D., “Properties and Applications of Commercial Magnetorheological Fluids,” *Journal of Intelligent Material Systems and Structures*, 10 (1), pp. 5-13, January 1999.

16. Jolly, M.R., Carlson, J.D., and Muñoz, B.C., "A Model of the Behavior of Magnetorheological Materials," *Smart Materials Structures*, 5, pp. 607-614, 1996.

17. Karnopp, D., “Design Principles for Vibration Control of Systems Using Semi-active Dampers”, *Transactions of the ASME*, Vol. 112, pp. 448-455, September 1990.

18. Karnopp, D. C. and Crosby, M. J., “System for Controlling the Transmission of Energy Between Spaced Members”, United States Patent #3,807,678, April 30, 1974.

19. Lord Corporation, “Rheonetic™ MR Damper RD-1005-3”, http://www.rheonetic.com/devices_damper_begin.htm, October 22, 2001.

20. Margida, A. J., Weiss, K. D., and Carlson, J. D., "Magnetorheological Materials Based on Iron Alloy Particles," in Proc. *5th International Conference on ER Fluids, MR fluids and Assoc. Tech.*, W. Bullough, Ed., World Scientific, Singapore (1996) pp. 544-550, July 1995.

21. Margolis, D. L. and Goshtasbpour, M., “The Chatter of Semi-Active On-Off Suspensions and its Cure”, *Vehicle System Dynamics*, 13, pp. 129-144, 1984.

22. Miller, L. R., “An Introduction to Semi-active Suspension Systems”, Lord Library of Technical Papers, LL-1204.

23. Miller, Lane, R. and Nobles, Charles, M., “Methods for Eliminating Jerk and Noise in Semi-Active Suspensions”, *SAE Technical Paper Series*, 902284, 1996.

24. Miller, L. R., Nobles, C. M., “The Design and Development of a Semi-active Suspension for a Military Tank”, *SAE Technical Paper Series*, 881133, 1988.

25. Nakano, M., Yamamoto, H. and Jolly, M.R., “Dynamic Viscoelasticity of a Magnetorheological Fluid in Oscillatory Slit Flow,” *International Journal of Modern Physics B*, 13 (14-16), pp. 2068-2076, June 1999

26. Phillips, C. L. and Harbor, R. D., Feedback Control Systems, fourth edition, Prentice Hall, New Jersey, 2000.

27. Poyner, J., “Innovative Designs for Magneto-Rheological Dampers”, Master of Science Thesis, Virginia Polytechnic and State University, Blacksburg, Virginia, August 2001.

28. Simon, D., “An Investigation of the Effectiveness of Skyhook Suspensions for Controlling Roll Dynamics of Sport Utility Vehicles Using Magneto-Rheological Dampers”, Ph.D. Dissertation, Virginia Polytechnic and State University, Blacksburg, Virginia, December 2001.

29. Song, X., “Design of Adaptive Vibration Control Systems with Application to Magneto-Rheological Dampers”, Ph.D. Dissertation, Virginia Polytechnic and State University, Blacksburg, Virginia, 1999.

Vitae

John W. Masi received his Bachelor of Arts degree from the University of Virginia in January 1996 and majored in Economics. Soon thereafter he enrolled in Virginia Tech in fall of 1997 to study engineering. He graduated with a Bachelor of Science in Mechanical Engineering in May 2000 and then started graduate school studies at Virginia Tech. John expects to graduate with a Master of Science in Mechanical Engineering in January 2002. Technology, inventions, and improvements over existing ways of doing things has always fascinated John and has led him to study engineering.